UNIVERSITY OF ZAGREB
FACULTY OF SCIENCE
DEPARTMENT OF PHYSICS

SREĆKO MOROVIĆ

MEASUREMENT OF W AND Z PAIR PRODUCTION AND SEARCH FOR WZ RESONANCES AT THE LARGE HADRON COLLIDER

(MJERENJE PRODUKCIJE PAROVA W I Z BOZONA I POTRAGA ZA NJIHOVIM REZONANCIJAMA NA VELIKOM HADRONSKOM SUDARIVAČU)

SUPERVISOR:
VUKO BRIGLJEVIĆ

ZAGREB, 2013

Abstract

This thesis presents a study of WZ production in proton proton collisions at a center of mass energy of 7 TeV. The measurements are based on data recorded by the CMS experiment at the Large Hadron Collider, corresponding to an integrated luminosity of approximately 5 fb^{-1}. The electron and muon decay channels of the W and Z bosons are used. A measurement of the inclusive cross section of the $pp \rightarrow$ WZ + X process is performed, restricted to the phase space for which the Z boson mass lies in the interval [71.18,111.18] GeV. The measurement result is compatible with the Standard model predictions. A search for exotic heavy resonances decaying to WZ is also presented. No significant excess above the expected SM background is found. New upper bounds at 95% confidence level are therefore set on the production cross section of the W' boson described by the sequential standard model, and lower bounds on W' bosons masses are set. Limits are also set on the production cross section and mass of the ρ_{TC} techni-hadron in the context of low-scale Technicolor models.

Key words:

Standard Model, Electroweak physics, Triple gauge coupling (TGC), WZ, Sequential Standard Model, Technicolor, Large Hadron Collider (LHC), Compact Muon Solenoid (CMS)

Acknowledgements

I would like to thank my supervisor Vuko, colleagues from my group: Tanja, Krešo, Tome, Senka, Jelena, Lucija, Darko, Vedran and Saša, as well as all other friends and colleagues at IRB and CERN for the nice working experience and for the opportunity to work at the leading-edge experiment in high-energy physics in recent years. Special thanks to my family, brother Dinko and parents Olja and Ivica, and all my friends.

Contents

Curriculum Vitae

List of Tables

List of Figures

Chapter 1

Introduction

As a fundamental theory of particle interactions, the Standard Model has been experimentally confirmed to extraordinary precision by many particle physics experiments. It is thus established that this theory is a correct description of electromagnetic and nuclear interactions at the so far verifiable energy scales.

Many observations, however, mainly astrophysical and cosmological, clearly identified phenomena that are not explained by the current model. Even the fundamental force of gravity has so far resisted theoretical attempts to be integrated with the other three fundamental forces described by the Standard Model. While the gravity is predicted to have emerged at the experimentally unreachable Planck scale in the early stages of the Universe, there is a hope that other observed phenomena, such as dark matter or matter-antimatter asymmetry in the universe, could emerge from a new form of interaction reachable at a much lower scale.

For central predictions of the Standard Model, as the existence of the Higgs boson, previous attempts to detect its presence were only able to set a lower limit on its possible mass. As a successor to the Tevatron, the previous hadron collider experiment, the Large Hadron Collider (LHC) is built to test the validity of the Standard Model at even higher interaction energies and attempt to find the Higgs boson. The LHC was envisioned also as an experiment that could test a variety of theoretical extensions at the TeV scale.

This thesis presents a study of diboson production in the WZ final state at the LHC. Diboson production modes are precisely predicted by the Standard Model. It is thus important to measure their cross section and other properties. In particular, the self-coupling strength of vector bosons, contributing to some of these modes, could be indirectly affected by some new physics even if it is not directly observable at the energy scale reachable by the LHC. In addition, it is also possible to directly search for new heavy resonances decaying to diboson final states.

Two results are presented based on proton-proton collisions at the center of mass energy of 7 TeV, produced by the LHC and recorded by the Compact Muon Solenoid (CMS) experiment. First is a cross section measurement of the WZ production, a Standard Model diboson production mode. Second is the search for new resonances decaying to the WZ signature as predicted in the scope of two Standard Model extensions, the Sequential Standard Model and Technicolor.

This thesis is organized in several chapters, starting with a theoretical description of the Standard Model, processes contributing to the WZ production and possible theoretical extensions. This is followed by a description of the LHC and the CMS detector. A detailed view of methods used to analyze a vast amount of data collected by the CMS is given. In the following chapter, the measurement of the Standard Model WZ process cross section is presented. The results are compared with theoretical predictions and measurements done by other experiments. This is followed by a chapter describing the analysis involved with testing theoretical hypotheses under which WZ process production is enhanced by a resonant signature, done on the same data as the cross section measurement. As a result, limits on the cross section and mass of the new resonances are established, and comparison drawn with other experimental results. Finally, the conclusion summarizes the presented results.

Chapter 2

Theoretical overview

The Standard Model of Particle Physics has been developed on the relativistic quantum field theory foundations in the course of the 20th century. It incorporates all current knowledge about the nature of elementary particles and their interactions through three of the four fundamental forces (electromagnetism, weak force and strong nuclear force), lacking only integration of the gravitational interaction, which is so far verifiably described only by the theories of relativity. An important milestone for the development of Standard Model was the unfication of electromagnetism and weak nuclear force into a single theory. For these achievements, Glashow, Salaam and Weinberg received the Nobel prize in 1979. Confirmation arrived through the experimental observation of the W and Z boson by the UA1 and UA2 experiments at CERN in 1983. To explain why elementary particles possess mass, the Higgs mechanism was incorporated into the theoretical framework [1–4]. A 2013 Nobel prize was awarded to Englert and Higgs for this work. In 1970's, Quantum chromodynamics emerged as an explanation of the strong interaction. In the following decades, the Standard Model has been tested and verified by experiments with ever-increasing precision at higher and higher energy scales. The top quark, the heaviest of all known elementary particles, was discovered by the Tevatron experiments CDF and D0 [5, 6]. More recently, the LHC experiments CMS and ATLAS discovered a particle consistent with the properties of a Higgs boson [7, 8].

This Chapter begins by describing fundamental aspects of the Standard Model, detailing mechanisms behind the electroweak interaction, the electroweak symmetry breaking and describing gauge boson self-couplings. This is followed by a description of the Sequential Standard Model and Technicolor theories predicting phenomena beyond the Standard Model, as potential manifestations of decay modes similar to processes emerging from the gauge boson self-coupling.

2.1 Overview of the Standard Model

Interactions in the Standard Model (SM) arise due to the requirement of gauge symmetry. Quantum Electrodynamics (QED), which describes electromagnetic interactions, is derived from the requirement of gauge invariance under the symmetry group $U(1)_{em}$. It is incorporated into the $SU(2)_L \otimes U(1)_Y$ symmetry requirement which gives rise to the electroweak interaction. In the same fashion, the strong interaction arises from the $SU(3)_C$ symmetry group. Overall, the Standard model is defined in terms of the symmetry group

$$SU(3)_C \otimes SU(2)_L \otimes U(1)_Y. \tag{2.1}$$

Elementary particles in the framework of the field theory are defined as nonlocal quantum fields which possess certain quantum numbers, such as charge. Based on the spin, they are divided in fermions, half-integer spin fields, and bosons, integer-spin particles. Fermions, listed along with several distinct properties[1] in Table 2.1, can be further divided into hadrons and leptons depending on whether they interact in terms of strong interaction or only through the electroweak interaction. For the electroweak interaction, the quantum numbers of charge, allowing fermions to interact, are the electromagnetic charge Q_{EM}, the third projection of the weak isospin T_3 and the weak hypercharge $Y_W = 2(\frac{Q_{EM}}{e} - T_3)$. Charges of the strong interaction are the colors red, green or blue (or respective anticolors). Quarks, which are elementary constituents of hadrons, carry a single color charge, while the force carriers, gluons, carry a combination of color and anti-color. Boson particles are mediators of interactions through the coupling to fermionic fields or to other boson fields.

Fermions can be described by the fermionic quantum field operator ψ of spin 1/2, or Dirac spinor. The Lagrangian of a free fermion with mass m is

$$\mathcal{L}_D = \bar{\psi}(i\gamma^\mu \, \partial_\mu - m)\psi \tag{2.2}$$

where γ_μ are Dirac matrices [2]. Dirac Lagrangian is trivially invariant under the global (constant) phase transformation $\psi \to e^{i\Phi}\psi$. The local gauge invariance requires the Dirac Lagrangian to be invariant under the field phase transformation $\psi \to e^{i\phi(x)}\psi$ where $\phi(x)$ is an arbitrary complex function of the space-time coordinates. For this, it is necessary to introduce a gauge field A^μ which

---

[1] A convention $c = 1$ is used throughout this thesis for units and relations of mass, momentum and energy.

[2] In the Weyl representation, γ matrices are defined as $\gamma_0 = \begin{pmatrix} 0 & \mathbb{1} \\ \mathbb{1} & 0 \end{pmatrix}$, $\gamma_i = \begin{pmatrix} 0 & -\sigma_i \\ \sigma_i & 0 \end{pmatrix}$ and $\gamma_5 = \begin{pmatrix} -\mathbb{1} & 0 \\ 0 & \mathbb{1} \end{pmatrix}$, where σ_i are Dirac spinors.

interacts with the fermion field and transforms simultaneously with the Dirac field as

$$\psi \to \psi' = e^{i\phi(x)}\psi \qquad A_\mu \to A'_\mu = A_\mu - \frac{1}{e}\partial_\mu \phi(x). \tag{2.3}$$

The Dirac Lagrangian incorporating the interaction term $e\bar{\psi}\gamma^\mu A_\mu \psi$ becomes

$$\mathcal{L}_D = \bar{\psi}(i\gamma^\mu\,(\partial_\mu + ieA_\mu) - m)\psi \equiv \bar{\psi}(i\gamma^\mu\,D_\mu - m)\psi. \tag{2.4}$$

where $D_\mu \equiv \partial_\mu + ieA_\mu$ is the covariant derivative. Under the local gauge transformation, the Lagrangian becomes

$$\mathcal{L}_D \to \bar{\psi}'(i\gamma^\mu\,(\partial_\mu + ieA'_\mu + i\partial_\mu\phi - i\partial_\mu\phi) - m)\psi' = \bar{\psi}'(i\gamma^\mu\,D'_\mu - m)\psi'. \tag{2.5}$$

The D_μ transforms in a same way as the ψ itself, leading to the gauge invariance of the Lagrangian. The Lagrangian term for the gauge field A_μ:

$$\mathcal{L} = -\frac{1}{4}F^{\mu\nu}F_{\mu\nu} \qquad F_{\mu\nu} \equiv \partial_\mu A_\nu - \partial_\mu A_\nu = D_\mu A_\nu - D_\nu A_\mu \tag{2.6}$$

represents the electromagnetic field and is also gauge invariant.

Boson fields found in the Standard Model are gluons, photons, W, Z, and the Higgs boson. Properties of these fundamental bosons are summarized in Table 2.2.

Table 2.1: Fundamental fermions in the Standard Model. Three generations of fermions are listed. For each listed fermion there is a corresponding antiparticle with identical mass and opposite quantum numbers. Presence of color (C) denotes that a quark particle carries one of the red, green or blue color.

	charge			1st generation		2nd generation		3rd generation	
	Q_{EM}	T^3	C	f	mass (GeV)	f	mass (GeV)	f	mass (GeV)
quarks	+2/3e	1/2	yes	u	$3 \cdot 10^{-}3$	c	1.27	t	172.9
	-1/3e	-1/2	yes	d	$5 \cdot 10^{-}3$	s	0.1	b	4.67
leptons	0	1/2	no	ν_e	$< 2.2 \cdot 10^{-9}$	ν_μ	$< 1.7 \cdot 10^{-4}$	ν_τ	< 0.0155
	-1e	-1/2	no	e	$5.11 \cdot 10^{-4}$	μ	0.106	τ	1.78

Table 2.2: Fundamental bosons in the Standard Model. Gluon carries a color and anticolor (C) from the red, green and blue triplet. Higgs boson properties are not yet fully experimentally confirmed.

boson	g	γ	W$^+$	W$^-$	Z	H
Q_{EM}	0	0	+e	-e	0	0
T_3	0	0	1	-1	0	0
C	1,-1	0	0	0	0	0
spin	0	1	1	1	1	0
mass (GeV)	0	0	80.385 ± 0.015		91.1876 ± 0.0021	$125 - 126$

2.1.1 Quantum chromodynamics

Quantum chromodynamics (QCD) is a theory of strong interactions. The interaction arises from the introduction of the $SU(3)$ gauge invariance. Boson fields which are introduced to preserve the local gauge invariance are called gluons. The QCD Lagrangian is

$$\mathcal{L}_{QCD} = \bar{\psi}_i(i(\gamma^\mu D_\mu)_{ij} - m\delta_{ij})\psi_j - \frac{1}{4}G^a_{\mu\nu}G^{\mu\nu}_a, \tag{2.7}$$

where quarks are described by a field $\psi_{i/j}$ with $i, j \in 1...3$ and the QCD covariant derivative is

$$D_\mu = \partial_\mu + ig_s A^a_\mu \lambda_a, \tag{2.8}$$

where g_s is a strong coupling constant, A^α_μ is a gluon gauge field and λ_a is one of the Gell-Mann matrices [9] with $a \in 1...8$.

As in QCD, the field term in 2.7 is allowed by the gauge invariance, with the field tensor $G^a_{\mu\nu}$ defined as

$$G^a_{\mu\nu} = \partial_\mu A^a_\nu - \partial_\nu A^a_\mu + g \cdot f^{abc} A^b_\mu A^b_\nu, \tag{2.9}$$

where the third term containing the f^{abc} structure constant and the gauge coupling parameter g reflects the non-abelian nature of QCD. In the Lagrangian, this term allows non-vanishing terms with three or four field tensors and therefore couplings between gluons.

A distinct property of the strong interaction is the asymptotic freedom: the strong interaction is weaker at short distances between quarks, and becomes stronger as they are pulled apart. The effective coupling in renormalizable theories is described by the beta function [10, 11] which describes variation of the theory's coupling constant depending on the scale of the momentum transfer (which increases at shorter distances). For $SU(N)$ groups with n_f quark flavors the beta function is

$$\beta_1(\alpha) = \frac{\alpha^2}{\pi}\left(\frac{-11N}{6} + \frac{n_f}{3}\right). \tag{2.10}$$

For QCD parameters $N = 3$ and $n_f = 6$, and the resulting beta function is negative, leading to the asymptotic freedom. As a consequence, colored particles are *confined*, i.e the interaction strength with other colored particles (e.g. proton constituents) increases with distance and prevents their separation. Only neutrally colored particle compositions can escape the confinement and be observed as free states.

2.1.2 Electroweak interaction

Weak interactions are known to violate parity as they are not acting symmetrically under the interchange of positive-helicity and negative-helicity fermions. Thus the left-handed and right-handed part of the Dirac field must be treated separately,

$$\psi = \psi_L + \psi_R \qquad \psi_L = P_L\psi \quad \psi_R = P_R\psi \tag{2.11}$$

where the left and right the projection operators are

$$P_L = \frac{1-\gamma_5}{2} \qquad P_R = \frac{1+\gamma_5}{2} \tag{2.12}$$

The electron, muon and tau leptons have both L and R components, while neutrinos only have L component[3]. Therefore the following "isospinors" can be constructed

$$\begin{array}{cccccccc} L_e & = & \begin{pmatrix} \nu_e \\ e_L \end{pmatrix} & L_\mu & = & \begin{pmatrix} \nu_\mu \\ \mu_L \end{pmatrix} & L_\tau & = & \begin{pmatrix} \nu_\tau \\ \tau_L \end{pmatrix} \\ R_e & = & e_R & R_\mu & = & \mu_R & R_\tau & = & \tau_R \end{array} \tag{2.13}$$

---

[3] There is no direct evidence of the right-handed neutrinos. The observed neutrino mixing, however, suggests that there is a possibility for R component to be observed.

The left doublets are assigned a weak isospin, $T = 1/2$ with a third projection $T_3 = 1/2$ for the neutrino component and $T_3 = -1/2$ for the charged lepton component, while right handed singlets have $T = 0$. The resulting Lagrangian

$$\mathcal{L} = \sum_{\ell=e,\mu,\tau} \left(i\bar{R}_\ell \partial\!\!\!/ R_\ell + i\bar{L}_\ell \partial\!\!\!/ L_\ell \right) \tag{2.14}$$

is invariant under rotations in the isospin ($SU(2)$) space. Under these rotations, only the left doublet transform, while right singlets remain invariant

$$\begin{aligned} L_\ell &\rightarrow e^{-i\frac{\vec{\tau}}{2}\cdot\vec{\alpha}} L_\ell \\ R_\ell &\rightarrow R_\ell, \end{aligned} \tag{2.15}$$

where $\vec{\tau}/2$ are generators of the $SU(2)$ group [4].

R_ℓ singlets only transform under the $U(1)_Y$ symmetry and the corresponding field B_μ. As electromagnetism is known to exist free of parity violation, this puts a requirement on doublets L_ℓ to also transform under this symmetry. The respective charge is the already mentioned weak hypercharge defined by the Gell-Mann-Nishijima relation $\frac{Q_{EM}}{e} = T_3 + \frac{Y}{2}$. From the definition of weak isospin

---

[4] $\tau_+ = \begin{pmatrix} 0 & \sqrt{2} \\ 0 & 0 \end{pmatrix}$, $\tau_- = \begin{pmatrix} 0 & 0 \\ \sqrt{2} & 0 \end{pmatrix}$, $\tau_0 = \begin{pmatrix} 1 & 0 \\ 0 & -1 \end{pmatrix}$.

for the left doublets and right singlets, it follows that L_ℓ has hypercharge $Y_W = -1$ and R_ℓ has $Y_W = -2$. Transformation under $U(1)_Y$ gauge group is therefore

$$\begin{aligned} &L_\ell \to e^{-i\frac{\beta}{2}} L_\ell \\ &R_\ell \to e^{-i\beta} R_\ell. \end{aligned} \tag{2.16}$$

The gauge invariant electroweak Lagrangian is obtained by constructing a covariant derivative through introduction of the three gauge fields $\vec{W}_\mu$ (denoted also with W_μ^i, where $i = 1, 2, 3$) associated to the $SU(2)_L$, and the $U(1)_Y$ B_μ field,

$$\begin{aligned} &D_\mu = \partial_\mu + ig\tfrac{\vec{\tau}}{2} \cdot \vec{W}_\mu + i\tfrac{g'}{2} Y_W B_\mu \quad (L) \\ &D_\mu = \partial_\mu + i\tfrac{g'}{2} Y_W B_\mu \qquad\qquad\qquad (R). \end{aligned} \tag{2.17}$$

The electroweak Lagrangian includes kinematic terms for the gauge fields as

$$-\frac{1}{4}\vec{W}_{\mu\nu}\vec{W}^{\mu\nu} - \frac{1}{4}B_{\mu\nu}B^{\mu\nu}, \tag{2.18}$$

where the field strength tensors are

$$\begin{aligned} \vec{W}_{\mu\nu} &= \partial_\mu \vec{W}_\nu - \partial_\nu \vec{W}_\mu + g\vec{W}_\mu \times \vec{W}_\nu \\ B_{\mu\nu} &= \partial_\mu B_\nu - \partial_\nu B_\mu. \end{aligned} \tag{2.19}$$

The full electroweak Lagrangian can be written as

$$\begin{aligned}\mathcal{L} = \; & -\tfrac{1}{4}\vec{W}_{\mu\nu}\vec{W}^{\mu\nu} - \tfrac{1}{4}B_{\mu\nu}B^{\mu\nu} \\ & +\bar{\psi}_L\gamma^{\mu}(i\partial_{\mu} - g\tfrac{\vec{\tau}}{2}\cdot\vec{W}_{\mu} - \tfrac{g'}{2}Y_W B_{\mu})\psi_L \\ & +\bar{\psi}_R\gamma^{\mu}(i\partial_{\mu} - \tfrac{g'}{2}Y_W B_{\mu}))\psi_R.\end{aligned} \tag{2.20}$$

The electromagnetic interaction acts identically on left handed and right handed fermions, and therefore the B field alone can not be responsible for it due to differing coupling strengths to left and right fields (due to different weak hypercharge). However it is possible to define physical fields A_μ and Z_μ (as well as $W_\mu^\pm$) as linear combinations:

$$\begin{aligned} Z_\mu &= \cos\theta_W W_\mu^3 - \sin\theta_W B_\mu \\ A_\mu &= \cos\theta_W B_\mu - \sin\theta_W W_\mu^3 \\ W_\mu^\pm &= \tfrac{1}{\sqrt{2}}\left(W_\mu^1 \mp W_\mu^2\right), \end{aligned} \tag{2.21}$$

where θ_W is the electroweak mixing angle, linking the electromagnetic charge e to the weak coupling constants

$$e = g\sin\theta_W = g'\cos\theta_W. \tag{2.22}$$

The field A_μ represents the electromagnetic interaction and generates a photon, while Z_μ, W_μ^+ and W_μ^- generate weak mediators, the Z and W$^\pm$ bosons.

Equivalent formalism of left and right field components under $SU(2)$ can be applied also to quarks:

$$\begin{aligned} L_1 &= \begin{pmatrix} u_L \\ d'_L \end{pmatrix} & L_2 &= \begin{pmatrix} c_L \\ s'_L \end{pmatrix} & L_3 &= \begin{pmatrix} t_L \\ b'_L \end{pmatrix} \\ R_1 &= d'_R & R_2 &= s'_R & R_3 &= b'_R \end{aligned} \tag{2.23}$$

The d' s' and b' are linear combinations of quark mass eigenstates with the mixing parametrized by the Cabibbo-Kobayashi-Masakawa (CKM) matrix [12, 13]

$$\begin{pmatrix} d' \\ s' \\ b' \end{pmatrix} = \begin{pmatrix} V_{ud} & V_{us} & V_{ub} \\ V_{cd} & V_{cs} & V_{cb} \\ V_{td} & V_{ts} & V_{tb} \end{pmatrix} \begin{pmatrix} d \\ s \\ b \end{pmatrix}. \tag{2.24}$$

While the Standard Model in general respects the combination of the two symmetries, charge-conjugation and parity symmetry (CP), leading to identical treatment of particles and antiparticles with inverted charges and parity and exactly the same mass, a possibility of violation arises as a consequence of a complex phase in the CKM matrix. CP violation has been detected experimentally first in K^0 meson decays [14] and later in other measurements. QCD also allows CP violation. However this has not been observer experimentally, thus resulting with the strong-CP problem where a CP-violating QCD parameter $\bar{\theta}$ appears to be unnaturally small.

2.1.3 The Higgs mechanism

In the described formulation, all fermionic fields and gauge bosons are massless which is of course not consistent with observations. It is not possible to simply include mass terms and preserve the gauge invariance. A solution to this problem lies in the introduction of the spontaneous symmetry breaking mechanism.

To achieve breaking of the global $SU(2) \otimes U(1)$ symmetry, a $SU(2)$ doublet with the weak hypercharge $Y_W = 1$ is constructed:

$$\Phi = \begin{pmatrix} \phi^+ \\ \phi^0 \end{pmatrix} = \frac{1}{\sqrt{2}} \begin{pmatrix} \phi_1 + i\phi_2 \\ \phi_3 + i\phi_4 \end{pmatrix}, \tag{2.25}$$

where $\phi_1 ... \phi_4$ are components of the complex field Φ, called the Higgs field. The doublet is invariant under $U(1)_Y$ transformations. A Lagrangian term for the field is introduced in form of a potential $V(\Phi)$

$$\mathcal{L}_\Phi = \left(D_\mu \Phi\right)^\dagger \left(D^\mu \Phi\right) - V(\Phi), \tag{2.26}$$

called the Higgs potential, which is defined as

$$V(\Phi) = \mu^2 \Phi^\dagger \Phi + \frac{\lambda}{4} \left(\Phi^\dagger \Phi\right)^2. \tag{2.27}$$

For a regime where $\lambda > 0$ and $\mu^2 < 0$, the potential forms a "Mexican hat" shape as a function of the field Φ, as illustrated in Figure 2.1. A minimum of the potential is not at the value of the field

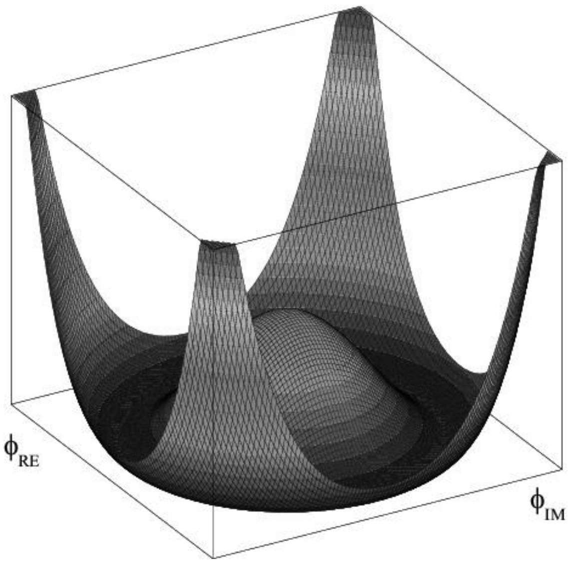

Figure 2.1: Higgs potential $V(\Phi) = \mu^2\Phi^\dagger\Phi + \frac{\lambda}{4}\left(\Phi^\dagger\Phi\right)^2$ in the regime where $\lambda > 0$ and $\mu^2 < 0$. Source: Wikimedia Foundation.

$\Phi = 0$ and is instead located at a continuous ring on a complex plane satisfying the condition

$$min(\Phi\Phi^\dagger) = -\frac{\mu^2}{2\lambda}. \tag{2.28}$$

This can be interpreted as the condition of the vacuum expectation value (vev)

$$\langle 0|\Phi^\dagger\Phi|0\rangle = v^2/2, \tag{2.29}$$

where $|0\rangle$, the initial (lowest potential) vacuum state, does not share the initial symmetry of the potential. The vev can be obtained through the measurement of the Fermi constant in muon decays,

$$\frac{G_F}{\sqrt{2}} = \frac{g^2}{8M_W} = \frac{1}{2v^2}. \tag{2.30}$$

The Fermi constant is $G_F = 1.6637 \cdot 10^{-5}\ \text{GeV}^{-2}$, resulting with $v \approx 246\ \text{GeV}$.

The appropriate choice of potential at the minimum is

$$\langle 0|\Phi_0|0\rangle = \frac{1}{\sqrt{2}} \begin{pmatrix} 0 \\ v \end{pmatrix}. \tag{2.31}$$

A consequence of such a choice of Φ_0 is breaking of three degrees of freedom associated with the flat plane of the potential, resulting with appearance of the three Goldstone bosons. These massless bosons are integrated as longitudinal spin components into W and Z boson fields which thus acquire mass. The photon remains massless, as the Φ_0 is neutral in charge and $U(1)_{EM}$ remains unbroken.

At the first order expansion around the minimum, the field expressed in terms of the real fields $\theta(x)_i$ $(i = 1, 2, 3)$ and $H(x)$ is

$$\Phi(x) = \frac{-\text{exp}(\vec{\theta}(x) \cdot \vec{\tau}/2)}{\sqrt{2}} \begin{pmatrix} 0 \\ v + H(x) \end{pmatrix}. \tag{2.32}$$

It can be shown that the $\vec{\theta}(x)$ fields can be gauged away by choosing an appropriate $SU(2)$ gauge, the so called *unitarity gauge* (see ref.[15]), and the expanded field becomes:

$$\Phi(x) = \frac{1}{\sqrt{2}} \begin{pmatrix} 0 \\ v + H(x) \end{pmatrix}, \tag{2.33}$$

The expanded scalar potential is thus

$$V = \frac{\mu^2}{2}(v+H)^2 + \frac{\lambda}{4}(v+H)^4. \tag{2.34}$$

The combined Lagrangian of the 2.18 and the Higgs is:

$$\begin{aligned}
\mathcal{L}_{G\Phi} \;=\; & \tfrac{1}{2}\partial_\mu H \partial^\mu H \\
& + \tfrac{1}{8}g^2(v+H)^2(W^1_\mu - iW^2_\mu)(W^{1\mu} + iW^{2\mu}) \\
& + \tfrac{1}{8}(v+H)^2(g'B_\mu - gW^3_\mu)(g'B^\mu - gW^{3\mu}) \\
& - \tfrac{\mu^2}{2}(v+H)^2 - \tfrac{\lambda}{16}(v+H)^4 \\
& - \tfrac{1}{4}\vec{W}_{\mu\nu}\vec{W}^{\mu\nu} - \tfrac{1}{4}B_{\mu\nu}B^{\mu\nu}.
\end{aligned} \tag{2.35}$$

In the fourth row there is a term proportional to H^2 which describes a scalar field with the mass $m_H = \sqrt{2}\mu = \sqrt{\lambda\nu/2}$. λ remains a free parameter and the Higgs mass is therefore not fixed in the model. In the same row there are also terms proportional to H^3 and H^4 which describe the Higgs self-coupling. After retaining only mass terms related to vector boson fields and using identities 2.21, the Lagrangian becomes:

$$\mathcal{L}_{\text{vector boson mass terms}} = \frac{vg^2}{4}W^+_\mu W^{\mu -} + \frac{v^2}{8}(g^2 + g'^2)(Z_\mu)^2 + 0(A_\mu)^2. \tag{2.36}$$

It follows that the masses acquired by the W and Z bosons are

$$m_W = \frac{1}{2}\sqrt{v^2 g^2} \qquad m_Z = \frac{1}{2}\sqrt{(g^2 + g'^2)v^2}, \tag{2.37}$$

while the photon does not acquire mass.

Mass terms for fermions can be introduced in a gauge invariant way through Yukawa couplings, where the scalar field couples left and right projection of fermionic fields (2.23 and 2.13):

$$\mathcal{L}_{\text{Yukawa}} = -g_f \left(\bar{L}_f \Phi R_f + \bar{R}_f \Phi^\dagger L_f \right) . \tag{2.38}$$

Substitution of the expanded Higgs field 2.33 results in

$$-g_f \frac{v + H(x)}{\sqrt{2}} (\bar{\psi}_L \psi_R + \bar{\psi}_R \psi_L) = -\frac{v}{\sqrt{2}} \bar{\psi}\psi - \frac{H(x)}{\sqrt{2}} \bar{\psi}\psi \tag{2.39}$$

with the first terms equivalent to the Dirac mass term, while the second term allows fermionic coupling to the Higgs field. Coupling strength is proportional to the fermion mass as

$$m_f = g_f \frac{v}{\sqrt{2}}. \tag{2.40}$$

2.1.4 Limitations of the Standard Model

It is widely believed that the currently known forces appear as separate interaction mechanisms below some high energy scale, possibly through symmetry breaking. Standard Model successfully unifies weak and electromagnetic interaction, however it fails to do so with QCD which for now remains a separate force.

The Higgs mechanism, which provides an elegant solution to the electroweak symmetry breaking, is accompanied by several open problems as well. The hierarchy problem represents the vast difference between the scales of gravity and weak force, as the weak force is 10^{32} times stronger. It is connected to a question of relatively small Higgs mass compared to the GUT (Planck) scale, mitigated in the SM by *unnaturally* large cancellations of perturbative contributions to the Higgs mass. One of the proposed solutions is provided by theories of supersymmetry which can remove these divergences through cancelling contributions of particles and their supersymmetric partners. The stability of the SM Higgs mechanism is also sensitive to the triviality problem which represents the problem of Higgs self-coupling corrections leading to a divergent λ parameter (2.27) above a certain scale. Similar is the the vacuum instability problem ($\lambda \to 0$) arising from corrections in quartic Higgs couplings to vector bosons and fermions [16]. Assuming the Higgs of mass $m_H \approx 125$ GeV, such regime could emerge at a scale as low as 10^8 GeV, requiring a new interaction to appear at this scale to preserve the stability. These theoretical problems are also resolved in supersymmetric models. In this thesis, one of the tested models is Higgsless (see Section 2.3.2), avoiding these issues altogether.

The Standard Model is also assuming a number of ad-hoc parameters, including fermion masses and coupling parameters. In the Higgs mechanism, the vacuum expectation value is not predicted by the model, and is instead determined only experimentally. It is hoped that a unifying theory would provide explanation on how these parameters emerge.

Finally, astronomical predictions as well as lack of theoretical integration with the general relativity show that SM can not explain all natural phenomena. For example, for the dark matter, which is the "invisible" matter in the universe observed only through its gravitational interaction, the SM provides no suitable elementary particle candidate. Even less is known about the nature of the repulsive *dark energy*, which causes the observed accelerated expansion of the universe. The matter-antimatter asymmetry of the universe also remains unresolved in the scope of the model, as observed CP violation modes are insufficient to explain the evident lack of antimatter.

Another emerging area of research are neutrino oscillations. The most trivial extension to the Standard Model follows the CKM approach, with neutrino masses explained as a consequence of the mass eigenstate mixing. This is parametrised by the PMNS matrix [17–19]. The mechanism by which fermions acquire mass in the SM however requires right handed neutrinos which have not been observed. One of the proposed explanations is the seesaw model [20, 21], where right-handed neutrinos are theorised to be *sterile* neutrinos with a disproportionally large mass.

2.2 WZ production in the Standard Model

The associated production of a W and Z boson is possible in the SM through several modes, one of which involves the direct coupling between heavy gauge bosons. The self-coupling is a consequence of the non-abelian nature of the $SU(2)$ gauge symmetry, where generators don't commute (as in the third $\vec{W}_{\mu\nu}$ term in 2.19). The $-\frac{1}{4}\vec{W}_{\mu\nu}\vec{W}^{\mu\nu}$ term of the electroweak Lagrangian can be expanded as

$$\begin{aligned}
\tfrac{1}{4}\vec{W}_{\mu\nu}\vec{W}^{\mu\nu} = \;& 2\left[\partial_\mu W^-_\nu - \partial_\nu W^-_\mu - ig\cos\theta_W(W^-_\mu Z_\nu - W^-_\nu Z_\mu) - ie(W^-_\mu A_\nu - W^-_\nu A_\mu)\right] \\
& \times\left[\partial_\mu W^{+\nu} - \partial^\nu W^{+\mu} + ig\cos\theta_W(W^{+\mu}Z^\nu - W^{+\nu}Z_\mu) + ie(W^{+\mu}A_\nu - W^{+\nu}A_\mu)\right] \\
& + \left[\cos\theta(\partial_\mu Z_\nu - \partial_\nu Z_\mu) + \sin\theta(\partial_\mu A_\nu - \partial_\nu A_\mu) + ig(W^-_\mu W^+_\nu - W^-_\nu W^+_\mu)\right] \\
& \times\left[\cos\theta(\partial^\mu Z^\nu - \partial^\nu Z^\mu) + \sin\theta(\partial^\mu A^\nu - \partial^\nu A^\mu) + ig(W^{-\mu}W^{+\nu} - W^{+\nu}W^{+\mu})\right].
\end{aligned} \tag{2.41}$$

The expansion contains terms allowing triple and quartic couplings of vector bosons. In case of the *triple gauge couplings* (TGC), the Lagrangian term, using identities in 2.21, becomes

$$\mathcal{L}^{TGC}_{WWV} = -ig_{WWV}\left[(W^-_{\mu\nu}W^{+\mu} - W^+_{\mu\nu}W^{-\nu})V^\nu + V_{\mu\nu}W^{+\mu}W^{-\nu}\right] \tag{2.42}$$

where the operator V^μ is A^μ or Z^μ, the field strength tensors are defined as $W^\pm_{\mu\nu} = \partial_\mu W^\pm_\nu - \partial_\nu W^\pm_\mu$ and $V_{\mu\nu} = \partial_\mu V_\nu - \partial_\nu V_\mu$, and the coupling constants are $g_{WWZ} = g\cos\theta_W$ and $g_{WW\gamma} = e$. It can be shown that only the TGC couplings involving $W^\pm$ boson fields are allowed in the Standard Model.

At the LHC, the WZ production mainly unfolds through quark-antiquark interaction in proton collisions. There is an excess of valence u over d quarks in protons leading to the asymmetry between the cross-section of W^+Z and W^-Z production [22]. Precisely, the probability for a charged current interaction of the u quark with the antiquark (where a W^+ is produced) is higher than the probability for the d quark interaction with the antiquark (where a W^- is produced).

(a) s-channel

(b) t-channel

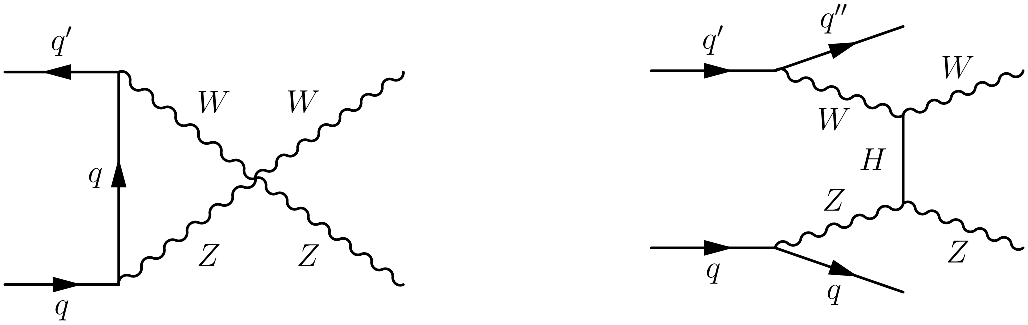

(c) quartic scattering

(d) Higgs-mediated scattering

Figure 2.2: Feynman diagrams of contributions to the WZ production at the LHC.

WZ is produced through several contributions, for which leading order Feynman diagrams are shown in Figure 2.2. The TGC or s-channel contribution is described by a diagram 2.2a and represents production of a virtual W boson with sufficiently high invariant mass to allow decay into the W and Z pair. In the t-channel mode (diagram 2.2b), W and Z are emitted by quark and antiquark exchange through a mediator quark. Contributions involving quartic scattering of longitudinally polarized W and Z and the Higgs contribution are described by diagrams 2.2c and 2.2d.

The W and Z decay can result in fully leptonic ($W \to \ell\nu$, $Z \to \ell^+\ell^-$), semi-leptonic ($W \to \ell\nu$, $Z \to jj$ or $W \to jj$, $Z \to \ell^+\ell^-$) or purely hadronic ($W \to jj$, $Z \to jj$) final states where ℓ, ν and j represent leptons, neutrinos and jets, respectively. Branching ratios of W and Z bosons are reported in Table 2.3. The low fraction of their leptonic decays results with only approx. 0.35%

Table 2.3: W and Z boson branching ratios [23] and branching ratios of WZ final states. ℓ, ν and j represent charged leptons, neutrinos and jets, respectively.

W decay	W BR(%)	Z decay	Z BR(%)
$e^{\pm}\nu$	10.75	$e^{+}e^{-}$	3.363
$\mu^{\pm}\nu$	10.57	$\mu^{+}\mu^{-}$	3.366
$\tau^{\pm}\nu$	11.25	$\tau^{+}\tau^{-}$	3.370
hadronic	67.60	hadronic	69.91
		$\bar{\nu}\nu$	20.00

WZ final states

	BR (%)		BR (%)
$eee\nu$	0.3615	$\mu\mu e\nu$	0.3555
$ee\mu\nu$	0.3618	$\mu\mu\mu\nu$	0.3558
$\ell\ell\ell\nu$	3.329	$4j$	47.26
$\ell\ell jj$	6.827	$\nu\nu l\nu$	6.51
$jjl\nu$	22.77	$\nu\nu jj$	13.52

WZ branching ratio for each combination of leptonic W and Z decay mode (channel). However, the leptonic final state has a very clean signature compared to decay modes with jets (hadronic modes), allowing a better discrimination from hadronic backgrounds which have a high presence at hadron colliders such as the LHC.

2.3 WZ production through non-Standard Model processes

2.3.1 Sequential Standard Model

Various extensions of the Standard Model predict the existence of a new heavy charged gauge boson, generically known as W' (or the W prime), that decays into a pair of W and Z bosons [24–29].

A new gauge boson could arise if there is an additional gauge symmetry present, often found in Grand Unifying Theories (GUTs) which try to encompass QCD and the electroweak sector under a unified gauge symmetry (e.g. $SU(5)$ [30]). This symmetry is proposed to break into the familiar Standard Model $SU(3) \otimes SU(2) \otimes U(1)$ symmetry. However, such breaking could not unfold without the rise of additional residual symmetries, such as $U(1)$ or $SU(2)$, which would result in additional charged vector bosons with Z-like or W-like properties. A mechanism for the appearance of massive vector boson resonances was also suggested by hidden extra-dimension models [31, 32] as a manifestation of excited states of the SM vector bosons in short-looped dimensions.

Previous $\mathrm{W}^{'}$ searches have typically interpreted their results in terms of the Sequential Standard Model (SSM) [33–38]. This is a simple extension of the Standard Model in which the couplings of the $\mathrm{W}^{'}$ to fermions are identical to those of the Standard Model W boson. Searches in many cases have been conducted in the leptonic ($\mathrm{W}^{'} \to \ell\nu$) decay mode, assuming that the $\mathrm{W}^{'} \to \mathrm{WZ}$ decay mode is suppressed. Under this assumption, the $\mathrm{W}^{'}$ boson with mass below 3.35 GeV has recently been excluded by the CMS Collaboration [39].

Searches for the $\mathrm{W}^{'} \to \mathrm{WZ}$ decay mode are thus complementary to searches in leptonic channels. Furthermore, for some Higgsless models [40–42] it is predicted that $\mathrm{W}^{'}$ couplings to fermions are suppressed [43]. Such scenario would lead to an enhanced triple gauge coupling strength to W and Z bosons [44, 45].

2.3.2 Technicolor

Technicolor (TC) belongs to a family of compositeness [46] theories which aim to describe distinct "elementary" particles in terms of smaller components, i.e. that they possess a substructure. The

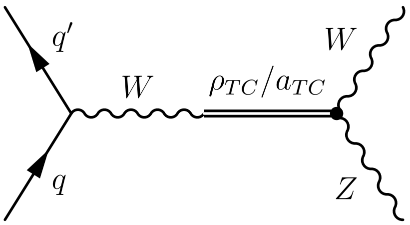

Figure 2.3: Feynman diagram of the ρ_{TC}/a_{TC} decay to WZ boson pair.

beauty of these theories lies in the potential reduction of the number of fundamental elementary particles and in the alternate formulation of the electroweak symmetry breaking. These models introduce a new QCD-like gauge interaction with no elementary scalar particles [47, 48], predicting instead an effective electroweak symmetry breaking mechanism in which the Z and W boson masses are dynamically generated through their coupling to composite fermions.

Technicolor is therefore a gauge theory with properties similar to those of QCD. A TC gauge group $SU(N_T)$ is introduced, having $N_T^2 - 1$ gauge bosons and massless chiral techniquarks Q_L^{ai} and Q_R^{ai}, where a refers to TC and i is a flavor index. In analogy to QCD, TC is assumed to be a confining theory and has an intrinsic (confinement) mass scale Λ_T, which must be of the order of the weak scale ($\approx vev/\sqrt{2}$). The confinement results with the formation of bound states possessing neutral Technicolor charge. Hence the spectrum of these so-called techni-hadrons consists of singlets that are either mesons or baryons composed of techniquarks. Since these objects are not found as stable states in nature, the theory must provide for the decay of techniquarks into the observed leptons and quarks. Although introduced as massless, techniquarks acquire constituent mass of the order Λ_T through the dynamics of the new interaction (in complete analogy to QCD).

Similar as in QCD, techni-hadrons with $I^G(J^{PC}) = 1^-(0^{-+})$, $1^+(1^{--})$, and $1^-(1^{++})$ are called π_{TC}, ρ_{TC}, and a_{TC} respectively.

Early Technicolor models were found to predict flavor-changing neutral currents (which have not been observed experimentally) and were thus quickly ruled out. More recently, extended Technicolor models [49] introduced a "walking" (slowly running) gauge coupling which resulted with suppression of the flavor-changing neutral currents. The walking coupling also predicts realistic fermionic masses that are lower than expected in previous models, leading to Low-Scale Technicolor (LSTC) [50, 51]. In LSTC the lightest techni-hadrons are expected to have masses below 700 GeV, well within reach of the LHC. A problem with walking Technicolor models has been a very large electroweak S-parameter prediction. This parameter has been used to quantify contributions to the electroweak radiative corrections by some kind of new physics and is, within the Standard Model, constrained to be zero [52]. The parameter can be extracted from a global fit to high-precision electroweak measurements at collider experiments and has been found to be in agreement with the Standard Model expectation. In recent TC models this problem has been solved by requiring ρ_{TC} and its axial vector partner a_{TC} to be nearly degenerate in mass. The charged ρ_{TC} and a_{TC} hadrons are interesting in the scope of this thesis due to possible decays to WZ boson pairs arising from the dynamic coupling to heavy vector bosons. A Feynman diagram of such ρ_{TC} decay is shown in Figure 2.3. As ρ_{TC} and a_{TC} are expected to be nearly mass-degenerate, they appear as a single resonance in the WZ invariant mass spectrum, and will hereafter be collectively referred to as ρ_{TC}.

Chapter 3

Experimental setup

3.1 The Large Hadron Collider

The Large Hadron Collider [53] is a superconducting proton accelerator and collider located at the Franco-Swiss border near Geneva, Switzerland. It is built in the underground 26.7 km long tunnel constructed and used originally for the CERN LEP experiment. The LHC achieves unprecedented collision energies and luminosity and trumps in complexity and magnitude of the human effort any previous collider experiment.

Proton-proton collision energy of up to $\sqrt{s} = 14$ TeV at luminosity of $L = 10^{34}$ cm^{-2}s^{-1} is envisioned by design, allowed by 8 T superconducting dipole magnets which keep protons in circulation in opposite directions in two closely placed beam pipes. Beams collide at four interaction points, around which four detector experiments are built. These are ATLAS [54] and CMS [55], two general purpose detectors located at diametral sides of the ring, ALICE [56], dedicated to studies of heavy ion collisions, and LHCb [57] which is designed for B-physics measurements. The LHC reuses the LEP injection chain. The machine schematic is shown in Figure 3.1. Protons are accelerated in Linac2 to 50 MeV using radio frequency (RF) cavities. The Proton Synchrotron Booster accelerates protons to 1.4 GeV and the Proton Synchrotron to 25 GeV. The Super Proton Synchrotron (SPS) further boosts protons to 450 GeV before they are injected in the LHC.

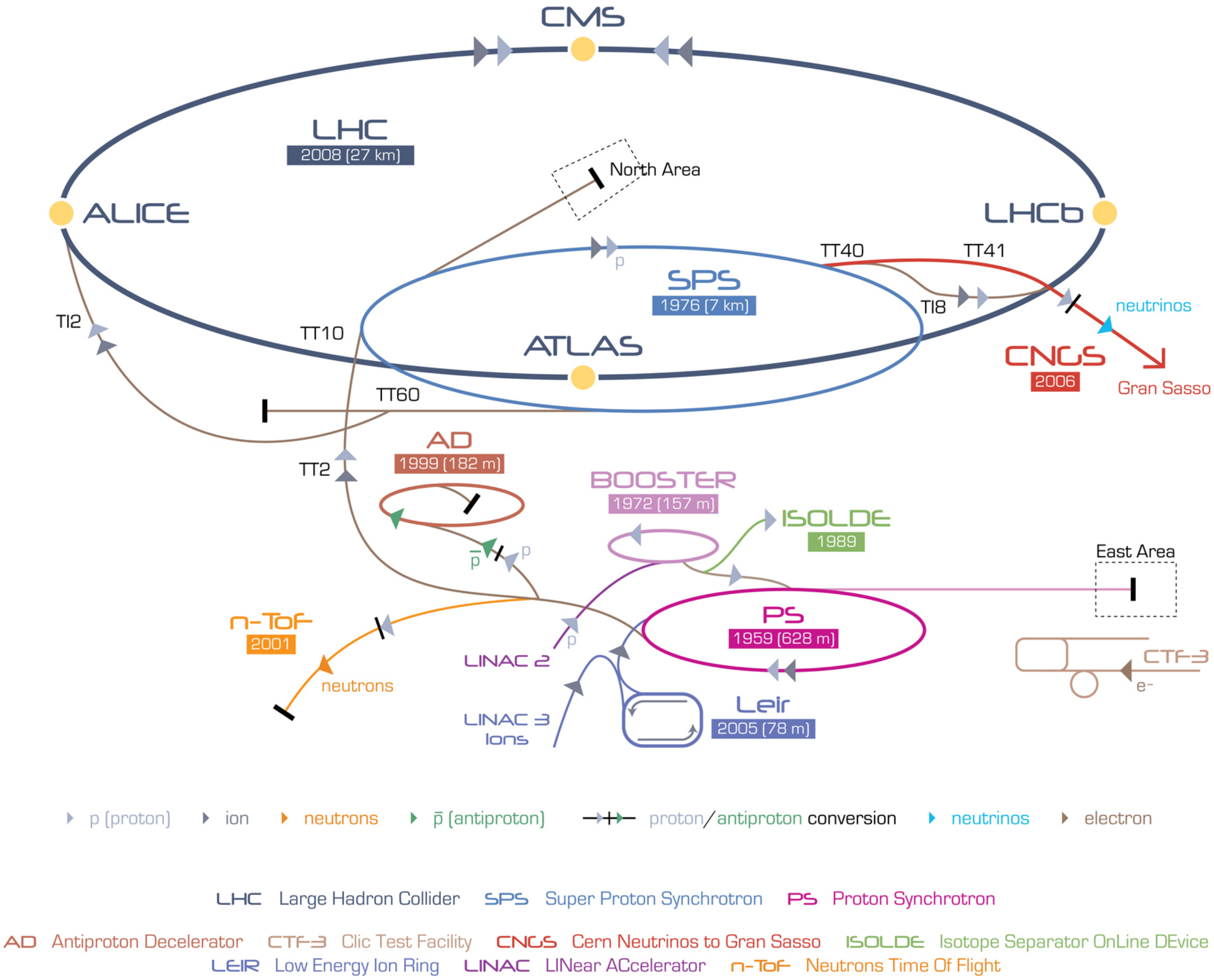

Figure 3.1: The CERN accelerator complex.

The LHC receives beam structured in *bunches*, proton packets separated by a vacuum gap. After the injection of bunches is finished, the acceleration phase starts, in which RF cavities are used to accelerate protons. Simultaneously, the electrical current in dipole magnets is raised to increase the magnetic field. This is followed by a squeezing phase, in which bunches are focused by quadrupole magnets to increase their density. Finally, in the adjust phase, beam trajectories at interaction points are tuned to achieve intersection. This marks the start of the bunch crossings and the resulting proton collisions.

The luminosity L is defined in terms of a number of collision events per unit of time, $\frac{dN}{dt}$, and the interaction cross section σ:

$$\frac{dN}{dt} = L \cdot \sigma. \tag{3.1}$$

For a collider containing a certain number of bunches n, each containing N particles, and colliding at revolution frequency f with the effective interacting area of two beams A_{eff}, the luminosity is

$$L = \frac{n \cdot N^2 f}{A_{eff}}. \tag{3.2}$$

LHC first provided proton proton collisions in November 2009 at the center of mass energy of 0.9 TeV and shortly after that, 2.36 TeV. In early 2010m the $\sqrt{s} = 7$ TeV energy was reached. In the same year, the LHC delivered approximately $\int Ldt = 40$ pb^{-1} of integrated luminosity. The LHC continued colliding at the same energy in 2011 reaching the instantaneous luminosity of $L = 10^{33}$ cm^{-2}s^{-1} and in that year delivered more than 5 fb^{-1} (Figure 3.2). In 2012 the energy was ramped up to 8 TeV, with the instantaneous luminosity approaching $8 \cdot 10^{33}$ cm^{-2}s^{-1}. By the

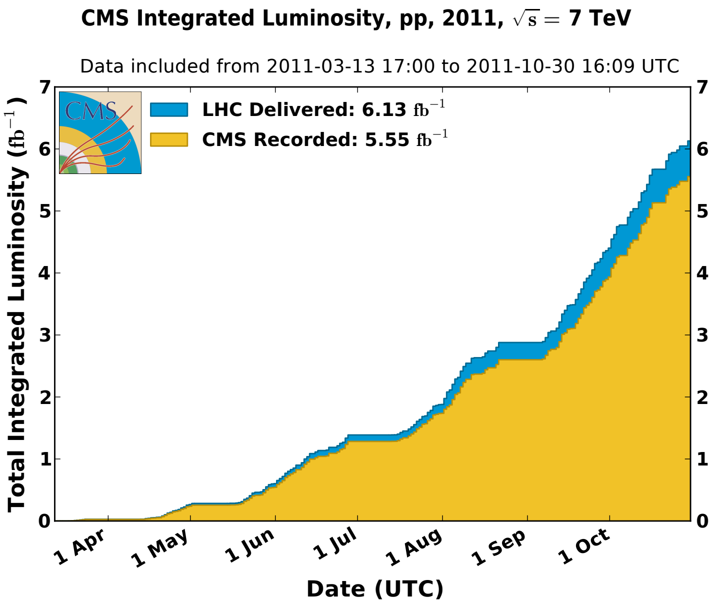

Figure 3.2: Cumulative pp integrated luminosity in 2011. delivered by the LHC and recorded by CMS.

end of proton-proton programme, the LHC delivered nearly 24 fb^{-1} of integrated luminosity at this energy.

3.1.1 Proton-proton collision phenomenology

Protons are composite particles with complex dynamic governed by QCD. Although the main constituents are asymptotically free valence quarks (uud), excitations are present and the proton contains a see of gluons and virtual quark-antiquark pairs. All of these particles, called *partons*, carry a certain amount of proton momentum and can participate in a collision. A probability density function to carry a certain fraction of the proton momentum, the so called Parton Density Function

(PDF), can be assigned to each parton type. These distributions are measured experimentally by deep inelastic scattering or other methods and are used in collision simulations.

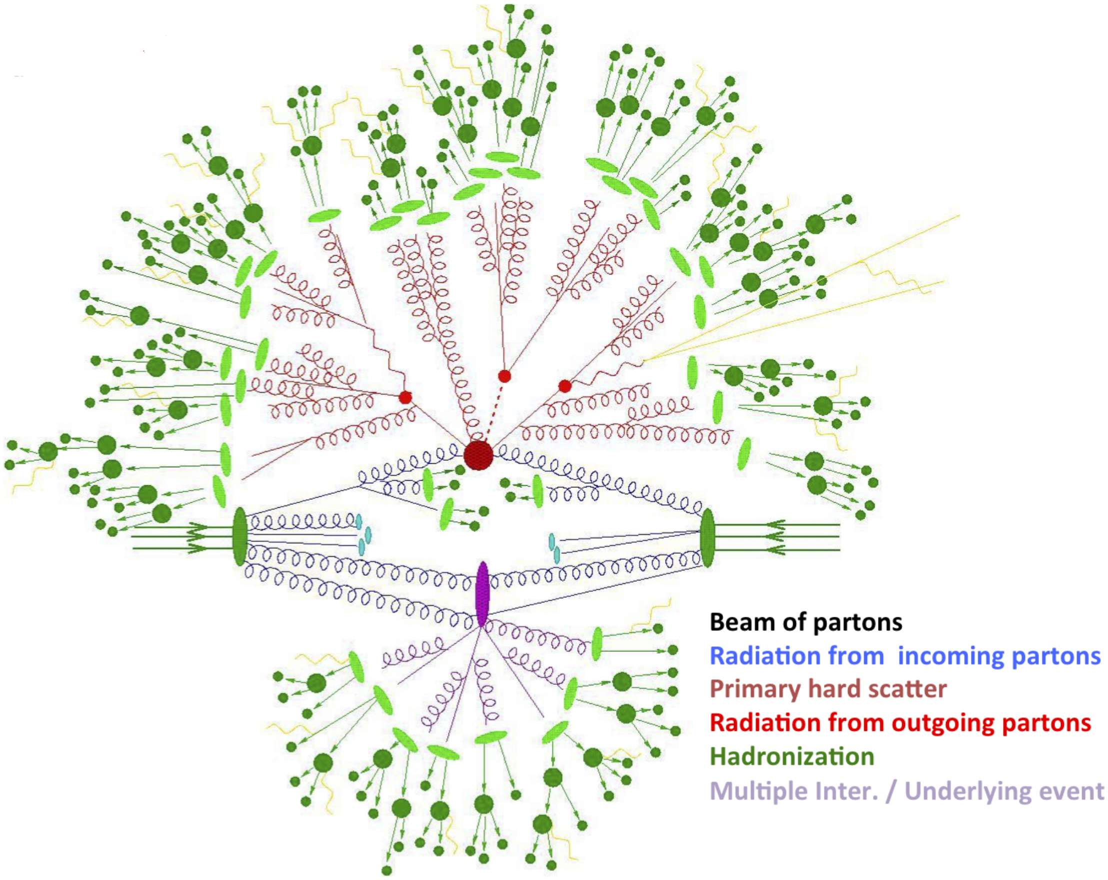

Figure 3.3: Illustration of a $p\bar{p}$ collision.

Generally, the proton momentum transverse to the beam is small. The large distance (*soft*) collisions will thus scatter mostly along the beam direction. Of the total proton-proton cross section at 7 TeV (approx. 110 mb), a dominant fraction are elastic and inelastic soft collisions, with the latter having a cross section of approx. 70 mb, as measured by CMS [58] and ATLAS [59] in 2010.

Rarer are the hard scattering interactions, with a significant momentum transfer, which generally occur through head-on collision of two partons. They are characterized by, on average, a large fraction of momentum dissipated in the direction perpendicular to the beam. Thus the *transverse momentum* of decay products often plays an important role as a discriminant in detecting the most interesting processes.

Remnants of proton that remain after a hard scattering are coupled to partons in the hard scattering process through color conservation. As a consequence, a multitude of new $q\bar{q}$ pairs gets pulled from the vacuum, resulting frequently in a large number of low energy hadrons (hadronic showers) emitted in the detector and causing additional activity. This is illustrated in Figure 3.3.

A significant effect at the LHC is the *pileup*, increased activity in the detector resulting from effects caused by collisions different than a hard scattering process which usually activates the trigger. Due to short intervals at which bunch crossings occur, it is possible for a detector to capture signals from bunch crossings adjacent to the one which is currently recorded, resulting in additional instrumental activity in the detector. The magnitude of this effect, called the *out of time* pileup, strongly depends on the spacing between bunches, which, in the period covered by this thesis, was 50 ns. Another contributing factor is the presence of multiple interactions (*vertex multiplicity*) in the same bunch crossing, which is significant at LHC luminosities. In 2011 there were, on average, O(10) interactions per bunch crossing with a large enough dissipation in transverse direction to affect the detector performance. This effect is called the *in-time* pileup.

3.2 The CMS detector

The Compact Muon Solenoid (CMS) [55] is a general-purpose experiment built at one of the proton beam interaction points. It is nearly hermetic, and follows a layered approach with tracker and calorimeter systems built inside of a strong solenoidal magnet, thus allowing improved resolution in electron and photon energy and momentum measurement. A set of outer detectors, largest in volume, is layered around the magnet to detect primarily muons, as well as other particles penetrating the inner layers. An overview of the CMS is shown in Figure 3.4.

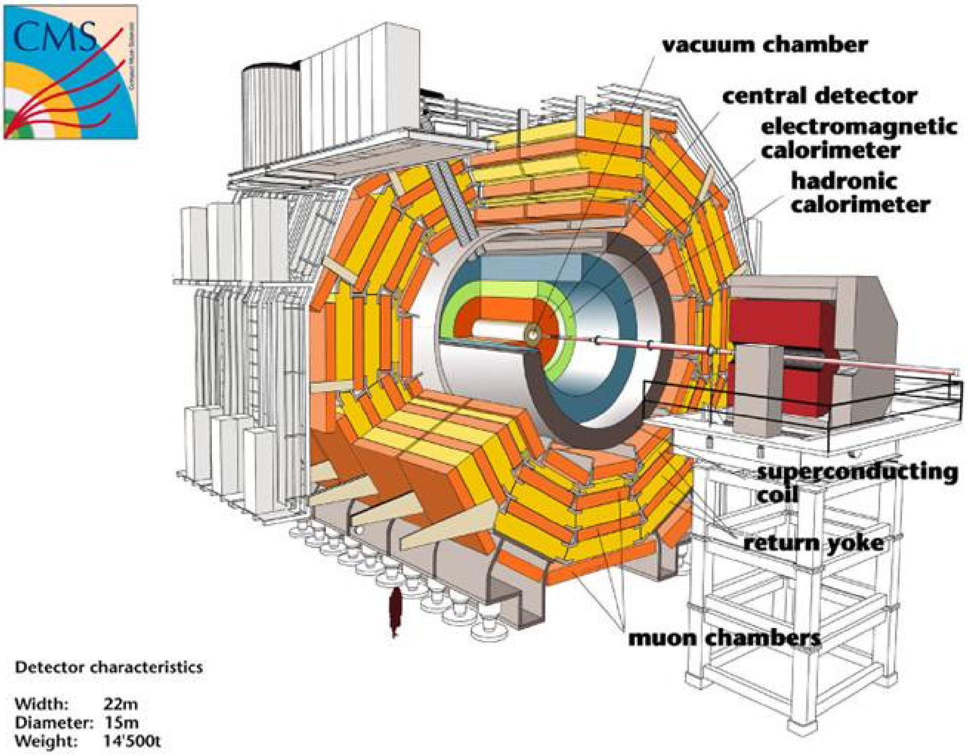

Figure 3.4: A view of the CMS detector internals.

3.2.1 Coordinate system

The detector is constructed to be cylindrically symmetrical around the beam axis. A point in the detector can be described simply by a cartesian system, where the origin is located in the center, virtually in the spot where beams collide. z coordinate denotes a direction of the beam, pointing west - i.e. in counterclockwise direction of the LHC ring. In perpendicular plane, x is the horizontal axis pointing towards the circle center, and y pointing upwards to the surface. As particles produced in collisions emerge nearly from the center, it is practical to use a system where $\phi = \arctan(y/x)$ is the rotation around the beam and $\theta = \arctan(\sqrt{x^2 + y^2}/z)$ is angle from the plane perpendicular to the beam. Often, however, θ metric is unsuitable as particles at high angles spread apart more due to Lorentz transformations, causing different detector occupancy at different θ ranges. A variable invariant to the increased spread is rapidity

$$y = \frac{1}{2} \ln \left[\frac{E + p_z}{E - p_z} \right] . \tag{3.3}$$

In the high-energy experimental physics the more often used variable is pseudorapidity η, a function of θ, which is a good approximation of rapidity in the relativistic limit ($E >> m$):

$$\eta = -\ln \left[\tan \frac{\theta}{2} \right] . \tag{3.4}$$

CMS is a modular detector, in the sense that it consists of subdetector modules grouped in the so called central *barrel* region, and detachable *endcaps* which are fitted on both sides of the central region. The pseudorapidity boundary at which the barrel region ends is roughly at $\eta \approx \pm 1.5$. The exact boundary, however, depends more precisely on the subdetector considered. Often, angular distances or cones are expressed by ΔR, defined as

$$\Delta R = \sqrt{\Delta\eta^2 + \Delta\phi^2}. \tag{3.5}$$

3.2.2 Detector components

Magnet

The CMS magnet provides a nearly homogeneous $B = 3.8$ T field in the whole inner volume of around 300 m^3. By the stored energy, it is the most powerful magnet ever built. The strong magnetic field results in higher particle trajectory curvature, which gives high sensitivity for estimating momentum of particles at the TeV scale. Muon detectors in the outside range operate under the 2 T field, enhanced by the massive iron yoke.

Silicon Pixel Tracker

The Silicon Pixel Tracker detector is the closest to the interaction point. It consists of 66 million silicon sensors, distributed in three layers in the barrel region and two endcap disks on each side. The three barrel layers are located at mean radii of 4.4 cm, 7.3 cm and 10.2 cm. The two endcap disks are placed on each side at $|z|$ = 34.5 cm and 46.5 cm.

A charged particle excites electrons which jump over the band gap, resulting with charged vacancies and free electrons. The high voltage imposed on the detector separates charges and they are collected as an electric pulse, indicating a particle "hit" or passage through the sensor. The pixel tracker is nearest to the beam and is crucial for the precise reconstruction of tracks, which is is needed to distinguish tracks originating from different primary interactions or identify tracks coming from decays of short lived particles, e.g. hadrons originating from b or c quark decays.

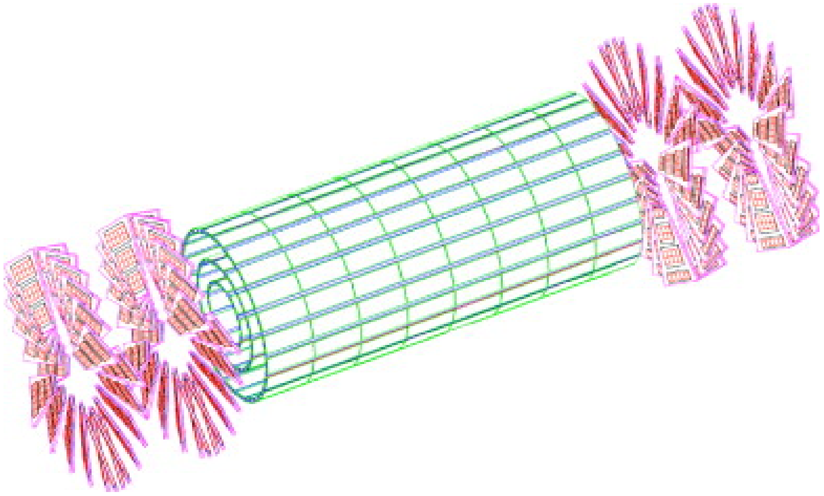

Figure 3.5: A view of the CMS Pixel Detector.

Silicon Strip Tracker

The Silicon Strip Tracker envelops the pixel tracker and occupies a much larger volume. Detector is built out of layers of metal strips in which the passing charged particle induces current. The collected current is then transferred to silicon detectors connected to the wires. The strip tracker measures particle hits at higher transversal distances than Pixel and is thus necessary for precise measurement of track properties. A view of the strip tracker is shown in Figure 3.6. The barrel section of the strip tracker consists of the Tracker Inner Barrel (TIB) made of 4 layers and the Tracker Outer Barrel (TOB) comprising 6 layers. The endcaps are divided into the Tracker End Cap (TEC) and the Tracker Inner Disks (TID). Each TEC comprises 9 disks and each TID comprises

3 small disks that fill the gap between the TIB and the TEC. The coverage in pseudorapidity is $|\eta| < 2.5$.

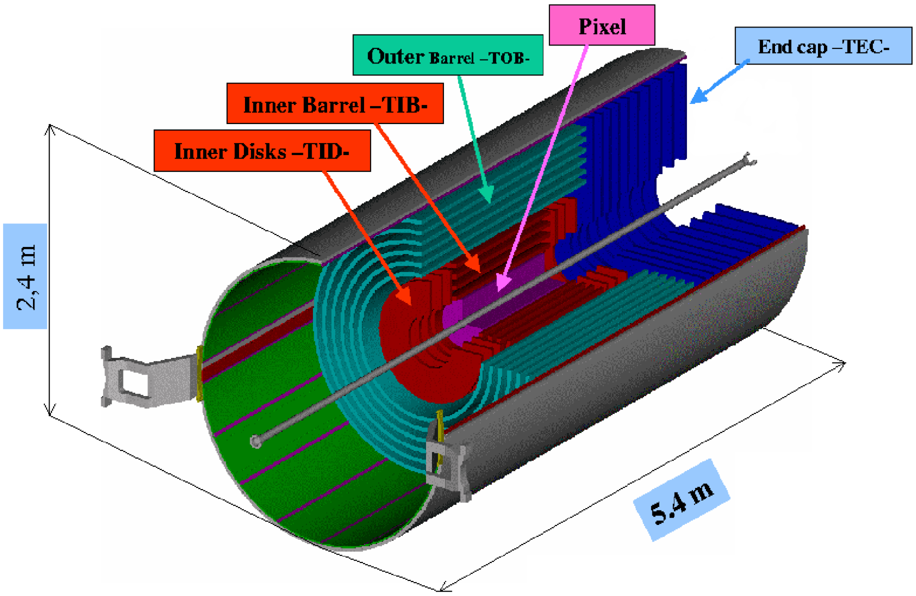

Figure 3.6: A view of the CMS Silicon Strip Tracker.

Electromagnetic calorimeter

The CMS electromagnetic calorimeter (ECAL) is built from $PbWO_4$ crystals which provide a high density (8.28 g/cm^3) and a small Molière radius (0.89 cm), resulting in short and narrow electromagnetic showers created on impact of high-energy electrons and photons. The subdetector is divided in the barrel region (EB), covering up to $|\eta| < 1.479$, arranged in 36 supermodules, and two endcaps (EE) covering up to $|\eta| < 3.0$. ECAL components are shown in Figure 3.7.

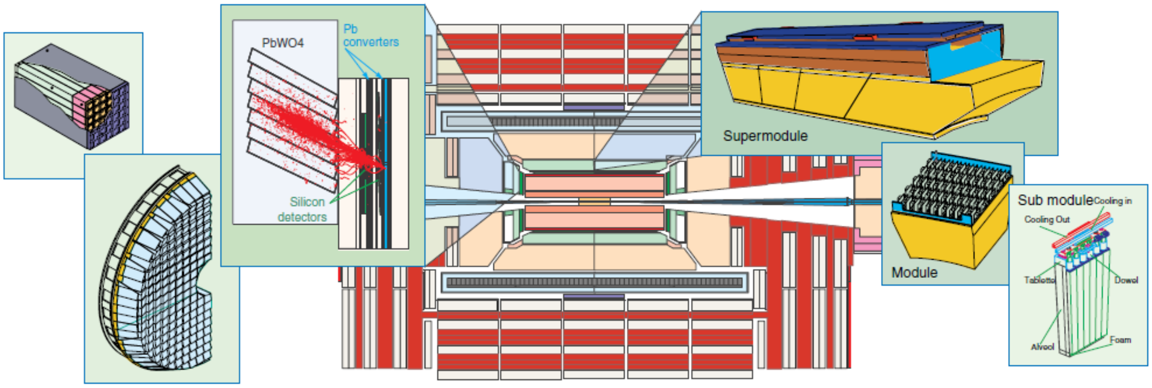

Figure 3.7: A view of ECAL components.

Hadronic calorimeter

The Hadronic calorimeter (HCAL) is shown in Figure 3.8. In the barrel region it consists of layers of brass, which acts as a non-ferromagnetic absorber, and plastic scintillator layers. Showers occurr mostly in brass layers, and are detected in scintillator layers where they are absorbed by fibres and reemitted in the narrow wavelength range which photodetectors collect. Endcap regions use steel as an absorber, and quartz as a scintillator for higher radiation resistance. The hadronic jet shower usually starts in ECAL and propagates into HCAL layers, so the measurements from both subdetectors contribute to the energy measurement. HCAL is the outermost detector located inside of the CMS magnet, with the exception of the Outer HCAL (HO).

Muon system

The muon system consists of several types of gaseous particle detectors. Drift Tubes (DT) are found in the barrel region. They are filled with gas ionized by passing particles and the charges

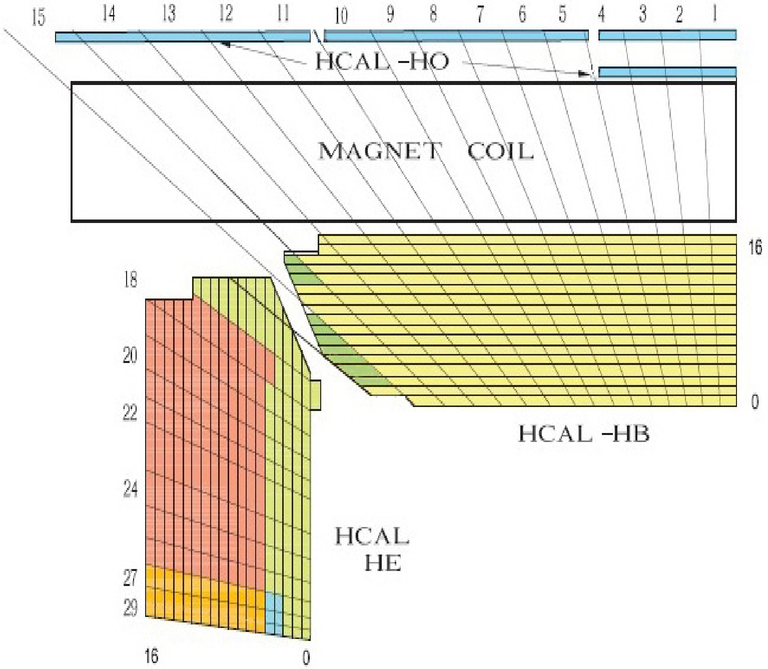

Figure 3.8: A view of HCAL regions.

are collected by wires held at high voltage. The position determination is based on the measured drift time of the collected charge. In endcaps, where DTs would be challenged by increased rate, Cathode Strip Chambers (CSC) are used. These are multi-wire proportional chambers composed of multiple anodes which collect charge from the gas ionization and serve as proportional counters. Resistive Plate Chambers (RPCs) are found in both barrel and endcaps. They consist of highly parallel plates imposing uniform electric field on the gas in the gap. Electrodes found on the plates are highly resistive and when the muon causes ionization, the resulting electron avalanche passes through the plates and is collected by external metallic strips. While inferior in spatial resolution compared to DTs and CSCs, RPCs provide superior time resolution and are able to identify muons coming from a specific bunch crossing. Therefore they are used for triggering. A schematic view of the muon system is shown in Figure 3.9.

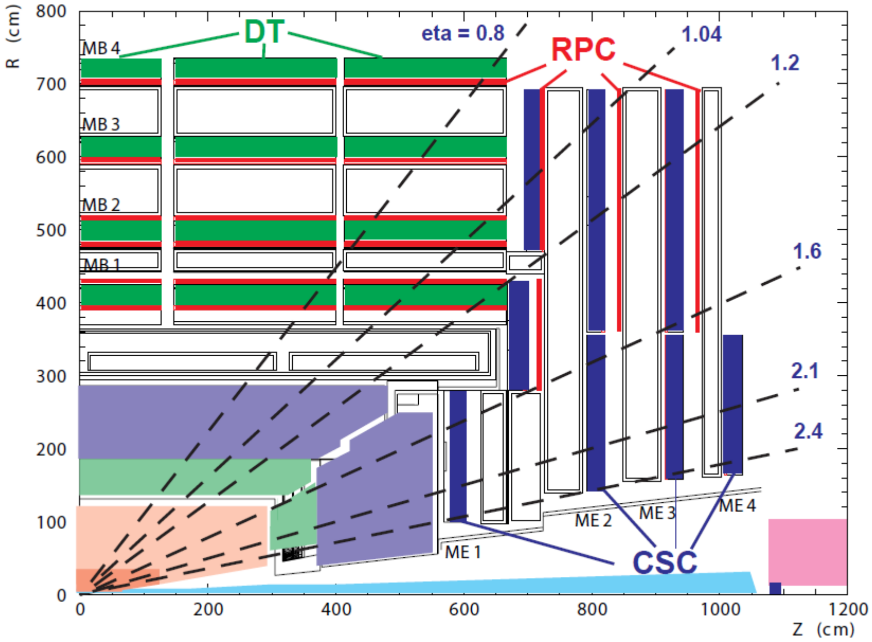

Figure 3.9: Overview of the CMS muon system.

3.2.3 Trigger and data acquisition system

The LHC has been designed to provide proton bunch collisions at a rate of 40 MHz. In the 2010-2012, the physics program has been executed at a rate of up to 20 MHz, corresponding to bunch crossing intervals of 50 ns. Detector records of interactions at each bunch crossing are called events. Since it is nearly impossible to store all events recorded at this high interaction rate, a drastic reduction in the rate has to be achieved. For this task, CMS includes a trigger system by which the rate is reduced in two steps: the Level-1 (L1) Trigger [60] and the High-Level Trigger (HLT) [61]. The system is designed to allow reduction at least by a factor of 10^6.

Level-1 Trigger

The Level-1 Trigger consists of custom-designed programmable electronic components, implemented with FPGAs or, in some cases, ASICs and programmable memory lookup tables. It decides on accepting the event for the HLT selection step based on coarsely segmented data from the calorimeter and muon systems. The latency of the system is 3.2 μs. In the meantime, full event records are held in pipelined memories in front-end electronics of each subdetector.

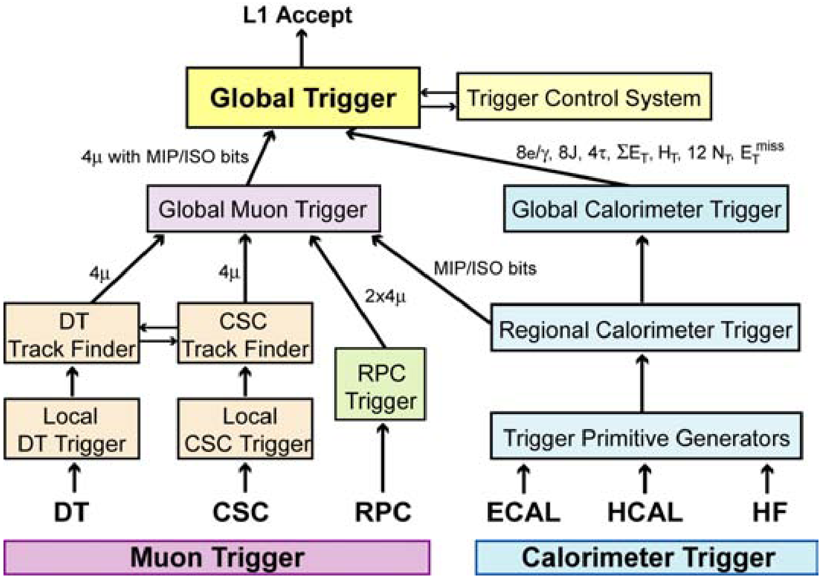

Figure 3.10: Overview of the Level-1 Trigger architecture.

The architectural overview of the Level-1 Trigger is shown in Figure 3.10. The first stage consists of Trigger Primitive Generators (TPGs), integrated with the on-detector electronics. In the calorimeters, TPGs are divided in trigger towers, radial blocks in ECAL and HCAL, each with (η,ϕ) coverage of 0.087×0.087, where energy deposits are calculated. In the muon systems, track segments or hit patterns are calculated. These trigger primitives are transmitted to the Regional Calorimeter Trigger and Regional Muon Trigger, respectively, which combine the information and use pattern logic to determine the rank and sort trigger objects in limited regions. The ranking is determined by the energy or momentum and the quality of L1 parameter measurements. The information across multiple subdetectors is aggregated in the Global Calorimeter Trigger and Global Muon Trigger with the ranking calculated for objects spanning across the entire experiment. At the top is the Global Trigger, which takes the decision to reject or accept the event for further evaluation by the HLT. This decision is communicated to the subdetectors through the Timing, Trigger and Control (TTC) system.

The L1 Trigger and readout systems are designed to deliver a sustained rate of accepted events of up to 100kHz for processing in the HLT.

Data acquisition system

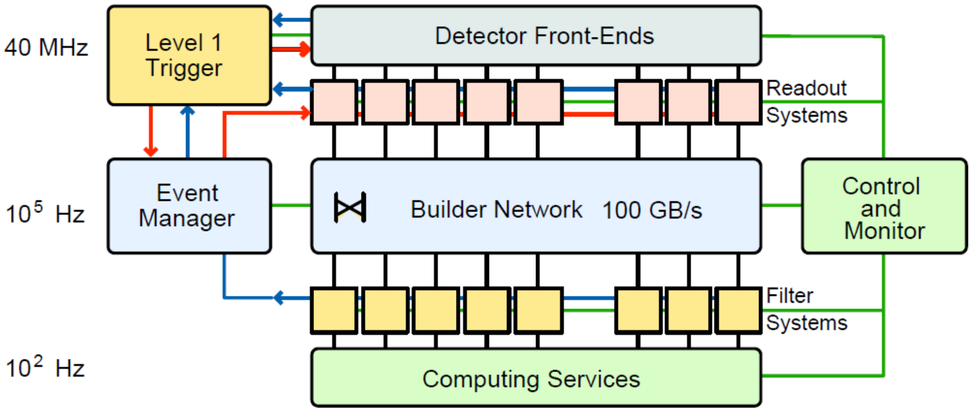

Figure 3.11: Architecture of the CMS DAQ system.

At the design input rate of 100kHz, the Data Acquisition System (DAQ), which performs both event data collection and HLT processing, must handle a data flow of 300 GByte/s coming from approximately 650 data sources. The architecture of the system is shown schematically in Figure 3.11.

Upon arrival of the L1 accept via the TTC, the corresponding data are extracted from the Front-End Drivers (FEDs). At the FED level, the data is zero-suppressed, i.e. subdetector regions without detected signal are excluded from the data that is prepared for readout into the DAQ, reducing significantly the required bandwidth. While the design of FEDs is subdetector specific, a common interface from the FED to the central DAQ system has been implemented using S-Link64 [62]. The data is transmitted from the S-Link64 sender card, capable of buffering up to 1.6 kBytes of data, to the Front-End Read-out Link (FRL) card which has two such input interfaces and is able to combine data from two FEDs into a single fragment. The size of the fragment is approximately 2 kByte for proton-proton collisions at design luminosity and each FRL is capable of buffering up to 64 kBytes of fragment data. On the output side, FRLs have an output interface implemented as a PCI connector for a Network Interface Card (NIC). In CMS there are a total of 512 FRLs.

The feedback from FEDs and associated FRLs is collected by the Trigger Throttling System (TTS) and provided to the Global Trigger. In case of problems, such as high buffer occupancy state or synchronization problems, the TTS allows prompt interruption of the data flow by stopping the trigger, after which automatic (or manual) recovery can be attempted by issuing L1-Resync or L1-Reset signals. On these signals, the electronics tries to resynchronize or restart the operation. For flexibility, FEDs are grouped in 32 TTC partitions which may be operated independently. TTS signals from all FEDs thus need to be merged per partition at low latency, which is performed by the dedicated Fast Merging Modules (FMMs) before being forwarded to the GT. In addition, FMMs provide extensive monitoring in order to diagnose which component is creating readout issues (dead-time).

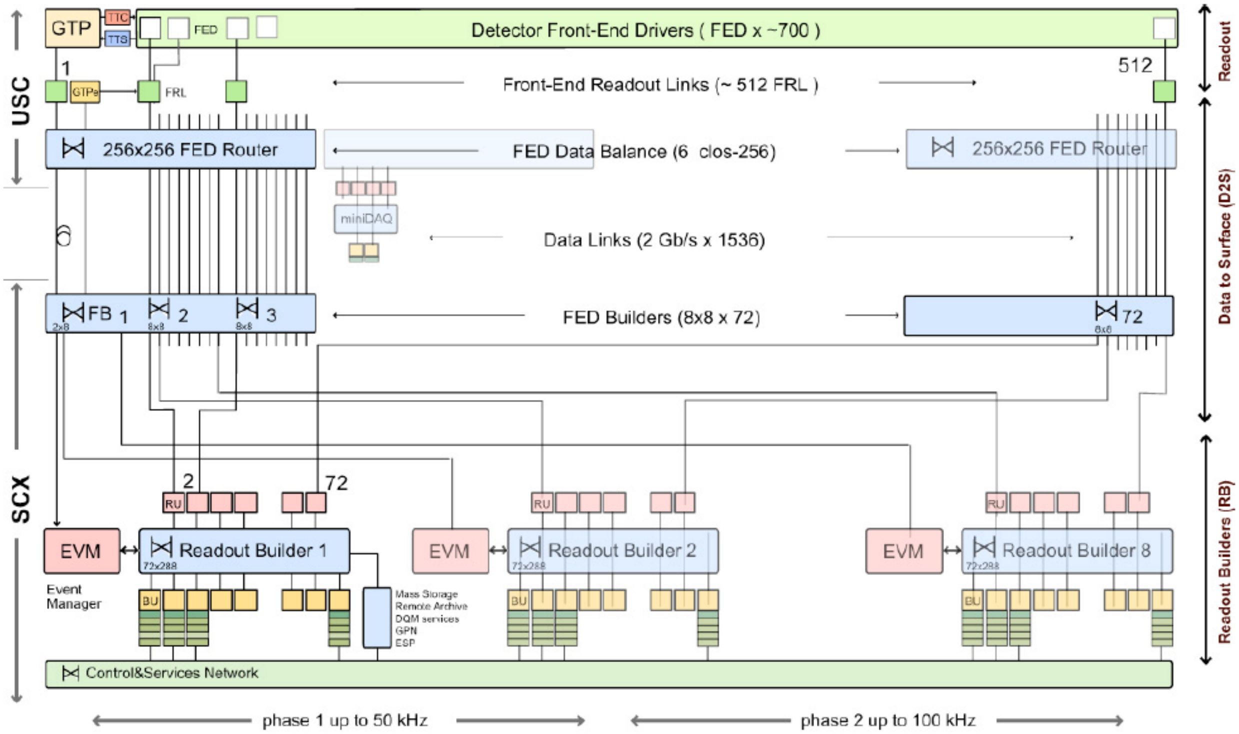

Figure 3.12: The Event Builder overview.

The Event Builder (Figure 3.12) is composed of two stages. The first stage is the FED-builder in charge of transporting fragments from FRLs to the surface building where they are combined into 72 superfragments and transported to Read-out unit PCs (RUs), where they are stored in large buffers, waiting for the second stage of event building (RU-builders). There can be up to 8 RU-builders, or DAQ slices, connected to the FED-builder. The FED-builder is based on the Myrinet [63] network technology. Both input NICs, hosted by FRLs, and output NICs, found on RU PCs, have two rails, each one connected to the independent FED-builder switching network. Fragments are multiplexed to each rail, achieving data flow of up to 4 Gbit/s per NIC and allowing for the effective aggregate output of ≈ 1.4 TBit/s, which is sufficient for CMS DAQ requirements. Each of the RU-builder slices assembles superfragments and builds complete events at a rate reaching 12.5 kHz. They comprise 72 RU PCs in standard configuration and a larger number of Builder-unit (BU) PCs, connected over a 10-gigabit ethernet switching network [64]. The Event manager (EVM) supervises the data flow by allocating events on request to BUs, which request fragments from RUs.

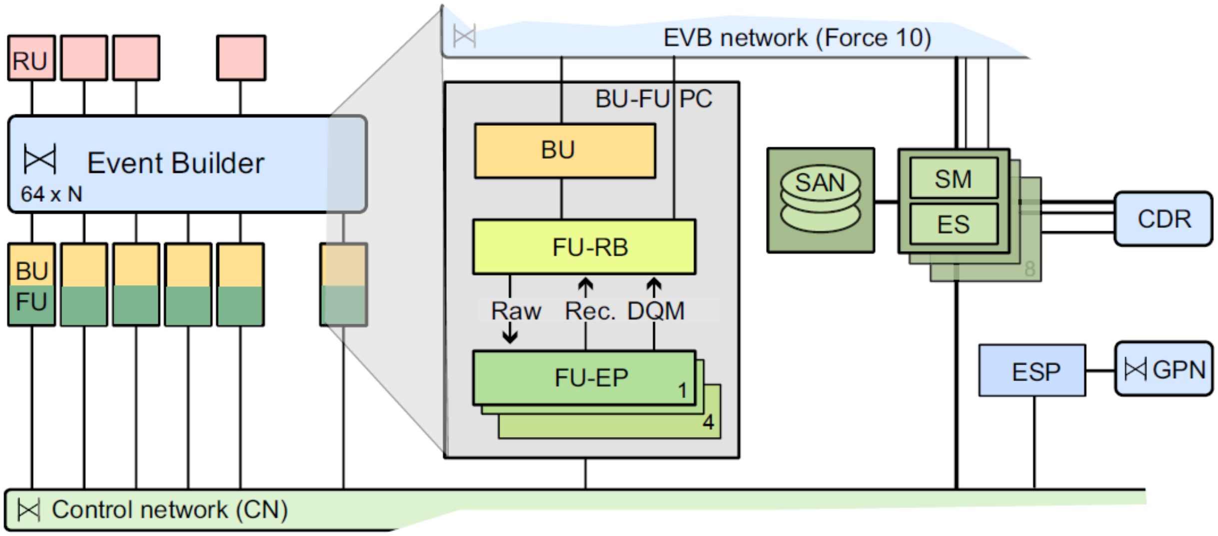

Figure 3.13: Architecture and data flow of the Filter Farm.

Each BU delivers complete events to the Event Filter responsible for the HLT event processing. In the present form, this task is done on a BU PC, which is thus called BU-FU (FU standing for the Filter Unit). The FU software (Figure 3.13) runs on the same PC and the data transfer is done locally, first to a Resource Broker (RB) application which is responsible for data bookkeeping and handling both input and reconstructed output of the HLT by using a local shared memory mechanism. BU-FUs comprise a large computing farm, located in the surface CMS buildings.

As of 2012 it consists of approximately 1250 computing nodes, with each spanning 8, 12 or 16 processor cores and some of them with the hyper-threading ability.

The HLT software is designed as a part of the CMS Software Framework (CMSSW) [65] implemented in C++, which is used both in the *offline* environment (e.g. for physics analysis) as well as for online tasks such as HLT. HLT processing is performed in form of HLT *paths*, each dedicated to a specific filtering task (e.g. electron finding). Each HLT path results in a decision to keep or reject the event[1]. The unified online and offline framework provides the advantage of sharing software implementations, for example the detailed local and global reconstruction of objects in the detector, for both offline tasks as well as for the online environments, such as HLT filtering. However this also results in various limitations, such as the inability to perform multi-threaded processing, increased memory footprint, or long startup times of applications. To work around these problems, the Event Processor (EP) application was designed, emulating the CMSSW environment in which the HLT configurations are executed, while allowing, through late process forking, utilization of the multi-core hardware found on BU-FUs. In addition, it also implements a fine-grained state machine model, which synchronizes the internal CMSSW state machine with the requirements of the whole online system. Additionally, the system is built to be robust against hardware (or software) malfunctions, allowing tolerance to failed HLT processes or even failures of single nodes.

The HLT processing stage is able to execute demanding reconstruction algorithms due to large available processing power and large buffering space. HLT achieves reduction of the rate by a further factor of 100, while retaining the most interesting events for physics analysis. While the design target output rate of the HLT was originally in the range of 100-300 Hz, in recent years the

---

[1] In some cases, the system is configured to *prescale* Level-1 or HLT path decisions. This means that only a fraction of such events is saved based on the defined prescaling factor.

CMS DAQ has been providing sustained output at rates up to 1500 Hz with the average HLT event processing time reaching ≈ 200 ms per event in high-luminosity LHC conditions.

The accepted HLT output is collected by up to 16 Storage Manager machines (two per slice) and stored on a 200 TByte SAN system. The collected data are then forwarded to the offline data processing center, the Tier-0, providing both permanent storage as well as facilities for detailed (offline) reconstruction of the collected data.

3.2.4 Run control system

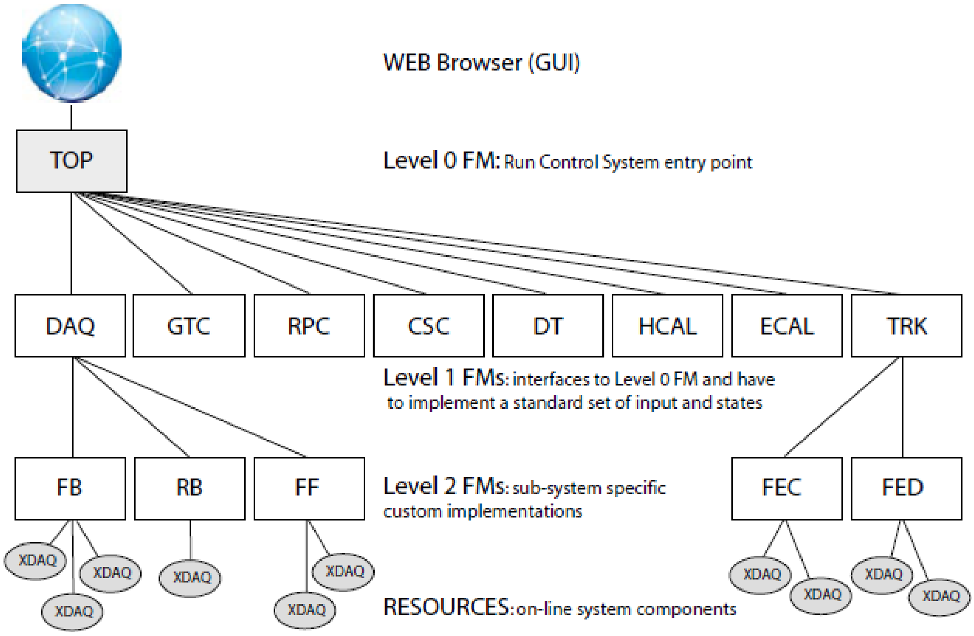

Figure 3.14: Architecture of the RCMS.

The Run Control and Management System (RCMS) provides a top-down control of all detector systems, ensuring that each subsystem is properly configured, and subsequently in the consistent state during the operational periods. For each of the operating (*running*) sessions, a unique identifier, the run number, is assigned for later tracking in data certification, analysis, and elsewhere.

The system is a modular and distributed set of state machines assembled into a hierarchy, with each subsystem represented by a module (Level-1 Function Manager or L1 FM) implemented as a Java application running in a dedicated web server [66]. On the top of the hierarchy, there is a Level-0 FM responsible for issuing global state change commands, using a standardized interface, to all L1 FMs. Depending on the subsystem, the L1 FMs can communicate with custom Level-2 FMs or implement a custom web UI used for standalone subdetector testing. RCMS is also designed to assemble, store and display log reports, useful for detection of problems and diagnostics. Architecture of the system is depicted in Figure 3.14.

3.2.5 Data quality monitoring

The Data Quality Monitoring (DQM) system [67] consists of the online DQM, a system used for real-time monitoring of detector state during the ongoing data-taking, as well as offline DQM, where the collected data are fully processed to certify that the detector was fully functional at given periods and thus provide a selection of the data collection periods that are suitable for physics analyses. Both DQM systems are largely based on extraction of detector state information from events.

The online DQM system (Figure 3.15) retrieves a selection of events (or histograms produced by the HLT) from all Storage Manager applications using the Storage Manager Proxy Server (SMPS) application. Additional filtering based on the HLT information as well as rate throttling is supported to limit the bandwidth of incoming data. Collected events and histograms are forwarded to

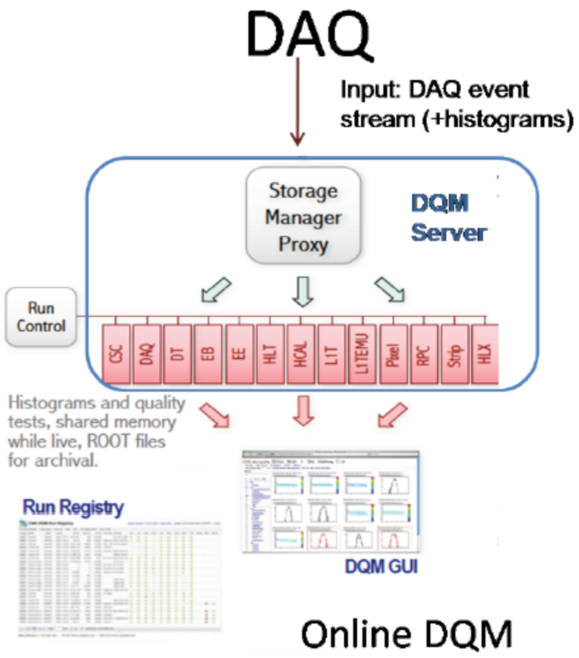

Figure 3.15: Architecture of the online DQM.

a DQM Server, where DQM analysis runs in a fashion similar to the HLT - there is a dedicated configuration for running specific CMSSW modules. To emulate the CMSSW environment, a dedicated DQM Event Processor, similar in design to the EP used in the HLT, is responsible for the execution of CMSSW configurations. The resulting information, assembled mostly in form of histograms, is forwarded to a DQM GUI, a web server application which provides a graphical view of the detector information. The information is easilly accessible live during the CMS operation, allowing monitoring of the data correctness and early warnings in case of malfunctioning detector subsystems.

3.3 Data processing and simulation

Detector readout is collected as tightly packed digital data (*raw* data) and is in such form not usable without detailed knowledge of the detector hardware. Moreover, this information is complemented by the detector condition data, such as calibration of the detector response, position of the luminous beam region, etc., which are stored separately. The data collected and stored by the DAQ are at a later step centrally processed by Tier-0, and, by using the accompanying condition information, higher level objects are reconstructed and stored in resulting events as ROOT [68] objects[2]. The data collected for physics analysis are then split into primary datasets, each defined by a collection of multiple HLT paths in which the events were accepted. Processed datasets are categorized and made available for the physics analysis which can run worldwide using a dedicated grid infrastructure which automates the processing of data distributed over many computing centers. A suite of software tools is centrally provided by the CMS collaboration to handle reconstructed objects that can be used in analysis software.

Additionally, a large amount of data is produced in simulation campaigns. Several Monte Carlo generators, capable of simulating hard scattering processes at matrix-element level, are utilized, including as input proton PDF sets which provide proper parametrization of the interacting parton momenta. Multiple types of simulated samples are generated, each with specific set of parameters and usually limiting the simulation to a certain group of physical processes (for example a Z boson production).

Generator information is staged into a full detector simulator where long-lived particles are propagated throughout the detector. For particles that may decay after traversing parts of the detector,

---

[2] CMSSW is based on the ROOT framework.

such as K_s^0, or Λ, the decay simulation is decoupled from the initial generator program and simulated at the later stage. A dedicated package is used to simulate parton showering, a process of decoupling color charges of partons coming out of a collision into colorless composite particles (resulting with jets), as well as the underlying event.

Based on the analog detector response resulting from all simulated particles propagating trough the detector, for which the GEANT4 [69] package is utilized, the readout of electronic components is emulated in the digitization step, followed by a simulation of the Level-1 Trigger. This output is then processed by HLT and the offline event reconstruction, done in an identical way as for the collected data.

In the rest of this section, several reconstruction methods which are relevant to the analysis described in this thesis, are detailed.

3.3.1 Luminosity measurement

The luminosity is measured by CMS either based on the activity in the forward hadronic calorimeter (HF) or the pixel tracker.

The HF measurement, performed in the pseudorapidity range $3 < |\eta| < 5$, relies on the fraction of non-empty calorimetric towers to estimate the number of interactions. The overall accuracy of the HF-based luminosity measurement in 2011 is 4.5% [70]. The dominant uncertainty comes from the nonlinear response of the HF to luminosity and the afterglow, wherein energy originating from a given bunch crossing creates a small response in subsequent bunch crossings. Accounting for these effects requires complex corrections with consequential increase in the systematic uncertainty.

The more precise luminosity measurement method was devised using the pixel tracker [71]. The advantage of this method is that pixel clusters are, due to their small cross section, rarely exposed to simultaneous hits of multiple tracks, resulting in low saturation, and thus a highly linear response to luminosity in the operating range of the LHC. The average number of cluster hits is proportional to the per-bunch instantaneous luminosity L_B as

$$< N_{\text{cluster}} >= \frac{\sigma_{\text{cluster}}}{f} L_B \tag{3.6}$$

where the orbital frequency $f = 11.246$ kHz and the pixel cluster cross section σ_{cluster} can be precisely estimated from the Van der Meer scan [72], a procedure involving dynamically modified transverse beam separation. The precision achieved by this method in 2011 is 2.2$\%$.

3.3.2 Reconstruction of physics objects

Muons

Muons are characterized by a track signature in the inner tracker and hits present in the muon chambers. Reconstruction [73] starts from a seed in the innermost muon chambers, used as a starting point by a *standalone* algorithm which uses a Kalman-fitter technique to fit individual tracks segments from chambers into a standalone muon track. This is followed by a *global muon* algorithm which matches the standalone track to a track found in the inner tracker, respecting their geometrical and kinematic compatibility. A global muon fit is performed, where a global momentum is calculated using hits from all available systems. Especially for muons with $p_{\text{T}} > 100$ GeV, this results in improved momentum precision compared to the standalone algorithm or a

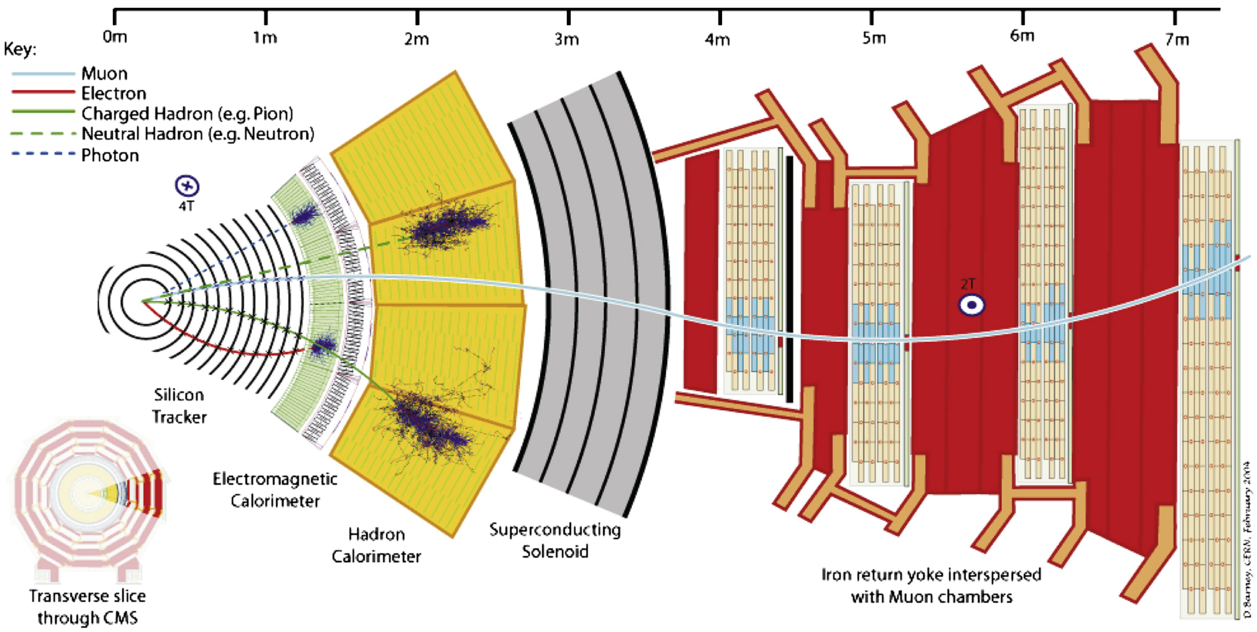

Figure 3.16: Illustration of electron, muon, photon and charged and neutral hadron propagation in transverse plane of the CMS.

tracker-only measurement due to better measurement of the track curvature. The resulting object is called a *global muon*. Alternatively, if the reconstruction is performed by matching the inner track with track segments in the muon system, a *tracker muon* is produced.

Electrons

The basic signature of electrons in the CMS detector is an energy deposit in the ECAL (produced by the electromagnetic shower created on impact) matched to a charged track built from hits in the pixel and strip tracker (ECAL-driven algorithm). In the ECAL, several neighboring cells containing energy deposits from the electromagnetic shower are joined to form a *cluster*. As the electron bends in the magnetic field and interacts with the detector material, it is likely to emit Bremsstrahlung photons. These photons produce clusters spread in a ϕ band, perpendicular to the magnetic field axis. These clusters are combined with the cluster formed by the electron impact to form a *supercluster* (SC).

A reconstructed electron contains inner tracker and ECAL information. Algorithms have to match these individual detector signatures into a unified object. The tracker-driven class of algorithms attempt this starting from a track object and try to match it to the ECAL signature. Such an approach is robust for electrons surrounded by high activity, and is mainly used for electrons with low transverse momenta, below 5 GeV.

As electrons originating from W and Z bosons have spectra predominantly over 20 GeV, the preferred method in this case is the *Gaussian Sum Filter* [74] algorithm, which attempts to match a supercluster with hit multiplet in the innermost (pixel) tracker to form a seed, followed by a tracking algorithm which builds a track propagating to the SC. In the process, the algorithm takes into account energy loss due to potential Bremsstrahlung photon emissions. Electrons reconstructed by this algorithm are called GSF-electrons.

Usually collision data undergo the reconstruction stage shortly after being recorded, thus lacking precise knowledge of ECAL transparency conditions which is an important calibration parameter. Due to this, there is often an additional recalibration used in form of energy corrections to the GSF electron energy and momentum. Proper integration of calibration updates into datasets requires repeating the whole reconstruction procedure. The analysis described in this thesis makes use of the former approximation. Similar treatment is performed with simulated samples to obtain a better agreement of the energy resolution between data and simulation.

Missing transverse energy

The missing transverse energy (or momentum[3]), E_T^{miss}, is the imbalance in the transverse momentum of all visible particles, i.e. particles that interact strongly or electromagnetically:

$$E_T^{miss} = - \sum_{\text{visible}} \vec{p}_T. \tag{3.7}$$

Because of momentum conservation in each direction, E_T^{miss} is a transverse momentum that must have been carried away by undetected, invisible particles[4]. Neutrinos are invisible to the detector, and E_T^{miss} is therefore an estimate of the neutrino transverse momentum.

E_T^{miss} reconstruction is demanding because it involves reconstruction of all visible particles, and is therefore sensitive to the quality of the detector calibration or inefficiencies. Several techniques are commonly employed to estimate E_T^{miss}depending on the type of objects used to estimate the visible energy deposited in the detector. Calorimetric E_T^{miss}algorithm uses only calorimetric information and additionally includes muon transverse momentum, as muons, which are minimum ionizing particles, deposit a small amount of energy in calorimeters. Improvement in energy resolution is provided using track-corrected E_T^{miss}, where information from the tracker is used to improve the estimation of energy deposits in the calorimeters.

The treatment of E_T^{miss}in this thesis is based on the particle flow method [75, 76], which consists in reconstructing and identifying each single particle with an optimized combination of all subdetector

---

[3] Energy of a particle is a function of mass and momentum, i.e. $E = p^2 + m_0^2$. Stable and long-lived particles produced in collisions at the LHC are mostly highly relativistic ($E \gg m_0$) and therefore it holds that $E \approx p$. In this regime, the missing transverse energy and the magnitude of the missing transverse momentum are nearly identical.

[4] The underlying event is mostly spread in longitudinal direction and can remain undetected. Thus at LHC it is only feasible to measure transverse component of the missing momentum.

information. In this method, the identification of the particle type (photon, electron, muon, charged hadron, neutral hadron) plays an important role in the determination of the particle direction and energy. Photons are identified as ECAL energy clusters. Electrons are identified as a primary charged particle track and ECAL energy clusters compatible with the track and potentially present Bremsstrahlung photons. Muons are identified as a track in the inner tracker consistent with signature in the muon system, associated to a small energy deposit in the calorimeters. Charged hadrons are identified as charged particle tracks neither identified as electrons, nor as muons. Finally, neutral hadrons are identified either as HCAL energy clusters not linked to any charged hadron trajectory, or as ECAL and HCAL energy excesses with respect to the expected charged hadron energy deposit. The energy of photons is directly obtained from the ECAL measurement, corrected for zero-suppression effects. The energy of electrons is determined from a combination of the track momentum at the main interaction vertex, the corresponding ECAL cluster energy, and the energy sum of all Bremsstrahlung photons attached to the track. The energy of muons is obtained from the corresponding track momentum. The energy of charged hadrons is determined from a combination of the track momentum and the corresponding ECAL and HCAL energy, corrected for zero-suppression effects, and calibrated for the nonlinear response of the calorimeters. Finally the energy of neutral hadrons is obtained from the corresponding calibrated ECAL and HCAL energy.

Vertex reconstruction

Two kinds of vertices can be reconstructed - primary and secondary vertices. A primary vertex is the interaction point of a proton-proton collision (there can be multiple primary vertices in the event). Secondary vertices are not true interaction points, and are instead reconstructed from decay of long-lived particles in the detector volume.

In the high luminosity conditions, multiple vertices frequently occur in bunch crossings. This creates a challenge of correctly assigning tracks to originating vertices and has prompted development of several vertex reconstruction algorithms.

The Standard Clustering (SC) algorithm starts from reconstructed tracks, selected to have a good quality χ^2 fit, minimal number of pixel and strip hits, and required to originate near the beamspot. Tracks are sorted by their z coordinate and clustered together if within distance of 2 mm to form vertex clusters, representing a single primary vertex. The AVF (Adaptive Vertex Fitting) algorithm is then applied, iteratively minimizing track distances and adapting the vertex position hypothesis [77]. The algorithm dynamically assigns a weight to each track with respect to vertices, giving higher weight (probability) to closer tracks. Weights w_i in range $[0, 1]$, enter the relation for the number of degrees of freedom

$$ndof = 2 \sum_{tracks} w_i - 2. \tag{3.8}$$

The hard interaction vertex is then found by selecting the candidate with highest $ndof$.

The Deterministic Annealing (DA) clustering algorithm [78] is designed to address problems of the standard clustering, which tends to merge vertices at high pileup, due to a χ^2 minimization procedure which tends to converge to local minima. The algorithm treats $< \chi^2 >$ as mean energy of the thermodynamic system and maximizes the entropy of the system. This leads to the gradual decrease of $< \chi^2 >$ with reduced bias of the z distance parameters. The DA algorithm is a default vertex reconstruction algorithm in CMS since 2011.

Chapter 4

WZ cross section measurement

This Chapter describes the measurement of the $pp \rightarrow$ WZ production cross section at $\sqrt{s} = 7$ TeV. The analysis focuses on leptonic decay modes of W and Z bosons, while the final measurement is extrapolated to the phase space of any possible W and Z decay mode (the inclusive cross section). Analysis is performed on the full 2011 dataset collected by the CMS and the results have been approved by the CMS Collaboration for presentation at the conferences [79].

The analysis focuses on the final state of WZ where the Z and W decays to leptons (e,μ) as discussed in Chapter 2. The $WZ \rightarrow 3l\nu$ decay signature is represented by a couple of same-flavor, opposite-charge and high p_{T} *isolated*[1] leptons with an invariant mass corresponding to a Z boson mass resonance, together with a third, high p_{T} isolated lepton and a significant amount of transverse energy (MET) associated to the escaping neutrino.

---

[1] Isolation is a requirement of geometrical separation from other detector activity.

Table 4.1: Definition of WZ channels based on the W and Z boson decay channel.

$3e$	$Z \rightarrow e^+e^-, W \rightarrow e^\pm\nu$
$2e1\mu$	$Z \rightarrow e^+e^-, W \rightarrow \mu^\pm\nu$
$2\mu1e$	$Z \rightarrow \mu^+\mu^-, W \rightarrow e^\pm\nu$
3μ	$Z \rightarrow \mu^+\mu^-, W \rightarrow \mu^\pm\nu$

Furthermore, the signal is by definition restricted to the phase space where Z boson mass lies within 20 GeV from the nominal Z boson mass ($M_Z \in [71.18, 111.18]$ GeV). The imposed mass window largely removes the interfering contribution from the $WW\gamma$ vertex as the virtual photon contribution is significant in the lower mass range.

Depending on the final state, the analysis is performed separately for four decay channels, defined by all possible combinations of Z and W leptonic decays, as shown in Table 4.1.

This Chapter is organized as follows. A description of significant background sources is found in Section 4.1. Section 4.2 details identification criteria required for charged lepton candidates or E_T^{miss} coming from the neutrino. The selection procedure to reconstruct the Z and W boson candidates is described in Section 4.3. The background estimation, including data-driven signal and background determination method, is described in Section 4.4. The study of systematic uncertainties is described and, finally, the cross section measurement is presented in Section 4.5. A comparison with results from other experiments is also drawn.

4.1 Backgrounds

The main instrumental[2] background sources come from events with:

- 1 to 3 jets misidentified as leptons: QCD, W with jets (W+jets), Z with jets (Z+jets) or WW pair with jets (WW+jets);
- leptons from heavy flavor jet decays: Z production with $b\bar{b}$ or $c\bar{c}$ (Z$b\bar{b}$, Z$c\bar{c}$), or $t\bar{t}$ (b and $\bar{b}$ jets, and leptonic W decays) ;
- conversion of photon to $e^{-}e^{+}$ pair (Zγ) ;

Most instrumental backgrounds contain jets, which are often detected as non-isolated leptons, and as such are different from the isolated signal leptons.

The fully leptonic ZZ decay results in four final state leptons. When all of these leptons are detected, it is possible to distinguish a background event from the signal. Sometimes, however, one lepton can escape detection. Such events are observed as having increased missing transverse energy and are not separable from the WZ signal. ZZ is therefore an irreducible physical background.

Alternatively, backgrounds can also be divided into resonant ones, containing a genuine Z boson (Z+jets incl. Z+bb and Z+cc, Zγ and ZZ), and non-resonant ones, without a genuine Z boson (QCD, W+jets, WW+jets and $t\bar{t}$).

The main background contributions are summarized by the Feynman diagrams shown in Figure 4.1.

---

[2] Backgrounds with the particles different from the signal ones, misidentified as isolated leptons or E_T^{miss}.

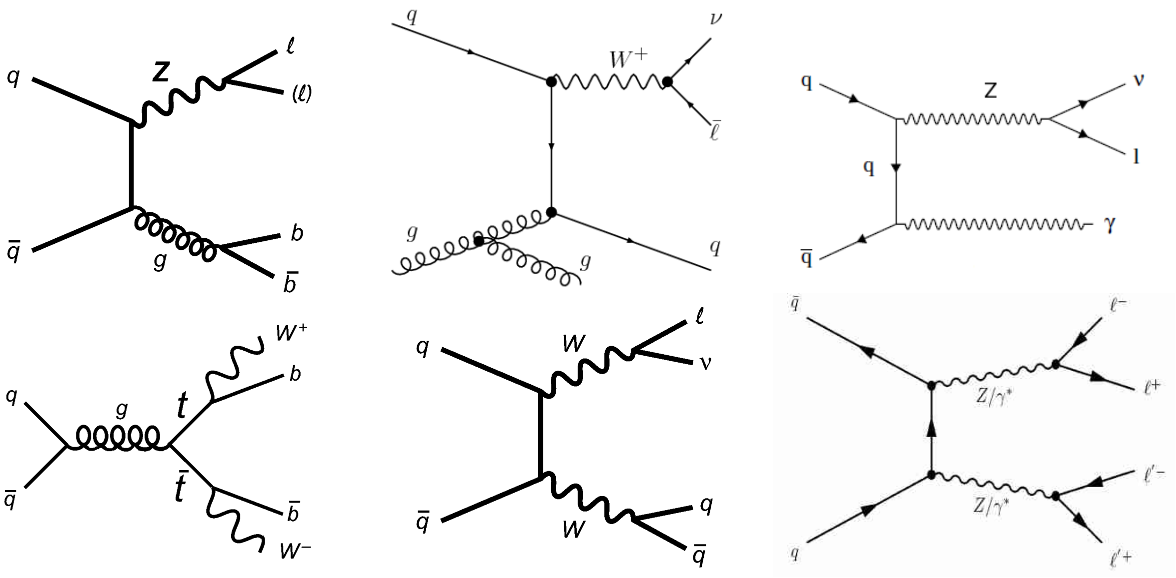

Figure 4.1: Feynman diagrams representing tree level contributions to Z+jets (Z+bb), W+jets, Zγ, $\mathrm{t\bar{t}}$, WW and ZZ production at the LHC.

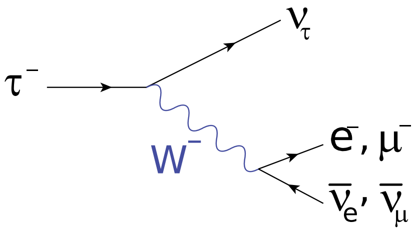

Figure 4.2: Feynman diagram of a leptonic τ decay.

A source of background can also come from the WZ process itself, where Z or W do not decay directly to muons or electrons. While hadronic WZ decays are easily rejected and their contribution to the selected sample remains negligible, the contribution of another WZ final state is significant, where W or Z decay leptonically to one or more τ leptons. τ decays result with an electron in 17.82% of cases, and with a muon in 18.39% of cases. A a fraction of momentum is however taken by the resulting neutrinos. The Feynman diagram of a leptonic τ decay is shown in Figure 4.2. This background can also be classified as irreducible when the final state satisfies imposed kinematic criteria. It has to be noted that the cross section is proportional to the one measured in this analysis.

4.2 Analysis objects

4.2.1 Muons

The CMS muon system instrumentation imposes a pseudorapidity requirement of $|\eta| < 2.4$. For any muon object considered, a transverse momentum requirement of $p_{\mathrm{T}} > 10$ GeV is imposed.

Global muons (see 3.3.2) are the only kind of reconstructed muon objects used in this analysis. Additional requirement are applied to ensure better rejection of backgrounds. The track has to be built with more than 10 hits in the inner tracker detector of which at least one hit has to be in the pixel detector. At least one hit in the muon system is also required. Moreover, at least two segments in two different muon stations should be matched to a track. The global muon fit is required to be of good quality by demanding $\chi^2/N_{dof} < 10$. These criteria ensure a good quality momentum measurement, and are effective at rejecting muons from hadrons decaying in flight or hadronic jets propagating to the muon detection system. Furthermore, the track transverse distance from the primary vertex position must be lower than 2 mm. This requirement helps to reject cosmic muons.

The muon is required to be isolated from other particles in order to reject muons from heavy flavor quark decays. The isolation variable is calculated using the particle flow algorithm described in 3.3.2, specifically taking into account photon, charged hadron and neutral hadron contributions.

Table 4.2: Muon identification and isolation requirements.

description	requirement
kinematical	$p_{\mathrm{T}} > 10$ GeV and $\lvert\eta\rvert < 2.4$
number of pixel hits	> 0
number of tracker hits	> 10
global fit $\chi^2/N_{\mathrm{d}of}$	< 10
number of muon hits	> 0
number of chambers with matched segments	> 1
vertex $\lvert d_0\rvert$	< 0.2 cm
relative isolation	< 0.12

To separate contributions coming from other vertices (pileup), charged hadrons are required to be associated to the primary vertex. These transverse momentum contributions are summed in the cone of $\Delta R < 0.4$ around the muon candidate. Average pileup transverse momentum is separately estimated for neutral hadrons and photons, and subtracted from the sum. The sum is divided by the muon candidate p_{T} to obtain the relative isolation variable, Iso_{rel}^{PF}, which is required to be smaller than 0.12. A summary of all muon identification and isolation requirements is reported in Table 4.2.

4.2.2 Electrons

Electrons are reconstructed using the GSF electron algorithm, as described in 3.3.2. Kinematic requirements on electrons in this analysis are $p_{\mathrm{T}} > 10$ GeV and the pseudorapidity has to be in the range $|\eta| < 2.5$. Electrons found within $\Delta R < 0.01$ of a muon are removed from the analysis due to high probability that they are false candidates built out of a muon track and an ECAL deposit.

A multivariate method (MVA) is utilized for electron identification. Electrons are selected based on the multivariate method output, which exploits correlations between the selection variables described in [74] to improve identification performance.

A preselection step is applied so that objects on which the MVA is applied are guaranteed to have satisfied also the *triggering* criteria. In this way, the quality of electrons on which the MVA is applied is guaranteed to be same as on the sample on which the MVA was trained on.

A preselection requirement is imposed on several electron variables [74, 80], so that objects on which the MVA is applied are guaranteed to have satisfied also the *triggering* criteria. In this way, properties of the electrons on which the MVA is applied are guaranteed to be same as in the sample on which the method was trained.

The electromagnetic cluster shower shape variable $\sigma_{i\eta i\eta}$ is particularly powerful in discriminating against electron energy deposition and showers produced by photons and fakes. It is defined as

$$\sigma_{i\eta i\eta} = \sqrt{\frac{\sum_i^{5x5} w_i(\eta_i - \eta_{seed})^2 \cdot \Delta\eta_{xtal}^2}{\sum_i^{5x5} w_i}} \tag{4.1}$$

with i running over all the crystals in a 5×5 block centered on the supercluster seed, $\eta_i - \eta_{seed}$ being the distance in number of crystals of the i^{th} crystal to the seed crystal in η direction, and $\Delta\eta_{xtal}^2$ being the average width of a single crystal. w_i is the weight of the i^{th} crystal defined as $w_i = \max(0, 4.7 + \ln E_i/E_{5\times5})$, where a single crystal energy is E_i and $E_{5\times5}$ is the total energy deposited in the 5×5 block.

The geometrical compatibility of the track and ECAL supercluster is controlled using the $\Delta\phi_{in}$ and $\Delta\eta_{in}$ variables, calculated as the absolute η and ϕ angular distance of the supercluster and the electron track extrapolated to the ECAL surface. A fraction of the calorimetric energy deposited in HCAL is calculated as the ratio of HCAL and ECAL energy deposits of the electron to discard candidates associated to the significant hadronic activity.The electron isolation is calculated as a sum of E_{T} deposits in ECAL and HCAL inside of the $\Delta R < 0.3$ cone around the candidate direction as computed from the interaction point, and as a p_{T} sum of tracks found in the $\Delta R < 0.3$ cone around the candidate track. The upper limit is required on isolation variables divided by the electron candidate p_{T} (the relative isolation variables). The electron compatibility with the primary vertex is evaluated using the electron track distance from the primary vertex in both transverse and longitudinal plane, the d_0 and d_z. Finally, the probability of a photon conversion is calculated by attempting to fit the electron track with another track under the hypothesis that they descend from a converted photon originating from the primary vertex. Unless this probability is sufficiently small, it can be a signature of the conversion. Conversions are also suppressed by requiring that the candidate track is built without missing hits in any of the inner tracker layers. The full preselection requirements are listed in Table 4.3.

Table 4.3: Preselection requirements applied on electrons.

variable	barrel region	endcaps
$\sigma_{i\eta i\eta}$	<0.01	<0.03
$\lvert\Delta\phi_{in}\rvert$	<0.15	<0.10
$\lvert\Delta\eta_{in}\rvert$	<0.007	<0.009
H/E	<0.12	<0.10
$\sum_{HCAL}^{\Delta R<0.3} E_T/p_T^e$	<0.2	<0.2
$\sum_{ECAL}^{\Delta R<0.3} E_T/p_T^e$	<0.2	<0.2
$\sum_{Tracker}^{\Delta R<0.3} p_T/p_T^e$	<0.2	<0.2
$\lvert d_0\rvert$	<0.02 cm	<0.02 cm
$\lvert d_z\rvert$	<0.1 cm	<0.1 cm
$P_{\text{matched conversion}}$	$<10^{-6}$	$< 10^{-6}$
$N_{\text{missing hits}}$	0	0

After the MVA quality requirement, the additional isolation requirement is applied on electrons. Isolation variable is calculated as E_{T} sum of particles reconstructed using the particle flow algorithm in the $\Delta R < 0.4$ cone around the electron, normalized with the electron candidate p_{T}. A selection is applied on particle flow candidates used for calculating the isolation. Flavor of the candidates is restricted to charged and neutral hadrons and photons. All candidates are required to have $p_{\mathrm{T}} > 1$ GeV. Charged hadron candidates have to be associated to the same primary vertex within 0.1 cm in z direction. Neutral hadrons are excluded if located in the inner cone $\Delta R < 0.07$ and photon candidates within $\eta < 0.0025$ around the electron.

The relative particle flow isolation, Iso_{rel}^{PF}, is required to be smaller than 0.13 for electrons in the ECAL barrel and smaller than 0.09 in endcaps.

4.2.3 Missing transverse energy

The missing transverse energy (E_T^{miss}) variable used in this measurement is computed with the particle flow algorithm described in 3.3.2. Additionally, the so-called *Type-I* correction [81] is used to improve the precision of the E_T^{miss}measurement by applying jet energy corrections for jets with with $p_{\mathrm{T}} > 10$ GeV.

4.3 Event selection

After the definition of basic building blocks, this section details the global event selection procedure. The selection procedure attempts to reconstruct decay products of the W and Z bosons, starting from lepton objects and E_T^{miss}reconstructed and identified in events. The selection requirements are designed to reject backgrounds differing in signature from the signal. The selection is applied on both collision data and simulated event samples, which are used for comparison of observed results with predictions.

4.3.1 Data and Monte Carlo samples

The analysis makes use of two primary datasets collected in the course of 2011 which combine particular HLT paths for detection of muons and electrons. These are named **DoubleElectron** and **DoubleMuon**.

The standard CMS selection of good runs and luminosity sections[3] is applied to ensure that all detector subsystems were fully functional in the considered periods. For this selection, the measured integrated luminosity amounts to approximately 4.9 fb^{-1}.

A collection of simulated samples of signal and background processes has been obtained using Monte Carlo simulation, as described in 3.3. These samples were produced as a part of the CMS 2011 official production campaign. Samples have been generated using the MadGraph [82], or powheg [83] generators. The background from QCD multi-jet events has also been studied in the simulation and found to be negligible after the Z-candidate selection is performed. The full list of Monte Carlo samples with the appropriate cross sections is summarized in Table 4.4.

---

[3] Luminosity section is a time unit used by the CMS. 1 ls $\simeq$ 23.1 s.

Table 4.4: Samples, Monte Carlo generators, leading order (LO) and higher-order cross sections for the signal and background samples considered in the WZ cross section analysis. The W+jets cross section is next-to-next-to-leading order (NNLO) while all others are next-to-leading order (NLO).

sample	Monte Carlo generator	σ_{LO} (pb)	$\sigma_{\mathrm{(N)NLO}}$ (pb)
$WZ \to \ell\nu\ell\ell$	MadGraph	0.7192	0.879
$Z(\to \ell\ell)$+jets	MadGraph	2474.0	3048
$t\bar{t}$	MadGraph	94.76	157.5
$W(\to \ell\nu)$+jets	MadGraph	27770.0	31314.0
$WW \to 2\ell 2\nu$	MadGraph	3.783	4.882
$V\gamma$+jets	MadGraph	56.64	65
$ZZ \to 4e$	powheg	—	0.0154
$ZZ \to 4\mu$	powheg	—	0.0154
$ZZ \to 4\tau$	powheg	—	0.0154
$ZZ \to 2e2\mu$	powheg	—	0.0308
$ZZ \to 2e2\tau$	powheg	—	0.0308
$ZZ \to 2\mu 2\tau$	powheg	—	0.0308

4.3.2 Monte Carlo corrections

While data-driven methods can be used to estimate certain types of background, there often remains a reliance on Monte Carlo simulation of the signal and some backgrounds. To account for the imprecision inherent to simulation software or differences caused by detector conditions unknown at the time of MC sample production, various correction factors are applied on Monte Carlo samples to account for these differences. Corrections are most often calculated from properties of individual MC event, such as lepton flavor, kinematic properties of leptons, or simulated pileup, and applied as individual event weight throughout the analysis. Triggering requirements on Monte Carlo samples are also simulated in a similar way, as described in Section 4.3.3.

Scale factors

Scale factors are corrections estimated by measuring lepton selection efficiencies, ϵ, in data and Monte Carlo. These factors are calculated as ratios

$$w_{\ell}^{SF} = \frac{\epsilon_{data}}{\epsilon_{MC}} \tag{4.2}$$

and applied as weights to MC events. The scale factors are measured and provided for standard lepton identification methods (see 4.2) by the responsible groups in the CMS Collaboration. Based on the flavor and kinematic properties of each lepton found in the event, the weight factor for each selected event is composed as a product of individual, (p_{T}, η)-dependent lepton scale factors w_{ℓ}^{SF}.

Pileup

As mentioned in 3.1.1, the pileup is significant at luminosities achieved by the LHC in 2011, when the average vertex multiplicity was approx. 9 simultaneous interactions. For the hard-scattering processes of interest, this results in additional activity in the detector, mainly in form of low p_{T} particles that can impact the quality reconstruction and detection algorithms and in many cases deteriorate the ability to efficiently identify particles, or discriminate them against backgrounds.

Monte Carlo samples used in this analysis include a simulation of pileup. They were however generated prior to the data taking and it was thus not possible to accurately predict the conditions influencing the amount of pileup that would be present in collected data. This disagreement is shown in Figure 4.3 for the 2011 data and Monte Carlo simulation used in this analysis.

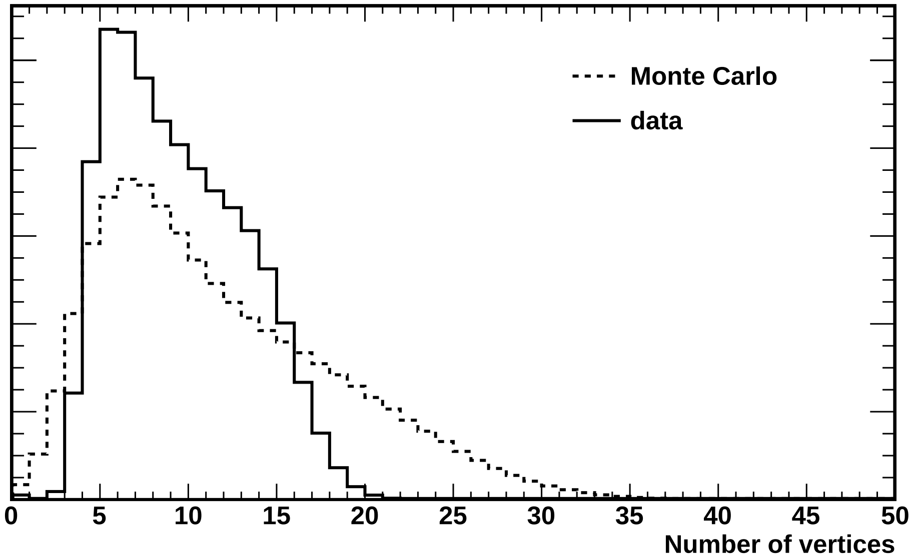

Figure 4.3: Vertex multiplicity (pileup) distribution in Monte Carlo and in data collected in 2011. The MC distribution is obtained using the true number of interactions provided in simulated events, while the data distribution is estimated using the inelastic proton-proton cross section of 68 mb and luminosity conditions in 2011.

To obtain a better modelling of the data, it is therefore necessary to apply additional correction on MC samples to obtain a pileup distribution that reflects the one in data. This is achieved by the *pileup-reweighting* procedure. The "target" pileup distribution is estimated for the analyzed collision period, calculated assuming that the proton-proton cross section is 68 mb. Then a set of factors is calculated that reweight the sample with the initial (Monte Carlo) distribution, to the sample respecting the final distribution. Based on the "true" input number of vertices in each Monte Carlo event which is provided by the generator, each event is assigned the individual weight w^{PU} which is propagated through the whole selection chain.

Electron energy and momentum smearing

Smearing corrections are applied on the electron energy and momentum in Monte Carlo samples to match the resolution in data. Corrections are derived from calibration information of the detector in periods when the data were collected. This improves the precision of the reconstructed Z boson width in the simulation.

4.3.3 Trigger requirements

The role of the trigger selection in CMS is elaborated in detail in Chapter 3. WZ signature consists of three leptons, of which at least two are same-flavor leptons. Therefore HLT paths requiring two electrons or muons were found to be appropriate for this analysis, particularly because of much lower thresholds and looser selection requirements than their single-lepton counterparts.

Double muon HLT paths require at least two muons built using information from the combined muon system and tracker. Because of the gradual increase in LHC luminosity throughout the 2011, several adjustments to the HLT menu were made, raising the selection thresholds for muon p_{T} (this is commonly done to reduce the accepted rate of a HLT path). Due to this, several different HLT paths have to be used to achieve a full coverage of the 2011 data collection period. In the analysis, tt least one of the following paths is required to pass for a data event, requiring also that the same HLT path is *unprescaled* (i.e. that the triggering system at the time of collection was configured to save each event passing the L1 and HLT selection in this path):

- `HLT_Double_Mu7_v*`: Threshold on both trigger muons is $p_{\mathrm{T}} > 7$ GeV.

- `HLT_Mu13_Mu8_v*`: Thresholds on trigger muons are $p_{\mathrm{T}} > 13$ and $p_{\mathrm{T}} > 8$ GeV.
- `HLT_Mu17_Mu8_v*`: Thresholds on trigger muons are $p_{\mathrm{T}} > 17$ and $p_{\mathrm{T}} > 8$ GeV.

In case of electrons, two HLT paths cover the entire 2011. period:

- `HLT_Ele17_CaloIdL_CaloIsoVL_Ele8_CaloIdL_CaloIsoVL_v*`
- `HLT_Ele17_CaloIdT_CaloIsoVL_TrkIdVL_TrkIsoVL_Ele8_CaloIdT_CaloIsoVL_TrkIdVL_TrkIsoVL_v*`

The first of these HLT paths selects exclusively based on calorimeter identification and isolation, while the second path includes also includes tracker information. For both HLT paths to pass, one selected electron with $E_{\mathrm{T}} > 17$ GeV is required, along with a second electron, selected with more relaxed criteria and E_{T} threshold above 8 GeV.

As described in Section 4.2, a preselection is applied on all electron candidates considered in the analysis to assure that they satisfy identification and isolation criteria imposed by the trigger before other selection criteria are applied.

For events which are considered in channels containing two muons (expected to come from a Z decay), the muon-based triggers are required, while the electron-based triggers are required in channels containing two electrons.

In Monte Carlo simulation, there is no HLT requirement and, instead, the efficiency of trigger requirement is simulated, utilizing independent measurement of the trigger efficiencies for the same data collection period. These measurements are provided as efficiencies for individual leptons passing HLT selection imposed on the first or the second lepton (*leg*) in the trigger, called *leading* and *trailing* requirements. The denominator of the measured efficiencies are leptons which satisfy the selection described in 4.2. Values provided in bins of η and p_{T} of lepton candidates are reported in Tables 4.5 and 4.6.

Table 4.5: Efficiencies for electrons satisfying the leading and trailing triggering criteria in the 2011 period.

p_{T} [GeV]		$10 < p_{\mathrm{T}} < 20$	$20 < p_{\mathrm{T}} < 30$	$p_{\mathrm{T}} > 30$
$\epsilon_{\text{leading}}$	$0 < \lvert\eta\rvert < 1.5$	0.5061	0.9849	0.9928
	$1.5 < \lvert\eta\rvert < 2.5$	0.3176	0.9774	0.9938
$\epsilon_{\text{trailing}}$	$0 < \lvert\eta\rvert < 1.5$	0.9854	0.9923	0.9948
	$1.5 < \lvert\eta\rvert < 2.5$	0.9938	0.9953	0.9956

Table 4.6: Efficiency for muons satisfying the leading and trailing triggering criteria in the 2011 period.

p_{T} [GeV]		$10 < p_{\mathrm{T}} < 13$	$13 < p_{\mathrm{T}} < 15$	$15 < p_{\mathrm{T}} < 17$	$17 < p_{\mathrm{T}} < 20$	$20 < p_{\mathrm{T}} < 30$	$p_{\mathrm{T}} > 30$
$\epsilon_{\text{leading}}$	$0 < \lvert\eta\rvert < 1.5$	0.070	0.908	0.939	0.966	0.9648	0.9666
	$0.8 < \lvert\eta\rvert < 1.2$	0.072	0.905	0.913	0.950	0.952	0.9521
	$1.2 < \lvert\eta\rvert < 2.1$	0.104	0.900	0.916	0.945	0.9480	0.9485
	$2.1 < \lvert\eta\rvert < 2.4$	0.131	0.807	0.848	0.888	0.876	0.877
$\epsilon_{\text{trailing}}$	$0 < \lvert\eta\rvert < 0.8$	0.960	0.959	0.971	0.967	0.9655	0.9670
	$0.8 < \lvert\eta\rvert < 1.2$	0.942	0.946	0.940	0.954	0.954	0.9537
	$1.2 < \lvert\eta\rvert < 2.1$	0.947	0.952	0.952	0.958	0.956	0.9530
	$2.1 < \lvert\eta\rvert < 2.4$	0.895	0.896	0.900	0.917	0.903	0.8992

In the WZ analysis, these values are used to estimate the probability that a signal-like event passes the trigger requirement. For channels containing three leptons of same flavor, the overall trigger efficiency is thus constructed as

$$\epsilon_{TRG}(3e,3\mu) = 1 - \begin{pmatrix} 1-\epsilon_{leading}(\eta_1,p_{T1})\times\epsilon_{leading}(\eta_2,p_{T2})\times\epsilon_{leading}(\eta_3,p_{T3}) \\ +\epsilon_{leading}(\eta_1,p_{T1})\times(1-\epsilon_{trailing}(\eta_2,p_{T2}))\times(1-\epsilon_{trailing}(\eta_3,p_{T3})) \\ +\epsilon_{leading}(\eta_2,p_{T2})\times(1-\epsilon_{trailing}(\eta_1,p_{T1}))\times(1-\epsilon_{trailing}(\eta_3,p_{T3})) \\ +\epsilon_{leading}(\eta_3,p_{T3})\times(1-\epsilon_{trailing}(\eta_1,p_{T1}))\times(1-\epsilon_{trailing}(\eta_2,p_{T2})) \end{pmatrix} \tag{4.3}$$

and for channels containing two same flavor leptons, as

$$\epsilon_{TRG}(2e,2\mu) = 1 - \begin{pmatrix} 1-\epsilon_{leading}(\eta_1,p_{T1})\times\epsilon_{leading}(\eta_2,p_{T2}) \\ +\epsilon_{leading}(\eta_1,p_{T1})\times(1-\epsilon_{trailing}(\eta_2,p_{T2})) \\ +\epsilon_{leading}(\eta_2,p_{T2})\times(1-\epsilon_{trailing}(\eta_1,p_{T1})) \end{pmatrix} \tag{4.4}$$

These efficiencies are applied to individual Monte Carlo events as event weights.

4.3.4 Selection of W and Z candidates

Prior to the Z candidate selection, the event is required to have exactly three identified electrons or muons satisfying the criteria described in 4.2.1 and 4.2.2. The purpose of this requirement is rejection of the multi-lepton backgrounds, mainly ZZ, which often consist of four lepton candidates.

The Z candidate is built from four-vectors of the two same-flavor, opposite-sign electron or muon candidates. The reconstructed Z mass must lie within the $[M_Z - 20, M_Z + 20]$ GeV window positioned around the Z boson nominal mass of $M_Z = 91.18$ GeV. If there is more than one possible Z candidate, the one with the invariant mass nearest to the nominal Z mass is selected.

If the Z candidate is successfully selected, the remaining lepton is chosen as the W candidate constituent if the lepton has $p_{\mathrm{T}} > 20$ GeV and is geometrically separated from the Z leptons by $\Delta R(\text{ W lepton, Z lepton}) > 0.1$. The latter requirement removes events where the final state radiation creates additional leptons or photons around Z decays, thus mimicking the WZ final state.

Based on the flavor of leptons building the selected Z and W candidates, events are grouped in one of the four channels as defined previously in Table 4.1.

As the last selection step, the transverse missing energy requirement of $E_T^{miss} > 30$ GeV is imposed. This largely removes backgrounds without a genuine neutrino. The E_T^{miss}distribution in each channel before this requirement and after other selection steps is shown in Figure 4.4. The distribution of the Z boson mass after all selection steps is shown in Figure 4.5.

Tables containing number of events after main selection steps are applied on data and Monte Carlo simulation are shown in Table 4.7 and, separately for each channel, in Table 4.8. Various distributions summed over all four channels are shown in Figure 4.6.

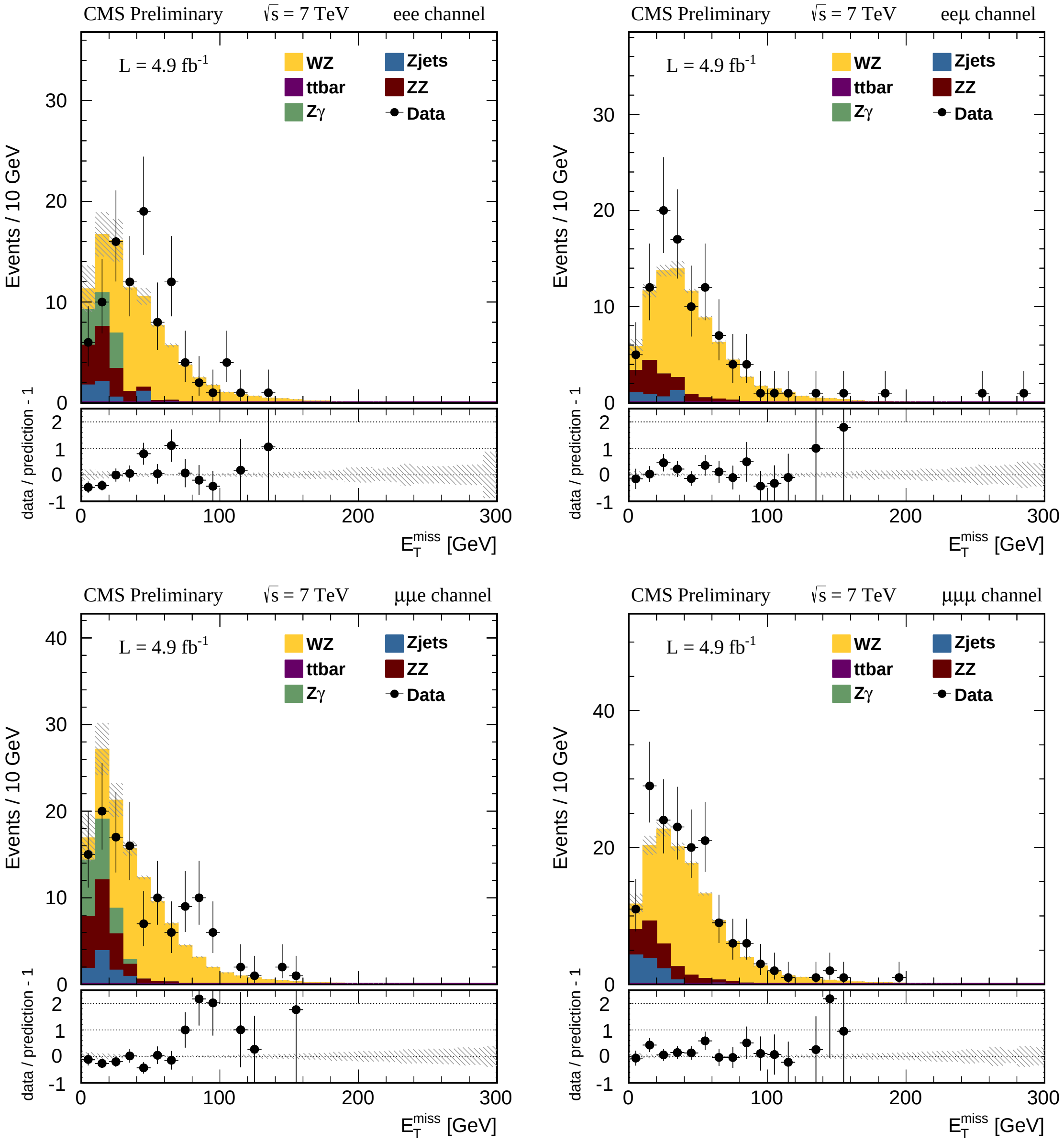

Figure 4.4: E_T^{miss}distribution after applying all of the selection criteria except the E_T^{miss}requirement. All expected distributions are estimated using the Monte Carlo simulation.

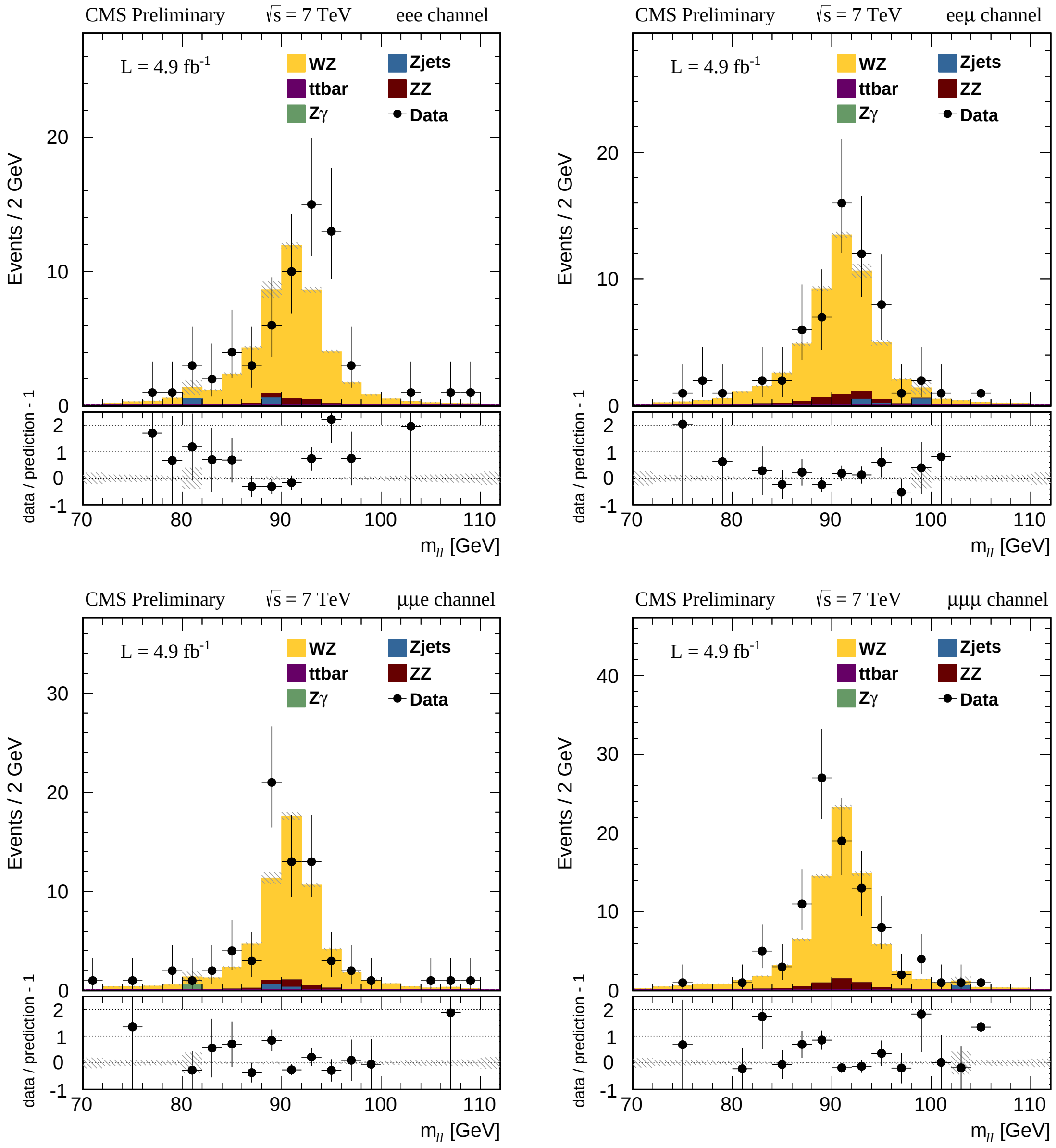

Figure 4.5: Z boson candidate invariant mass distribution after applying all of the selection criteria. All expected distributions are estimated using the Monte Carlo simulation.

Table 4.7: Yields of selected events in data together with the expected yields from the simulation of signal and background processes after main selection steps. Numbers correspond to an integrated luminosity of 4.9 fb^{-1}. Errors are statistical.

sample	Z selection + 3 leptons	W selection	E_T^{miss}selection
$Z + jets$	184.7	28.3	3.9 ± 1.4
$W + jets$	0	0	0
$t\bar{t}$	4.5	2.9	2.4 ± 0.2
ZZ	77.7	64.8	13.25 ± 0.04
$V\gamma$	30.8	27.4	0.5 ± 0.5
WW	0	0	0
WZ	375	318	224 ± 1
total MC	673	441	244 ± 2
data	725	478	293

Table 4.8: Yields of selected events in data together with the expected yields from the simulation of signal and background processes after main selection steps in individual channels. Numbers correspond to an integrated luminosity of 4.9 fb^{-1}. Errors are statistical.

sample	Z selection + 3 leptons		W selection				E_T^{miss}selection			
	$Z \to ee$	$Z \to \mu\mu$	3e	2e1μ	1e2μ	3μ	3e	2e1μ	1e2μ	3μ
$Z + jets$	64.6	120.1	5.7	3.7	8.2	10.7	1.2 ± 0.8	1.2 ± 0.9	0.8 ± 0.6	0.6 ± 0.6
$W + jets$	0	0	0	0	0	0	0	0	0	0
$t\bar{t}$	1.6	2.9	0.33	0.65	0.66	1.29	0.30 ± 0.07	0.55 ± 0.09	0.56 ± 0.09	1.04 ± 0.13
ZZ	30.9	46.8	14.3	11.6	21.0	17.9	2.01 ± 0.04	3.48 ± 0.04	2.66 ± 0.03	5.09 ± 0.06
$V\gamma$	13.7	17.1	10.4	0	17.0	0	0	0	0.5 ± 0.5	0
WW	0	0	0	0	0	0	0	0	0	0
WZ	153	222	61.8	70.8	78.9	106.6	44.7 ± 0.5	49.8 ± 0.5	56.0 ± 0.5	73.8 ± 0.6
total MC	264	409	92.5	86.8	125.8	136.5	48.2 ± 1.0	55.0 ± 1.0	60.5 ± 1.1	80.5 ± 0.9
data	284	441	96	99	122	161	64	62	70	97

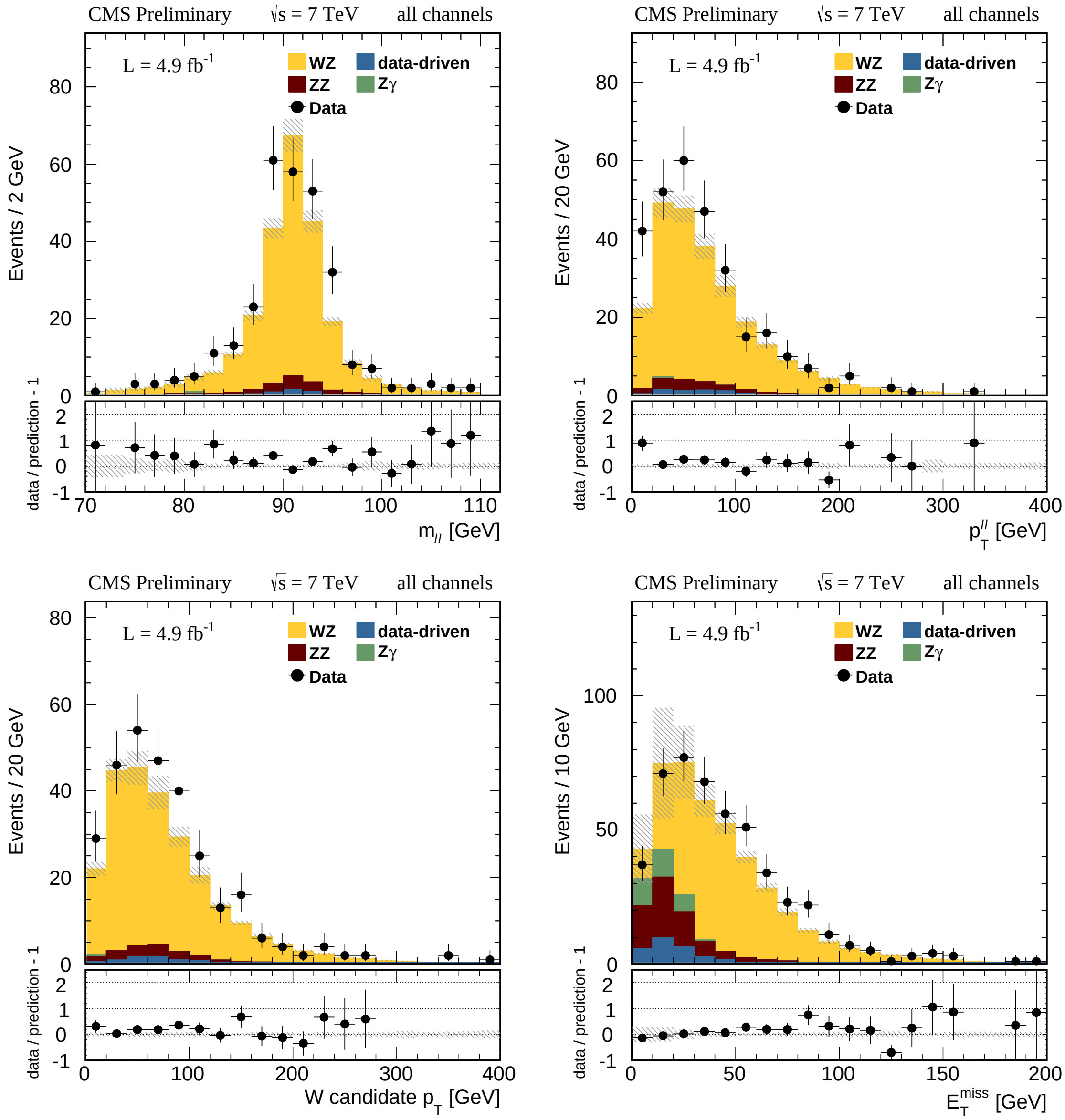

Figure 4.6: Kinematic distributions after applying all of the WZ selection criteria in the four channels: invariant mass of the Z candidate (top left), transverse momentum of the Z candidate (top right), transverse momentum of the W candidate (bottom left), and the $E_T^{miss}$of the event before applying the E_T^{miss}selection (bottom right). The top and Z+jets backgrounds are estimated using the data-driven method described in Section 4.4.2.

4.4 Background estimation

4.4.1 WZ decays with $Z \to \tau\tau$ or $W \to \tau\nu$

Special consideration is given to WZ decays containing τ leptons, as their cross section is directly proportional to the signal cross section. Their contribution is therefore not taken as absolute yield, and is instead taken as a fraction (f_τ) of the $WZ \to 3l$ events passing the full selection in each channel. This fraction, estimated directly from the Monte Carlo, can then be factored out from the signal estimate. As shown in Table 4.9, this background consists predominantly of events containing exclusively τ decays resulting in a final-state electrons or muons. Contributions of events with $Z \to \tau\tau$ and $W \to \tau\nu$, as well as f_τ fractions for each channel are also reported.

Table 4.9: Number of WZ→ $3l$ Monte Carlo events in selection channels containing τ decays of W or Z boson, obtained after all selection steps are applied. Various categories based on generator level restrictions are reported; requiring leptonic or hadronic τ decays, or requiring τ decays of W or Z bosons to be present. f_τ values are also included. Errors are statistical.

sample	$3e0\mu$	$2e1\mu$	$2e1\mu$	$0e3\mu$
$N_{\tau\to e,\mu}$	2.90 ± 0.12	3.64 ± 0.13	3.58 ± 0.12	5.44 ± 0.15
$N_{\tau\to\text{hadronic}}$	0.02 ± 0.01	0.003 ± 0.003	0.02 ± 0.01	0.002 ± 0.002
$N_{W\to\tau\nu}$	2.83 ± 0.11	3.54 ± 0.13	3.49 ± 0.12	5.28 ± 0.15
$N_{Z\to\tau\tau}$	0.08 ± 0.02	0.11 ± 0.02	0.10 ± 0.02	0.17 ± 0.003
f_τ	0.065 ± 0.002	0.073 ± 0.002	0.064 ± 0.002	0.074 ± 0.002

4.4.2 Background determination from data

Monte Carlo simulations are affected by theoretical predictions and numerous approximations, from modelling the PDFs, higher order radiative contributions, hadronization modelling, to imperfections in the detector simulation. To avoid dependency on inaccuracies coming from these issues, various techniques are used to perform estimations and cross-checks of signal or backgrounds based on information extracted from collision data, called *data-driven* methods.

For this analysis, a method has been developed to estimate the number of reducible background events remaining in the sample after all WZ selection criteria have been applied. The method only applies to backgrounds containing jets misidentified as leptons, or produced from a heavy quark decay, resulting in leptons produced as a part of a hadronic jet. In this sense, two categories of observable leptons are distinguished according to their real origin:

- *Prompt lepton*, a true lepton originating from heavy boson decays. They will usually be isolated from other particles in the final state.
- *Misidentified lepton*, any lepton not originating from heavy boson decays, or a particle misidentified as lepton.

In the following, the index j is used to denominate misidentified leptons, while index ℓ is used to denominate prompt leptons, in the following order for the WZ final state: W lepton, Z lepton with higher p_{T} (*leading*), and Z lepton with lower p_{T} (*trailing*).

The sample of selected collision events has contributions from the following event categories:

- $\ell\ell\ell$: the three leptons originate from prompt leptons. WZ signal events contribute to this category, as well as the irreducible ZZ background.
- $j\ell\ell$: this category is mostly composed of Z+jets and $\mathrm{t\bar{t}}$ events, in which the two Z leptons are prompt, while the lepton associated to the W decay is a misidentified lepton.

- $\ell\ell j$ and $\ell j\ell$: This category is again composed of $\mathrm{t\bar{t}}$ and Z+jets events, in which one of the two Z leptons is combined with a misidentified lepton to form a Z, while the other Z lepton is associated to the W decay.

- $jj\ell$, $j\ell j$, ℓjj, jjj: Two or all three misidentified leptons. Several processes may contribute to this category: W+jets, Z+jets (in which one or both leptons escape undetected), $\mathrm{t\bar{t}}$ (with fully hadronic top decays), or QCD multijet processes.

Given a relaxed set of lepton selection criteria, called the loose selection, leptons passing this base selection are furthermore distinguished as *passing* or *failing* the non-relaxed selection, or the tight selection, which corresponds to the nominal selection used in the analysis. The following probabilities, that are generally dependent on η and p_T of the reconstructed lepton, are defined:

- ϵ_i is the probability for a prompt lepton that passes the loose selection for the i-th lepton to also pass the tight selection.

- p_i is the probability that a misidentified lepton, which passes the loose selection as the i-th lepton, also passes the tight selection.

where the meaning of the index $i = 1...3$ represents the order: W lepton, leading Z lepton and trailing Z lepton.

The definition of the loose and tight criteria is chosen to be same for all W and Z leptons. Loose muons have a relaxed isolation criteria: $Iso_{rel}^{PF} < 1.0$. Loose electrons have the MVA identification and isolation requirements removed, and only the MVA preselection is retained. For both electrons and muons, the relaxed criteria are tighter than the trigger selection to avoid bias.

The starting point is the sample of collision events in which all three leptons are satisfying the loose selection criteria and otherwise passing all other WZ selection requirements. This sample can be decomposed in different contributions according to the origin of the selected leptons,

$$N_{LLL} = n_{\ell\ell\ell} + n_{\ell\ell j} + n_{\ell j\ell} + n_{\ell jj} + n_{j\ell\ell} + n_{j\ell j} + n_{j\ell j} + n_{jjj}. \tag{4.5}$$

The same sample can then be split in subsamples depending on whether each of the three leptons[4] passes or fails the tight requirement. The number of events in each subsample is labeled N_{ijk} with $i, j, k = \{T, F\}$ where T indicates leptons passing the tight selection and F stands for leptons failing the tight selection. The number of events in each category can be expressed with the efficiencies p_i and ϵ_i. The category with all three leptons satisfying the tight requirement is constructed as

$$\begin{aligned} N_{TTT} = \quad & n_{j\ell\ell} p_1 \epsilon_2 \epsilon_3 + n_{j\ell j} p_1 \epsilon_2 p_3 + n_{jj\ell} p_1 p_2 \epsilon_3 + n_{jjj} p_1 p_2 p_3 \\ & + n_{\ell\ell\ell} \epsilon_1 \epsilon_2 \epsilon_3 + n_{\ell\ell j} \epsilon_1 \epsilon_2 p_3 + n_{\ell j\ell} \epsilon_1 p_2 \epsilon_3 + n_{\ell jj} \epsilon_1 p_2 p_3, \end{aligned} \tag{4.6}$$

with the equations for all other N_{ijk} constructed analogously. By solving this system of equations, solutions to $n_{\ell\ell\ell} ... n_{jjj}$ are obtained. The signal is contained in the category of three prompt leptons that satisfy the loose selection:

---

[4] Identified lepton objects for which it is not known if they are prompt or misidentified leptons.

$$\begin{aligned}
n_{\ell\ell\ell} \quad = \quad & \frac{1}{(\epsilon_1 - p_1)(\epsilon_2 - p_2)(\epsilon_3 - p_3)} \\
& [\ N_{TTT}(1-p_1)(1-p_2)(1-p_3) \\
& -N_{TTF}(1-p_1)(1-p_2)(\ p_3) \\
& -N_{TFT}(1-p_1)(\ p_2)(1-p_3) \\
& +N_{TFF}(1-p_1)(\ p_2)(\ p_3) \\
& -N_{FTT}(\ p_1)(1-p_2)(1-p_3) \\
& +N_{FTF}(\ p_1)(1-p_2)(\ p_3) \\
& +N_{FFT}(\ p_1)(\ p_2)(1-p_3) \\
& -N_{FFF}(\ p_1)(\ p_2)(\ p_3)]. \qquad (4.7)
\end{aligned}$$

The coefficients for the number of events in each category N_{ijk} in equation (4.7) define weights which are applied to each event depending on category in which it belongs. These weights are then summed over all events in the loose sample. The reason of using weights instead of simply summing each N_{ijk} contribution is that e_i and p_i values depend on the kinematic (p_{T}, η) properties of lepton objects in each event. To obtain the number of events remaining after requiring all leptons to pass the tight selection, an additional weight is applied in form of efficiencies for loose prompt leptons to pass tight selection, i.e. $n^T_{\ell\ell\ell} = \epsilon_1\epsilon_2\epsilon_3 n_{\ell\ell\ell}$.

Efficiencies e_i and p_i are determined using separate physical processes selected to obtain a sample of prompt or misidentified objects resembling, as closely as possible, those found in the selected sample.

Determination of prompt lepton efficiencies

For prompt leptons, efficiencies are determined from $Z \to \ell\ell$ decays using the *Tag and Probe* (T&P) method. The estimation is done on data samples selected to contain genuine Z decays. The method is described in more detail in the next Chapter (see 5.4) where it was used in the scope of heavy resonance searches. Results of the electron and muon efficiency estimation are given in Table 4.10.

Table 4.10: Electron and muon prompt efficiencies for the tight criteria.

	electrons		muons
	$0.0 < \|\eta\| < 1.479$	$1.479 <= \|\eta\| < 2.5$	$0.0 < \|\eta\| < 2.4$
$10 < p_{\mathrm{T}} < 15$	0.8415 ± 0.0033	0.6048 ± 0.0053	0.7778 ± 0.0024
$15 < p_{\mathrm{T}} < 20$	0.8145 ± 0.0033	0.6048 ± 0.0053	0.7778 ± 0.0024
$20 < p_{\mathrm{T}} < 25$	0.9031 ± 0.0014	0.8058 ± 0.0026	0.8670 ± 0.0015
$25 < p_{\mathrm{T}} < 30$	0.9244 ± 0.0009	0.8406 ± 0.0020	
$30 < p_{\mathrm{T}} < 50$	0.9572 ± 0.0002	0.8980 ± 0.0005	0.9489 ± 0.0002
$50 < p_{\mathrm{T}} < \mathrm{inf}$	0.9736 ± 0.0004	0.9387 ± 0.0011	0.9792 ± 0.0004

Determination of misidentified lepton efficiencies

As misidentified leptons are largely jets or leptons from heavy quark decays, the method for efficiency determination focuses on obtaining sample (the *control sample*) where the selection criteria can be tested on such objects with the ability of measuring the probability of a misidentified loose lepton satisfying tight criteria.

A special set of selection requirements, optimized for isolating QCD processes containing jets, is used to select the control sample. This QCD enriched sample is selected using single electron or single muon HLT paths. The loose criteria are carefully selected to impose requirements stricter than the selection used in single lepton HLT paths and thus avoid the bias coming from the trigger. The selection is mainly optimized to suppress the presence of prompt electrons from real W or Z boson decays. The transverse missing energy is restricted to $E_T^{miss} < 20$ GeV, the resonant Z invariant mass is excluded by requiring $M_{ee} \notin [60, 120]$ GeV, while prompt muons from W and Z decays are restricted to $E_T^{miss} < 20$ GeV. The transverse mass of the lepton and E_T^{miss}system is restricted to $M_T < 20$ GeV and the resonant Z mass region $M_{\mu\mu} \notin [76, 106]$ GeV is excluded. To exclude contamination by leptons from the Drell-Yan decay[5], the invariant mass of two the leptons is required to be above 20 GeV.

For each event, the transverse energy (E_T^{LeadJet}) of the leading jet is required to be above a certain threshold, affecting the E_T spectrum of the jet misidentified as lepton, which itself is selected as lepton object separated by $\Delta R > 1$ from the leading jet. This requirement ensures that there is no bias from the leading jet and that the misidentified object is recoiling against it. The E_T^{LeadJet} threshold is selected in a such way that the QCD E_T spectra are as similar as possible to E_T spectrum of the background sample. For the WZ fake rate measurement, the optimal threshold value was found to be $E_T^{\text{LeadJet}} > 50$. Measured electron and muon misidentification rates are reported in Tables 4.12 and 4.11.

Table 4.11: Measured rate of muon misidentification as a function of the transverse momentum and η of the muon. Errors are statistical.

	$0.0 < \|\eta\| \leq 1.0$	$1.0 < \|\eta\| \leq 1.479$	$1.479 < \|\eta\| \leq 2.0$	$2.0 < \|\eta\| \leq 2.5$
$10.0 < p_t \leq 15.0$	0.0343 ± 0.0066	0.0504 ± 0.0122	0.0567 ± 0.0146	0.0523 ± 0.0226
$15.0 < p_t \leq 20.0$	0.0077 ± 0.0042	0.0291 ± 0.0126	0.0615 ± 0.0224	0.0004 ± 0.0003
$20.0 < p_t \leq 25.0$	0.0108 ± 0.0011	0.0146 ± 0.0019	0.0249 ± 0.0031	0.0305 ± 0.0059
$25.0 < p_t \leq 30.0$	0.0097 ± 0.0012	0.0094 ± 0.0018	0.0159 ± 0.0030	0.0230 ± 0.0062
$30.0 < p_t \leq \infty$	0.0156 ± 0.0010	0.0171 ± 0.0016	0.0260 ± 0.0025	0.0221 ± 0.0044

---

[5] Dilepton decay (or decay to a quark-antiquark pair) of the virtual photon which is significant in the low invariant mass region of the virtual photon.

Table 4.12: Measured rate of electron misidentification as a function of the transverse momentum and η of the electron. Errors are statistical.

	$0.0 < \lvert\eta\rvert \leq 1.0$	$1.0 < \lvert\eta\rvert \leq 1.479$	$1.479 < \lvert\eta\rvert \leq 2.0$	$2.0 < \lvert\eta\rvert \leq 2.5$
$10.0 < p_t \leq 18.0$	0.0630 ± 0.0360	0.0420 ± 0.0290	0.0080 ± 0.0100	0.0340 ± 0.0340
$18.0 < p_t \leq 26.0$	0.0260 ± 0.0120	0.0340 ± 0.0160	0.0080 ± 0.0100	0.0410 ± 0.0240
$26.0 < p_t \leq 34.0$	0.0610 ± 0.0150	0.0600 ± 0.0180	0.0540 ± 0.0180	0.0510 ± 0.0180
$34.0 < p_t \leq \infty$	0.0520 ± 0.0140	0.0240 ± 0.0120	0.0330 ± 0.0150	0.0440 ± 0.0160

Data driven method result

Table 4.13 contains the result of the background determination method. The first row contains the signal estimation and statistical error which includes statistical uncertainties propagated from $N_{i,j,k}$ and efficiencies ϵ_i and p_i. These values with the corresponding errors are taken as input of the cross section measurement.

Table 4.13: Data-driven background determination method results.

	$3e$	$2e1\mu$	$2\mu1e$	3μ
$\epsilon_1\epsilon_2\epsilon_3 n_{\ell\ell\ell}$	61.83 ± 8.08	60.48 ± 7.93	67.59 ± 8.42	95.23 ± 9.89
$N_{TTT} - \epsilon_1\epsilon_2\epsilon_3 n_{\ell\ell\ell}$	2.17 ± 0.40	1.52 ± 0.28	2.41 ± 0.36	1.77 ± 0.24
N_{TTT}	64	62	70	97
N_{TTF}	16	14	43	47
N_{TFT}	13	7	13	8
N_{TFF}	5	1	3	6
N_{FTT}	33	59	42	64
N_{FTF}	11	8	19	15
N_{FFT}	5	6	0	8
N_{FFF}	1	8	3	6

4.4.3 Other backgrounds

The backgrounds which are signal-like can not be removed using the data driven method. The ZZ background is largely rejected by requiring exactly three leptons in the selection, while the remaining irreducible contribution is estimated from the Monte Carlo. The Zγ background is largely rejected by the electron conversion rejection requirements in the electron preselection. The remaining contribution contains photons not efficiently removed by the data-driven method, as they are isolated. This background is therefore also estimated from the Monte Carlo. ZZ and Zγ estimates are given in Tables 4.7 and 4.8.

4.5 Cross section measurement

The measurement of the cross section is derived from the relation

$$\sigma = \frac{N_{\text{sig}}}{A \times \epsilon \cdot \mathcal{L}}, \tag{4.8}$$

where N_{sig} is the estimated number of signal events, $A \times \epsilon$ is the detector acceptance and efficiency for signal and $\mathcal{L}$ is the integrated luminosity for the period over which the observed events were recorded. The number of signal events is defined as

$$N_{\text{sig}} = (1 - f_{\tau}) \cdot (N_{signal}^{data-driven} - N_{ZZ} - N_{Z\gamma}), \tag{4.9}$$

where the f_{τ} is the fraction of WZ to τ decays reported in Table 4.9, N_{ZZ} and $N_{Z\gamma}$ are the number of selected ZZ and $Z\gamma$ background events shown in Table 4.8, $N_{signal}^{data-driven}$ is the number of signal-like events obtained by the background determination method as shown in Table 4.13, and $A \times \epsilon$ is detector acceptance and efficiency for signal. The values calculated separately for each selection channel are used in eq. 4.9.

4.5.1 Acceptance and efficiency

A relevant quantity for measuring the production cross section of signal is the overall fraction of produced signal events that is detected and selected. Only a fraction of produced events will decay in such a way that the phase space of all detectable final state particles is covered by functional (*fiducial*) parts of the detector. The fraction of the phase space for which this is satisfied is called acceptance (A). Among events within the acceptance, not all are successfully detected due to inefficiencies or not satisfying selection criteria imposed by the trigger or the analysis. Overall, acceptance and efficiency are estimated together as the single fraction.

The product of acceptance and selection efficiency is estimated for the WZ signal simulation as a single parameter, defined as

$$A \times \epsilon = \frac{\text{number of selected } WZ \to \ell\ell\nu \text{ events}}{\text{number of produced signal events}}. \tag{4.10}$$

It is calculated for each channel separately. In the numerator, the number of selected events in the WZ Monte Carlo sample is counted in each channel. In the denominator, only signal events in a particular channel are counted, by applying the generator-level restrictions on the flavor of leptons from W and Z decays and on the generated Z boson mass ($M_Z \in [71.18, 111.18]$ GeV).

$A \times \epsilon$ is derived from the Monte Carlo signal simulation and needs to be additionally corrected to account for differences in detector efficiency between data and Monte Carlo. Using corrections described in 4.3.2 and 4.3.2, and trigger efficiency simulation described in 4.3.3, the corrected acceptance and efficiency is

$$(A \times \epsilon)^{ch}_{\text{corr}} = \frac{\sum_{i=1...N}^{selected(ch)} \prod_{\ell=1...3} w^{SF}_{i\ell} \cdot w^{PU}_{i} \epsilon^{i}_{TRG(ch)}}{N^{ch}_{gen}} \tag{4.11}$$

Values of the $(A \times \epsilon)^{ch}_{\text{corr}}$ for each channel are found in Table 4.14.

Table 4.14: $(A \times \epsilon)^{ch}_{\text{corr}}$ for each selection channel.

channel	$A \times \epsilon)^{ch}_{\text{corr}}$
eee	$0.1362 \pm 0.0012(stat)$
$ee\mu$	$0.1523 \pm 0.0012(stat)$
$\mu\mu e$	$0.1704 \pm 0.0013(stat)$
$\mu\mu\mu$	$0.2265 \pm 0.0014(stat)$

A number of systematic uncertainties arising from various theoretical and instrumental effects are estimated on acceptance and efficiency. This is elaborated in Section 4.5.2.

4.5.2 Systematic uncertainties

Systematic effects can contribute through any of the parameters used to calculate the cross section. The acceptance is affected by PDF uncertainties, while it can also be affected by the the accuracy of the (N)NLO simulation in generators. The efficiency ϵ is susceptible to instrumental uncertainties in the reconstruction and identification of analysis objects, such as those of the electron and muon reconstruction, identification, energy and momentum scale or E_T^{miss}reconstruction. The efficiency is also affected by the pileup simulation, where the main uncertainty is on the inelastic proton-proton cross section. Additionally, most of these uncertainties are also inherent to ZZ and Zγ Monte Carlo based estimation, affecting similarly their acceptance and selection efficiency. In this analysis, all uncertainties affecting the signal efficiency are considered to be fully correlated with the corresponding background uncertainties. As the absolute ZZ and Zγ simulated yields are used for the cross section calculation, an error is assigned to the cross section of these backgrounds. The data-driven background estimation is affected by uncertainties in determination of misidentified lepton efficiencies.

Each systematic contribution is evaluated as the effect on the overall cross section following the prescription

$$\Delta^i_{rel}(\sigma_{WZ}) = max\left(\frac{|\sigma^i_{up} - \sigma(WZ)^i|}{\sigma(WZ)^i}, \frac{|\sigma_{down}(WZ)^i - \sigma(WZ)^i|}{\sigma(WZ)^i}\right) \tag{4.12}$$

where σ_{up} and σ_{down} denote the cross section for the upward and downward effect of variation by the respective uncertainty. This estimate is performed for each particular channel and contribution i. Finally, all contributions are added in quadrature to obtain the overall systematic uncertainty estimate $\Delta_{syst} = \sqrt{\sum_i (\Delta^i_{rel}(\sigma_{WZ}))^2}$.

Methods used to determine systematic uncertainty from each individual contribution are discussed in the following, with the results of each method summarized in Table 4.17.

PDF, QCD and factorization scale

PDF uncertainties have an effect both on the predicted cross section of the process as well as on the fraction of selected events, affected due to modified kinematic properties. These uncertainties are estimated by applying PDF parameter variations on the $A \times \epsilon$, affecting simultaneously its nominator and denominator. The Method used to estimate PDF uncertainty using the CTEQ6 [84] PDF set is described in Ref.[85]. For each parameter within the PDF set, the up or down variation is applied, resulting in modified weights in each Monte Carlo event. The corresponding difference in acceptance is calculated for each of these variations. Results are then grouped depending on whether they have positive or negative effect on the acceptance and summed in quadrature to obtain $|\Delta_{rel}(PDF_{+})|$ and $|\Delta_{rel}(PDF_{-})|$. For the resulting uncertainty, a larger of the these values is used. PDF uncertainty for signal acceptance is estimated at 1.4%.

The effect of uncertainties on the used factorization and renormalization scales on the geometric acceptance of the described selection is studied with the MCFM program by varying each scale by a factor of two up and down with respect to its nominal value which is set to the average mass of the final state bosons. The variation of the acceptance can be seen in Table 4.15. The largest variation is 1.3%, which is taken as systematic uncertainty.

Pileup

The efficiency and acceptance used in the cross section determination are obtained using Monte Carlo samples that were reweighted to reproduce the expected distribution of the number of pileup interaction in data. The target distribution for data is generated using the central minimum bias cross section ($\sigma_{pp} = 68$ mb). The same procedure is repeated for a minimum bias cross section

Table 4.15: Geometrical acceptance of the WZ selection as a function of renormalization and factorization scales.

QCD Scale (GeV)	factorization scale (GeV)	acceptance	relative difference
42	42	0.3703	0.548 %
42	85	0.3687	0.101 %
42	170	0.3678	-0.140 %
85	42	0.3683	-0.002 %
85	85	0.3683	0.000 %
85	170	0.3666	-0.469 %
170	42	0.3663	-0.529 %
170	85	0.3636	-1.285 %
170	170	0.3658	-0.669 %

scaled up and down by 5%. The relative difference of acceptance and efficiency from the central one is taken as systematic uncertainty from pileup (choosing the higher value from the up or down variation result)

Lepton momentum and energy scale

Electron energy scale and muon momentum scale uncertainties are determined by scaling the corresponding lepton type four-momentum, and performing the full selection procedure with lepton objects modified in such way[6] and obtaining a relative difference on the acceptance or a number of selected events. For electrons, a 2% uncertainty is assumed in the ECAL barrel region and 5% in endcap regions. Muons are assumed to have 1% uncertainty on the momentum scale.

---

[6] Including recalculation of the relative isolation variable.

Lepton corrections and trigger simulation

The uncertainty on the lepton efficiency for each lepton object in a fully selected sample is propagated through the selection process to estimate the effect on each individual scale factor (see Section 4.3.2). These values are then summed in quadrature to obtain the overall effect. Statistical errors for electron and muon scale factors are of the order of 2%. Uncertainties coming from the T&P measurement method are assumed on individual muon efficiencies; 0.5% (identification), 0.2%(isolation) and 0.2%(single-muon HLT path). The uncertainties on electron reconstruction efficiencies are 1.3% and 1.5% in barrel and endcap regions, respectively.

To estimate the overall uncertainty on the trigger efficiency simulated in Monte Carlo (see Section 4.3.3), the uncertainty is calculated for each event from individual lepton HLT object efficiency errors by performing error propagation (corresponding to equations 4.3 and 4.4). Then these errors are summed over events in the sample and added to lepton scale factor uncertainties in quadrature. The systematic uncertainty from trigger is however negligible in comparison to uncertainties on lepton identification.

Missing transverse energy

The missing transverse energy is a composite object and is highly dependent on the resolution and scale of its components. To obtain the uncertainty, $E_T^{miss}$is factored into components which are separately varied by their respective uncertainties, determined from dedicated studies. This is done for the following components:

- jet energy scale and jet energy resolution

- unclustered energy (10%)
- tau leptons (3%)
- electrons and photons (0.6% in barrel region and 1.5% in endcaps)
- muons (0.2%)

Backgrounds determined from data

By selecting an appropriate E_T threshold on the leading jet in the QCD enriched sample used to measure the efficiency of misidentified leptons (see Section 4.4.2), the E_T spectrum of misidentified lepton objects is tuned to be as similar as possible to the one in backgrounds (mainly $\mathrm{t\bar{t}}$ and Z+jets). The optimal threshold was found to be $E_T^{\text{LeadJet}} < 50$ GeV for Z+jets, while for $\mathrm{t\bar{t}}$ the optimal requirement was found to be $E_T^{\text{LeadJet}} < 30$ GeV for muons and $E_T^{\text{LeadJet}} < 35$ GeV for electrons. Those results have been obtained by matching the leading jet E_T spectra to the respective background sources in Monte Carlo. To account for the systematic effect of the $E_T^{\text{LeadJet}} < 50$ GeV choice, the signal estimation, described in 4.4.2, is repeated using lowered thresholds. The variation in signal yield from the yield obtained using the nominal threshold is taken as systematic uncertainty. Results of the signal estimation for multiple leading jet E_T threshold choices are reported in Table 4.16.

Table 4.16: Signal estimation in the N_{TTT} sample using different $E_T^{LeadJet}$ selection of the QCD control sample.

	$3e$	$2e1\mu$	$2\mu1e$	3μ
$E_T^{LeadJet} > 15$ GeV	59.75 ± 8.18	55.72 ± 8.06	62.46 ± 8.58	87.71 ± 10.09
$E_T^{LeadJet} > 35\ (30)$ GeV	60.32 ± 8.14	57.06 ± 8.02	63.78 ± 8.51	90.23 ± 10.02
$E_T^{LeadJet} > 50$ GeV (nominal)	61.83 ± 8.08	60.48 ± 7.93	67.59 ± 8.42	95.23 ± 9.89

Backgrounds derived from Monte Carlo

The uncertainties on the ZZ and Zγ cross sections are taken from the uncertainty on $\sqrt{s} = 7$ TeV CMS measurement results; 14% uncertainty for ZZ [86] and 7% for Zγ [87].

Table 4.17: Summary of systematic uncertainties for the WZ $\rightarrow 3\ell$ cross section measurement.

		eee	$ee\mu$	$\mu\mu e$	$\mu\mu\mu$
source	systematic uncertainty	effect on WZ cross section			
electron energy scale	2%(EB),5%(EE)	1.9%	0.75%	1.2%	n/a
muon p_T scale	1%	n/a	0.60%	0.43%	1.06%
E_T^{miss}Resolution and scale		3.7%	3.4%	4.3%	3.7%
lepton scale factors and trigger		2.9%	2.7%	2.0%	1.4%
pileup		0.27%	0.50%	1.00%	0.64%
PDF	1.4%	1.4%	1.4%	1.4%	1.4%
QCD and factorization scale	1.3%	1.3%	1.3%	1.3%	1.3%
ZZ cross section	14%	0.50%	0.92%	0.62%	0.85%
$Z\gamma$ cross section	7%	0.%	0.	0.04%	0
background determination		2.7%	6.5%	6.3%	6.0%
source	systematic uncertainty	effect on luminosity			
luminosity	2.2%	2.2%	2.2%	2.2%	2.2%

4.5.3 Cross section measurement in individual channels

Table 4.18: The WZ cross section for $\int \mathcal{L}\, dt = 4.9$ fb^{-1} in each channel.

channel	cross section [pb]	inclusive cross section (σ_{ch}(WZ)$/BR_{ch}$) [pb]
$3e$	$0.0834 \pm 0.0110(stat) \pm 0.0051(syst) \pm 0.0018(lumi)$	$23.08 \pm 3.12(stat) \pm 1.41(syst) \pm 0.51(lumi)$
$2e\mu$	$0.0702 \pm 0.0098(stat) \pm 0.0055(syst) \pm 0.0015(lumi)$	$19.75 \pm 2.75(stat) \pm 1.54(syst) \pm 0.43(lumi)$
$2\mu e$	$0.0719 \pm 0.0094(stat) \pm 0.0058(syst) \pm 0.0016(lumi)$	$19.86 \pm 2.60(stat) \pm 1.60(syst) \pm 0.44(lumi)$
3μ	$0.0749 \pm 0.0082(stat) \pm 0.0054(syst) \pm 0.0016(lumi)$	$21.06 \pm 2.31(stat) \pm 1.53(syst) \pm 0.46(lumi)$

The cross section measurement is obtained for each channel using the equation 4.8. The results are reported in Table 4.18 and extrapolated to estimate the inclusive cross section by dividing the channel cross section with the branching ratio of the W and Z decays in particular channel. The branching ratios listed in Table 2.3 are used. The result includes propagation of all statistical errors listed in Table 4.17 as well as statistical error from the data-driven background estimation (Table 4.13) and the 2.2% uncertainty on the luminosity measurement described in 3.3.1.

4.5.4 Combination of channels

The cross section measurement results in each channel are combined, taking into account all the correlations in systematic uncertainties using the Best Linear Unbiased Estimator (BLUE) [88]. The combined cross section, $\sigma(WZ \to 3l)$, is taken to be a linear combination of the measured cross sections in the four channels given in Table 4.18:

$$\sigma(WZ \to 3l) = \alpha_1 \sigma_{WZ\to eee\nu} + \alpha_2 \sigma_{WZ\to ee\mu\nu} + \alpha_3 \sigma_{WZ\to \mu\mu e\nu} + \alpha_4 \sigma_{WZ\to \mu\mu\mu\nu}, \tag{4.13}$$

where α_1, α_2, α_3 and α_4 are weight factors determined by minimizing the variance of σ and subject to the constraint $\sum_{i=1..4} \alpha_i = 1$.

The variance of σ^2 can be expressed as

$$\sigma^2 = \tilde{\alpha} E \alpha, \tag{4.14}$$

where **E** is the error matrix, α is the vector of the weight factors α_i, and $\tilde{\alpha}$ is its transpose. Using the method of Lagrangian multipliers we obtain

$$\alpha = E^{-1}U/(\tilde{U}E^{-1}U), \tag{4.15}$$

where U is a vector whose four components are all unity and E^{-1} is the inverse error matrix.

The error matrix is defined as follows:

$$E = \begin{pmatrix} \sigma_1^2 & \sigma_{12}^{\text{corr}}\sigma_{21}^{\text{corr}} & \sigma_{13}^{\text{corr}}\sigma_{31}^{\text{corr}} & \sigma_{14}^{\text{corr}}\sigma_{41}^{\text{corr}} \\ \sigma_{21}^{\text{corr}}\sigma_{12}^{\text{corr}} & \sigma_2^2 & \sigma_{23}^{\text{corr}}\sigma_{32}^{\text{corr}} & \sigma_{24}^{\text{corr}}\sigma_{42}^{\text{corr}} \\ \sigma_{31}^{\text{corr}}\sigma_{13}^{\text{corr}} & \sigma_{32}^{\text{corr}}\sigma_{23}^{\text{corr}} & \sigma_3^2 & \sigma_{34}^{\text{corr}}\sigma_{43}^{\text{corr}} \\ \sigma_{41}^{\text{corr}}\sigma_{14}^{\text{corr}} & \sigma_{42}^{\text{corr}}\sigma_{24}^{\text{corr}} & \sigma_{43}^{\text{corr}}\sigma_{34}^{\text{corr}} & \sigma_4^2 \end{pmatrix}, \tag{4.16}$$

where the σ_i^2 are variances of the individual WZ cross section measurements and $\sigma_{ij}^{\text{corr}}$ are the correlated components of the uncertainties in those measurements for a combination of channels.

The following cross section systematic uncertainties are taken to be fully correlated between channels:

- The PDF uncertainties on the WZ signal acceptance and efficiency;
- The uncertainty on cross section of subtracted backgrounds which are estimated from Monte Carlo (ZZ and Zγ);
- The uncertainty on MET resolution and energy scale;
- The uncertainty on the minimum bias cross-section used for the pileup simulation

- The uncertainty on electron energy scale (channels with electrons);
- The uncertainty on muon momentum scale (channels with muons);
- The uncertainty on electron reconstruction (channels with electrons);
- The uncertainty on muon identification, isolation and T&P method used in determination of HLT efficiencies (channels with muons);
- The uncertainty on double electron trigger efficiency (channels with $Z \to e^+e^-$);
- The uncertainty on double muon trigger efficiency (channels with $Z \to \mu^+\mu^-$);

The error matrix is constructed from statistical and systematic uncertainties entering diagonal elements and from systematic uncertainties correlated between channels entering non-diagonal elements:

$$E = \begin{pmatrix} 11.7 & 1.05 & 1.19 & 0.87 \\ 1.04 & 9.93 & 0.94 & 0.77 \\ 1.19 & 0.94 & 9.30 & 0.92 \\ 0.87 & 0.77 & 0.92 & 7.67 \end{pmatrix} pb^2. \tag{4.17}$$

Values of the α_{ch} obtained are $\alpha_1 = 0.190$, $\alpha_2 = 0.239$, $\alpha_3 = 0.248$ and $\alpha_4 = 0.323$, giving the combined inclusive WZ cross section

$$\sigma_{incl.WZ} = 20.83 \pm 1.32 \text{ (stat.)} \pm 1.14 \text{ (syst.)} \pm 0.46 \text{ (lumi.) pb} \tag{4.18}$$

The graphical representation of the measured cross section and theoretical cross section estimate of $\sigma_{incl.WZ}(NLO) = 17.8^{+0.7}_{-0.5}$ pb obtained with the MCFM program is shown in Figure 4.7. It is interesting to observe that the result has a small excess over the theoretical prediction between one and two standard deviations (visible in Figure 4.7), however not significant enough to claim disagreement with the Standard Model.

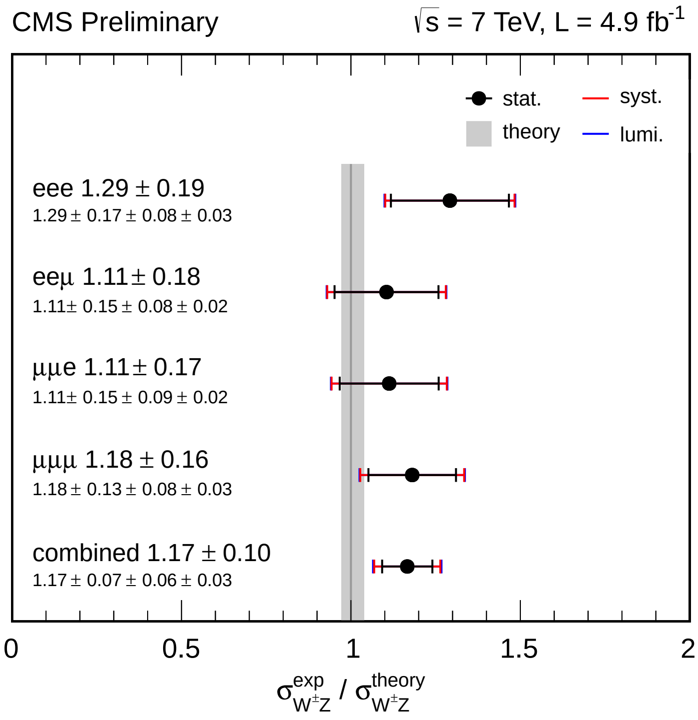

Figure 4.7: Ratio of the measured inclusive cross-section to the theoretical prediction $\sigma^{\text{theo}}_{\text{WZ}} = 17.8$ pb for WZ production at $\sqrt{s} = 7$ TeV.

4.5.5 Other results

Currently WZ production has been observed at the Tevatron and the LHC, as summarized in Table 4.19. After a first definite observation in 2007, the D0 [89] and CDF [90] experiments published their latest results for $p\bar{p}$ $\sqrt{s} = 1.96$ TeV in 2011. Their analysis is performed for the leptonic final states for the integrated luminosity of 4.1 and 7.1 fb^{-1}, respectively. First LHC results were presented by CMS[7] [91] and ATLAS in 2011 for $\approx 1\,\text{fb}^{-1}$ at $\sqrt{s} = 7$ TeV.

The ATLAS Collaboration published an updated 7 TeV measurement in 2012 [92], and in 2013 presented results measured on the 8 TeV data [93]. Results from ATLAS are provided for the $M_Z \in [66, 116]$ GeV window defined as the signal phase space.

Table 4.19: WZ inclusive cross section results from D0 and CDF measured on $p\bar{p}$ collisions at 1.96 TeV, and ATLAS results measured on pp collisions at 7 TeV and 8 TeV.

	$\sqrt{s}$	$\int Ldt$	measured $\sigma_{inclusive}(WZ)[pb]$	theory: $\sigma_{NLO}(WZ)[pb]$
D0	1.96 TeV ($p\bar{p}$)	4.1 fb^{-1}	$3.89^{+1.02}_{-0.85}$(stat. + syst.) $\pm$ 0.31(lumi.)	3.25 ± 0.19
CDF	1.96 TeV ($p\bar{p}$)	7.1 fb^{-1}	$3.9^{+0.8}_{-0.7}$(stat. + syst.)	3.46 ± 0.21
ATLAS	7 TeV (pp)	4.6 fb^{-1}	$19.0^{+1.4}_{-1.3}$(stat.) $\pm$ 0.9(syst.) $\pm$ 0.4(lumi.)	$17.6^{+1.1}_{-1.0}$
ATLAS	8 TeV (pp)	13 fb^{-1}	$20.3^{+0.8}_{-0.7}$(stat.)$^{+1.2}_{-1.1}$(syst.)$^{0.7}_{0.6}$(lumi.)	20.3 ± 0.8

Similar excesses as in the result presented in this thesis were also seen in other charged VV state measurements at ATLAS and CMS [87, 94–96], including the CMS WZ measurement at 8 TeV [79] which used the same phase space and kinematic requirements as this analysis and was presented together with the 7 TeV results. As such small deviations could easily be of statistical nature, more detailed studies and comparisons of different processes will be required, including studies at higher collision energies.

A summary of the measured cross sections of electroweak processes by the CMS Collaboration is shown in the Figure 4.8.

---

[7] Measurements presented in this thesis are a continuation of the work on the first WZ cross section measurement at CMS.

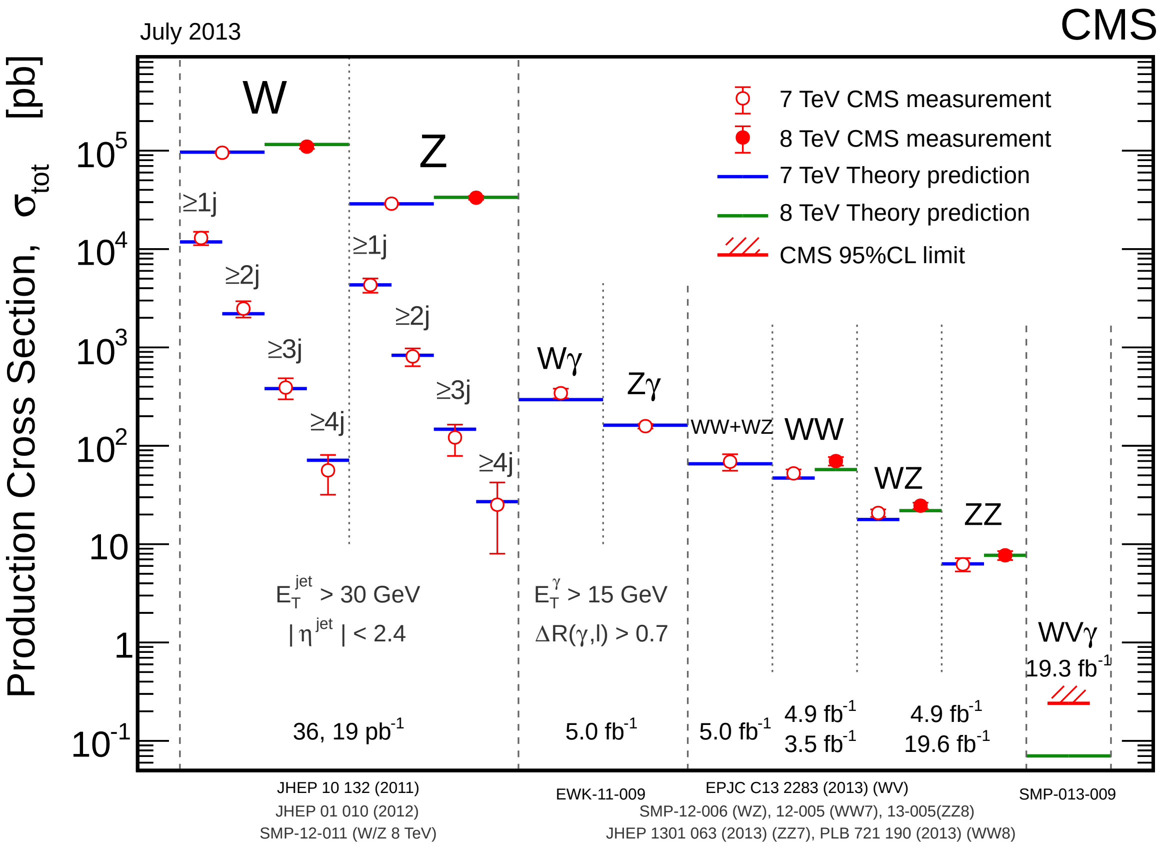

Figure 4.8: A summary of the cross sections of electroweak and multiboson processes measured by CMS.

Chapter 5

Search for WZ resonances

This Chapter presents a search for WZ resonances in the scope of the SSM and Technicolor models. Chronologically, the analysis was developed during 2011 and was finalized prior to the cross section measurement. While both share a similar approach, the cross section analysis was updated and refined in many aspects and some differences will be discussed. Results presented in this Chapter have been published in 2012 [97].

The analysis tests multiple hypotheses of the WZ resonance mass (*mass points*) in terms of SSM and Technicolor models. Some of the selection criteria are optimized for each case. For mass regions where an upper limit can be set on the cross sections for WZ resonance production, models predicting the production of a heavy WZ resonance can be excluded if the predicted cross section is larger than the limit.

5.1 Signal definition

Heavy WZ resonances share a common final state signature with the Standard Model WZ process, resulting in W and Z boson decays. This analysis, as the cross section measurement, is performed in the context of leptonic decays of the WZ pair. However due to potentially high mass of the hypothetical new resonances, both the overall process cross section and the kinematic phase space of the final state will generally differ, opening up possibilities to further optimize the selection. Unlike in the Chapter 4, Standard Model WZ production is considered as background in scope of this search.

The PYTHIA [98] generator implements Monte Carlo simulation for both SSM and Technicolor (LSTC) models (see 2.3). The resulting kinematic distributions for the ρ_{TC} and $\mathrm{W}'$are similar and the PYTHIA W'implementation was used to for the simulation of both models[1].

For the W'search, a set of samples covering a total of fifteen different mass points between 200 GeV and 1500 GeV were generated. As PYTHIA includes only leading order (LO) matrix element calculation, it results in an underestimated cross section. Therefore, the NNLO correction factors (k-factors)

$$k = \frac{\sigma_{NNLO}}{\sigma_{LO}} \tag{5.1}$$

are applied to the cross section of each mass point. A summary of W'cross section values and k-factors for the studied mass points is shown in Table 5.1.

For the Technicolor search, the identical set of samples was used, however assuming the LSTC Technicolor cross sections. The LO cross section value was estimated by PYTHIA for various

---

[1] Technicolor implementation in PYTHIA suffers from errors in the implementation leading to incorrect fraction of longitudinally polarized techni-hadrons.

Table 5.1: An overview of the $\mathrm{W}' \rightarrow WZ \rightarrow \ell\nu\ell\ell$ signal samples considered in this analysis, giving the W' mass along with the associated leading order (LO) and next-to-next-to-leading order (NNLO) cross sections in the SSM. The cross sections include the branching ratios for the bosonic decays into charged leptons (e, μ, or τ).

$M(\mathrm{W}')$ [GeV]	σ_{LO} (pb)	σ_{NNLO} (pb)	k-factor
200	1.324	1.797	1.357
250	1.118	1.517	1.357
300	0.6337	0.8599	1.357
400	0.204	0.2768	1.357
500	0.07915	0.1074	1.357
600	0.0362	0.0489	1.351
700	0.01806	0.0244	1.352
800	0.009857	0.01328	1.347
900	0.005551	0.00744	1.341
1000	0.003322	0.00442	1.332
1100	0.002041	0.002704	1.325
1200	0.001289	0.001690	1.311
1300	0.0008333	0.001082	1.298
1400	0.0005395	0.000690	1.279
1500	0.0003606	0.000456	1.265

LSTC parameter space configurations, and the k-factor was applied on the cross section of each mass point. The cross section is affected by the branching ratios of techni-hadron decays to WZ, BR($\rho_{TC} \rightarrow WZ$), which strongly depends on the relation between $M(\rho_{TC})$ and $M(\pi_{TC})$. When $M(\rho_{TC}) > M(\pi_{TC})$ the WZ branching ratio is below 10% while it is nearly 100% if $M(\rho TC) < M(\pi_{TC}) + M(W)$. For this analysis, the assumed parameter space is respecting the relation

$$M(\pi_{TC}) = \frac{3}{4}M(\rho_{TC}) - 25\,\mathrm{GeV}. \tag{5.2}$$

This parameter space, also known as *Les Houches* parameter set. was used in previous CMS investigations [51]. In addition, the result is evaluated for dependence on other relations of the $M(\rho TC)$ and $M(\pi_{TC})$ and several configurations of the $\sin\chi$ parameter. The list of parameters used per mass point for Technicolor is reported in Table 5.2.

Table 5.2: Parameter sets of the Technicolor signal samples. BR refers to the product of the branching ratios of the ρ_{TC}/a_{TC} to WZ, and the subsequent decay of W and Z to electrons, muons, or τ leptons.

$M(\rho_{TC})$ = $M(\omega_{TC})$[GeV]	$M(a_{TC})$[GeV]	$M(\pi_{TC})$[GeV]	$\sigma_{\text{LO}} \times BR$(pb)	$\sigma_{\text{NNLO}} \times BR$(pb)
200	220	125	0.3872	0.5254
250	275	163	0.2144	0.2909
300	330	200	0.09616	0.1305
400	440	275	0.02889	0.03920
500	550	350	0.01172	0.01590
600	660	425	5.612×10^{-3}	7.582×10^{-3}
700	770	500	2.943×10^{-3}	3.979×10^{-3}
800	880	575	1.670×10^{-3}	2.249×10^{-3}
900	990	650	0.974×10^{-3}	1.306×10^{-3}

5.2 Analysis objects

Unlike in the cross section analysis, different selection requirements were applied on leptons associated to the W and Z decays. A more relaxed *loose* selection criteria is required on leptons building the Z boson candidate, while the stricter (*tight*) criteria are required on a lepton building the W candidate [2]. This approach is warranted by efficient removal of backgrounds without a Z boson, for which the Z built from loose leptons, and the Z mass window constraint are efficient rejection criteria. This is not the case for the $W \to l\nu$ selection, where there is high probabil-

---

[2] This definition of loose and tight criteria should not be confused with the relaxed criteria used for the data-driven background estimation in Chapter 4.

ity of selecting a misidentified jet. The tight lepton selection is thus made stricter to reduce this probability.

5.2.1 Muons

Muon identification, with the exception of isolation (where the loose and tight criteria are set), is identical to the approach described in 4.2.

5.2.2 Electrons

The multivariate electron identification described in 4.2 was introduced for the cross section measurement, while this analysis is based on an older, *cut-based*, approach. Such approach, unlike the multivariate methods, does not exploit correlations between variables and is generally considered less efficient.

Electrons must lie within the detector acceptance ($|\eta| < 2.5$), and satisfy several criteria. Electrons found within $\Delta R < 0.01$ of a muon are removed from the analysis. The constraints are placed on $\sigma_{i\eta i\eta}$, $\Delta\phi_{in}$, $\Delta\eta_{in}$) and E_{HCAL}/E_{ECAL}, the identical variables as in 4.2.2. To suppress photon conversion to electron-positron pair, the track must not have any missing hits before the first measured hit in the inner tracker. For electrons assigned to W, there is also a veto if additional tracks are found within 0.2 mm of the candidate track or their angular separation θ is not sufficient to satisfy the requirement $\Delta cot(\theta) > 0.02$. Electrons found within $\Delta R < 0.01$ of a muon are removed from the analysis due to high probability that they are false candidates built out of a muon track and the ECAL deposit. The full summary of electron selection requirements is given in Table 5.3.

5.2.3 Lepton isolation

Compared to the electron and muon isolation treatment described in 4.2.2 and 4.2.1 of the previous Chapter, the particle flow algorithm is not used. Instead, the isolation variable is calculated from separate contributions from several subdetector systems (*detector-based* isolation). The approach is identical for both electrons and muons, differing only in the selection imposed on the isolation variable. The transverse energy contributions are summed if found within a geometrical cone ($\Delta R < 0.3$) around each electron or muon candidate trajectory. This includes tracks in the inner tracker and energy deposits in ECAL and HCAL. The sum can be written as

$$E_T^{iso} = \sum_i^{tracker} p_{\mathrm{T}}(i) + \sum_i^{ECAL} E_{\mathrm{T}}(i) + \sum_i^{HCAL} E_{\mathrm{T}}(i) \tag{5.3}$$

and the isolation is normalized to the lepton transverse momentum, $Iso_{rel} = E_T^{iso}/p_{\mathrm{T}}(l)$.

The isolation is sensitive to pileup as additional interactions lead to more background activity. Detector based isolation is in particular more sensitive than particle flow based approach, and a correction has to be used to ensure a more stable efficiency with respect to the number of pileup interactions. The FASTJET algorithm [99, 100] is used to calculate the average energy density from jets coming from the pileup and underlying event, which is then integrated over the same ΔR cone and subtracted from the isolation variable. The FASTJET algorithm was however found to overcorrect the isolation variable, leading to a worse background rejection performance. A smaller effective cone was therefore chosen for the corrected isolation:

$$Iso_{rel}^{corr} = Iso_{rel} - \rho \cdot \pi R^2 \tag{5.4}$$

where the optimal values of the effective area R were estimated to be $R = 0.18$ (barrel) and $R = 0.19$ (endcaps). The effects of pileup and correction of the isolation variable are shown in Figure 5.1.

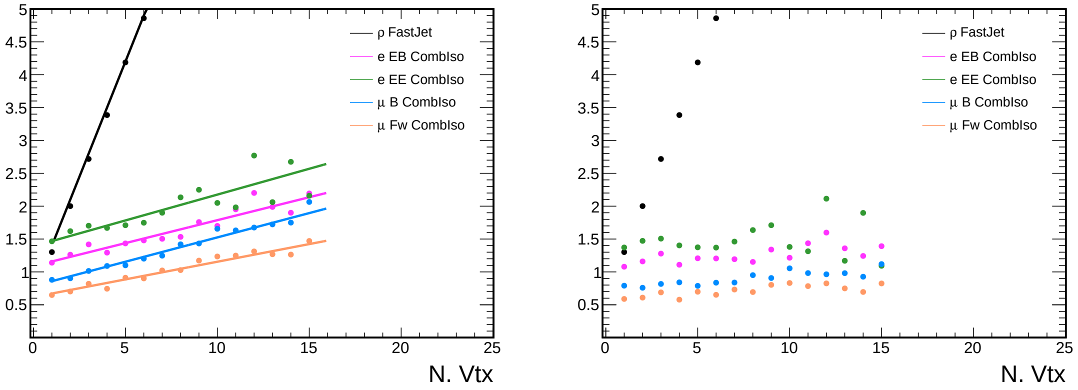

Figure 5.1: Mean value of the combined isolation variable as a function of the number of reconstructed primary vertices before and after the pileup correction. The black line is a fit to the energy density ρ as obtained from the FASTJET [99, 100] algorithm which is used to subtract the pileup contribution.

The selection criterion imposed on Iso_{rel}^{corr} varies depends on the lepton being assigned to the Z or W boson candidate in the selection process. For muons from a Z decay, the relaxed (loose) requirement $Iso_{rel}^{corr} < 0.15$ is used, and for a muon from W decay the stricter (tight) requirement $Iso_{rel}^{corr} < 0.10$ is used. Isolation requirements imposed for electrons vary also by the ECAL region and are summarized in Table 5.3.

Table 5.3: Electron selection requirements.

	electrons from Z	electrons from W
requirement	barrel (endcaps)	barrel (endcaps)
kinematic	$p_{\mathrm{T}} > 10$ GeV $\|\eta\| < 2.5$	$p_{\mathrm{T}} > 20$ GeV $\|\eta\| < 2.5$
max. $\sigma_i\eta i\eta$	0.012(0.031)	0.010(0.31)
max. $\|\Delta\phi_{in}\|$	0.8(0.7)	0.027(0.021)
max. $\|\Delta\eta_{in}\|$	0.007(0.011)	0.005(0.006)
max. track missing hits	0	0
min. distance between tracks(cm)	-	0.02
min. $\Delta cot(\phi)$ between tracks	-	0.02
max. Iso_{rel}^{corr}	0.15(0.10)	0.07(0.06)

5.2.4 Transverse missing energy

The transverse missing energy is reconstructed using the particle flow algorithm, as described in 3.3.2. Unlike in the cross section analysis, the particle flow $E_T^{miss}$was not corrected for the jet energy scale.

5.3 Event selection

5.3.1 Data and Monte Carlo samples

The data samples used in this analysis are identical to the ones used in the cross section measurement (see 4.3.1). A slightly different selection of valid detector runs was used, corresponding to a integrated luminosity of approximately 5.0 fb^{-1}.

The set of Monte Carlo simulation samples for backgrounds is identical to the one used in cross section analysis (see Table 4.4 in Section 4.3.1), while the used signal samples simulating W' and Technicolor are described in Section5.1.

MC simulation samples are reweighted in order to reproduce the distribution of number of pp interactions per bunch-crossing (pileup) observed in data, using the method similar to the one described in Section 4.3.2. The difference from the cross section analysis is that the earlier recommendation of the minimum bias cross section was $\sigma_{pp} = 73.5pb$. Also, an older reweighting algorithm is used, differing in the detail of how the realistic number of vertex interactions is extracted from Monte Carlo samples[3].

5.3.2 Summary of event selection criteria

The list of the required trigger (HLT) paths is nearly identical as in the cross section analysis, with the only exception of omitting the calorimeter-only double-electron HLT path in this analysis. The Z candidate is built from the two opposite-sign same flavor leptons which satisfy loose electron or muon selection, and the candidate is valid only if the type of the passing double lepton trigger corresponds to the flavor of Z constituents. In case of multiple possible candidates, the one whose mass is closest to the nominal Z boson mass is selected. It is required that the Z candidate invariant mass lies $[60, 120]$ GeV window.

In contrast to the cross section analysis, leptons building the Z candidate are required to geometrically (within $\Delta R < 0.1$ cone) match corresponding lepton objects constructed by the HLT and used in the trigger selection. Threshold for the matched HLT lepton objects are set to be 17 and

---

[3] Comparison between the two methods established that they produce nearly identical result.

8 GeV for the leading and trailing lepton, respectively. Since the trigger matching has certain efficiency, it is measured using the T&P method and corresponding scale factors (see Section 4.3.2) are calculated. This is detailed in Section 5.5.

Another significant difference to the cross section analysis is the rejection veto. Instead of rejecting events with more than three identified good leptons, a less strict approach is used, rejecting only events where a second Z candidate with the invariannt mass within the $[60, 120]$ GeV window can be constructed out of remaining leptons. In this case, the loose selection is required on these additional leptons and $p_{\mathrm{T}} > 10$ is required on both candidates building the second Z boson. These leptons are not required to be matched to leptons used in the trigger selection.

The W candidate is built using leptons remaining after the Z selection step, if they satisfy the tight selection. The candidate with the highest p_{T} is selected in case of multiple remaining leptons. The ΔR separation between leptons building Z and W is not imposed in this analysis.

The missing transverse energy (E_T^{miss}) computed with the particle flow algorithm, is required to be above 30 GeV.

5.3.3 Suppression of the WZ background

While the previous selection steps are favoring the common final state signature of both the Standard Model WZ and heavy WZ resonances, it is ultimately necessary to efficiently suppress the SM WZ background.

One of these differences is that final state particles from a heavy WZ resonance decay can carry a large amount of transverse momentum. Therefore the scalar sum of charged lepton momenta is used as an additional selection requirement in the analysis:

$$L_T = \sum_{i=1...3} |\vec{p}_T(l_i)|, \tag{5.5}$$

The mass of the WZ resonance is another important distinguishing factor. However, while kinematics of the Z boson and a W charged lepton can be precisely determined, the neutrino longitudinal momentum p_z^ν can not be measured in proton-proton collisions as the p_z of all escaping particles in a pp collision is not reconstructed. Therefore, it is impossible to fully reconstruct the WZ mass. However it still considered useful if any approximate measure of the WZ mass could be extracted to identify events with very large resonant mass. A method was developed to estimate the WZ mass, assuming that the mass of the W boson in the event is known. This assumption leads to a quadratic equation for p_z^ν, which has real solutions in case of a choice of the nominal W boson mass ($M_W = 80.385$ GeV) if the reconstructed transverse W mass:

$$M_T(W) \equiv \sqrt{2 \cdot |E_T^{miss}| \cdot |p_T^{lepton}| \cdot (1 - \cos\Delta\phi(p_T^{lepton}, E_T^{miss}))} \tag{5.6}$$

is smaller than the nominal W boson mass. When the reconstructed $M_T(W)$ is larger than the nominal mass, the M_W choice which leads to real solutions is used: $M_W = M_T(W)$. It was found from a Monte Carlo simulation study that in 75% of the cases the solution with lower magnitude corresponds to the p_z^ν.

Since the efficiency of the L_T and the WZ mass window requirements strongly depends on the mass hypothesis of the WZ resonance, these requirements were optimized separately for each mass point. The optimization is performed in steps of 10 GeV in the value of WZ mass window edges and the L_T requirement. The method varies requirements on both variables until the optimal working point is found. In this case the full calculation of the expected limit was used as a criterion for finding a combination providing the best limit (the limit finding procedure is later described in 5.6). In the higher mass range ($M_{WZ} > 800$ gev) the fluctuations due to low statistics limit the effectiveness of optimizing the L_T requirement. A fixed requirement of $L_T > 400$ GeV at higher masses is therefore used. The full set of optimized WZ mass window and L_T requirements is shown in Table 5.9.

The distribution of the reconstructed invariant WZ mass for the mass point $M_{\mathrm{W}'} = 600$ GeV is shown in Figure 5.2.

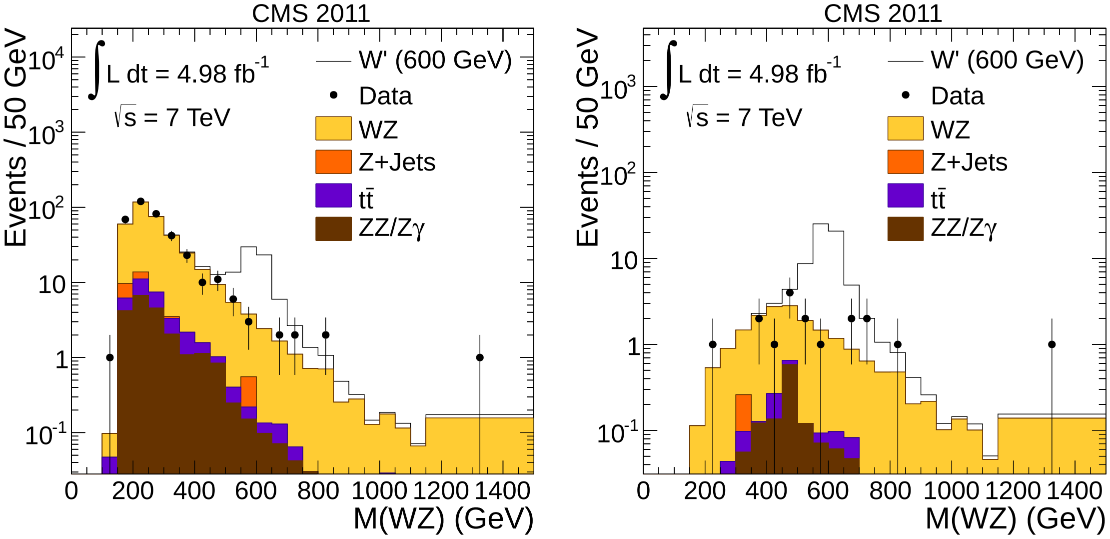

Figure 5.2: Distribution of the WZ invariant mass (left) before application of the L_T requirement and (right) after applying the L_T requirement ($L_T > 290$ GeV) for the W' mass point at 600 GeV.

5.4 Lepton efficiency measurement

This section describes measurements of the lepton selection efficiencies in data and Monte Carlo simulation, done with Tag and Probe method with the goal of obtaining data over Monte Carlo correction factors (scale factors) for the lepton reconstruction and identification.

Tag and Probe is a technique based on the analysis of leptonic Z decays, where the Z boson constituents are treated asymmetrically; There is a *tag*, lepton selected with strong selection criteria, and a *probe*, with the same flavor and opposite sign of the tag, on which arbitrary selection criteria are applied with the goal of measuring their efficiency. A mass window around the nominal Z mass is required, after which backgrounds of the Z process are largely suppressed.

It is possible to estimate the Z boson signal from the remaining background contributions by a fitting procedure, where the non-resonant background shape is parametrized by an exponential function and the resonant Z mass distribution shape is parametrized using the Gaussian function (it is also possible to use the Breit-Wigner function). The overall scale and the scale ratio of these functions is scaled until the sum of the two contributions reaches the best fit with the overall distribution (minimal χ^2). After fitting, the integral of the Z shape is taken as the signal event count. The procedure is performed before and after applying the selection requirement on probe so that the ratio of these two signal integrals measures selection efficiency.

Special HLT paths are used to select data and MC samples for tag and probe fits. In order not to bias the probe, minimal or no requirements must be imposed on a secondary object selected by the HLT path. The path used for electron measurements requires a combination of a super cluster and a more tightly selected electron in HLT[4]. The efficiency of finding a super-cluster is nearly 100% and only minimally biases probes. For muons, several single muon HLT paths are used. In all cases, the tag lepton is always required to be matched to a HLT electron or muon object.

For muons, the reconstruction efficiency in tracker or muon system (*stand-alone*) is measured, as well as the identification, isolation and HLT matching efficiencies, applied on the probe in respective order. The results are reported in Table 5.5.

The measurement of electron reconstruction efficiency was performed for electrons with $E_{\mathrm{T}} > 20$ GeV in different pseudorapidity bins. The results are presented in Table 5.4. A very good agreement is seen between data and Monte Carlo efficiencies. The scale factors are averaged over the η bins using the momentum distribution of electrons decaying from W and Z bosons in the WZ MC sample and the value of $\rho^{ele}_{RECO} = 0.997$ is obtained[5].

Table 5.4: Electron reconstruction efficiencies in different η regions on data and MC. Efficiencies are in %. Systematic uncertainties are added in quadrature in the given data/MC ratios.

	data	MC	$\left(\frac{\mathrm{Data}}{\mathrm{MC}}\right)$
$0 < \lvert\eta\rvert \leq 0.78$	$97.0 \pm 0.11(stat.) \pm 0.98(syst.)$	$98.08^{+0.03}_{-0.04}$	0.999 ± 0.010 (stat. + syst.)
$0.78 < \lvert\eta\rvert \leq 1.444$	$97.35^{+0.17}_{-0.19}(stat.) \pm 1.22(syst.)$	97.6 ± 0.04	0.997 ± 0.012 (stat. + syst.)
$1.444 < \lvert\eta\rvert \leq 1.566$	$94.18 \pm 0.57(stat.) \pm 0.12(syst.)$	$95.74^{+0.17}_{-0.18}$	0.983 ± 0.006 (stat. + syst.)
$1.566 < \lvert\eta\rvert \leq 2.0$	$95.24 \pm 0.25(stat.) \pm 0.14(syst.)$	96.0 ± 0.07	0.992 ± 0.003 (stat. + syst.)
$2.0 < \lvert\eta\rvert \leq 2.5$	$93.66^{+0.31}_{-0.32}(stat.) \pm 0.14(syst.)$	93.48 ± 0.1	1.002 ± 0.004 (stat. + syst.)

The measurement of electron identification, isolation and HLT matching efficiencies is presented in Table 5.6.

---

[4] This path is used due to very high E_{T} selection thresholds found in single electron HLT paths excluding most of the Z boson phase space.

[5] In the cross section analysis this factor was not used due to a very consistent agreement between data and Monte Carlo, however the appropriate systematic uncertainty was assigned to the overall scale factor of each electron.

Table 5.5: Muon efficiency values obtained from the T&P fits. For each efficiency, given is the value obtained from data, the value obtained from MC simulation, and the data/MC ratio. Errors are statistical.

efficiency	data	MC	ratio $\left(\frac{\text{Data}}{\text{MC}}\right)$
$\epsilon_{\text{stand-alone}}$	0.984 ± 0.001	0.982 ± 0.005	1.002 ± 0.005
ϵ_{track}	0.989 ± 0.001	0.993 ± 0.005	0.995 ± 0.005
ϵ_{ID}	0.971 ± 0.001	0.977 ± 0.001	0.994 ± 0.001
$\epsilon_{\text{isolation}}$	0.952 ± 0.001	0.925 ± 0.002	1.030 ± 0.002
$\epsilon_{\text{HLT}}(17)$	0.953 ± 0.001	0.949 ± 0.001	1.004 ± 0.001
$\epsilon_{\text{HLT}}(8)$	0.953 ± 0.001	0.949 ± 0.001	1.004 ± 0.001

Table 5.6: Electron efficiency values obtained from the T&P fits. For each efficiency, given is the value obtained from data, the value obtained from MC simulation, and the data/MC ratio. Errors are statistical.

efficiency	data	MC	ratio $\left(\frac{\text{Data}}{\text{MC}}\right)$
$\epsilon_{\text{ID}}(\text{W})$	0.848 ± 0.001	0.849 ± 0.001	0.999 ± 0.001
$\epsilon_{\text{isolation}}(\text{W})$	0.856 ± 0.001	0.817 ± 0.001	1.047 ± 0.002
$\epsilon_{\text{ID}}(\text{Z})$	0.974 ± 0.001	0.976 ± 0.000	0.998 ± 0.001
$\epsilon_{\text{isolation}}(\text{Z})$	0.979 ± 0.001	0.973 ± 0.000	1.006 ± 0.001
$\epsilon_{\text{HLT}}17$	0.958 ± 0.001	0.982 ± 0.000	0.976 ± 0.001
$\epsilon_{\text{HLT}}8$	0.958 ± 0.001	0.982 ± 0.000	0.976 ± 0.001

Using the scale factors listed in this Section, a weight factor is constructed and applied to each MC event, considering leptons building the W or Z candidate. This follows the approach used in the cross section analysis, with a difference that the scale factors are applied as a function of kinematic properties of individual leptons. For all the three leptons, the reconstruction, identification and isolation scale factors are applied. For leptons building the Z candidate, also the HLT matching factor is applied.

5.5 Systematic uncertainties

Every contribution to the systematic uncertainty is estimated for each mass point on the signal and background Monte Carlo simulation sample. The estimate is given as the uncertainty on the number of selected events after the final selection for each mass point, summed over over all (e,μ) WZ channels. Because for W' and Technicolor the same MC simulation sample is used (differing only in the branching ratios), the resulting systematic uncertainty estimates for the two models are identical. Results, for the procedures described in the following, are summarized in Table 5.7.

The uncertainty on the luminosity measurement described in 3.3.1 is 2.2%.

Pileup

The method uses a procedure similar to the description in 4.5.2, with the difference that the varied distributions are obtained by shifting the Poisson mean of the central distribution by $\Delta N_{vtx} = \pm 1$.

Background cross sections

As seen in the Table 5.9, the number of background events is small for higher mass points. Therefore the final version of this analysis did not have a sufficient statistical sample to perform background estimation from data for all mass points[6]. Instead, backgrounds were estimated using Monte Carlo, with the uncertainty assumed on the used cross section. Theoretical cross section uncertainty affecting the ZZ background is estimated using the MCFM [22] program, and the Zγ cross section uncertainty is estimated by the CMS measurement in 2010 [101].

---

[6] The study was, however performed. It is an early version of the study described in 4.4.2.

Table 5.7: Summary of E_T^{miss}, pileup and lepton momentum and energy scale systematic uncertainties for backgrounds (B) and $\mathrm{W}'/\rho_{\mathrm{TC}}$ signal (S) given at each mass point.

Type	E_T^{miss}scale		E_T^{miss}resolution		pileup		muon p_{T} scale		electron E_{T} scale	
mass point(GeV)	B(%)	S(%)	B(%)	S(%)	B(%)	S(%)	B(%)	S(%)	B(%)	S(%)
200	0.99	0.01	0.52	1.9	1.7	0.31	0.45	3.1	1.0	1.9
250	0.24	0.90	0.59	1.3	2.2	0.58	2.5	1.6	3.1	2.5
300	1.1	0.49	0.72	0.97	1.9	2.0	2.2	0.51	4.3	1.3
400	1.7	0.43	0.77	0.53	2.2	0.71	1.9	1.0	4.2	2.2
500	1.8	0.38	0.91	0.36	2.6	2.3	1.7	0.71	3.6	1.5
600	1.3	0.10	1.4	0.30	1.7	1.6	3.1	0.55	4.8	1.6
700	2.4	0.15	1.7	0.23	3.0	0.82	5.3	0.91	4.2	1.7
800	3.9	0.28	1.9	0.20	4.0	1.4	3.9	0.87	4.3	1.7
900	2.3	0.24	1.9	0.13	3.6	1.6	3.0	0.72	6.4	0.94
1000	2.7	0.03	2.4	0.12	0.36	1.4	5.0	0.37	8.7	0.49
1100	1.1	0.16	2.2	0.13	0.83	1.1	2.6	0.15	6.7	0.51
1200	0.16	0.13	2.6	0.12	1.3	1.2	2.8	0.34	13	0.54
1300	0.70	0.10	2.9	0.12	1.3	1.9	4.7	0.12	5.7	0.38
1400	4.7	0.10	3.7	0.14	2.3	1.4	4.2	0.46	8.2	0.85
1500	0.01	0.02	4.2	0.19	0.92	2.6	0.72	0.37	11	1.3

The theoretical cross section uncertainty was also estimated for the WZ background. For this study, the MadGraph generator was used for the WZ process simulation. MadGraph simulates explicit production of additional jets at the matrix element level and is is expected to give a correct kinematic description of the process which includes higher order corrections, and the prediction is only rescaled with a global factor to the total NLO cross section computed with MCFM [102]. To estimate uncertainties from remaining differences between the spectra predicted by MadGraph and true NLO predictions, several kinematic distributions for WZ were compared between MadGraph and MCFM and were found to agree within 10%. As an example, the distribution of the WZ mass is shown in Fig. 5.3.

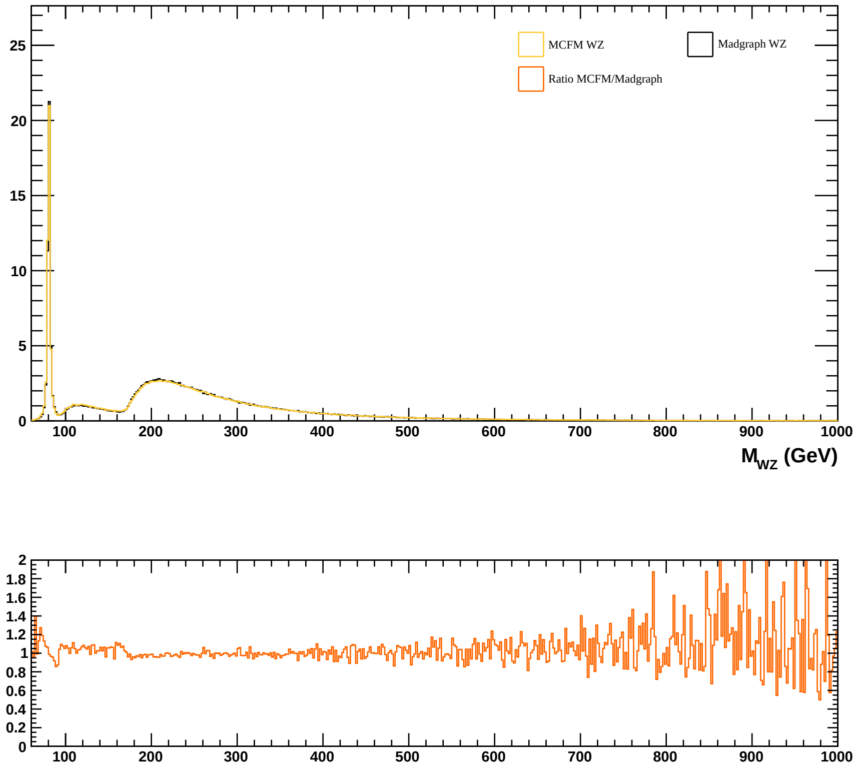

Figure 5.3: Distributions and ratio of the WZ mass spectrum for the electroweak WZ production obtained by MadGraph and MCFM generators.

Transverse missing energy

The E_T^{miss}resolution depends on how well the visible part of the event is measured in the detector and can not be affected by the neutrino itself. The method described in Ref.[103] uses Z→ $\ell\ell$

events where neutrino is simulated by a well measured Z boson. The transverse hadronic recoil vector, measuring the response and resolution of $E_T^{miss}$is defined as

$$\vec{u} = -\vec{\not{E}}_T - \vec{p}_T^{Z} \tag{5.7}$$

where $\vec{p}_T^{Z}$ is determined from generator-level MC information. With perfect resolution it would be $\vec{u} = -\vec{p}_T^{Z}$. The recoil vector is decomposed in the components u_1 and u_2, parallel and orthogonal to $\vec{p}_T^{Z}$, respectively. The mean value of $|u_1|$ measures the E_T^{miss}*response* and the spread of u_1 and u_2 measure the E_T^{miss}resolution. The dependence of $|u_i|$ and σ_{u_i} on p_T^Z is fitted on both data and MC to obtain the uncertainty which is used to vary the WZ hadronic recoil vector in Monte Carlo WZ events

$$\vec{u}_T^{WZ} = -\vec{\not{E}}_T - \vec{p}_T^{Z} - \vec{p}_T^{Wlept} \tag{5.8}$$

A scale shift is applied to $\vec{u}_T^{WZ}$ and $E_T^{miss}$is recomputed in each MC event using eq. 5.8 to calculate the difference in the number of selected events, which is taken as uncertainty on the E_T^{miss}scale.

For the resolution effect, the full event selection is repeated in $O(500)$ pseudoexperiments for each event, where each time the E_T^{miss}recoil in each event is randomly smeared by the resolution uncertainty. Finally, a distribution of the number of events passing the final selection is obtained, and the σ of this distribution is taken as the systematic effect.

For the cross section analysis, the method described here was replaced with the more accurate method, described in Chapter 4.

Lepton selection and trigger matching efficiency

Lepton efficiency scale factors and their respective uncertainties are calculated as described in 5.4. The full uncertainty is obtained by adding in quadrature contributions from reconstruction, identification, isolation and trigger matching. The procedure does not provide individual weights for each event. Instead, contributions from different lepton η and p_{T} bins are weighted using the spectrum of leptons from W and Z decays to estimate the effect.

Lepton momentum and energy scale

A 1% muon momentum scale and 2% electron energy scale uncertainty is assumed. The method for estimating the effect follows the procedure described in 4.5.2. The selection procedure is fully repeated with scaled leptons to calculate the effect on the number of events obtained after final selection.

PDFs

The PDF uncertainty procedure follows the prescription described in 4.5.2. The estimation was in this instance not done on full Monte Carlo simulation samples, but instead using the MCFM program, which does not provide detector simulation. Kinematic requirements on leptons, E_T^{miss}were simulated on true generator-level leptons. The resulting uncertainties for the WZ background and signal at considered mass points are given in Table 5.8.

Table 5.8: PDF uncertainties for the $\mathrm{W}^{'}(\rho_{TC})$ production given at each mass point.

mass (GeV)	PDF uncertainty (%)	
	signal	WZ background
200	2.370	3.2
250	2.370	3.4
300	2.370	3.3
400	2.764	3.2
500	3.181	3.6
600	3.704	4.0
700	4.198	4.7
800	4.624	4.8
900	5.135	6.3
1000	5.695	8.9
1100	6.088	7.8
1200	6.516	12.0
1300	7.349	28.0
1400	7.760	7.8
1500	8.471	0.0

5.6 Selection and search limit results

5.6.1 Event selection results

The final number of selected events for each mass point for the signal and background Monte Carlo samples and in data is shown in Table 5.9. Together with the systematic uncertainty estimation (Table 5.7) these results are used as input in the limit estimation. Monte Carlo event numbers are corrected for the difference in selection efficiency in data and Monte Carlo as described in Section 5.4.

Table 5.9: Minimum L_T requirements and search windows for each W$'(\rho_{TC})$ mass point along with the number of expected background events, observed events and signal efficiency. Errors represent statistical and systematic uncertainties combined in quadrature.

$M(\mathrm{W}'/\rho_{TC})$ (GeV)	L_T (GeV)	WZ mass window (GeV)	N_{Bkg}^{MC}	data	ϵ_{sig} (%)
200	0	190-210	50.0 ± 9.1	52	8.0 ± 0.4
250	150	230-270	34.1 ± 6.2	40	8.8 ± 0.4
300	160	280-320	23.9 ± 4.5	23	18 ± 1
400	220	360-440	12.8 ± 2.4	7	29 ± 1
500	230	450-550	8.1 ± 1.5	9	41 ± 1
600	290	540-660	3.4 ± 0.7	2	45 ± 1
700	360	620-780	1.79 ± 0.38	2	48 ± 1
800	400	710-890	1.02 ± 0.22	1	52 ± 2
900	400	760-1040	1.03 ± 0.23	0	61 ± 2
1000	400	820-1180	0.77 ± 0.19	0	65 ± 2
1100	400	890-1310	0.55 ± 0.13	0	63 ± 1
1200	400	940-1460	0.42 ± 0.11	0	58 ± 1
1300	400	1020-1580	0.34 ± 0.12	0	50 ± 1
1400	400	1110-1690	0.18 ± 0.05	0	36 ± 1
1500	400	1200-1800	0.13 ± 0.04	0	30 ± 1

5.6.2 Statistical approach

The statistical technique used to set cross section limits is the CL$_S$ [104], implemented as part of the RooStats [105] software package.

The expected limit will be affected both by the statistical uncertainties and systematic uncertainties on any significant "nuisance parameters". The latter are quantities which affect the result. In this measurement, the nuisance parameters are the luminosity, and the detector acceptance and efficiency.

The method introduces likelihoods (L) which assume either the presence of signal and background (S+B) or of background only (B). For a finite sample of $n*$ events, the likelihood under both hypotheses, S and S+B, is computed and the logarithmic ratio of the two, LLR $\equiv -2\ln L$(S+B)$/L$(B), is taken. The expected distribution of LLR values under both hypotheses is then obtained in the following way in two steps by generating pseudo-data sets corresponding to the luminosity used in the data. Each of the nuisance parameters is first smeared by a Gaussian distribution whose variance is set to be equal to the systematic uncertainty on the parameter, as listed in Table 5.7. The number of events is then generated according to a Poisson distribution for both signal and background samples[7].

For a tested n^*, one can obtain the probability to see more events than n^* under the B hypothesis (1-CL$_B$), or to see less events under the S+B hypothesis (CL$_{S+B}$), by performing integration over the respective log-likelihood distributions. The confidence level for the upper limit on the number of signal events n_s is then $1-$ CL$_S$, where the CL$_S$ is:

$$\mathrm{CL}_S = \frac{\mathrm{CL}_{S+B}}{\mathrm{CL}_B}. \tag{5.9}$$

By convention, the confidence level used for exclusion limits is 95$\%$. The largest value of n_s for which CL$_S$ is below 5$\%$ is taken as the upper limit on the number of signal events at confidence level of 95$\%$. The limit on n_s is converted to a limit on the signal cross section by scaling appropriately by luminosity, acceptance and branching ratio.

For this measurement, the expected limit is obtained using the background only hypothesis. $O(1000)$ pseudoexperiments are performed for each mass point, In each pseudoexperiment,

---

[7] For the B only hypothesis, the number of expected signal events is zero.

the number of background events (N^{*}_{exp}) is chosen from the background distribution, which is generated from a Poisson distribution as described above after smearing the value of nuisance parameters. For the Poisson mean, the expected number of background events obtained after selection is taken. N^{*}_{exp} represents a sum of signal and background ($N^{*}_{exp} = n_b + n_s$) on which the CL$_S$ method is applied. The upper limit on n_s at 95% confidence level is then found for each pseudoexperiment. From the n_s limit distribution obtained from all pseudoexperiments, the expected limit is taken as a median value of the distribution, while the width of the distribution is used to extract its $\pm 1\sigma$ and $\pm 2\sigma$ uncertainty bands (usually drawn in green and yellow color, as seen in Figure 5.4). To estimate the observed limit, the same approach is used, assuming instead that the observed number of events represents a sum of background and signal: $N_{obs} = n_b + n_s$.

In practice, instead of the CL$_S$ method, a less computationally intensive Bayesian method is used (the approach is described in [106]), as it is suitable for measurements where there is a good agreement between observation and background expectation. For the results presented in this thesis it was found to estimate negligibly different limits from the ones estimated with the CL$_S$ method.

5.6.3 Limit results

The W$^{'}$cross section upper limit set for the sensitive mass range is shown in Figure 5.4. The sensitivity boundary, under which the observed cross section limit becomes lower than the cross section expected under signal hypothesis, sets the lower limit on the mass of W$^{'}$at $M_{\mathrm{W}'} > 1143$ GeV.

Technicolor limits for various parameter space configurations of $M(\rho_{TC})$ and $M(\pi_{TC})$, as discussed in Section 5.1, are shown in Figure 5.5. Limits were obtained by applying the branching

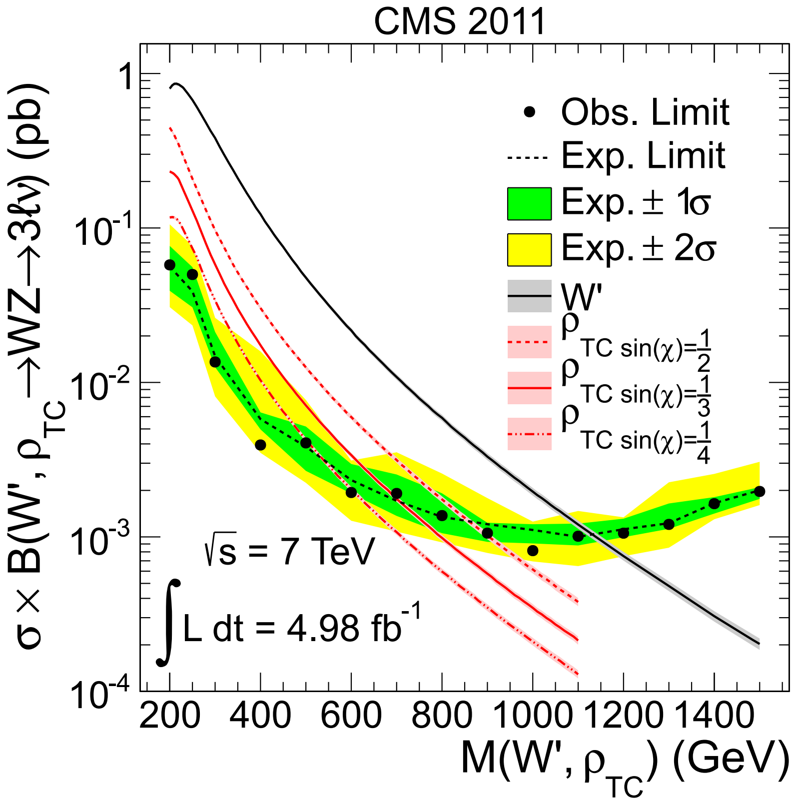

Figure 5.4: W$'$ and ρ_{TC} cross section limits for the observed and expected (background) events, and the expected signal cross section with the theoretical uncertainty band. The theoretical ρ_{TC} cross section is given for the three values of $\sin\chi$ with the $\sin\chi = 1/3$ being the nominal value of the model.

ratio rescaling dependent on the model parameters, under the assumption that kinematic properties of the final state, and thus acceptance, are not affected.

For the reference phase space ($M(\pi_{TC}) = \frac{3}{4}M(\rho_{TC}) - 25$ GeV), ρ_{TC} hadrons are excluded for $M(\rho_{TC})$ between 167 GeV and 687 GeV. For the parameter space chosen by the D0 experiment ($M(\rho_{TC}) < M(\pi_{TC}) + M(W)$), the result is the $M(\rho_{TC})$ exclusion between 180 GeV and 938 GeV.

The Figure 5.4 shows sensitivity dependence for the three $\sin\chi$ Technicolor parameter values, $\sin\chi = 1/2, 1/3$ and $1/4$, which can affect the branching ration of $\rho_{TC} \to WZ$, as recently proposed [107]. The $\sin\chi = 1/3$ is assumed as nominal value of the model.

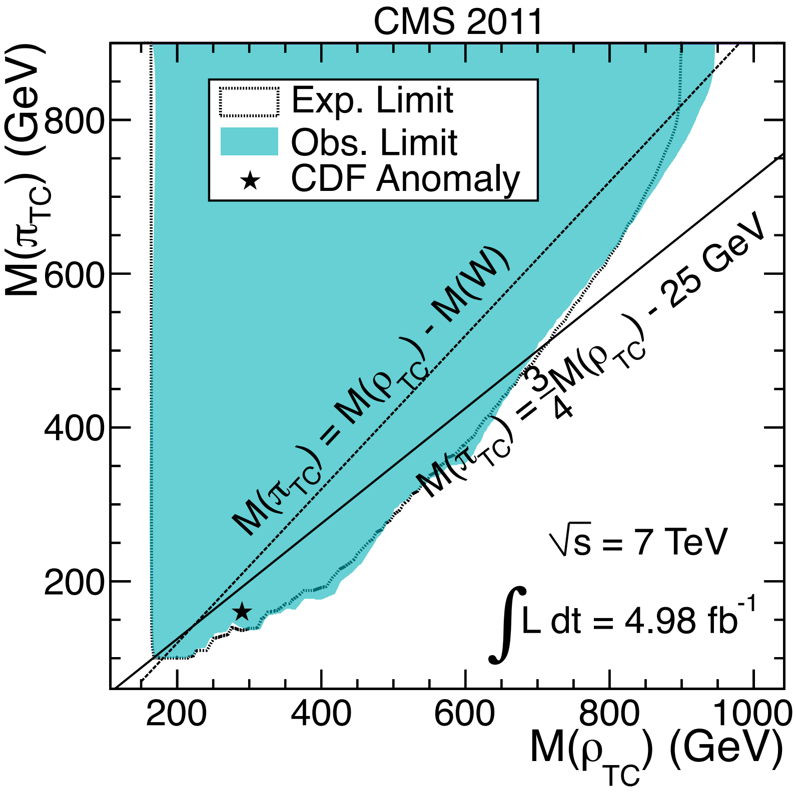

Figure 5.5: ρTC cross section limits for the expected (background) and observed number of events. Various phase space combinations are produced by varying the branching ratio according to model predictions.

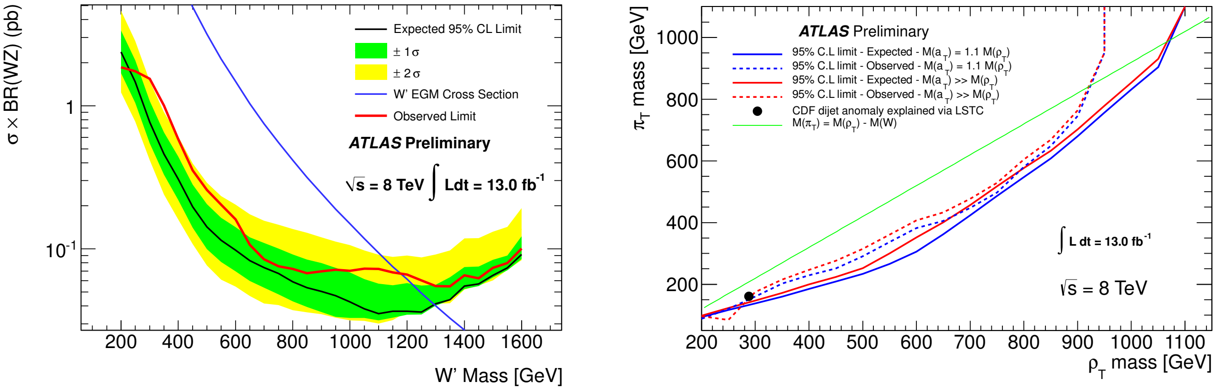

Figure 5.6: ATLAS $\sqrt{s} = 8$ TeV W$'$limits (left) and limits on the $M(\rho_{TC})$ and $M(\pi_{TC})$ parameter space(right).

5.6.4 Other results

The search for SSM W$'$and Technicolor signature was studied extensively by the D0 Collaboration [35] in addition to the cross section measurement. The limit calculation procedure depends on the reconstructed WZ system transverse mass. This results in an exclusion of W$'$masses within between 188 GeV and 520 GeV. In the Technicolor interpretation, the excluded $M(\rho_{TC})$ region is between 208 GeV and 408 GeV for the parameter space $M(\rho_{TC}) < M(\pi_{TC}) + M(W)$.

The CDF Collaboration observed in 2011 a peak in the $M(jj)$ distribution in the W+jj channel dubbed the "CDF anomaly" [108]. The possible Technicolor interpretation [109] is excluded by the CMS result presented in this thesis.

ATLAS has currently published $\sqrt{s} = 8$ TeV Technicolor and SSM W$'$search results in the WZ channel for the 13 fb^{-1} [110] of data. W$'$bosons are excluded for masses up to 1180 GeV and ρ_{TC} for masses up to 920 GeV, including the parameter space configuration $M(\rho_{TC}) < M(\pi_{TC}) + M(W)$ and $M(\rho_{TC}) = 1.1M(a_{TC})$ or $M(\rho_{TC}) >> M(a_{TC})$. Limits are shown in Figure 5.6.

The analysis similar to the one described in this thesis was performed on the 8 TeV dataset of 19.6 fb^{-1} collected by CMS, excluding the W'mass between 170 and 1450 GeV and setting also new limits on the ρ_{TC} mass (detailed in ref.[111]).

Chapter 6

Conclusion

The inclusive cross section of WZ production was measured using the full 2011 dataset collected by CMS. The measureed inclusive cross section $\sigma_{incl.WZ} = 20.83 \pm 1.32$ (stat.) $\pm$ 1.14 (syst.) $\pm$ 0.46 (lumi.) pb exhibits a small excess over the theoretical prediction of $\sigma_{incl.WZ}(NLO) = 17.8^{+0.7}_{-0.5}$ pb. This result is interesting because of a similar excess seen by ATLAS and CMS in several charged VV states: WW [94, 95], Wγ [87, 96] and WZ [79, 92]. Thus it will be important to perform further studies, including measurements at higher collision energies.

The search for the signature of Technicolor ρ_{TC} and SSM W' in WZ mode has not resulted in any sign of excess over Standard Model prediction. The limit on the mass of heavy resonances was set in scope of SSM and Technicolor as the 95% C.L. exclusion limit, excluding $M(W')$ below 1143 GeV and excluding $M(\rho_{TC})$ between 167 and 687 GeV for the parameter space used in previous

CMS searches, and between 180 and 938 GeV for the parameter space previously analyzed by the D0 Collaboration.

Poglavlje 7

Prošireni sažetak: Mjerenje produkcije parova W i Z bozona i potraga za njihovim rezonancijama na Velikom hadronskom sudarivaču

7.1 Uvod

Kao fundamentalna teorija čestičnih interakcija, Standardni model do sada je bio potvrđivan u mnogim eksperimentima fizike čestica s velikom preciznošću. Stoga se može tvrditi da je ta teorija točan opis čestičnih interakcija na do sada ispitanim skalama energije. S druge strane, mnoga opažanja, posebno astrofizička i kozmološka, detektirala su pojave koje se ne mogu objasniti unutar

Standardnog modela. I sama gravitacija do sada nije bila uspješno integrirana u model. Također, nije razjašnjeno porijeklo tamne materije za koju unutar Standardnog modela ne postoje prikladni čestični kandidati, kao ni uzrok asimetrije materije i antimaterije u svemiru.

Neka od centralnih predviđanja Standardnog modela, kao što je postojanje Higgsova bozona, do nedavno nisu bila eksperimentalno potvrđena. Veliki hadronski sudarivač (LHC od eng. *Large Hadron Collider*) primarno je sagrađen da bi se pronašla ta zadnja karika modela. No LHC-ova je namjena također, osim provjere valjanosti Standardnog modela, i provjera velikog broja teorijskih predviđanja fizike izvan Standardnog modela na TeV-skoj skali.

Modovi produkcije više baždarnih bozona precizno su predviđeni unutar Standardnog modela. Stoga je za potvrdu Standardnog modela izuzetno važno izmjeriti njihov udarni presjek na LHC energijama. Posebno je zanimljivo mjerenje jačine međusobnih vezanja baždarnih bozona jer ona mogu biti osjetljiva na doprinose fizike izvan Standardnog modela čak i ako se ona izravno manifestira tek na višoj skali energije, izvan dosega LHC-a. Uz to, moguće je vršiti i izravne potrage za teškim rezonancijama koje se raspadaju u dibozonska konačna stanja.

U ovom radu predstavljena su dva važna rezultata mjerenja protonskih sudara CMS detektorom na LHC-u na energiji sustava centra mase $\sqrt{s} = 7$ TeV-a. Izmjeren je udarni presjek produkcije parova W i Z bozona čije je postojanje predviđeno unutar Standardnog modela. Također su prezentirani rezultati potrage za teškim rezonancijama, predviđenim unutar Tehnikolor modela i Sekvencijalnog standardnog modela, koje se raspadaju u WZ par te su postavljena ograničenja na predviđanja tih modela.

7.2 Teorijski pregled

Standardni model (SM) fizike čestica razvijen je na osnovama relativističke kvantne teorije polja. Uključuje svo današnje znanje o prirodi elementarnih čestica i njihovih interakcija kroz tri od četiri fundamentalne sile (elektromagnetizam, jaka sila i slaba sila). SM ujedinjuje slabu silu i elektromagnetizam, a postojanje mase objašnjeno je Higgsovim mehanizmom [1–4]. 70-ih godina prošlog stoljeća, formirana je kvantna elektrodinamika (QCD od eng. *Quantum Chromodynamics*) koja opisuje jaku interakciju.

U SM-u se interakcije pojavljuju uvođenjem baždarne simetrije. Kvantna elektrodinamika (QED od eng. *Quantum Electrodynamics*) je izvedena iz zahtjeva lokalne baždarne invarijantnosti na grupu simetrija $U(1)_{em}$. Ona je integrirana u $SU(2)_L \otimes U(1)_Y$ simetriju elektroslabe interakcije gdje se također pojavljuju baždarna polja. Interakcije u QCD-u proizlaze iz $SU(3)_C$ grupe simetrija. Sveukupno, simetrija SM je

$$SU(3)_C \otimes SU(2)_L \otimes U(1)_Y. \tag{7.1}$$

Elementarne čestice su u fizici polja definirane kao nelokalna kvantna polja s određenim kvantnim brojevima, kao primjerice naboj. Prema spinu, dijele se na fermione (necijelobrojni spin) i bozone (cijelobrojni spin). Fermioni u SM-u prikazani su[1] u tablici 7.1. Za elektroslabu interakciju, kvantni brojevi su električni naboj Q_{EM}, treća projekcija slabog izospina T_3 i slabi hipernaboj[2] $Y_W = Q_{EM} - T_3$. Kod jake interakcije, to su tri naboja boje. Kvarkovi (antikvarkovi) nose jednu boju (anti-boju), a gluoni nose kombinaciju boje i anti-boje.

Bozoni u SM-u su gluoni, fotoni, W, Z i Higgsov bozon. Njihova svojstva prikazana su u tablici 7.2.

---

[1] Konvencija $c = 1$ koristi se u ovom radu za mjerne jedinice i relacije mase, impulsa i energije.

[2] U izrazu se koristi konvencija $e = 1$.

Tablica 7.1: Fundamentalni fermioni Standardnog modela.

	naboj			1. generacija		2. generacija		3. generacija	
	Q_{EM}	T^3	C	f	mass (GeV)	f	mass (GeV)	f	mass (GeV)
kvarkovi	+2/3e	1/2	da	u	$3 \cdot 10^{-3}$	c	1.27	t	172.9
	-1/3e	-1/2	da	d	$5 \cdot 10^{-3}$	s	0.1	b	4.67
leptoni	0	1/2	da	ν_e	$< 2.2 \cdot 10^{-9}$	ν_μ	$< 1.7 \cdot 10^{-4}$	ν_τ	< 0.0155
	-1e	-1/2	da	e	$5.11 \cdot 10^{-4}$	μ	0.106	τ	1.78

Tablica 7.2: Fundamentalni bozoni Standardnog modela.

bozon	g	γ	W$^+$	W$^-$	Z	H
Q_{EM}	0	0	+	-	0	0
T_3	0	0	1	-1	0	0
C	1,-1	0	0	0	0	0
spin	0	1	1	1	1	0
masa (GeV)	0	0	80.385 ± 0.015		91.1876 ± 0.0021	$125 - 126$

7.2.1 WZ produkcija u Standardnom modelu

Produkcija WZ parova je, unutar SM-a, moguća putem nekoliko kanala, od kojih se u jednom pojavljuje izravno vezanje teških baždarnih bozona. Takvo vezanje izravna je posljedica neabelovske prirode $SU(2)$ baždarne simetrije, s obzirom da generatori grupe međusobno ne komutiraju. To rezultira mogućnošću vezanja u WWZ i WWγ verteksima, tzv. trostrukim baždarnim vezanjima (TGC od eng. *Triple Gauge Couplings*), a moguća su i kvartična baždarnim vezanja. Član Lagrangiana koji opisuje TGC vezanja dan je izrazom:

$$\mathcal{L}^{TGC}_{WWV} = -ig_{WWV}\left[(W^-_{\mu\nu}W^{+\mu} - W^+_{\mu\nu}W^{-\nu})V^\nu + V_{\mu\nu}W^{+\mu}W^{-\nu}\right], \tag{7.2}$$

gdje operator V^μ predstavlja A^μ ili Z^μ, tenzori jakosti polja definirani su kao $W^\pm_{\mu\nu} = \partial_\mu W^\pm_\nu - \partial_\nu W^\pm_\mu$ i $V_{\mu\nu} = \partial_\mu V_\nu - \partial_\nu V_\mu$. Konstante vezanja su $g_{WWZ} = -g \cos\theta_W$ i $g_{WW\gamma} = e$ gdje je θ_W kut slabog miješanja, a g i g' su $SU(2)_L$ i $U(1)_Y$ konstante vezanja. Može se pokazati da su unutar SM-a dupuštena samo TGC vezanja koja uključuju W bozone. U protonskim sudarima na LHC-u WZ produkcija se najčešće odvija putem kvark-antikvark interakcija. U protonima su učestaliji u nego d kvarkovi, što vodi do asimetrije između udarnih presjeka W^+Z i W^-Z produkcije [22]. Preciznije, vjerojatnost interakcije u kvarka s antikvarkom, gdje se producira W^+, veća je nego ona interakcije d kvarka s antikvarkom, gdje se producira W^- bozon.

Nekoliko procesa, prikazanih na Feynmanovim dijagramima na slici 7.1, pridonosi WZ produkciji. TGC ili s-kanal dijagram u kojem se producira virtualni W bozon dovoljno velike mase za raspad u W i Z par prikazan je na slici 7.1a. U t-kanalu (7.1b), W i Z bozoni emitirani su u izmjeni kvarka i antikvarka. Dijagrami koji opisuju kvartično raspršenje longitudinalno polariziranih W i Z bozona te doprinos Higgsovog bozona prikazani su na slikama 7.1c i 7.1d.

Raspad W ili Z bozona može rezultirati leptonskim ($W \to \ell\nu$, $Z \to \ell^+\ell^-$) ili hadronskim ($W \to jj$, $Z \to jj$) konačnim stanjima, gdje ℓ označava leptone ($\ell = e, \mu, \tau$), ν neutrine, a j hadronske mlazove. Omjeri grananja W i Z bozona kao i omjeri grananja za WZ konačna stanja navedeni su u tablici 7.3. Pojedini leptonski kanali WZ raspada imaju mali omjer grananja ($\approx 0.35\%$). S druge strane, leptonska konačna stanja stvaraju vrlo jasno razlučiv signal u detektoru u usporedbi s hadronskima i lakše ih je razlikovati od pozadina koje sadrže mlazove.

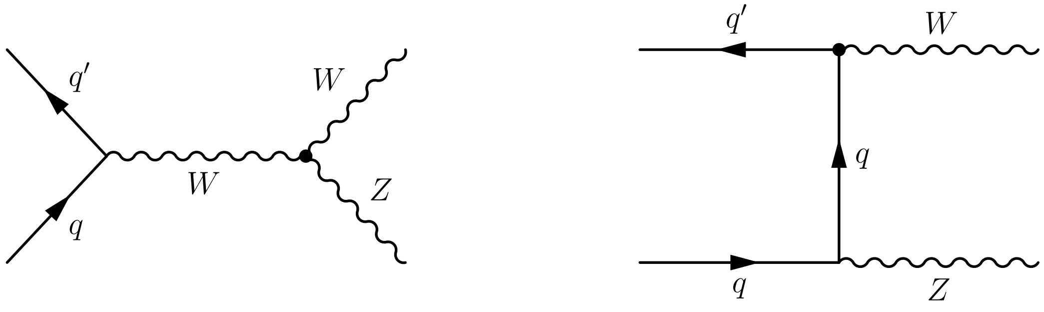

(a) s-kanal

(b) t-kanal

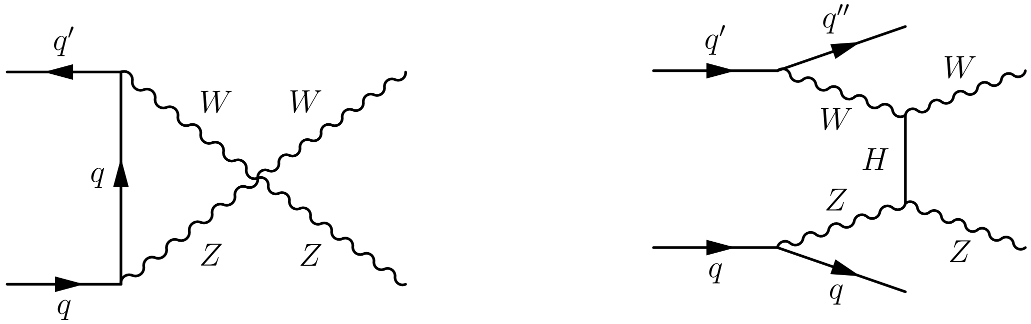

(c) kvartično raspršenje

(d) raspršenje putem Higgs-medijatora

Slika 7.1: Feynmanovi dijagrami procesa koji doprinose WZ produkciji na LHC-u.

Tablica 7.3: Omjeri grananja (BR) W i Z bozona [23] i omjeri grananja WZ konačnih stanja. ℓ označava nabijene leptone, ν neutrine, a j hadronske mlazove.

W raspad	W BR(%)	Z raspad	Z BR(%)
$e^{\pm}\nu$	10.75	$e^{+}e^{-}$	3.363
$\mu^{\pm}\nu$	10.57	$\mu^{+}\mu^{-}$	3.366
$\tau^{\pm}\nu$	11.25	$\tau^{+}\tau^{-}$	3.370
hadronski	67.60	hadronski	69.91
		$\bar{\nu}\nu$	20.00
WZ konačna stanja			
	BR (%)		BR (%)
$eee\nu$	0.3615	$\mu\mu e\nu$	0.3555
$ee\mu\nu$	0.3618	$\mu\mu\mu\nu$	0.3558
$\ell\ell\ell\nu$	3.329	$4j$	47.26
$\ell\ell jj$	6.827	$\nu\nu l\nu$	6.51
$jjl\nu$	22.77	$\nu\nu jj$	13.52

7.2.2 WZ produkcija izvan Standardnog modela

Sekvencijalni standardni model

Neka proširenja Standardog modela predviđaju postojanje novih teških nabijenih baždarnih bozona, poznatih kao W' (eng. W *prime*), koji se raspadaju u par W i Z bozona [24–29].

Takav novi bozon je moguć ukoliko postoje dodatne baždarne simetrije. One su često prisutne u teorijama velikog ujedinjenja (GUT od eng. *Grand Unification Theory*), koje nastoje obuhvatiti QCD i elektroslabi sektor SM-a u unificiranu baždarnu teoriju (npr. $SU(5)$ [30]). Takva simetrija lomi se u poznatu $SU(3) \otimes SU(2) \otimes U(1)$ simetriju SM-a. Lomljenje simetrije dovodi do pojave novih rezidualnih simetrija, npr. $U(1)$ ili $SU(2)$, što rezultira generiranjem dodatnih nabijenih vektorskih bozona sa svojstvima sličnim W ili Z bozonu. U teorijama ekstra-dimenzija također su predviđeni mehanizmi nastajanja masivnih rezonancija vektorskih bozona [31, 32] kao pobuđenih stanja poznatih SM vektorskih bozona u dodatnim dimenzijama.

Prijašnje potrage za W' bozonom obično su bile vršene u kontekstu Sekvencijalnog standardnog modela (SSM-a) [33–38]. To je jednostavno proširenje SM-a u kojem su vezanja W' bozona i fermiona identična vezanjima W bozona u SM-u. Te su potrage često bile rađene u leptonskim ($\mathrm{W}' \to \ell\nu$) kanalima raspada, pretpostavljajući da je $\mathrm{W}' \to \mathrm{WZ}$ kanal raspada potisnut. Uz ovu pretpostavku, postojanje W' bozona mase manje od 3.35 GeV-a nedavno je isključeno na CMS-u [39].

Potrage za $\mathrm{W}' \to \mathrm{WZ}$ kanalom raspada su stoga komplementarne onima u leptonskim kanalimaa raspada. Štoviše, u nekim modelima bez Higgsovog bozona [40–42] predviđeno je da su W' vezanja na fermione potisnuta [43]. Takav scenarij vodio bi na pojačanu jakost trostrukog baždarnog vezanja W', W i Z bozona [44, 45].

Tehnikolor

Tehnikolor (TC od eng. *Technicolor*) pripada obitelji kompozitnih teorija [46] koje predviđaju da pojedine "elementarne" čestice posjeduju substrukturu. Takve teorije također mogu objasniti lomljenje simetrije u slabom sektoru SM-a kroz dinamiku nove interakcije u analogiji s QCD-om te ne zahtijevaju postojanje elementarnih skalarnih bozona [47, 48]. U ovim modelima, W i Z bozoni dobivaju masu kroz njihovo vezanje na kompozitne fermione.

Tehnikolor je dakle baždarna teorija sa svojstvima sličnim QCD-u. Uvodi se TC baždarna grupa simetrije $SU(N_T)$ s $N_T^2 - 1$ baždarnih bozona i bezmasenim kiralnim tehnikvarkovima Q_L^{ai} i Q_R^{ai}, gdje a označava TC, a i je indeks okusa. U analogiji s QCD-om, TC karakterizira zatočenje. Intrinzična masena skala TC-a (Λ_T) reda je slabe skale ($O(100)$ GeV). Zatočenje rezultira formiranjem vezanih stanja s neutralnim TC nabojem, barionima ili mezonima sastavljenim od tehnikvarkova. S obzirom da takva stanja nisu stabilna u prirodi, teorija mora omogućiti raspad tehnikvarkova u poznate leptone i kvarkove.

Slično kao i u QCD-u, tehni-hadroni s $I^G(J^{PC}) = 1^-(0^{-+})$, $1^+(1^{--})$ i $1^-(1^{++})$ nazivaju se π_{TC}, ρ_{TC}, and a_{TC}.

Noviji Tehnikolor modeli [49] uvode "šetajuće" baždarno vezanje koje rezultira potisnućem nedozvoljenih neutralnih struja s mijenjanjem okusa. Takvo vezanje također predviđa realistične fermionske mase te vodi do tzv. LSTC (od eng. *Low-Scale Technicolor*) [50, 51] modela. U LSTC-u,

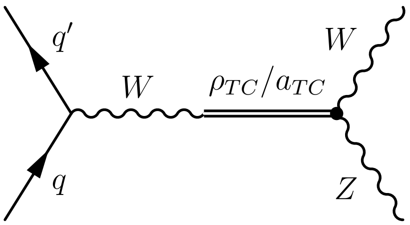

Slika 7.2: Feynmanov dijagram koji prikazuje raspad ρ_{TC}/a_{TC} čestice u par W i Z bozona.

najlakši tehni-hadroni imaju očekivanu masu ispod 700 GeV, daleko unutar dosega LHC-a. Noviji TC modeli rješavaju problem velikog elektroslabog S-parametra [52] zahtjevom da su ρ_{TC} i njegov aksijalno-vektorski partner a_{TC} gotovo iste mase (degenerirani). Te dvije nabijene čestice su zanimljive u okviru ovog rada iz aspekta njihovog mogućeg raspada u WZ par. Feynmanov dijagram takvog ρ_{TC} raspada prikazan je na slici 7.2. Budući da se očekuje da su ρ_{TC} i a_{TC} gotovo iste mase, vidljivi su kao jedna rezonancija u spektru WZ invarijantne mase te ih se stoga u daljnjem tekstu zajednički naziva ρ_{TC}.

7.3 Eksperimentalna postava

7.3.1 Veliki hadronski sudarivač

Veliki hadronski sudarivač [53] je supravodljivi ubrzivač protona smješten na švicarsko-francuskoj granici blizu grada Ženeve. Nalazi se u podzemnom tunelu duljine 26.7 km te je prvotno konstruiran i korišten za CERN-ov LEP sudarivač. LHC je dizajniran za rad na energiji sudara i luminozitetu nedostižnima na prijašnjim ubrzivačima, a po kompleksnosti i razmjeru ljudskog sudjelovanja nadmašuje bilo koji prijašnji sudarivač.

Dizajnom je predviđeno sudaranje protona na energiji sustava centra mase do $\sqrt{s} = 14$ TeV-a pri luminozitetu od $L = 10^{34} cm^{-2} s^{-1}$, što omogućuju supravodljivi dipolni magneti koji postižu magnetsko polje od 8 T i time održavaju kruženje snopova protona u suprotnom smjeru u dvije blisko postavljene cijevi snopa.

Snopovi se sudaraju u četiri interakcijske točke, na kojima su sagrađena četiri detektora: ATLAS [54], CMS [55], dva detektora opće namjene, te ALICE [56], namijenjen istraživanju sudara teških iona, i LHCb [57] koji je dizajniran za mjerenja B-fizike. LHC koristi LEP-ov sustav injekcije snopa, čija je shema prikazana na slici 7.3.

Snop se u LHC ubrizgava u obliku paketa protona pripremljenih u sustavu za predubrzavanje snopa te se nakon toga ubrzava u LHC-u pomoću radio-frekventnih (RF) komora. Luminozitet je definiran kao $\frac{dN}{dt} = L \cdot \sigma$ gdje σ udarni presjek snopova, a $\frac{dN}{dt}$ broj sudara u jedinici vremena. Luminozitet sudarivača za određen broj paketa *n*, koji sadrže *N* protona i sudaraju se orbitalnom frekvencijom f, definiran je kao

$$L = \frac{n \cdot N^2 f}{A_{eff}}, \tag{7.3}$$

gdje je A_{eff} interakcijska površina dva snopa.

2011. godine LHC je postizao trenutni luminozitet of $L = 10^{33} cm^{-2} s^{-1}$ na energiji sudara $\sqrt{s} = 7$ TeV-a te je prikupljeno više od 5 fb^{-1} (slika 7.4) integriranog luminoziteta.

Fenomenologija protonskih sudara

Protoni su složene čestice s kompleksnom dinamikom koju definira QCD. Glavni konstituenti su valentni kvarkovi (uud) koje okružuje more gluona i virtualnih kvark-antikvark parova. Sve te

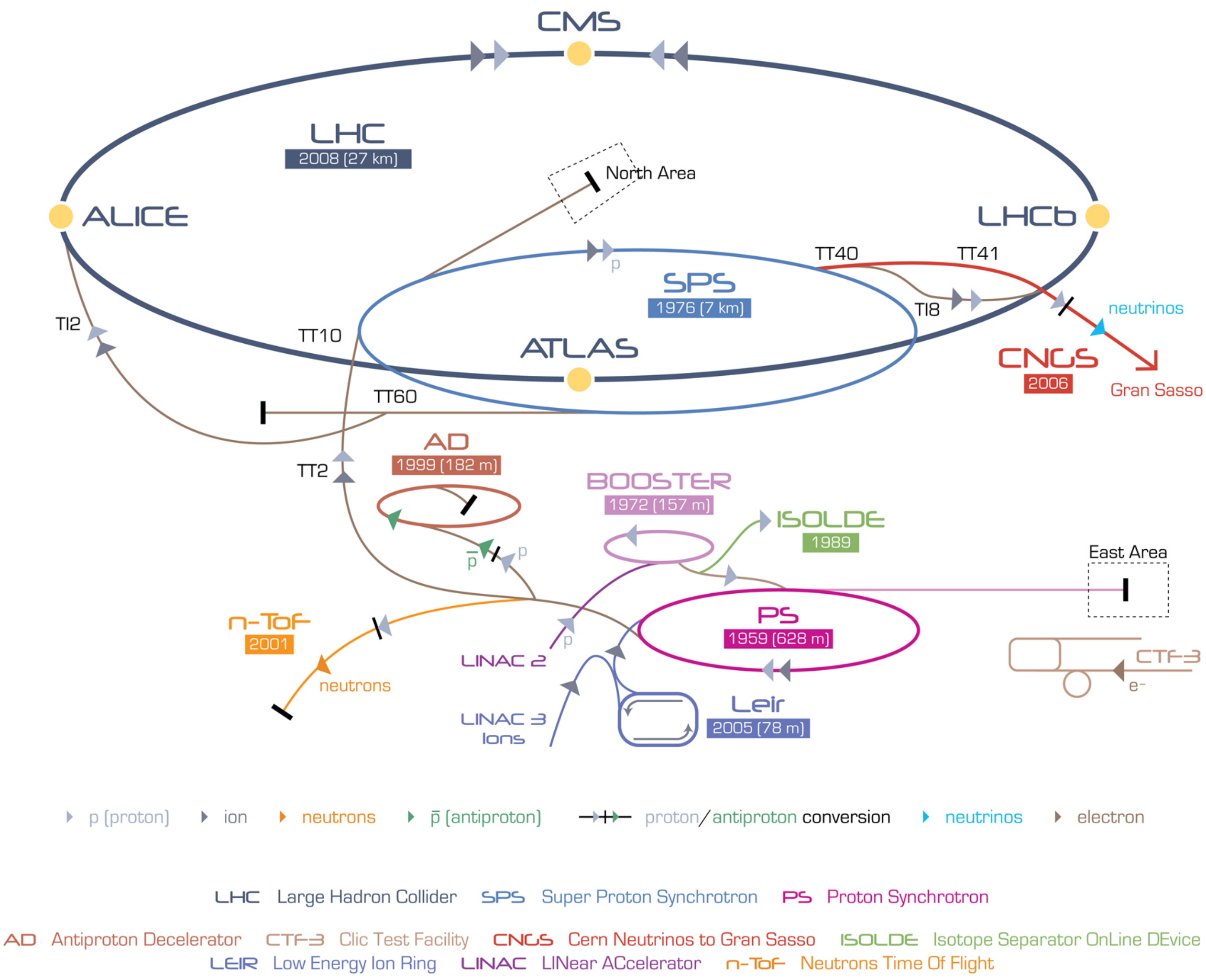

Slika 7.3: Akceleratorski kompleks LHC-a.

čestice, tzv. partoni, nose dio impulsa protona, što se može opisati funkcijama gustoće vjerojatnosti (PDF od eng. *Parton Density Function*). U ubrzivačima većina je impulsa protona, odnosno partona, sadržana u komponenti u smjeru snopa. Dalekodosežne interakcije (s malom izmjenom impulsa između partona) u sudarima protona rezultiraju produkcijom čestica koje se raspršuju pretežno u smjeru snopa. Rijeđi su tzv. tvrdi sudari (s velikim prijenosom impulsa) partona koji mogu dovesti do produkcije čestica velikog izlaznog impulsa u smjeru okomitog na snop (transverzalnog

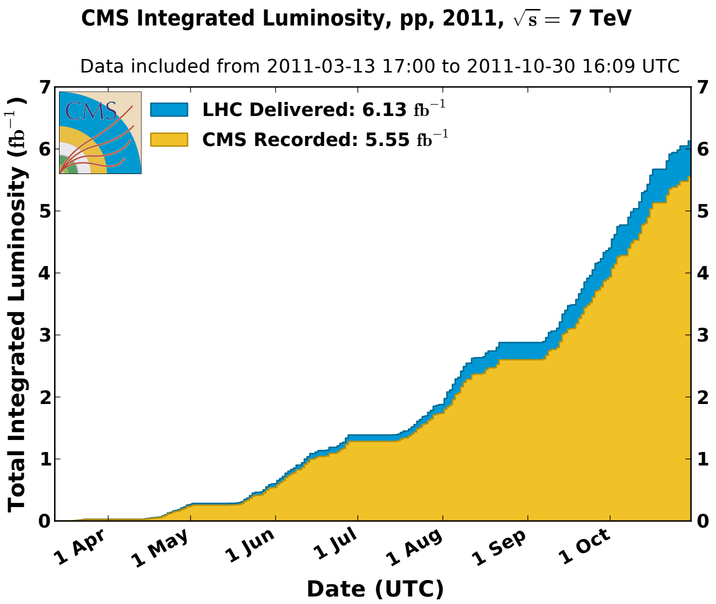

Slika 7.4: Ukupni pp integrirani luminozitet postignut na LHC-u te prikupljen na CMS eksperimentu 2011. godine.

impulsa). Iz tog razloga transverzalni je impuls važna veličina u prepoznavanju najzanimljivijih tvrdih procesa.

Značajna pojava na LHC-u je tzv. preklop događaja (eng. *pileup*), povećana aktivnost u detektoru, kao posljedica višestrukih sudara u jednom križanju paketa snopova ili kao aktivnost detektora iz susjednih križanja paketa. U 2011. godini prosječan broj sudara u križanju paketa bio je reda $O(10)$.

7.3.2 CMS detektor

Compact Muon Solenoid (CMS) [55] detektor je opće namjene sagrađen na jednoj od točaka interakcije na LHC sudarivaču. Gotovo hermetički zatvara točku interakcije te je slojevito strukturiran, s tragačem i kalorimetrima u unutrašnjosti solenoidnog magneta te vanjskim sustavima za detekciju miona. Struktura CMS detektora prikazana je na slici 7.5.

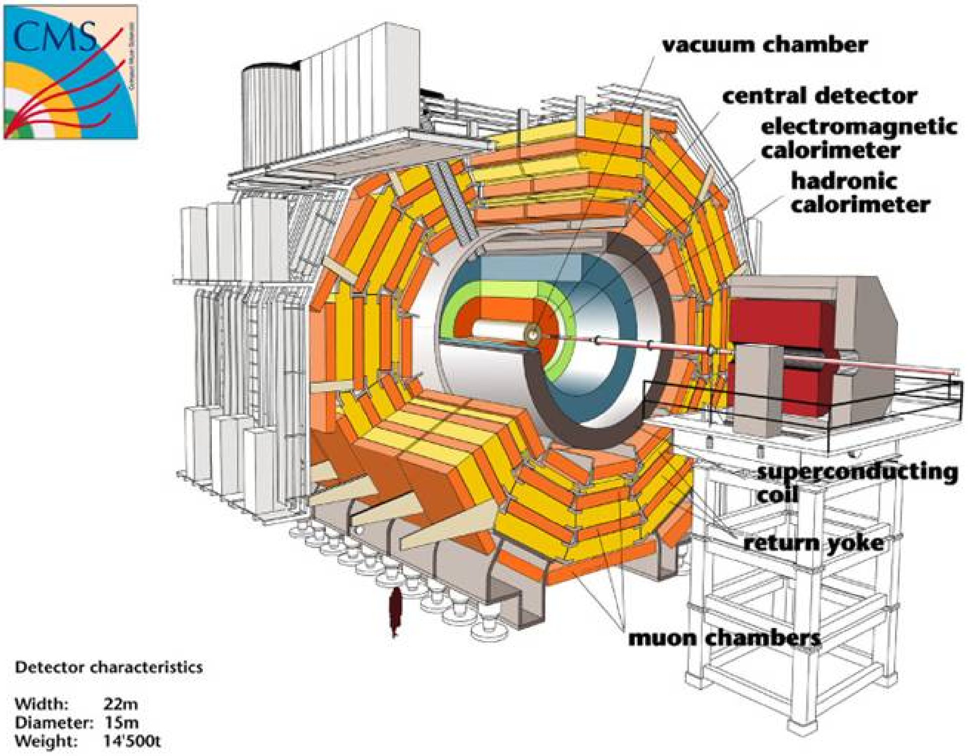

Slika 7.5: Prikaz unutrašnjosti CMS detektora.

Detektor je gotovo cilindrično simetričan oko osi snopa koja predstavlja z koordinatu. Ishodište je postavljeno u središtu detektora. x i y osi postavljene su okomito na smjer snopa. Često se koristi sustav koordinata $\phi = \arctan(y/x)$ te $\theta = \arctan(\sqrt{x^2+y^2}/z)$. Umjesto koordinate θ često se koristi pseudurapiditet definiran kao

$$\eta = -\ln\left[\tan\frac{\theta}{2}\right]. \tag{7.4}$$

CMS se dijeli na središnji dio (EB od eng. *ECAL Barrel*) koji se proteže do $\eta \approx \pm 1.5$ (gdje završava središnji dio ECAL poddetektora) te bočne dijelove (EE od eng. *ECAL Endcaps*). CMS-ov magnet generira magnetsko polje jakosti $B = 3.8$ T u cijelom unutarnjem volumenu. Ono zakreće putanje nabijenih čestica koje izlaze iz točke interakcije snopova, omogućujući time precizno mjerenje njihovog impulsa. Polje u području mionskih detektora pojačano je vanjskom čeličnom konstrukcijom te je jakosti $B = 2$ T.

Silikonski piksel detektor tragova postavljen je najbliže snopu. Sastoji se od velikog broja silicijskih senzora koji detektiraju prolazak nabijenih čestica. Razmješteni su u tri sloja u središnjem dijelu te po dva sloja u bočnim dijelovima CMS-a. Oko njega je postavljen trakasti detektor tragova. Njegov volumen premrežen je žicama na kojima se inducira naboj kod prolaska nabijenih čestica te se provodi do silicijskih senzora. Detektori tragova pokrivaju područje pseudorapiditeta do $|\eta| < 2.5$.

Elektromagnetski kalorimetar (ECAL) sagrađen je od PbWO_4 kristala velike gustoće (8.28 g/cm^3) i malog Molièreovog radijusa (0.89 cm), što rezultira kratkim i uskim elektromagnetskim pljuskom pri udaru elektrona ili fotona visoke energije.

Hadronski kalorimetar (HCAL) sastoji se od slojeva mjedenih absorbera i plastičnih scintilatora u središnjem dijelu te čeličnih absorbera i kvarcnih scinitilatora u bočnim dijelovima. Absorberi zaustavljaju hadronske snopove, te se rezultirajući pljusak čestica detektira u scintilatorima.

Mionski sistem sastoji se od nekoliko vrsta detektora punjenih plinom. Driftne komore (DT od eng. *Drift Tubes*) smještene su u središnjem dijelu. Napunjene su plinom koji se ionizira prolaskom miona. Katodne trakaste komore (CSC od eng. *Cathode Strip Chambers*) nalaze se u bočnim dijelovima te funkcioniraju na sličan način, no isprepletene su velikim brojem žica koje prikupljaju naboj. Potonji su detektori otporniji na veliku frekvenciju prolazaka čestica. Komore s otpornim pločama (RPC od eng. *Resistive Plate Chambers*) sastoje se od paralelnih ploča velike otpornosti između kojih je plin. U slučaju prolaska čestice dolazi do ionizacije plina i pljuska elektrona koji detektiraju eksterni trakasti detektori. Njih karakterizira visoka vremenska razlučivost ($\approx$ 1 ns) te se stoga koriste kao dio sustava za okidanje.

Okidač i Sustav za prikupljanje podataka

LHC je u mogućnosti producirati sudare protonskih paketa frekvencijom do 40 MHz. Snimanje svih tih sudara bilo bi od malog značaja, s obzirom da je udio tvrdih protonskih sudara razmjerno malen. Današnje tehnologije također ne omogućuju kostrukciju sustava za prikupljanje podataka takve namjene po prihvatljivoj cijeni. Stoga se u svim detektorima na LHC-u koriste tzv. okidači (sustavi za filtriranje podataka) koji odlučuju o zapisu pojedinih sudara ovisno o njihovim fizikalnim karakteristikama.

CMS-ov okidač obuhvaća dva stupnja filtriranja podataka u dva zasebna sustava. Prvostupanjski (L1 od eng. *Level-1*) okidač je hardverski okidač koji analizira podskup podata iz kalorimetara i mionskih sustava. Vrijeme odziva sustava je 3.2 ms. U tom vremenu podaci sudara čuvaju se u memorijskim spremnicima detektorske elektronike. Sustav može analizirati podatke frekvencijom do 40 MHz, a maksimalna frekvencija prihvaćenih zapisa sudara (tzv. događaja) je 100 kHz. Arhitektura L1 okidača prikazana je na slici 7.6.

U slučaju prihvaćenog događaja, svi pripadajući podaci prenose se u sustav za prikupljanje podataka (DAQ od eng. *Data Acquisition System*), čija je arhitektura prikazana na slici 7.7.

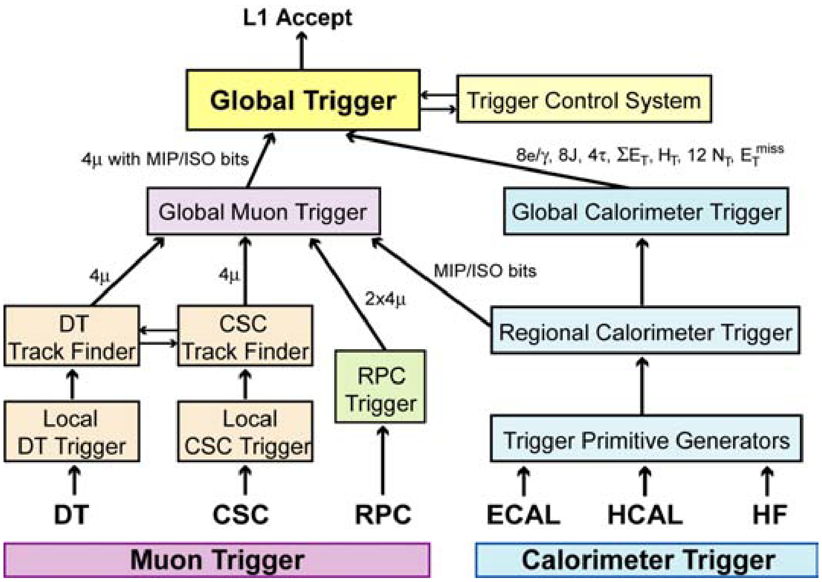

Slika 7.6: Prikaz arhitekture L1 okidača.

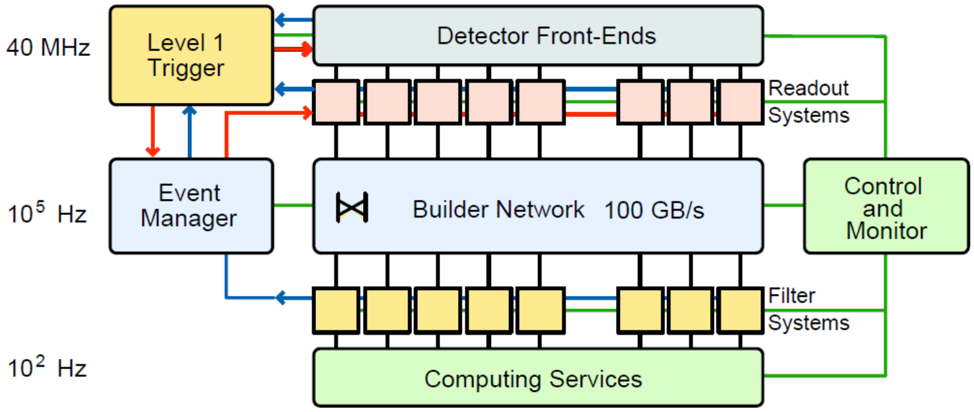

Slika 7.7: Architektura DAQ sustava.

Nakon odluke o prihvaćanju događaja u L1 okidaču, podaci (tzv. fragmenti) događaja se iščitavaju iz FED (od eng. *Front End Detector*) elektronike svakog podsustava do FRL (od eng. *Front-End Read-out Link*) kartica putem S-Link64 [62] veze. Veličina svakog fragmenta je oko 2 kB.

FRL kartice su povezane na EVB (od eng. *Event Builder*) sustav koji je izgrađen na Myrinet [63] mrežnoj tehnologiji. Njegova zadaća je povezivanje fragmenata u više superfragmenata, ukupno 72, koji se kompletiraju na RU (od eng. *Readout Unit*) računalima. S RU računala fragmenti se prenose do BU (od eng. *Builder Unit*) računala gdje se prikupljaju podaci događaja iz svih FED-ova te se cijeli događaj spaja u jedan zapis. Na BU računalima ujedno se vrši i obrada podataka, te se takvo računalo naziva i BU-FU (eng. *Builder Unit-Filter Unit*). FU softver izvodi se na tim računalima te zaprima ulazne podatke korištenjem lokalne djeljene memorije iz BU spremnika, a podaci se zatim analiziraju. Farma BU-FU računala čini drugostupanjski okidač ili HLT (od eng. *High Level Trigger*), gdje se dovršava filtriranje podataka. Za razliku od L1 okidača, analiziraju se potpuni podaci iz svih dijelova detektora. Takva analiza je zahtjevna i pri velikom luminozitetu LHC-a može trajati do 200 ms po događaju pa je potreban velik broj računala da bi se mogli analizirati svi događaji koje je prihvatio L1 okidač. BU-FU računalna farma koja se sastoji od probližno 1250 računala s 8, 12 ili 16 procesorskih jezgri.

HLT softver dizajniran je kao dio CMSSW (od eng. *CMS Software Framework*) [65] softverskog okružja koje se koristi i za kasniju obradu podataka. Takva unifikacija omogućuje korištenje istih softverskih implementacija za zadaće u više okruženja, primjerice za detaljnu rekonstrukciju događaja. HLT obrada se vrši u okviru HLT *staza*, od kojih je svaka zadužena za jedan mod filtriranja (npr. detekciju leptona). Za efikasno pokretanje HLT softvera razvijena je posebna softverska aplikacija, EP (od eng. *Event Processor*), koja omogućava efikasno korištenje višejezgrenih računala te integrira HLT softver u okruženje DAQ sustava. HLT filtriranje smanjuje količinu prihvaćenih događaja za dodatni faktor 100 te se konačno odabrani događaji snimaju koristeći STM (od eng. *Storage Manager*) aplikacije na zasebnim radnim stanicama. Ukupni kapacitet sustava za snimanje podataka je približno 1000 Hz.

Sustav za praćenje kvalitete podataka

Sustav za praćenje kvalitete podataka (DQM od eng. *Data Quality Monitoring*) zadužen je za analizu dijela prikupljenih događaja i histograma koje producira HLT. Podaci se dohvaćaju sa STM aplikacija i analiziraju na DQM serveru, gdje se izvršavaju zasebne CMSSW DQM aplikacije za analizu podataka. Svaka od tih aplikacija producira histograme ili drukčiji oblik informacija o trenutnom stanju pojedinog poddetektora. Informacije se prenose na DQM korisničko sučelje, gdje se može nadgledati stanje svih poddetektora te se omogućuje brza detekcija problema. DQM također uključuje i sustav za kasniju detaljnu analizu kvalitete prikupljenih podataka i proces certifikacije za daljnje analize.

7.3.3 Obrada podataka i simulacija

Podaci koje prikuplja i pohranjuje DAQ naknadno se prebacuju i obrađuju na tzv. Tier-0 sustavu za obradu podataka. Pri tome se podaci dijele u primarne skupove podataka, od kojih je svaki definiran tako da su prihvaćene određene HLT staze. Primarni se setovi podataka nakon procesiranja globalno distribuiraju putem grid sustava te su dostupni za daljnju analizu.

Velika količina podataka također se generira u simulacijskim kampanjama. Koristi se nekoliko Monte Carlo generatora kojima se simuliraju fizikalni procesi u protonskim sudarima. Odziv detektora na tako generirane događaje simulira se GEANT4 [69] paketom. Simulira se digitalni zapis detektora i L1 okidača. Na tim podacima zatim se primjenjuju uvjeti HLT-a, kao i potpuna rekonstrukcija događaja, istovjetno kao i na prikupljenim podacima.

Mjerenje luminoziteta

U CMS eksperimentu luminozitet se može odrediti koristeći prednji hadronski kalorimetar (HF) ili silicijski piksel detektor tragova. Potonja metoda je preciznija i koristi se u rezultatima prikazanim o ovom radu [71]. Piksel klasteri, blokovi silicijskih senzora, zbog svog su malog udarnog presjeka pogodni za takvo mjerenje jer su rijetko izloženi višestrukim istovremenim prolascima čestica, što rezultira gotovo linearnim odzivom u uvjetima rada LHC-a. Prosječan broj pogođenih klastera proporcionalan je luminozitetu sudarenih paketa protona L_B kao

$$< N_{\text{cluster}} >= \frac{\sigma_{\text{cluster}}}{f} L_B, \tag{7.5}$$

gdje je orbitalna frekvencija $f = 11.246$ kHz, a udarni presjek klastera σ_{cluster} se može precizno odrediti tzv. *Van der Meer Scan* metodom [72]. Nepouzdanost opisane metode mjerenja luminoziteta za podatke prikupljene 2011. godine iznosi 2.2%.

Rekonstrukcija fizikalnih objekata

Mione karakterizira trag u unutarnjem tragaču kao i tragovi u mionskim komorama. Rekonstrukcija [73] kreće od mionskih sustava gdje se Kalman prilagodbom rekonstruira trag (tzv. *standalone muon* algoritam). Zatim se izgrađuje globalni mion gdje se taj trag povezuje s tragom u tragaču. Alternativno, rekonstrukcija također može započeti od traga u unutarnjem tragaču (tzv. *tracker muon* algoritam).

Elektrone karakterizira energijski depozit u ECAL-u, iz kojeg se izgrađuje klaster, te trag u tragaču. Pri prolasku kroz materijal detektora elektron može emitirati Bremsstrahlung fotone koji stvaraju

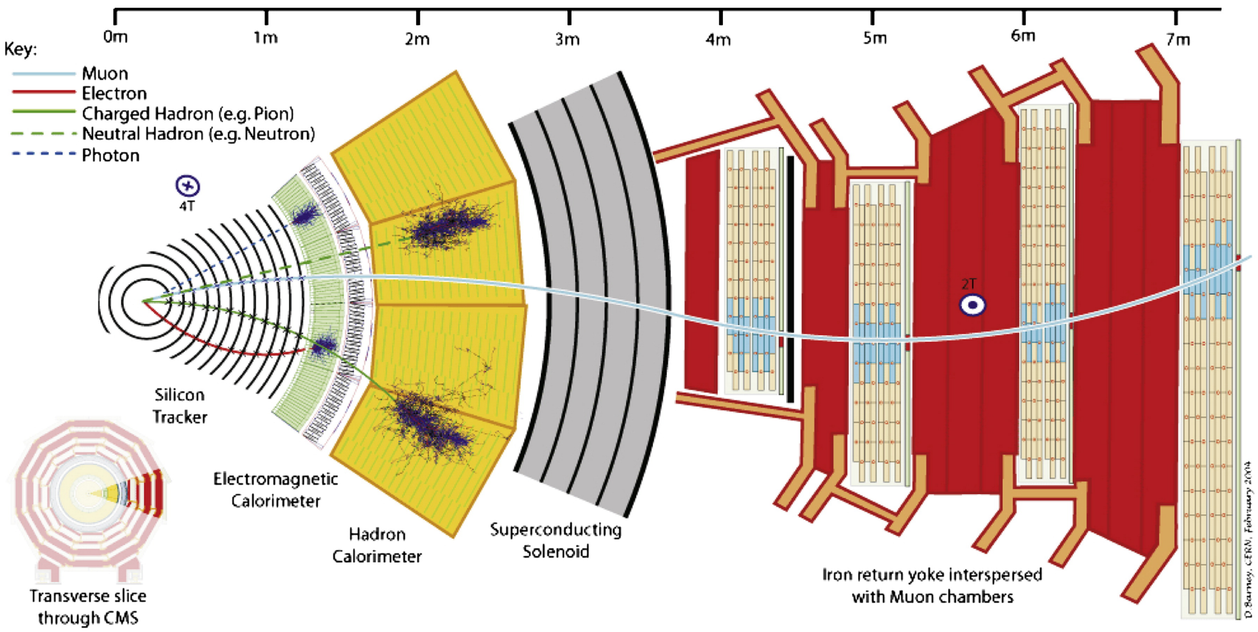

Slika 7.8: Ilustracija propagacije elektrona, miona, fotona i nabijenog i neutralnog hadrona u transverzalnoj ravnini CMS-a.

dodatne klastere u ECAL-u razmještene duž ϕ koordinate. Iz svih tih klastera izgrađuje se superklaster (SC od eng. *supercluster*). Primarna metoda rekonstrukcije elektrona bazirana je na tzv. *Gaussian Sum Filter* [74] algoritmu, koji povezuje SC s tragovima u piksel detektoru tragova. Iz tako formirane jezgre pokušava se rekonstruirati trag prema SC-u, uzimajući u obzir mogućnost Bremsstrahlunga.

Nedostajuća transverzalna energija (MET od eng. *Missing Transverse Energy*) je neravnoteža u transverzalnom impulsu svih vidljivih čestica[3],

$$\vec{E}_T^{miss} = - \sum_{\text{visible}} \vec{p}_T. \tag{7.6}$$

S obzirom da je impuls očuvan, E_T^{miss}mjeri transverzalni impuls kojeg odnose nevidljive čestice, kao npr. neutrini. E_T^{miss}je vrlo osjetljiv na kvalitetu kalibracije te neefikasnosti detektora. U mjerenjima prezentiranima u ovom radu za E_T^{miss}rekonstrukciju koristi se PF (od eng. *particle flow*) metoda [75, 76] koja pokušava pojedinačno identificirati sve čestice nastale u sudaru, za što se koriste informacije iz cijelog detektora.

Rekonstrukcija verteksa je proces određivanja točaka interakcije (ili točke nastanka čestica) u snimljenim događajima. Primarni verteks je točka interakcije protona iz snopova, dok sekundarni verteksi nastaju raspadom dugoživućih čestica i u pravilu su udaljeni od primarne točke interakcije. U uvjetima visokog luminoziteta često dolazi do više interakcija u jednom križanju paketa te ih je zahtjevno točno rekonsturirati. U tu svrhu razvijeno je nekoliko metoda koje koriste tragove za rekonstrukciju. SC (od eng. *Standard Clustering*) metoda [77] grupira tragove prema njihovoj udaljenosti u z smjeru te vrši iterativnu prilagodbu uz minimizaciju χ^2. Algoritam koji se koristi u analizi opisanoj u ovom radu, DA (od eng. *Deterministic Annealing*) [78], razlikuje se u tome da tretira $< \chi^2 >$ kao srednju energiju termodinamičkog sustava i maksimizira njegovu entropiju, što vodi do postupnog smanjenja $< \chi^2 >$ veličine čime se smanjuje mogućnost pogrešne rekonstrukcije.

---

[3] Energija čestica dana je relacijom $E = p^2 + m_0^2$. Stabilne i dugoživuće čestice producirane u sudarima na LHC-u najčešće su visoko relativističke ($E \gg m_0$) te stoga vrijedi $E \approx p$. U tom režimu, apsolutna vrijednost nedostajućeg transverzalnog impulsa i nedostajuća transverzalna energija gotovo su jednake.

7.4 Mjerenje WZ udarnog presjeka

Udarni presjek $pp \rightarrow$ WZ na energiji sustava centra mase $\sqrt{s} = 7$ TeV-a mjeren je preko leptonskih (elektronskih i mionskih) kanala raspada W i Z bozona. Dobiveni rezultati ekstrapolirani su na fazni prostor svih W i Z kanala raspada te je određen tzv. inkluzivni udarni presjek. Analiza je izvršena na ukupnom skupu podataka prikupljenih u 2011. godini CMS detektorom, a CMS kolaboracija odobrila je predstavljanje rezultata na konferencijama [79]. Konačno stanje $WZ \rightarrow 3l\nu$ karakterizirano je parom elektrona ili miona suprotnog naboja koji su nastali raspadom Z bozona te elektronom ili mionim i nedostajućom transverzalnom energijom neutrina iz raspada W bozona. Područje signala Z bozona ograničeno je na interval invarijantne mase $M_Z \in [71.18, 111.18]$ GeV-a. Tijekom analize događaji su podijeljeni u četiri kategorije (selekcijska kanala) ovisno o kanalu raspada W i Z bozona.

7.4.1 Pozadine

WZ pozadine dijele se na instrumentalne, tj. pozadine koje sadrže pogrešno identificirane čestice, te fizikalne, koje imaju isto konačno stanje nastalo od raspada drugih čestica. Instrumentalne pozadine čine događaji s jednim ili više mlazova (QCD, W+mlazovi, Z+mlazovi, WW+mlazovi) koji su pogrešno identificirani kao leptoni te događaji s leptonima nastalim u mlazovima teških kvarkova (Z$b\bar{b}$, Z$c\bar{c}$, $t\bar{t}$) ili nastalim konverzijom fotona (Zγ). Fizikalnoj i ireducibilnoj pozadini doprinosi raspad ZZ$\rightarrow 4l$ u slučaju kada se identificiraju samo tri leptona. Pozadine se također dijele na rezonantne (sa Z bozonom) i nerezonantne (bez Z bozona).

Pozadinu također čini WZ produkcija gdje se W ili Z raspadaju u τ leptone, a oni u elektron i neutrine u 17.82% slučajeva ili u mion i neutrine u 18.39% slučajeva. S obzirom da su to raspadi realnog WZ stanja, udarni presjek ove pozadine proporcionalan je signalu.

7.4.2 Objekti analize

Mioni

Na globalni mion, koji se koristi u ovoj analizi, postavljaju se dodatni zahtjevi s ciljem smanjivanja pozadine: bolja kvaliteta traga, kompatibilnost s primarnim verteksom i broj detektiranih pogodaka u pojedinim poddetektorima. Također se zahtijeva je da je mion izoliran, tj. da se ne nalazi u blizini drugih čestica. U postupku određivanja izolacije koristi se PF algoritam kojim se rekonstruiraju individualni fotoni i hadroni u događaju. Zbroj transverzalnih impulsa čestica u konusu[4] $\Delta R < 0.4$ oko miona podijeljen je s transverzalnim impulsom miona, dajući varijablu relativne izolacije. Zahtjevi na mione sažeti su u tablici 7.4.

Tablica 7.4: Selekcijski zahtjevi na mione.

opis	zahtjev
kinematski	$p_{\mathrm{T}} > 10$ GeV i $\lvert\eta\rvert < 2.4$
broj pogodaka u piksel detektoru	> 0
broj pogodaka u detektoru tragova	> 10
globalna prilagodba χ^2/N_{dof}	< 10
broj mionskih pogodaka	> 0
broj komora s odgovarajućim segmentima	> 1
transverzalna udaljenost od verteksa	< 0.2 cm
relativna izolacija	< 0.12

---

[4] $\Delta R = \sqrt{\Delta\eta^2 + \Delta\phi^2}$.

Elektroni

Za selekciju elektrona upotrebljava se multivarijatna analiza (MVA) koja koristi elektronske varijable opisane u [74]. Prethodno se na elektrone primjenjuje predselekcija koja osigurava da su elektroni prošli zahtjeve okidača. U predselekciji se koristi više elektronskih varijabli [74, 80]. Širina elektromagnetskog snopa u ECAL-u, $\sigma_{i\eta i\eta}$, karakteristično je uska za elektrone u odnosu na druge čestice. Elektron mora imati superklaster geometrijski kompatibilan s tragom ekstrapoliranim do iste točke ($\Delta\phi_{in}$ i $\Delta\eta_{in}$). Također, elektronski kandidat mora imati mali udio energije u HCAL-u, mora biti kompatibilan s primarnim verteksom, imati malu mogućnost da je nastao konverzijom fotona i zadovoljavati uvjete izolacije u kalorimetrima i tragaču, analogne onima postavljenim u stazama okidača. Predselekcijski zahtjevi na elektrone sažeti su u tablici 7.5.

Tablica 7.5: Predselekcijski zahtjevi na elektrone.

varijabla	centralni dio	bočni dijelovi
p_T	c > 10 GeV	
$\|\eta\|$	c < 2.5	
$\sigma_{i\eta i\eta}$	<0.01	<0.03
$\|\Delta\phi_{in}\|$	<0.15	<0.10
$\|\Delta\eta_{in}\|$	<0.007	<0.009
H/E	<0.12	<0.10
$\sum_{HCAL}^{\Delta R<0.3} E_T/p_T^e$	<0.2	<0.2
$\sum_{ECAL}^{\Delta R<0.3} E_T/p_T^e$	<0.2	<0.2
$\sum_{Tracker}^{\Delta R<0.3} p_T/p_T^e$	<0.2	<0.2
$\|d_0\|$	<0.02 cm	<0.02 cm
$\|d_z\|$	<0.1 cm	<0.1 cm
$P_\text{konverzije}$	<10^{-6}	$< 10^{-6}$
$N_\text{nedostajućih pogodaka}$	0	0

Za određivanje izolacije elektrona, koja se, uz MVA, primjenjuje kao zahtjev potpune selekcije, također se koristi PF algoritam. Zbrajaju se transverzalni impulsi čestica u konusu $\Delta R < 0.4$ te se postavlja zahtjev na relativnu izolaciju Iso_{rel}^{PF} koja mora biti manja od 0.13 u središnjem dijelu i 0.09 u bočnim dijelovima detektora.

Nedostajuća transverzalna energija

U analizi se koristi nedostajuća transverzalna energija, E_T^{miss}, određena PF algoritmom. Također se primjenjuju dodatne, tzv. *tip-I* korekcije energijske skale mlazova [81].

7.4.3 Uzorci

U analizi se koriste dva primarna skupa podataka iz 2011. godine, tzv. **DoubleElectron** i **DoubleMuon**, ukupnog integriranog luminoziteta pribiližno 4.9 fb^{-1}. Za simuliranje signala i pozadine korišteni su Monte Carlo generatori MadGraph [82] i powheg [83]. Popis MC uzoraka dan je u tablici 7.6.

Na MC uzorke primjenjuju se korekcije da bi se ispravile nepreciznosti u simulaciji.

Korekcije efikasnosti elektrona (faktori skaliranja) mjere se na MC uzorcima i podacima te se njihov omjer $w_\ell^{SF} = \epsilon_{data}/\epsilon_{MC}$ pridjeljuje svakom leptonu u događaju. Omjeri ovise o transverzalnom impulsu i pseudorapiditetu leptona.

Preklop događaja obično se razlikuje između podataka i simulacije budući da se MC uzorci obično generiraju prije samog LHC-ovog radnog perioda te se ne mogu unaprijed znati uvjeti luminoziteta, a time i konačna raspodjela preklopa. Da bi se izjednačila dodatna aktivnost u detektoru u podacima i MC uzorcima, MC događajima je potrebno prilagođavati težinu kako bi se dobila ras-

Tablica 7.6: Uzorci, Monte Carlo generator, udarni presjeci prvog (LO) i višeg reda za MC uzorke. Udarni presjek višeg reda za uzorak W+mlazovi određen je u NNLO redu, dok su svi ostali NLO reda.

uzorak	Monte Carlo generator	σ_{LO} (pb)	$\sigma_{\mathrm{(N)NLO}}$ (pb)
$WZ \to \ell\nu\ell\ell$	MadGraph	0.7192	0.879
$Z(\to \ell\ell)$+mlazovi	MadGraph	2474.0	3048
$t\bar{t}$	MadGraph	94.76	157.5
$W(\to \ell\nu)$+mlazovi	MadGraph	27770.0	31314.0
$WW \to 2\ell 2\nu$	MadGraph	3.783	4.882
$V\gamma$+mlazovi	MadGraph	56.64	65
$ZZ \to 4e$	powheg	—	0.0154
$ZZ \to 4\mu$	powheg	—	0.0154
$ZZ \to 4\tau$	powheg	—	0.0154
$ZZ \to 2e2\mu$	powheg	—	0.0308
$ZZ \to 2e2\tau$	powheg	—	0.0308
$ZZ \to 2\mu 2\tau$	powheg	—	0.0308

podjela preklopa istovjetna podacima. Procjena preklopa u podacima dobiva se uz pretpostavku neelastičnog pp udarnog presjeka od $\sigma_{pp} = 68$ mb.

Na MC uzorke primjenjuje se i razmazivanje impulsa i energije elektrona, da bi rezolucija odgovarala onoj u podacima.

Okidač

U WZ analizi zahtijeva se da je događaj prošao stazu HLT-a s dva miona ili dva elektrona. S obzirom da svaki WZ događaj ima barem dva leptona iste vrste, efikasnost ovakvog zahtjeva je velika. Odabrane su staze koje pokrivaju cijeli period u 2011. godini. Pragovi na p_{T} leptona razlikuju se ovisno o stazi te se zahtijeva prag od 17 GeV-a za jedan lepton i 8 GeV-a za drugi lepton u stazama koje su bile korištene pri velikom luminozitetu LHC-a.

U Monte Carlo uzorcima efikasnost okidača je simulirana. Za to se koriste efikasnosti pojedinih leptona u okidaču, izmjerene u neovisnim uzorcima. Efikasnosti se u dileptonskim HLT stazama razlikuju za leptone većeg i manjeg impulsa.

7.4.4 Selekcija događaja

Prvi korak selekcije je zahtjev da događaj sadrži točno tri leptona s idenitifikacijskim zahtjevima opisanim u odjeljku 7.4.2, čime se odbacuje velik udio ZZ pozadine. Za rekonstrukciju Z bozona povezuju se dva leptona istog okusa i različitih naboja, od kojih barem jedan mora imati $p_{\mathrm{T}} > 20$ GeV-a. U slučaju više mogućih kombinacija, izabire se Z kandidat koji je najbliže PDG Z masi ($M_Z = 91.18$ GeV-a). [23]. Masa također mora biti u prozoru $[M_Z - 20, M_Z + 20]$ GeV-a, a okus leptona iz raspada Z kandidata mora odgovarati stazi okidača koja je prihvaćena.

Nakon rekonstrukcije Z bozona slijedi rekonstrukcija W bozona. Treći, preostali lepton mora imati p_{T} veći od 20 GeV-a. Također mora biti geometrijski razdvojen od Z leptona te se zahtijeva $\Delta R(\text{W lepton, Z lepton}) > 0.1$. E_T^{miss}mora biti veći od 30 GeV-a čime se odbacuje velik udio pozadina bez neutrina.

Ovisno o okusima leptona, događaji se svrstavaju u četiri kanala: $3e$, $2e\mu$, 2μ i 3μ. Broj događaja nakon glavnih koraka selekcije prikazan je u tablici 7.7. Odabir kinematskih raspodjela prikazan je na slici 7.9.

Tablica 7.7: Broj događaja u podacima i simulaciji nakon glavnih koraka selekcije. Greške su statističke. Vrijednosti odgovaraju integriranom luminozitetu od 4.9 fb^{-1}.

uzorak	Z selekcija + 3 leptona		W selekcija				E_T^{miss}selekcija			
	$Z \to ee$	$Z \to \mu\mu$	3e	2e1μ	1e2μ	3μ	3e	2e1μ	1e2μ	3μ
$Z + mlazovi$	64.6	120.1	5.7	3.7	8.2	10.7	1.2 ± 0.8	1.2 ± 0.9	0.8 ± 0.6	0.6 ± 0.6
$W + mlazovi$	0	0	0	0	0	0	0	0	0	0
$t\bar{t}$	1.6	2.9	0.33	0.65	0.66	1.29	0.30 ± 0.07	0.55 ± 0.09	0.56 ± 0.09	1.04 ± 0.13
ZZ	30.9	46.8	14.3	11.6	21.0	17.9	2.01 ± 0.04	3.48 ± 0.04	2.66 ± 0.03	5.09 ± 0.06
$V\gamma$	13.7	17.1	10.4	0	17.0	0	0	0	0.5 ± 0.5	0
WW	0	0	0	0	0	0	0	0	0	0
WZ	153	222	61.8	70.8	78.9	106.6	44.7 ± 0.5	49.8 ± 0.5	56.0 ± 0.5	73.8 ± 0.6
Ukupno MC	264	409	92.5	86.8	125.8	136.5	48.2 ± 1.0	55.0 ± 1.0	60.5 ± 1.1	80.5 ± 0.9
Podaci	284	441	96	99	122	161	64	62	70	97

7.4.5 Procjene pozadina

WZ konačna stanja s $Z \to \tau\tau$ i $W \to \tau\nu$ raspadima

WZ raspadi s τ leptonima imaju udarni presjek gotovo istovjetan kanalima signala. Stoga se njihov doprinos tretira kao relativni udio $WZ \to 3l$ u svakom kanalu (f_τ) koji se oduzima od selektiranih događaja. Udio (f_τ) se procjenjuje iz MC uzorka signala. U tablici 7.8 prikazan je f_τ za svaki kanal te broj događaja za nekoliko različitih kategorija WZ raspada u τ leptone.

Tablica 7.8: Broj selektiranih događaja u WZ$\to$ $3l$ uzorku za τ raspade W ili Z bosona. Također je prikazan broj događaja za hadronske i leptonske raspade τ leptona i vrijednosti f_τ. Greške su statističke.

uzorak	$3e0\mu$	$2e1\mu$	$2e1\mu$	$0e3\mu$
$N_{\tau \to e,\mu}$	2.90 ± 0.12	3.64 ± 0.13	3.58 ± 0.12	5.44 ± 0.15
$N_{\tau \to \text{hadronic}}$	0.02 ± 0.01	0.003 ± 0.003	0.02 ± 0.01	0.002 ± 0.002
$N_{W \to \tau\nu}$	2.83 ± 0.11	3.54 ± 0.13	3.49 ± 0.12	5.28 ± 0.15
$N_{Z \to \tau\tau}$	0.08 ± 0.02	0.11 ± 0.02	0.10 ± 0.02	0.17 ± 0.003
f_τ	0.065 ± 0.002	0.073 ± 0.002	0.064 ± 0.002	0.074 ± 0.002

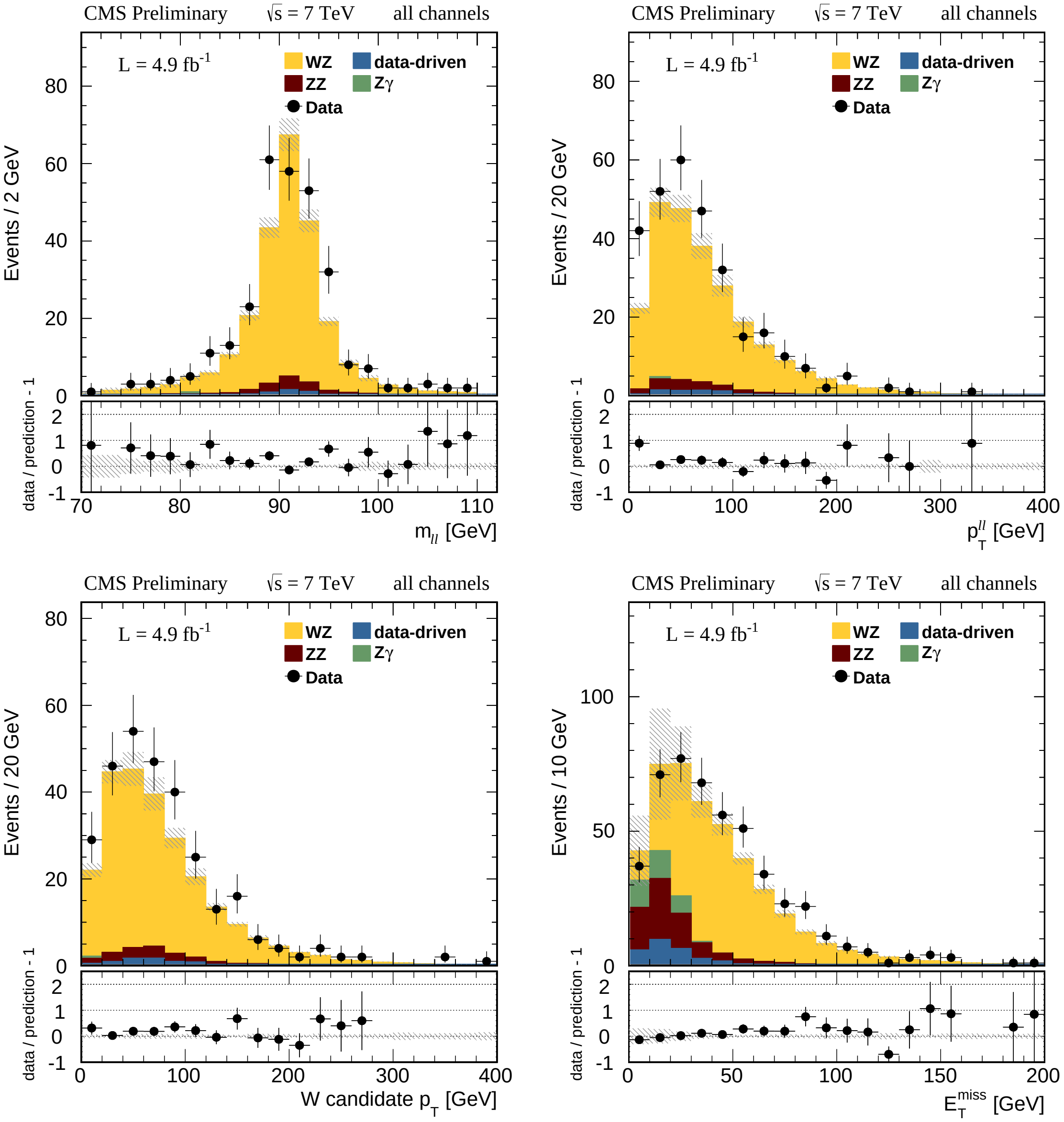

Slika 7.9: Kinematske raspodjele nakon primjene svih selekcijskih kriterija zbrojene za sva četiri kanala: invarijantna masa Z kandidata (gore lijevo), transverzalni impuls Z kandidata (gore desno), transverzalni impuls W kandidata (dolje lijevo), i E_T^{miss}prije primjene E_T^{miss}zahtjeva (dolje lijevo). t kvark i Z+mlazovi pozadine procijenjene su iz podataka, koristeći metodu opisanu u odjeljku 7.4.5.

Procjena pozadina iz podataka

Zbog nepreciznosti MC simulacija, u WZ analizi se koristi metoda procjene pozadina iz podataka. Ona se odnosi na pozadine koje sadrže jedan ili više mlazova koji su pogrešno identificirani kao leptoni. Glavno svojstvo takvih objekata je da nisu izolirani i, za razliku od leptona iz W i Z raspada, kroz detektor se propagiraju kao snop čestica. U tom smislu definiraju se pravi leptoni (označeni s ℓ) koji su najčešće izolirani i pogrešno identificirani leptoni (označeni s j), objekti koji nisu izolirani, a mogu biti ili mlazovi ili leptoni nastali u mlazovima.

Signal i ireducibilne pozadine imaju tri prava leptona, dok Z+mlazovi s leptonskim Z raspadima i $\mathrm{t\bar{t}}$ najčešće imaju po jedan pogrešno identificirani lepton. Ostale pozadine većinom imaju po dva ili više pogrešno identificirana leptona.

Definira se relaksirana (L od eng. *loose*) selekcija miona i elektrona te se leptone koji prolaze tu selekciju naziva L leptonima, a one koji prolaze punu selekciju T (od eng. *tight*) leptonima. Za relaksaciju mionske selekcije oslabljuje se zahtjev izolacije na $Iso^{PF}_{rel} < 1.0$, dok se za elektrone uklanja MVA selekcija i zahtjev izolacije. Pravi i pogrešno identificirani L leptoni tada imaju generalno različite efikasnosti prolaska T kriterija: ϵ_i i p_i, gdje se indeks $i = 1, 2, 3$ koristi za označavanje, redom, Z leptona s većim p_{T}-om, Z leptona s manjim p_{T}-om i W leptona.

Početni uzorak sadrži udio različitih kategorija ovisno o broju pravih ili pogrešno identificiranih leptona:

$$N_{LLL} = n_{\ell\ell\ell} + n_{\ell\ell j} + n_{\ell j\ell} + n_{\ell jj} + n_{j\ell\ell} + n_{j\ell j} + n_{jj\ell} + n_{jjj}. \tag{7.7}$$

Isti uzorak može se razdijeliti po kategorijama broja leptona koji prolaze ili ne prolaze T zahtjev, N_{abc} s $a, b, c = \{T, F\}$ gdje T indicira T lepton, a F indicira lepton koji ne prolazi T zahtjev. Broj događaja u svakoj kategoriji može se izraziti putem efikasnosti ϵ_i i p_i, primjerice u N_{TTT} uzorku koji je upravo broj događaja u konačnoj WZ selekciji:

$$
\begin{aligned}
N_{TTT} = \quad & n_{j\ell\ell} p_1 \epsilon_2 \epsilon_3 + n_{j\ell j} p_1 \epsilon_2 p_3 + n_{jj\ell} p_1 p_2 \epsilon_3 + n_{jjj} p_1 p_2 p_3 \\
& + n_{\ell\ell\ell} \epsilon_1 \epsilon_2 \epsilon_3 + n_{\ell\ell j} \epsilon_1 \epsilon_2 p_3 + n_{\ell j\ell} \epsilon_1 p_2 \epsilon_3 + n_{\ell jj} \epsilon_1 p_2 p_3 .
\end{aligned}
\tag{7.8}
$$

Ostale kategorije se konstruiraju analogno te se takav sustav jednadžbi može riješiti. Tada za $n_{\ell\ell\ell}$ dobivamo:

$$
\begin{aligned}
n_{\ell\ell\ell} \quad = \quad & \frac{1}{(\epsilon_1 - p_1)(\epsilon_2 - p_2)(\epsilon_3 - p_3)} \\
& [\ N_{TTT}(1 - p_1)(1 - p_2)(1 - p_3) \\
& - N_{TTF}(1 - p_1)(1 - p_2)(\ p_3) \\
& - N_{TFT}(1 - p_1)(\ p_2)(1 - p_3) \\
& + N_{TFF}(1 - p_1)(\ p_2)(\ p_3) \\
& - N_{FTT}(\ p_1)(1 - p_2)(1 - p_3) \\
& + N_{FTF}(\ p_1)(1 - p_2)(\ p_3) \\
& + N_{FFT}(\ p_1)(\ p_2)(1 - p_3) \\
& - N_{FFF}(\ p_1)(\ p_2)(\ p_3)].
\end{aligned}
\tag{7.9}
$$

Udio događaja s tri prava leptona u konačno selektiranom uzorku je $n^T_{\ell\ell\ell} = \epsilon_1 \epsilon_2 \epsilon_3 n_{\ell\ell\ell}$. Iako to nije prikazano, vrijednosti se zbrajaju preko svih događaja pri čemu im se dodjeljuje težina, s obzirom da su ϵ_i i p_i ovisni o kinematskim varijablama svakog pojedinog leptona.

Efikasnosti ϵ_i se procjenjuju iz $Z \to \ell\ell$ događaja korištenjem T&P (od eng. *Tag and Probe*) metode. U toj metodi se događaji selektiraju tako da se dobije uzorak pravih Z raspada. Efikasnost kriterija zatim se procjenjuje na tako izoliranim pravim leptonima.

Efikasnosti p_i procjenjuje se na uzorku QCD događaja koji je selektiran tako da se izolira što čišći uzorak događaja s nekoliko mlazova. U tako selektiranim događajima zatim se postavlja zahtjev na minimalnu transverzalnu energiju vodećeg mlaza $E_T^{\text{LeadJet}} > 50$ GeV. Mlaz na kojem se procjenjuje efikasnost p_i mora biti geometrijski razdvojen od vodećeg mlaza za $\Delta R > 1$. U uzorku mlazova zatim se traže elektroni pogrešno identificirani kao L leptoni te se iz udjela koji prolazi T selekciju dobiva mjerenje p_i.

Konačan rezultat opisane metode prikazan je u tablici 7.9.

Tablica 7.9: Rezultati metode procjene pozadina iz podataka.

	$3e$	$2e1\mu$	$2\mu 1e$	3μ
$\epsilon_1\epsilon_2\epsilon_3 n_{\ell\ell\ell}$	61.83 ± 8.08	60.48 ± 7.93	67.59 ± 8.42	95.23 ± 9.89
$N_{TTT} - \epsilon_1\epsilon_2\epsilon_3 n_{\ell\ell\ell}$	2.17 ± 0.40	1.52 ± 0.28	2.41 ± 0.36	1.77 ± 0.24
N_{TTT}	64	62	70	97
N_{TTF}	16	14	43	47
N_{TFT}	13	7	13	8
N_{TFF}	5	1	3	6
N_{FTT}	33	59	42	64
N_{FTF}	11	8	19	15
N_{FFT}	5	6	0	8
N_{FFF}	1	8	3	6

Ostale pozadine

Pozadine koje su slične signalu ne mogu se ukloniti metodom opisanom u odjeljku 7.4.5, budući da je efikasnost selekcije leptona u njima slična ili istovjetna signalu. ZZ pozadina većinom se odbacuje zahtjevom za postojanjem točno tri leptona u događajima, a preostali udio procjenjuje se iz MC uzoraka. Zγ pozadina većinom se odbacuje zahtjevima koji odbacuju konverziju fotona u elektrone, a preostali udio, koji sadrži fotone detektirane kao izolirane elektrone, također se procjenjuje iz MC-a. Procjene doprinosa ovih pozadina navedene su u tablici 7.7.

7.4.6 Mjerenje udarnog presjeka

Mjerenje udarnog presjeka zasniva se na relaciji

$$\sigma = \frac{N_{\text{sig}}}{A \times \epsilon \cdot \mathcal{L}}, \tag{7.10}$$

gdje je N_{sig} procijenjeni broj događaja signala, $A \times \epsilon$ je akceptanca detektora i efikasnost selekcije, a $\mathcal{L}$ je integrirani luminozitet za mjereni period. N_{sig} je definiran kao

$$N_{\text{sig}} = (1 - f_\tau) \cdot (N_{signal}^{data-driven} - N_{ZZ} - N_{Z\gamma}), \tag{7.11}$$

gdje su $N_{signal}^{data-driven}$, N_{ZZ} i $N_{Z\gamma}$ redom rezultati procjene signala iz podataka te ZZ i Zγ pozadina iz MC uzoraka u konačnoj selekciji.

$A \times \epsilon$ (u daljnjem tekstu akceptanca) se procjenjuje iz MC uzorka signala:

$$A \times \epsilon = \frac{\text{broj selektiranih } WZ \to \ell\ell\ell\nu \text{ događaja}}{\text{broj produciranih događaja signala}}. \tag{7.12}$$

Akceptanca se računa za svaki kanal zasebno. U brojniku su zbrojeni svi $WZ \to \ell\ell\ell\nu$ događaji koji prolaze selekciju za određeni kanal, a u nazivniku svi događaji koji prema generatorskoj informaciji dostupnoj u događaju pripadaju tom kanalu. Na sve događaje u brojniku primjenjuje se korekcija preklopa događaja, faktori skaliranja leptona, kao i simulacija efikasnosti okidača. Tako dobivene vrijednosti navedene su u tablici 7.10.

Tablica 7.10: $(A \times \epsilon)^{ch}_{\mathrm{corr}}$ za svaki kanal selekcije.

Kanal	$(A \times \epsilon)^{ch}_{\mathrm{corr}}$
eee	$0.1362 \pm 0.0012(stat)$
$ee\mu$	$0.1523 \pm 0.0012(stat)$
$\mu\mu e$	$0.1704 \pm 0.0013(stat)$
$\mu\mu\mu$	$0.2265 \pm 0.0014(stat)$

Sistematske nesigurnosti

Sistematske nesigurnosti u analizu ulaze kroz bilo koji od parametara korištenih u računu udarnog presjeka. Na akceptancu A utječu nesigurnosti u određivanju PDF raspodjele [84, 85] i nesigurnosti u QCD skali i skali faktorizacije [22].

Efikasnost ϵ ovisi o instrumentalnim nesigurnostima vezanim za objekte analize. Pri rekonstrukciji i identifikaciji elektrona i miona, mjerenje faktora skaliranja također uključuje i procjenu sistematskih nesigurnosti. Uzima se također i prilično konzervativna procjena nesigurnosti skale energije ili impulsa elektrona (2-5%) i miona (1%). E_T^{miss}nesigurnost određuje se razmazivanjem skale energije i impulsa svih PF objekata za pripadajuće nesigurnosti. Simulacija okidača unosi nesigurnost mjerenja efikasnosti okidača u selekciji leptona. Nesigurnost u neelastičnom udarnom presjeku pp sudara je $\pm 5\%$ što utječe na preciznost simulacije preklopa događaja.

Na procjenu pozadine iz podataka najviše utječe QCD uzorak koji se koristi za izračun p_i. S obzirom da su dominantne pozadine s mlazovima uglavnom Z+mlazovi i $\mathrm{t\bar{t}}$, nepoznat je njihov pravi omjer u mjerenom uzorku, tako da preciznost p_i ovisi da li je taj omjer točno pogođen u

QCD uzorku. Da bi se to uzelo u obzir, varira se E_T^{LeadJet} čime se spektar mlazova mijenja od jedne krajnosti, spektra sličnog Z+mlazovi pozadini, do druge gdje je sličan $\mathrm{t\bar{t}}$ pozadini. U ta dva slučaja dobiva se različita procjena signala te se razlika uzima kao nesigurnost na $N_{signal}^{data-driven}$.

Pozadinama procijenjenim iz MC uzoraka pridjeljuju se nesigurnosti iz CMS mjerenja njihovog udarnog presjeka, 14% za ZZ[86] i 7% za Zγ [87].

Kao što je opisano u odjeljku 7.3.3, nesigurnost na mjerenje luminoziteta je 2.2%. Sve nesigurnosti se propagiraju kao utjecaj na pripadajuće parametre te se propagiraju kroz relaciju 7.10 da bi se procijenio utjecaj na udarni presjek. Rezultati procjene sistematskih grešaka prikazani su u tablici 7.11.

Tablica 7.11: Sažetak mjerenja sistematskih nesigurnosti mjerenja WZ udarnog presjeka.

		eee	$ee\mu$	$\mu\mu e$	$\mu\mu\mu$
izvor	sistematska nesigurnost	utjecaj na WZ udarni presjek			
skala energije elektrona	2%(EB),5%(EE)	1.9%	0.75%	1.2%	n/a
p_T skala miona	1%	n/a	0.60%	0.43%	1.06%
E_T^{miss}rezolucija i skala		3.7%	3.4%	4.3%	3.7%
leptonski faktori skaliranja i okidač		2.9%	2.7%	2.0%	1.4%
preklop događaja		0.27%	0.50%	1.00%	0.64%
PDF	1.4%	1.4%	1.4%	1.4%	1.4%
QCD i skala faktorizacije	1.3%	1.3%	1.3%	1.3%	1.3%
ZZ udarni presjek	14%	0.50%	0.92%	0.62%	0.85%
$Z\gamma$ udarni presjek	7%	0.%	0.	0.04%	0
procjena pozadina iz podataka		2.7%	6.5%	6.3%	6.0%
izvor	sistematska nesigurnost	utjecaj na luminozitet			
luminozitet	2.2%	2.2%	2.2%	2.2%	2.2%

Mjerenje udarnog presjeka u pojedinim kanalima i kombinacija

Rezultati mjerenja udarnog presjeka u pojedinim kanalima dani su u tablici 7.12. Pri određivanju inkluzivnog udarnog presjek korištene su vrijednosti omjera grananja navedene u tablici 7.3.

Tablica 7.12: WZ udarni presjek za $\int \mathcal{L}\, dt = 4.92$ fb^{-1} u svakom kanalu.

kanal	udarni presjek [pb]	inkluzivni udarni presjek ($\sigma_{ch}(\mathrm{WZ})/BR_{ch}$) [pb]
$3e$	$0.0834 \pm 0.0110(stat) \pm 0.0051(sist) \pm 0.0018(lumi)$	$23.08 \pm 3.12(stat) \pm 1.41(sist) \pm 0.51(lumi)$
$2e\mu$	$0.0702 \pm 0.0098(stat) \pm 0.0055(sist) \pm 0.0015(lumi)$	$19.75 \pm 2.75(stat) \pm 1.54(sist) \pm 0.43(lumi)$
$2\mu e$	$0.0719 \pm 0.0094(stat) \pm 0.0058(sist) \pm 0.0016(lumi)$	$19.86 \pm 2.60(stat) \pm 1.60(sist) \pm 0.44(lumi)$
3μ	$0.0749 \pm 0.0082(stat) \pm 0.0054(sist) \pm 0.0016(lumi)$	$21.06 \pm 2.31(stat) \pm 1.53(sist) \pm 0.46(lumi)$

Rezultati mjerenja kombinirani su BLUE metodom [88], kojom se kombinirani udarni presjek određuje kao linearna kombinacija rezultata u pojedinim kanalima

$$\sigma(WZ \to 3l) = \alpha_1 \sigma_{WZ\to ee e\nu} + \alpha_2 \sigma_{WZ\to ee\mu\nu} + \alpha_3 \sigma_{WZ\to \mu\mu e\nu} + \alpha_4 \sigma_{WZ\to \mu\mu\mu\nu}. \tag{7.13}$$

α_1, α_2, α_3 i α_4 su težinski faktori određeni minimiziranjem nesigurnosti kombiniranog udarnog presjeka te vrijedi $\sum_{i=1..4} \alpha_i = 1$. Metoda također uzima u obzir sistematske nesigurnosti koje su korelirane među pojedinim kanalima.

Dobivene vrijednosti α faktora su $\alpha_1 = 0.190$, $\alpha_2 = 0.239$, $\alpha_3 = 0.248$ i $\alpha_4 = 0.323$ što za kombinirani udarni presjek daje

$$\sigma_{incl.WZ} = 20.83 \pm 1.32 \text{ (stat.)} \pm 1.14 \text{ (sist.)} \pm 0.46 \text{ (lumi.) pb}. \tag{7.14}$$

Očekivani teorijski WZ udarni presjek dobiven MCFM programom iznosi $\sigma_{incl.WZ}(NLO) = 17.8^{+0.7}_{-0.5}$ pb. Omjer mjerenog i teorijskog udarnog presjeka prikazan je na slici 7.10.

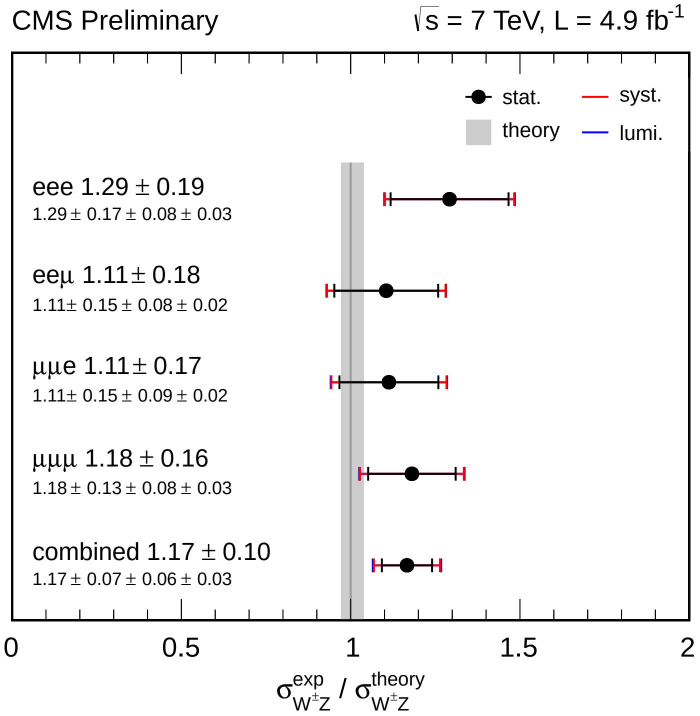

Slika 7.10: Omjer mjerenog i očekivanog teorijskog udarnog presjeka $\sigma^{\mathrm{theo}}_{\mathrm{WZ}} = 17.8$ pb za WZ produkciju na $\sqrt{s} = 7\,\mathrm{TeV}$.

7.4.7 Rezultati drugih eksperimenata i diskusija

Produkcija para W i Z bozona mjerena je na Tevatronu i ATLAS eksperimentu na LHC-u. Dobiveni rezultati sažeti su u tablici 7.13.

Rezultati mjerenja udarnog presjeka WZ produkcije predstavljeni u ovom radu nešto su viši od predviđanja Standardnog modela. Odstupanje kombiniranog udarnog presjeka je unutar dvije stan-

Tablica 7.13: Mjerenja WZ inkluzivnog udarnog presjeka na drugim eksperimentima.

	$\sqrt{s}$	$\int Ldt$	izmjereni $\sigma_{inclusive}(WZ)[pb]$	teorijski $\sigma_{NLO}(WZ)[pb]$
D0[89]	1.96 TeV ($p\bar{p}$)	4.1 fb^{-1}	$3.89^{+1.02}_{-0.85}$(stat. + sist.) ± 0.31(lumi.)	3.25 ± 0.19
CDF[90]	1.96 TeV ($p\bar{p}$)	7.1 fb^{-1}	$3.9^{+0.8}_{-0.7}$(stat. + sist.)	3.46 ± 0.21
ATLAS[92]	7 TeV (pp)	4.6 fb^{-1}	$19.0^{+1.4}_{-1.3}$(stat.) ± 0.9(sist.) ± 0.4(lumi.)	$17.6^{+1.1}_{-1.0}$
ATLAS[93]	8 TeV (pp)	13 fb^{-1}	$20.3^{+0.8}_{-0.7}$(stat.)$^{+1.2}_{-1.1}$(sist.)$^{0.7}_{0.6}$(lumi.)	20.3 ± 0.8

dardne devijacije, kao što je vidljivo na slici 7.10. Slično ponašanje primijećeno je pri mjerenju WZ udarnog presjeka na energiji sustava centra mase $\sqrt{s} = 8$ TeV-a na CMS-u [79], kao i pri mjerenjima udarnih presjeka nekoliko drugih multibozonskih kanala [87, 94–96] na CMS-u i ATLAS-u. Međutim, u nijednom od ovih mjerenja odstupanje nema veliku signifikantnost (veću od tri standardne devijacije) pa je moguće da su takvi rezultati posljedice statističkih fluktuacija te su potrebne detaljnije analize i usporedbe, uključujući i mjerenja na većim energijama sudara.

Sažetak mjerenja udarnih presjeka elektroslabih procesa na CMS-u prikazan je na slici 7.11.

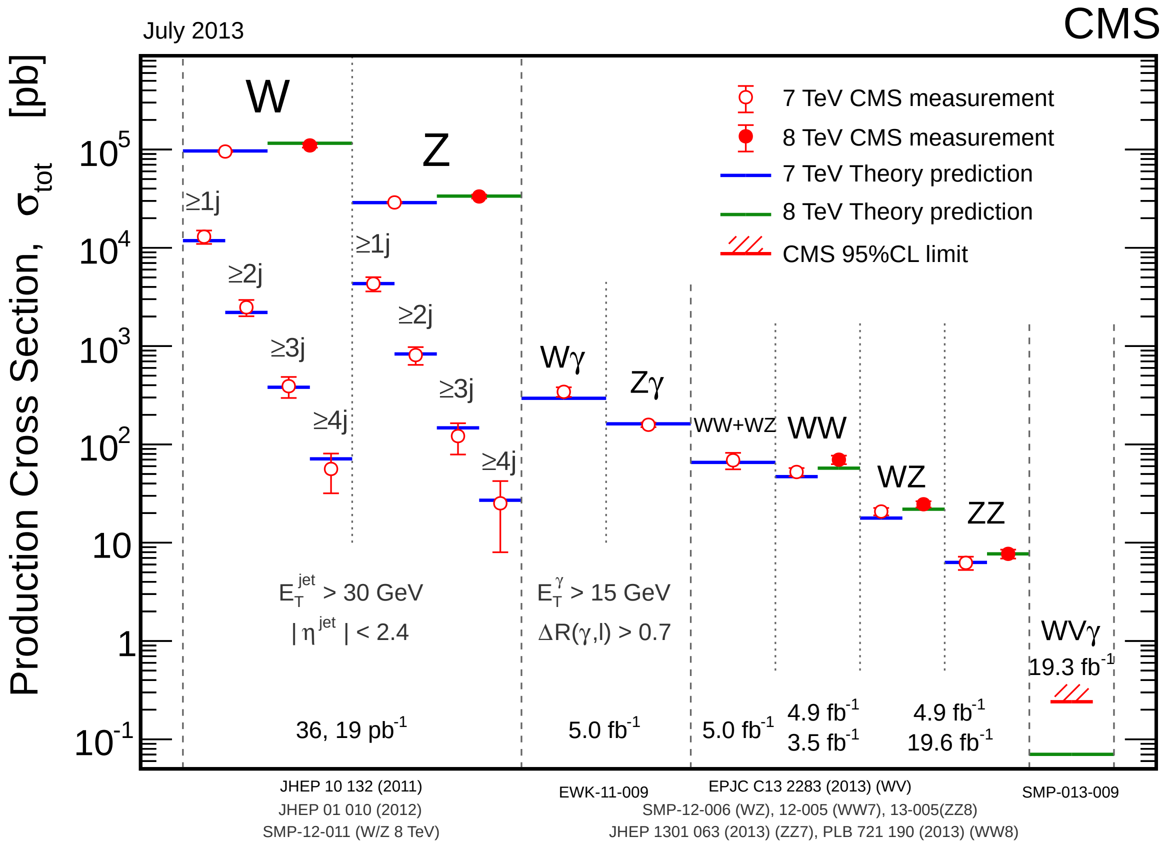

Slika 7.11: Prikaz mjerenih udarnih presjeka elektroslabih procesa na CMS-u.

7.5 Potraga za WZ rezonancijama

U ovom odjeljku opisana je analiza i rezultati potrage za SSM i Tehnikolor rezonancijama u WZ kanalu raspada. Predstavljeni rezultati su objavljeni (ref.[97]). Ova je analiza slična onoj kod mjerenja udarnog presjeka i završena je prije nego što je započeto mjerenje udarnog presjeka. Stoga postoje razlike u identifikaciji leptona i glavnim koracima WZ selekcije, kao i neki dodatni zahtjevi u analizi. Sve te razlike biti će navedene i opisane u ovom odjeljku.

7.5.1 Opis signala i uzorci

Glavna konceptualna razlika jest da je pozadina novim rezonancijama upravo WZ proces predviđen SM-om. Iako je konačno stanje WZ rezonancija identično WZ-u, zbog njihove velike mase kinematske se raspodjele znatno razlikuju.

Analizirani su podaci iz 2011. godine na energiji 7 TeV-a, uzevši u obzir nešto veći skup prikupljenih podataka, ukupnog integriranog luminoziteta približno 5.0 fb^{-1}. Za opis pozadina koriste se identični MC uzorci kao i u analizi WZ udarnog presjeka. Za generiranje MC uzoraka koji simuliraju W' i ρ_{TC} rezonancije korišten je PYTHIA [98] generator. Zbog problema u TC implementaciji, u konačnici su korišteni samo W' uzorci s pripadajućim TC udarnim presjekom, s obzirom na slična kinematska svojstva W' i ρ_{TC} rezonancija. Generirano je ukupno 15 uzoraka za mase W' rezonancije u rasponu od 200 GeV-a do 1500 GeV-a. S obzirom da PYTHIA podržava samo račun matričnih elemenata prvog reda (LO), na udarni presjek svakog uzorka primijenjeni su NNLO korekcijski faktori (k-faktori). MC uzorci W' produkcije s pripadajućim udarnim presjecima prikazani su u tablici 7.14.

Za Tehnikolor su korišteni LSTC udarni presjeci dobiveni pomoću PYTHIA generatora te k-faktori za parametarski prostor koji zadovoljava relaciju

$$M(\pi_{TC}) = \frac{3}{4}M(\rho_{TC}) - 25\,\mathrm{GeV}, \tag{7.15}$$

korišten u prethodnim CMS potragama (poznat i kao *Les Houches* parametarski prostor) [51]. TC udarni presjeci za masene točke korištene u analizi navedeni su u tablici 7.15.

Tablica 7.14: Pregled W$^{'}$ $\rightarrow WZ \rightarrow \ell\nu\ell\ell$ uzoraka SSM W$^{'}$ signala korištenih u analizi. Udarni presjeci uključuju omjere grananja bozonskih raspada u nabijene leptone (e, μ ili τ).

$M(\mathrm{W}^{'})$ [GeV]	σ_{LO} (pb)	σ_{NNLO} (pb)	k-faktor
200	1.324	1.797	1.357
250	1.118	1.517	1.357
300	0.6337	0.8599	1.357
400	0.204	0.2768	1.357
500	0.07915	0.1074	1.357
600	0.0362	0.0489	1.351
700	0.01806	0.0244	1.352
800	0.009857	0.01328	1.347
900	0.005551	0.00744	1.341
1000	0.003322	0.00442	1.332
1100	0.002041	0.002704	1.325
1200	0.001289	0.001690	1.311
1300	0.0008333	0.001082	1.298
1400	0.0005395	0.000690	1.279
1500	0.0003606	0.000456	1.265

Variranjem omjera grananja WZ kanala raspada ρ_{TC} rezonancija dobiveni su i rezultati za veći fazni prostor parametara $M(\rho TC)$ i $M(\pi_{TC})$, uključujući i fazni prostor korišten u potragama na D0 eksperimentu ($M(\rho TC) < M(\pi_{TC}) + M(W)$).

Tablica 7.15: Tehnikolor parametri za masene točke korištene u analizi. Udarni presjeci uključuju omjere grananja bozonskih raspada u nabijene leptone (e, μ ili τ).

$M(\rho_{TC})$ = $M(\omega_{TC})$[GeV]	$M(a_{TC})$[GeV]	$M(\pi_{TC})$[GeV]	$\sigma_{\mathrm{LO}} \times BR$(pb)	$\sigma_{\mathrm{NNLO}} \times BR$(pb)
200	220	125	0.3872	0.5254
250	275	163	0.2144	0.2909
300	330	200	0.09616	0.1305
400	440	275	0.02889	0.03920
500	550	350	0.01172	0.01590
600	660	425	5.612×10^{-3}	7.582×10^{-3}
700	770	500	2.943×10^{-3}	3.979×10^{-3}
800	880	575	1.670×10^{-3}	2.249×10^{-3}
900	990	650	0.974×10^{-3}	1.306×10^{-3}

Na sve MC uzorke primjenjuju se težinski faktori kako bi se dobila raspodjela preklopa događaja koja odgovara podacima, na sličan način kao i kod mjerenja udarnog presjeka (odjeljak 7.4.3). Korišten je neelastični pp udarni presjek $\sigma_{pp} = 73.5pb$.

7.5.2 Selekcija

Identifikacija objekata analize

Na leptone koji su pridruženi Z bozonu primijenjeni su relaksirani uvjeti (L), dok su na leptone pridružene W bozonu primijenjeni stroži uvjeti (T).

Identifikacija i selekcija miona je, osim u izolaciji, identična selekciji opisanoj u odjeljku 7.4.2.

Međutim, identifikacija elektrona značajno se razlikuje te se ne koristi MVA metoda već selekcija zasnovana na rezovima. U tu svrhu korištene su neke od varijabli opisanih u odjeljku 7.4.2, a za odbacivanje elektrona nastalih konverzijama koristi se zahtjev na udaljenost tragova i ograničenje vrijednosti kuta između tragova $\Delta cot(\theta) > 0.02$. Zahtjevi su navedeni u tablici 7.16.

Izolacija leptona (Iso_{rel}) određuje se iz izolacije u pojedinim poddetektorima (HCAL-u, ECAL-u i detektoru tragova) u konusu $\Delta R < 0.3$ oko leptonskog kandidata:

$$E_T^{iso} = \sum_i^{tracker} p_{\mathrm{T}}(i) + \sum_i^{ECAL} E_{\mathrm{T}}(i) + \sum_i^{HCAL} E_{\mathrm{T}}(i). \tag{7.16}$$

Ta se veličina normalizira s leptonskim transverzalnim impulsom $p_T(\ell)$: $Iso_{rel} = E_T^{iso}/p_{\mathrm{T}}(l)$. Od dobivene vrijednosti oduzima se procijenjena količina dodatne aktivnosti od preklopa događaja, izračunata korištenjem FASTJET algoritma [99, 100], te se dobiva korigirana varijabla izolacije, Tablica 7.16: Selekcijski zahtjevi na elektrone.

	elektroni iz Z	Elektroni iz W
zahtjev	EB (EE)	EB (EE)
kinematski	$p_{\mathrm{T}} > 10$ GeV	$p_{\mathrm{T}} > 20$ GeV
	$\|\eta\| < 2.5$	$\|\eta\| < 2.5$
maks. $\sigma_i\eta i\eta$	<0.012(0.031)	<0.010(0.31)
maks. $\|\Delta\phi_{in}\|$	<0.8(0.7)	<0.027(0.021)
maks. $\|\Delta\eta_{in}\|$	<0.007(0.011)	<0.005(0.006)
broj nedostajućih pogodaka	0	0
udaljenost između tragova(cm)	-	>0.02
$\Delta cot(\phi)$	-	<0.02
Iso^{corr}_{rel}	<0.15(0.10)	<0.07(0.06)

Iso^{corr}_{rel}. U slučaju miona vrijednost reza na tu varijablu iznosi $Iso^{corr}_{rel} < 0.15$ (L selekcija) ili $Iso^{corr}_{rel} < 0.10$ (T selekcija), dok su vrijednosti rezova korištene u izolaciji elektrona navedene u tablici navedene u tablici 7.16.

Efikasnosti identifikacije leptona procjenjuju se na MC uzorcima i podacima te se računaju MC korekcije koje se primjenjuju na selektirane MC događaje. Za to se, kao i kod mjerenja udarnog presjeka, koristi T&P metoda.

Za E_T^{miss} rekonstrukciju koristi se PF algoritam te se ne koriste dodatne korekcije.

Selekcija događaja

Selekcija je također definirana zasebno za četiri selekcijska WZ kanala ovisno o tome da li su W i Z rekonstruirani iz elektrona ili miona. Na kraju se selektirani događaji u svim kanalima zbrajaju i koriste kod određivanja granica na udarni presjek produkcije novih rezonancija.

S iznimkom korištenja samo jedne HLT staze za selekciju elektrona, korišten je identičan skup HLT staza kao u 7.4.3. U ovom slučaju HLT zahtjevi se također primjenjuju na MC uzorke, korištenjem ekvivalentnih HLT staza prisutnih u uzorcima. Leptoni iz raspada Z kandidata također moraju biti geometrijski kompatibilni s leptonima selektiranim u okidaču (unutar konusa $\Delta R < 0.1$) na koje se postavljaju i zahtjevi transverzalnog impulsa većeg od 17 i 8 GeV-a. Z kandidat mora imati invarijantnu masu u prozoru $m_Z \in [60, 120]$ GeV-a.

Također se zahtijeva da ne postoji drugi Z kandidat u prozoru mase Z bozona $m_Z \in [60, 120]$ GeV-a s leptonima pridruženim Z bozonu koji zadovoljavaju L selekciju. Ti leptoni moraju imati $p_\mathrm{T} > 10$ GeV-a, a njihova kompatibilnost s leptonima iz okidača se ne zahtijeva.

Treći lepton u događaju ne mora biti geometrijski izoliran od leptona iz raspada Z kandidata, već mora zadovoljavati T selekciju i imati $p_\mathrm{T} > 20$ GeV-a. Zahtjev na nedostajuću transverzalnu energiju je $E_T^{miss} > 30$ GeV-a.

Dodatni zahtjevi postavljeni su da bi se potisnula WZ pozadina. Zbog veće količine ukupnog transverzalnog momenta u događajima signala, postavlja se rez na skalarnu sumu transverzalnog impulsa sva tri nabijena leptona iz raspada W i Z bozona:

$$L_T = \sum_{i=1...3} |\vec{p}_T(l_i)|. \tag{7.17}$$

Također se može postaviti rez na WZ invarijantnu masu. Problem predstavlja nepoznat longitudinalni impuls neutrina, p_z, koji se može grubo procjeniti uz pretpostavku da je masa W bozona jednaka nominalnoj PDG masi $M_W = 80.385$ GeV-a, što vodi na kvadratnu jednadžbu za p_z. Ta jednadžba ima realna rješenja ako je transverzalna masa W bozona

$$M_T(W) \equiv \sqrt{2 \cdot |E_T^{miss}| \cdot |p_T^{lepton}| \cdot (1 - \cos\Delta\phi(p_T^{lepton}, E_T^{miss}))} \tag{7.18}$$

manja od nominalne, a u suprotnom se u jednadžbu uvrštava $M_T(W)$. Iz MC simulacije signala zaključeno je da rješenje za p_z manje apsolutne vrijednosti odgovara longitudinalnom impulsu neutrina u 75% slučajeva.

Rezovi na vrijednost invarijantne WZ mase obuhvaćaju prozor u području oko vrijednosti pojedine masene točke. Točna vrijednost granica dobiva se simultanom optimizacijom L_T reza i granica $M(WZ)$ prozora tako da je osjetljivost na postavljanje granica na udarni presjek nove rezonancije što veća. Primjer distribucije WZ mase za W$'$ generiran na 600 GeV-a prikazan je na slici 7.12.

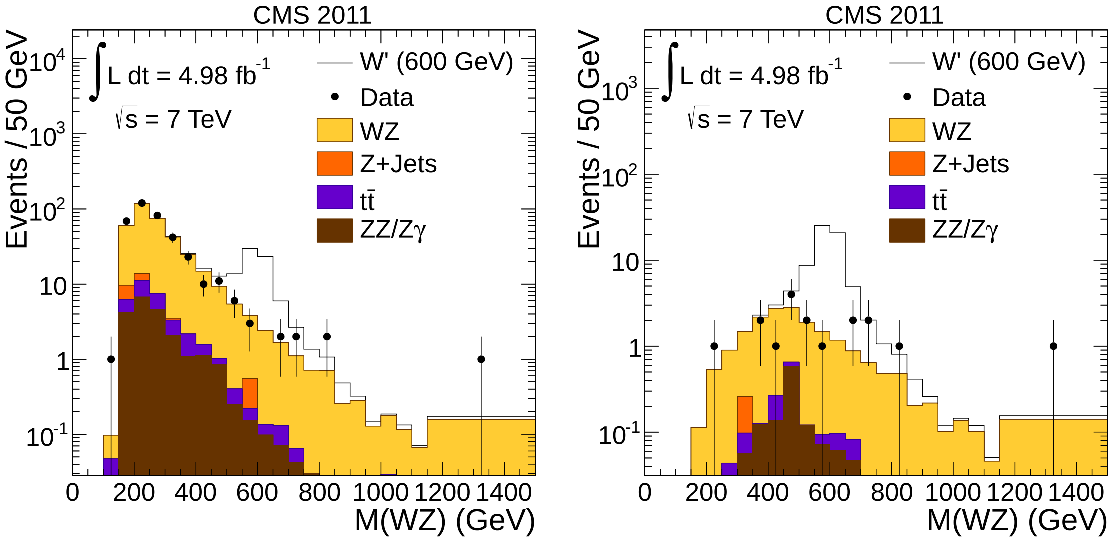

Slika 7.12: Distribucija WZ invarijantne mase prije (lijevo) i nakon (desno) zahtjeva $L_T > 290$ GeV za W$'$ masenu točku na 600 GeV-a.

7.5.3 Sistematske nesigurnosti

Svaka od nesigurnosti procijenjuje se zasebno za signal i pozadine svake selektirane masene točke. S obzirom da se u konačnom rezultatu koristi zbroj događaja iz sva četiri selekcijska kanala, sistematske pogreške su izračunate samo za zbroj kanala, odnosno dane kao utjecaj na očekivani broj događaja. Izračun PDF nesigurnosti identičan je kao i u 7.4.6 te su procijenjene nesigurnosti za različite masene točke u rasponu od 2% do 28% za WZ pozadinu te u rasponu od 2% do 8% za signal.

Za skalu energije i impulsa koristi se pristup variranja kinematskih varijabli, u rasponu od 1% za mione te 2% za elektrone. Nesigurnosti faktora skaliranja, dobivene iz T&P mjerenja, propagiraju se kroz selekciju da bi se procijenio njihov efekt, a slična procedura primjenjuje se i za zahtjev geometrijskog poklapanja leptona s onima iz okidača. Procjena E_T^{miss} nesigurnosti razlikuje se od metode korištene za mjerenje udarnog presjeka. i detaljno je opisana u ref.[103]. Nesigurnost preklopa događaja dobivena je variranjem broja verteksa u MC događajima za ± 1. Utjecaj ovih nesigurnost sažet je u tablici 7.17.

Nesigurnosti udarnih presjeka pozadina procijenjene su korištenjem programa [22] osim u slučaju Zγ pozadine gdje je korišten mjereni udarni presjek na energiji 7 TeV-a [101] iz 2010. godine. Nesigurnost mjerenja luminoziteta je 2.2%.

7.5.4 Postavljanje ograničenja

Broj događaja dobiven nakon selekcije u svakoj masenoj točki, kao i rezultati optimizacije rezova na L_T i $M(WZ)$ za očekivani signal i pozadinu te za podatke, prikazani su u tablici 7.18. Broj

Tablica 7.17: Sažetak efekta sistematskih nesigurnosti E_T^{miss}, preklopa događaja i skale impulsa i energije leptona na selektirani broj događaja za pozadine (B) i signal (S), dan za svaku masenu točku.

Type	E_T^{miss}skala		E_T^{miss}rezolucija		preklop događaja		mionska p_{T} skala		elektronska E_{T} skala	
masena točka(GeV)	B(%)	S(%)	B(%)	S(%)	B(%)	S(%)	B(%)	S(%)	B(%)	S(%)
200	0.99	0.01	0.52	1.9	1.7	0.31	0.45	3.1	1.0	1.9
250	0.24	0.90	0.59	1.3	2.2	0.58	2.5	1.6	3.1	2.5
300	1.1	0.49	0.72	0.97	1.9	2.0	2.2	0.51	4.3	1.3
400	1.7	0.43	0.77	0.53	2.2	0.71	1.9	1.0	4.2	2.2
500	1.8	0.38	0.91	0.36	2.6	2.3	1.7	0.71	3.6	1.5
600	1.3	0.10	1.4	0.30	1.7	1.6	3.1	0.55	4.8	1.6
700	2.4	0.15	1.7	0.23	3.0	0.82	5.3	0.91	4.2	1.7
800	3.9	0.28	1.9	0.20	4.0	1.4	3.9	0.87	4.3	1.7
900	2.3	0.24	1.9	0.13	3.6	1.6	3.0	0.72	6.4	0.94
1000	2.7	0.03	2.4	0.12	0.36	1.4	5.0	0.37	8.7	0.49
1100	1.1	0.16	2.2	0.13	0.83	1.1	2.6	0.15	6.7	0.51
1200	0.16	0.13	2.6	0.12	1.3	1.2	2.8	0.34	13	0.54
1300	0.70	0.10	2.9	0.12	1.3	1.9	4.7	0.12	5.7	0.38
1400	4.7	0.10	3.7	0.14	2.3	1.4	4.2	0.46	8.2	0.85
1500	0.01	0.02	4.2	0.19	0.92	2.6	0.72	0.37	11	1.3

događaja zbrojen je za sve kanale selekcije. Navedene vrijednosti koriste se kao ulazni podaci za postavljanje ograničenja na udarni presjek.

Za određivanje ograničenja na udarni presjek koristi se CL$_S$ metoda [104], implementirana u RooStats [105] softverskom paketu.

Očekivano ograničenje osjetljivo je na statističke nesigurnosti, kao i na sistematske nesigurnosti parametara koji utječu na rezultat. U ovom mjerenju, ti parametri su luminozitet te akceptanca detektora i efikasnost.

Metoda uvodi vjerojatnosti (L) koje pretpostavljaju prisutnost samo pozadine (B od eng. *background*) ili i signala i pozadine (S+B). Za konačan uzorak događaja (n^*), vjerojatnost za obje hipoteze računa se kao njihov omjer, LLR $\equiv$ L(B)/L(S+B). Očekivana raspodjela LLR vrijednosti za obje

Tablica 7.18: Zahtjevi na najmanji L_T i ograničenja na prozor mase za svaku W′ (ρ_{TC}) masenu točku. Dani su također broj očekivanih događaja pozadina i signala, broj opaženih događaja i efikasnost signala. Sistematske i statističke nesigurnosti su zbrojene u kvadraturi.

$M(\mathrm{W}'/\rho_{TC})$ (GeV)	L_T (GeV)	prozor WZ mase (GeV)	N_{Bkg}^{MC}	podaci	ϵ_{Sig} (%)
200	0	190-210	50.0 ± 9.1	52	8.0 ± 0.4
250	150	230-270	34.1 ± 6.2	40	8.8 ± 0.4
300	160	280-320	23.9 ± 4.5	23	18 ± 1
400	220	360-440	12.8 ± 2.4	7	29 ± 1
500	230	450-550	8.1 ± 1.5	9	41 ± 1
600	290	540-660	3.4 ± 0.7	2	45 ± 1
700	360	620-780	1.79 ± 0.38	2	48 ± 1
800	400	710-890	1.02 ± 0.22	1	52 ± 2
900	400	760-1040	1.03 ± 0.23	0	61 ± 2
1000	400	820-1180	0.77 ± 0.19	0	65 ± 2
1100	400	890-1310	0.55 ± 0.13	0	63 ± 1
1200	400	940-1460	0.42 ± 0.11	0	58 ± 1
1300	400	1020-1580	0.34 ± 0.12	0	50 ± 1
1400	400	1110-1690	0.18 ± 0.05	0	36 ± 1
1500	400	1200-1800	0.13 ± 0.04	0	30 ± 1

pretpostavke tada se dobiva u dva koraka u pseudoeksperimentima u kojima se generiraju uzorci odgovarajući luminozitetu u podacima. Prvo se variraju parametri koji utječu na rezultat prema Gaussovoj distribuciji čija je varijanca određena sistematskim nesigurnosti na pojedine parametre, navedenim u tablici 5.7. Zatim se generira broj događaja za signal i pozadine prema Poissonovoj distribuciji[5]

Za neki n^*, može se izračunati vjerojatnost da ima više od n^* događaja pod B predpostavkom (1-CL$_B$), kao i da ima manje od n^* događaja pod S+B pretpostavkom (CL$_{S+B}$), integracijom preko pripadajućih distribucija vjerojatnosti. Stupanj pouzdanosti za gornju granicu na broj događaja

---

[5] Za B pretpostavku broj događaja signala je nula.

signala n_s tada je $1 - \mathrm{CL}_S$, gdje je CL_S:

$$\mathrm{CL}_S = \frac{\mathrm{CL}_{S+B}}{\mathrm{CL}_B}. \tag{7.19}$$

Konvencijom se za postavljanje isključenja zahtijeva stupanj pouzdanosti od 95%. Najveća vrijednost n_s za koju je CL_S ispod 5% uzima se kao gornja granica na broj događaja signala uz stupanj pouzdanosti od 95%. Gornja granica na n_s pretvara se u gornju granicu na udarni presjek signala dijeljenjem s luminozitetom, akceptancom i omjerom grananja.

U ovom mjerenju, očekivano ograničenje dobiva se uz pretpostavku samo pozadine. Izvršava se $O(1000)$ pseudoeksperimenta za svaku masenu točku. U svakom od njih odabire se jedna vrijednost (N^*_{exp}) iz distribucije pozadine generirane iz Poisson raspodjele nakon varijacije sistematskih vrijednosti parametara, kao što je opisano. Kao srednja vrijednost Poisson raspodjele uzima se broj događaja pozadine dobiven nakon selekcije. N^*_{exp} predstavlja zbroj signala i pozadine ($N^*_{exp} = n_b + n_s$) na koju se primijenjuje CL_S metoda. Zatim se određuje gornja granica na n_s uz stupanj pouzdanosti od 95%. Iz pseudoeksperimenata se dobiva raspodjela gornjih granica n_s. Za konačnu gornju granicu uzima se središnja vrijednost te raspodjele, a iz nje se određuju i pojasevi nesigurnosti (najčešče prikazani žutom i zelenom bojom, kao na slici 7.13). Za očekivano ograničenje provodi se identičan postupak uz pretpostavku $N_{obs} = n_b + n_s$.

U slučaju mjerenja gdje je dobro poklapanje očekivane pozadine i opažanja, često se koristi i Bayesova metoda (pristup je opisan u [106]), koja je manje računski zahtjevna. U odnosu na CL_S metodu, Bayesova metoda daje neznatno različite rezultate za ograničenja postavljena u ovom radu.

7.5.5 Rezultati

Opažena gornja granica na W'udarni presjek u masenom području od 200 GeV-a do 1.5 TeV-a prikazana je na slici 7.13. Na slici su također, u svakoj masenoj točki, prikazani predviđeni udarni presjek W'produkcije s pojasom teorijske nesigurnosti i očekivana gornja granica udarnog presjeka uz pretpostavku postojanja samo pozadine. U dijelu masenog spektra gdje je opažena gornja granica ispod očekivanog udarnog presjeka, postojanje W'bozona je isključeno, odnosno postavljena je donja granica na masu W'rezonancije, $M_{\mathrm{W}'} > 1143$ GeV-a.

Gornja ograničenja ρ_{TC} udarnog presjeka za različite konfiguracijama TC parametarskog prostora prikazana su na slici 7.14. Za referentni fazni prostor ($M(\pi_{TC}) = \frac{3}{4}M(\rho_{TC}) - 25$ GeV) isključen je ρ_{TC} mase između 167 GeV-a i 687 GeV-a. Za parametarski prostor $M(\rho TC) < M(\pi_{TC}) + M(W)$ korišten u mjerenjima D0 eksperimenta, isključen je ρ_{TC} mase između 180 GeV-a i 938 GeV-a.

Slika 7.13 prikazuje također osjetljivost ograničenja ρ_{TC} udarnog presjeka za tri vrijednosti $\sin\chi$ TC parametra, $\sin\chi = 1/2, 1/3$ i $1/4$, koji može utjecati na omjer grananja $\rho_{TC} \to WZ$ [107]. $\sin\chi = 1/3$ se koristi kao nominalna vrijednost modela.

Rezultatih drugih potraga

Detaljne potrage za SSM W'i TC signalom rađene su na D0 eksperimentu [35] te je isključena masa W'bozona u području između 188 GeV-a i 520 GeV-a. Za fazni prostor TC modela $M(\rho TC) < M(\pi_{TC}) + M(W)$ isključena je $M(\rho_{TC})$ u području između 208 GeV-a i 408 GeV-a. CDF kolaboracija objavila je 2011. godine opažanje odstupanja u distribuciji M(2 mlaza) u kanalu W+2 mlaza,

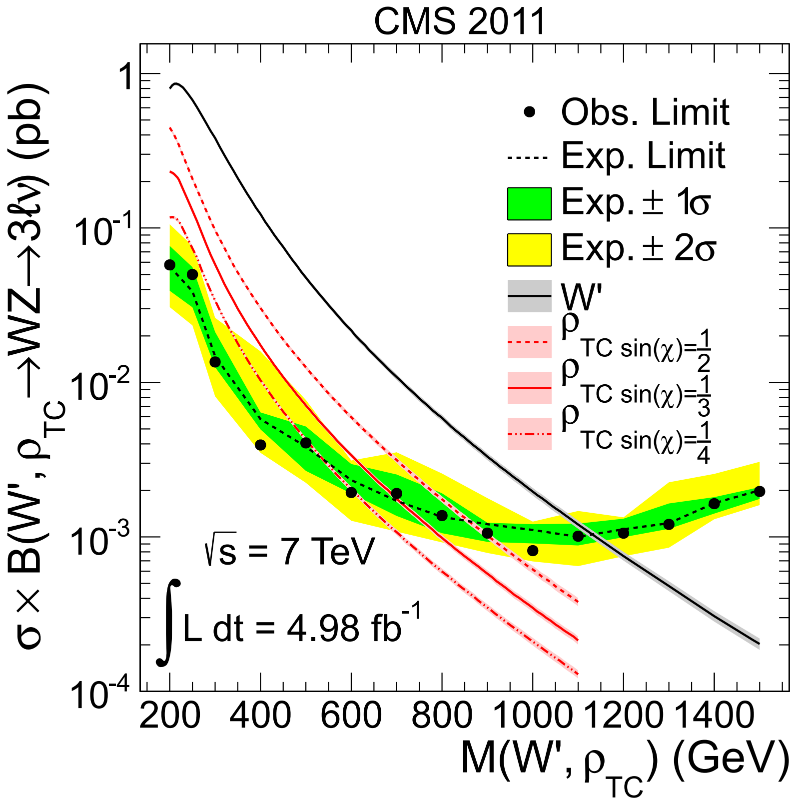

Slika 7.13: Gornja granica W$'$ i ρ_{TC} udarnog presjeka za očekivani i opaženi broj događaja te očekivani udarni presjek signala s pojasom teorijske nesigurnosti. Teorijski ρ_{TC} udarni presjek dan je za tri vrijednosti $\sin\chi$ parametra.

kasnije nazvano "CDF anomalija" [108]. Moguća TC interpretacija [109] isključena je rezultatom prezentiranim u ovom radu.

ATLAS je do sada objavio rezultate potrage za W$'$i ρ_{TC} rezonancijama u WZ kanalu izmjerene na ukupnom integriranom luminozitetu od 13 fb^{-1} na energiji 8 TeV-a [110]. W$'$bozon je isključen za mase do 1180 GeV-a, a ρ_{TC} za mase do 920 GeV-a, pretpostavljajući parametarski prostor $M(\rho TC) < M(\pi_{TC}) + M(W)$ i $M(\rho_{TC}) = 1.1M(a_{TC})$ ili $M(\rho_{TC}) >> M(a_{TC})$.

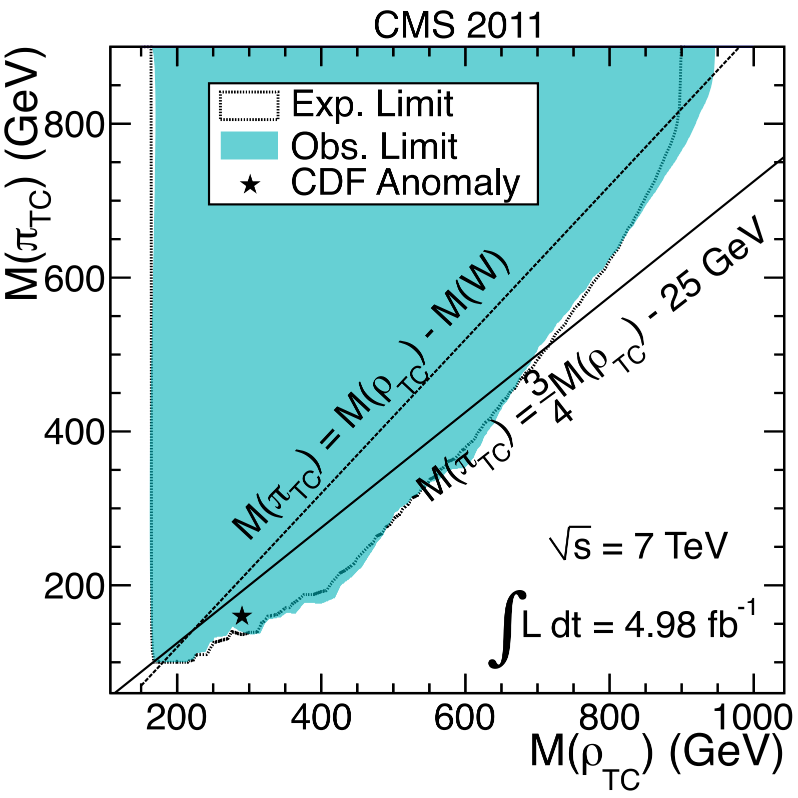

Slika 7.14: Gornja granica na ρTC udarni presjek za opaženi i očekivani broj događaja za različite konfiguracije parametara modela.

Na CMS-u je također napravljena potraga za W' i ρ_{TC} rezonancijama na energiji 8 TeV-a s 19.6 fb^{-1} integriranog luminoziteta. Isključeno je postojanje W' bozona mase između 170 i 1450 GeV-a te su postavljene nove granice na masu ρ_{TC} rezonancije. Radi se o analizi koja je slična analizi prezentiranoj u ovom radu te je detaljnije opisana u ref.[111].

7.6 Zaključak

Inkluzivni udarni presjek WZ produkcije izmjeren je na ukupnom skupu podataka prikupljenim CMS detektorom u 2011. godini te iznosi $\sigma_{incl.WZ} = 20.83 \pm 1.32$ (stat.) $\pm$ 1.14 (sist.) $\pm$ 0.46 (lumi.) pb. Izmjereni udarni presjek pokazuje malo odstupanje unutar dvije standardne devijacije od teorijski predviđene vrijednosti $\sigma_{incl.WZ}(NLO) = 17.8^{+0.7}_{-0.5}$ pb. Taj rezultat zanimljiv je budući da je u nekoliko drugih mjerenja nabijenih VV stanja na ATLAS-u i CMS-u opaženo slično odstupanje: WW [94, 95], Wγ [87, 96] i WZ [79, 92]. Stoga je važno napraviti detaljnije studije tih procesa, uključujući mjerenja na većim energijama sudara.

Potraga za Tehnikolor ρ_{TC} i SSM W$'$rezonancijama u WZ kanalu raspada nije rezultirala odstupanjem od predviđanja Standardnog modela. Donje granice na mase tih teških rezonancija postavljene su uz stupanj pouzdanosti od 95% te je isključena masa W$'$bozona manja od 1143 GeV-a, masa ρ_{TC} rezonancije između 167 i 687 GeV-a za parametarski prostor korišten u prijašnjim CMS mjerenjima te masa ρ_{TC} rezonancije između 180 i 938 GeV-a za parametarski prostor koji je prethodno analizirao D0 eksperiment.

Bibliography

[1] S. Weinberg. "A Model of Leptons". In: *Phys.Rev.Lett.* 19 (1967), pp. 1264–1266.

[2] P.W.Higgs. "Broken Symmetries and the Masses of Gauge Bosons". In: *Phys. Rev. Lett.* 13 (1964), pp. 508–509.

[3] F.Englert and R.Brout. "Broken Symmetry and the Mass of Gauge Vector Mesons". In: *Phys. Rev. Lett.* 13 (1964), pp. 321–323.

[4] G.S. Guralnik and C.R: Hagen. "Global Conservation Laws and Massless Particles". In: *Phys. Rev. Lett.* 13 (1964), pp. 585–587.

[5] D0 Collaboration. "Search for High Mass Top Quark Production in pp Collisions at $\sqrt{s} =$ 1.8 TeV". In: *Phys.Rev.Lett.* 74(13) (1995), pp. 2422–2426.

[6] CDF Collaboration. "Observation of Top Quark Production in pp Collisions with the Collider Detector at Fermilab". In: *Phys.Rev.Lett.* 74(14) (1995), pp. 2626–2631. DOI: `10.1103/PhysRevLett.74.2626`.

[7] CMS Collaboration. "Observation of a new boson with a mass near 125 GeV". In: *CMS Physics Analysis Summary* CMS-PAS-HIG-12-020 (2012).

[8] ATLAS Collaboration. "Observation of an Excess of Events in the Search for the Standard Model Higgs boson with the ATLAS detector at the LHC". In: *ATLAS Note* ATLAS-CONF-2012-093 (2012).

[9] M. Gell-Mann. In: *Physics* 1 (1964), p. 63.

[10] H.David Politzer. "Reliable Perturbative Results for Strong Interactions?" In: *Phys.Rev.Lett.* 30 (1973), 1346–1349. DOI: `10.1103/PhysRevLett.30.1346`.

[11] D.J. Gross and F. Wilczek. "Asymptotically Free Gauge Theories. 1". In: *Phys.Rev. D* 8 (1973), 3633–3652. DOI: `10.1103/PhysRevD.8.3633`.

[12] N. Cabibbo. "Unitary Symmetry and Leptonic Decays". In: *Phys. Rev. Lett.* 10(12) (June 1963), p. 531 533. DOI: `10.1103/PhysRevLett.10.531`.

[13] M. Kobayashi and K. Maskawa. "CP-Violation in the Renormalizable Theory of Weak Interaction". In: *Prog. Theor. Phys.* 49(2) (Feb. 1973), pp. 652–657. DOI: `10.1143/PTP.49.652`.

[14] V. L. Fitch J. H. Christenson J. W. Cronin and R. Turlay. "Evidence for the 2pi Decay of the K20 Meson". In: *Phys. Rev. Lett.* 13 (1964), p. 138.

[15] Müller Greiner Walter and Berndt. 2010. Chap. Spontaneous Symmetry Breaking: The Higgs Sector. ISBN: 978-3-540-87843-8.

[16] G. Degrassi et.al. "Higgs mass and vacuum stability in the Standard Model at NNLO". In: (2012). URL: `http://arxiv.org/abs/1205.6497`.

[17] M. Nakagawa Z. Maki and S. Sakata. "Remarks on the Unified Model of Elementary Particles". In: *Progress of Theoretical Physics* 28 (1962), p. 870. DOI: `10.1143/PTP.28.870`.

[18] B. Pontecorvo. "Mesonium and anti-mesonium". In: *Zh. Eksp. Teor. Fiz.* 33 (1957), 549–551.

[19] B. Pontecorvo. "Neutrino Experiments and the Problem of Conservation of Leptonic Charge". In: *Zh. Eksp. Teor. Fiz.* 53 (1967), p. 1717.

[20] G. Senjanovic N. Mohapatra. "Neutrino Mass and Spontaneous Parity Nonconservation". In: *Phys. Rev. Lett.* 44 (14) (1980), 912–915. DOI: `10.1103/PhysRevLett.44.912`.

[21] J. J. Schechter J.W.F.Valle; Valle. "Neutrino masses in SU(2)xU(1) theories". In: *Phys. Rev.* 22 (9) (1980), 2227–2235. DOI: `10.1103/PhysRevD.22.2227`.

[22] Ciaran Williams John Campbell Keith Ellis. "Vector boson pair production at the LHC". In: *JHEP* 07 (2011), p. 018. arXiv: `hep-ph/1105.0020v1`.

[23] J. Beringer et al. (Particle Data Group). "Review of particle physics". In: *Phys. Rev. D* 86 (2012), p. 010001. DOI: `10.1103/PhysRevD.86.010001`.

[24] Jogesh C. Pati and Abdus Salam. "Lepton number as the fourth 'color'". In: *Phys. Rev. D* 10.1 (July 1974), pp. 275–289. DOI: `10.1103/PhysRevD.10.275`.

[25] G. Altarelli, B. Mele, and M. Ruiz-Altaba. "Searching for new heavy vector bosons in $p\bar{p}$ colliders". In: *Zeitschrift für Physik C Particles and Fields* 45 (1 1989). 10.1007/BF01556677, pp. 109–121. ISSN: 0170-9739. URL: `http://dx.doi.org/10.1007/BF01556677`.

[26] Andreas Birkedal, Konstantin Matchev, and Maxim Perelstein. "Collider phenomenology of the Higgsless models". In: *Phys. Rev. Lett.* 94 (2005), p. 191803. DOI: `10.1103/PhysRevLett.94.191803`. arXiv: `hep-ph/0412278`.

[27] Maxim Perelstein. “Little Higgs models and their phenomenology”. In: *Progress in Particle and Nuclear Physics* 58.1 (2007), pp. 247 –291. ISSN: 0146-6410. DOI: `DOI:10.1016/j.ppnp.2006.04.001`. URL: `http://www.sciencedirect.com/science/article/pii/S0146641006000469`.

[28] Kaustubh Agashe et al. “LHC Signals for Warped Electroweak Charged Gauge Bosons”. In: *Phys. Rev. D* 80 (2009), p. 075007. DOI: `10.1103/PhysRevD.80.075007`. arXiv: `0810.1497 [hep-ph]`.

[29] Christophe Grojean, Ennio Salvioni, and Riccardo Torre. “A weakly constrained W’ at the early LHC”. In: *JHEP* 07 (2011), p. 002. DOI: `10.1007/JHEP07(2011)002`. arXiv: `1103.2761v3 [hep-ph]`.

[30] H. Georgi and S.L. Glashow. “Unity of All Elementary Particle Forces”. In: *Phys. Rev. Lett.* 32 (1974), pp. 438–441.

[31] O. Klein. “Quantentheorie und Fünfdimensionale Relativitätstheorie”. In: *Zeitschrift für Physik* 37 (Dec. 1926), pp. 895–906.

[32] D.A. Dicus R.S. Chivukula and H.-J. “Unitarity of Compactified Five Dimensional Yang-Mills Theory”. In: *Phys. Lett. B* 525 (2002), pp. 175–182. DOI: `10.1016/S0370-2693(01)01435-6`.

[33] Georges Aad et al. “Search for a heavy gauge boson decaying to a charged lepton and a neutrino in 1 fb^{-1} of pp collisions at $\sqrt{s} = 7$ TeV using the ATLAS detector”. In: *Phys. Lett. B* 705 (2011), p. 28. DOI: `10.1016/j.physletb.2011.09.093`. arXiv: `1108.1316 [hep-ex]`.

[34] S. Chatrchyan et al. “Search for leptonic decays of W’ bosons in pp collisions at $\sqrt{s}$=7 TeV”. In: *JHEP* 08 (2012), p. 023. DOI: `10.1007/JHEP08(2012)023`. arXiv: `1204.4764 [hep-exp]`.

[35] V. M. Abazov et al. “Search for a resonance decaying into WZ boson pairs in $p\bar{p}$ collisions”. In: *Phys. Rev. Lett.* 104 (2010), p. 061801. DOI: `10.1103/PhysRevLett.104.061801`. arXiv: `0912.0715 [hep-ex]`.

[36] T. Aaltonen et al. “Search for WW and WZ Resonances Decaying to Electron, Missing E_T, and Two Jets in $p\bar{p}$ Collisions at $\sqrt{s} = 1.96$ TeV.” In: *Phys. Rev. Lett.* 104 (2010), p. 241801. DOI: `10.1103/PhysRevLett.104.241801`. arXiv: `1004.4946 [hep-ex]`. URL: `http://link.aps.org/doi/10.1103/PhysRevLett.104.241801`.

[37] V. M. Abazov et al. “Search for Resonant WW and WZ Production in $p\bar{p}$ Collisions at $\sqrt{s} = 1.96$ TeV”. In: *Phys. Rev. Lett.* 107 (2011), p. 011801. DOI: `10.1103/PhysRevLett.107.011801`. arXiv: `1011.6278 [hep-ex]`.

[38] ATLAS Collaboration. “Search for resonant WZ production in the WZ to l ν l’ l’ channel in $\sqrt{s}$ = 7 TeV pp collisions with the ATLAS detector”. Submitted to Phys. Rev. D. 2012.

[39] CMS Collaboration. “Search for leptonic decays of W’ bosons”. In: *CMS Physics Analysis Summary* EXO-12-060 (2013). URL: `http://cds.cern.ch/record/1522476?ln=en`.

[40] C. Csaki et al. “Gauge Theories on an Interval: Unitarity without a Higgs”. In: *Phys.Rev.D* 69 (2003). DOI: `10.1103/PhysRevD.69.055006`.

[41] M. J. May K. Agashe A. Delgado and R. Sundrum. “RS1, Custodial Isospin and Precision Tests”. In: *JHEP* 0308 (2008), p. 050. DOI: `10.1088/1126-6708/2003/08/050`.

[42] C. Csaki et al. “Towards a Realistic Model of Higgsless Electroweak Symmetry Breaking”. In: *Phys. Rev. Lett.* 92 (2003). DOI: `10.1103/PhysRevLett.92.101802`.

[43] R.S. Chivukula et al. “Multi-Gauge-Boson Vertices and Chiral Lagrangian Parameters in Higgsless Models with Ideal Fermion Delocalization”. In: *Phys. Rev. D* 72 (2005). DOI: `10.1103/PhysRevD.72.075012`.

[44] M.C. Chen et al. “The Review of Particle Physics: W’-Boson Searches”. In: *J. Phys.* G37 (2010), p. 075021. DOI: `10.1088/0954-3899/37/7A/075021`.

[45] Hong-Jian He, Yu-Ping Kuang, Yong-Hui Qi, et al. “CERN LHC signatures of new gauge bosons in the minimal Higgsless model”. In: *Phys. Rev. D* 78 (2008), p. 031701. DOI: `10.1103/PhysRevD.78.031701`. arXiv: `0708.2588v2 [hep-ph]`. URL: `http://link.aps.org/doi/10.1103/PhysRevD.78.031701`.

[46] R. Sekhar Chivukula. “Lectures on Technicolor and Compositeness”. In: (2000), pp. 12–39. URL: `http://arxiv.org/abs/hep-ph/0011264`.

[47] Steven Weinberg. “Implications of Dynamical Symmetry Breaking: An Addendum”. In: *Phys. Rev.* D19 (1979), pp. 1277–1280. DOI: `10.1103/PhysRevD.19.1277`.

[48] Leonard Susskind. “Dynamics of Spontaneous Symmetry Breaking in the Weinberg- Salam Theory”. In: *Phys. Rev.* D20 (1979), pp. 2619–2625. DOI: `10.1103/PhysRevD.20.2619`.

[49] Bob Holdom. “Raising the Sideways Scale”. In: *Phys. Rev.* D24 (1981), p. 1441. DOI: `10.1103/PhysRevD.24.1441`.

[50] Kenneth Lane. “Technihadron production and decay in low-scale technicolor”. In: *Phys. Rev. D* 60.7 (Sept. 1999), p. 075007. DOI: `10.1103/PhysRevD.60.075007`.

[51] Estia Eichten and Kenneth Lane. “Low-scale technicolor at the Tevatron and LHC”. In: *Physics Letters B* 669.3-4 (2008), pp. 235 –238. ISSN: 0370-2693. DOI: `DOI:10.1016/j.physletb.2008.09.047`. URL: `http://www.sciencedirect.com/science/article/pii/S0370269308011908`.

[52] Michael Edward Peskin and Tatsu Takeuchi. “A New constraint on a strongly interacting Higgs sector”. In: *Phys. Rev. Lett.* 65 (1990), pp. 964–967. DOI: `10.1103/PhysRevLett.65.964`.

[53] LHC Collaboration. “LHC Machine”. In: (2008). URL: `http://iopscience.iop.org/1748-0221/3/08/S08001`.

[54] ATLAS Collaboration. “The ATLAS Experiment at the CERN Large Hadron Collider”. In: (2008). URL: `http://iopscience.iop.org/1748-0221/3/08/S08003`.

[55] R. Adolphi et al. “The CMS Experiment at the CERN LHC”. In: *JINST* 3 (2008), S08004. DOI: `10.1088/1748-0221/3/08/S08004`.

[56] ALICE Collaboration. “he ALICE experiment at the CERN LHC”. In: (2008). URL: `http://iopscience.iop.org/1748-0221/3/08/S08002`.

[57] LHCb Collaboration. “The LHCb Detector at the LHC”. In: (2008). URL: `http://iopscience.iop.org/1748-0221/3/08/S08005`.

[58] CMS Collaboration. “Measurement of the inelastic pp cross section at s=7 TeV with the CMS detector”. In: *Physics Analysis Summary* FWD-11-001 (2011).

[59] ATLAS Collaboration. “Measurement of the Inelastic Proton-Proton Cross-Section at s=7 TeV”. In: (2011). URL: `http://arxiv.org/pdf/1104.0326v1`.

[60] CMS collaboration. “The TriDAS project, technical design report. Volume 1: The level-1 trigger”. In: CERN-LHCC-2000-038 (). URL: `http://cdsweb.cern.ch/record/706847`.

[61] CMS collaboration. “The TriDAS project, technical design report. Volume 2: Data acquisition and high-level trigger technical design report”. In: CERN-LHCC-2002-026 (). URL: `http://cdsweb.cern.ch/record/578006`.

[62] R. McLaren A. Racz and E. van der Bij. “The S-Link64 bit extension specification: S-Link64”. In: (). URL: `http://hsi.web.cern.ch/HSI/s-link`.

[63] N.J. Boden et al. “Myrinet — A gigabit per second local area network”. In: *IEEE Micro* 15 (1995), p. 29.

[64] G. Bauer et al. “CMS DAQ event builder based on gigabit ethernet”. In: *IEEE Trans. Nucl. Sci.* 55 (2008), p. 198.

[65] C.-D. Jones et al. “The new CMS data model and framework, in Proocedings of the Conference on Computing in High Energy Physics, Mumbai India (2006).” In: ().

[66] “The Apache Tomcat servlet container”. In: (). URL: `http://tomcat.apache.org`.

[67] Segoni I. Tuura L. Meyer A. and Della Ricca G. “CHEP09, Computing in High Energy Physics, 2009 CMS data quality monitoring: systems and experiences Proc. (Prague, Czech Republic)”. In: (2009).

[68] R. Brun and F. Rademakers. “ROOT — An object oriented data analysis framework”. In: *Nucl. Instrum. Meth. A* 389 (1997), p. 81. URL: `http://root.cern.ch`.

[69] S. J. Allison et al. In: *IEEE Trans. Nucl. Sci.* 53 (2006), p. 270.

[70] *Absolute Calibration of the CMS Luminosity Measurement: Summer 2011 Update*. CMS Physics Analysis Summary CMS PAS EWK-11-001. CERN. URL: `http://cdsweb.cern.ch/record/1376102`.

[71] CMS Collaboration. “Absolute Calibration of the Luminosity Measurement at CMS: Winter 2012 Update”. In: *CMS Physics Analysis Summary* SMP-12-008 (2012). DOI: `1434360.`.

[72] S. Van der Meer. *Calibration of the effective beam height in the ISR*. Tech. rep. CERN-ISR-PO/68-31. 1968.

[73] CMS Collaboration. “Performance of muon identification in pp collisions at $\sqrt{s} = 7$ TeV”. In: *CMS Physics Analysis Summary* CMS-PAS-MUO-10-002 (2010). URL: `http://cdsweb.cern.ch/record/1279140`.

[74] CMS Collaboration. “Electron reconstruction and identification at $\sqrt{s} = 7$ TeV”. In: *CMS Physics Analysis Summary* CMS-PAS-EGM-10-004 (2010). URL: `http://cdsweb.cern.ch/record/1299116`.

[75] CMS Collaboration. *Particle–Flow Event Reconstruction in CMS and Performance for Jets, Taus, and E_T^{miss}*. CMS Physics Analysis Summary CMS-PAS-PFT-09-001. 2009. URL: `http://cdsweb.cern.ch/record/1194487`.

[76] CMS Collaboration. *Commissioning of the Particle-flow Event Reconstruction with the first LHC collisions recorded in the CMS detector*. CMS Physics Analysis Summary CMS-PAS-PFT-10-001. 2010. URL: `http://cdsweb.cern.ch/record/1247373`.

[77] The CMS Collaboration. “Tracking and vertexing results from first Collisions”. In: *TRK-10-001* (2010).

[78] The CMS Collaboration. “Vertex Reconstruction at the CMS Experiment”. In: *Journal of Physics* 110 (2007), pp. 81–86.

[79] CMS. “Measurement of the production cross section of W bosons in association with two b jets in pp collisions at $\sqrt{s}$=7 TeV”. In: CMS-PAS-SMP-2012-006 (2013). URL: `http://cds.cern.ch/record/1537320?ln=en`.

[80] S. Baffioni et al. “Electron reconstruction in CMS”. In: *Eur. Phys. J.* C49 (2007), pp. 1099–1116. DOI: `10.1140/epjc/s10052-006-0175-5`.

[81] CMS Collaboration. “Missing transverse energy performance of the CMS detector”. In: *J. Instrum.* 6 (2011). DOI: `10.1088/1748-0221/6/09/P09001`.

[82] Johan Alwall, Pavel Demin, Simon de Visscher, et al. “MadGraph/MadEvent v4: The New Web Generation”. In: *JHEP* 09 (2007), p. 028. arXiv: `0706.2334v1 [hep-ph]`.

[83] Stefano Frixione, Paolo Nason, and Carlo Oleari. "Matching NLO QCD computations with parton shower simulations: the POWHEG method". In: *JHEP* 11 (2007), p. 070. DOI: `10.1088/1126-6708/2007/11/070`. arXiv: `0709.2092 [hep-ph]`.

[84] J. Pumplin et al. "New Generation of Parton Distributions with Uncertainties from Global QCD Analysis". In: *JHEP* 07 (2002), p. 012. eprint: `hep-ph/0201195`.

[85] John M. Campbell, J.W. Huston, and W.J. Stirling. "Hard Interactions of Quarks and Gluons: A Primer for LHC Physics". In: *Rept.Prog.Phys.* 70 (2007), p. 89. DOI: `10.1088/0034-4885/70/1/R02`. arXiv: `hep-ph/0611148 [hep-ph]`.

[86] *Observation of Z to 4l production in pp collisions at 7 TeV.* CMS Physics Analysis Summary CMS PAS SMP-12-009. CERN. URL: `http://cdsweb.cern.ch/record/1431862`.

[87] CMS. *Measurement of the* $\mathrm{W}\gamma$ *and* $\mathrm{Z}\gamma$ *Cross Sections and Limits on Anomalous Triple Gauge Couplings at* $\sqrt{s} = 7$ *TeV.* CMS Physics Analysis Summary CMS-PAS-EWK-2011-009. 2011. URL: `http://cds.cern.ch/record/1537415`.

[88] Louis Lyons, Duncan Gibaut, and Peter Clifford. "How to combine correlated estimates of a single physical quantity". In: *Nucl.Instrum.Meth.* A270 (1988), p. 110. DOI: `10.1016/0168-9002(88)90018-6`.

[89] V.M. Anderson *et al.* "Measuremenent of the $WZ \to \ell\nu\ell\ell$ cross section and limits on anomalous triple gauge couplings in $p\bar{p}$ collisions at $\sqrt{s} = 1.96$ TeV". In: *Phys. Lett. B* 695 (2011), p. 67. DOI: `10.1016/j.physletb.2010.10.047`.

[90] A. Abulencia *et al.* "Observation of WZ production". In: *Phys. Rev. Lett* 98 (2007), p. 161801. DOI: `10.1103/PhysRevLett.98.161801`.

[91] "Measurement of the WW, WZ, and ZZ cross sections at CMS". In: *CMS Physics Analysis Summary* EWK-11-010 (2011).

[92] ATLAS Collaboration. "Measurement of the WZ production cross section and limits on anomalous triple gauge couplings in proton-proton collisions at $\sqrt{s}$ = 7 Te V with the ATLAS detector". In: *Phys. Lett. B* 709 (2012), p. 341. DOI: `10.1016/j.physletb.2012.02.053`. arXiv: `1111.5570 [hep-ex]`. URL: `http://www.sciencedirect.com/science/article/pii/S0370269312001943`.

[93] ATLAS Collaboration. "A Measurement of $\mathrm{W}^{\pm}\mathrm{Z}$ Production in Proton-Proton Collisions at $\sqrt{s} = 8$ TeV with the ATLAS Detector". In: *ATLAS Note* ATLAS-CONF-2013-021 (2013). URL: `http://cdsweb.cern.ch/record/1525557`.

[94] CMS. *Measurement of WW production rate in pp collisions at* $\sqrt{s}$ *= 7 TeV.* CMS Physics Analysis Summary CMS-PAS-SMP-2012-005. 2012. URL: `http://cds.cern.ch/record/1440234?ln=en`.

[95] Serguei Chatrchyan et al. “Measurement of $\mathrm{W^+W^-}$ and ZZ production cross sections in pp collisions at $\sqrt{s} = 8$ TeV”. In: *Phys.Lett.* B721 (2013), pp. 190–211. DOI: `10.1016/j.physletb.2013.03.027`. arXiv: `1301.4698 [hep-ex]`.

[96] “Measurement of W gamma and Z gamma production cross sections in pp collisions at sqrt(s) = 7 TeV and limits on anomalous triple gauge couplings with the ATLAS detector”. In: *Phys. Lett. B* 717 (2012), pp. 49–69. DOI: `10.1016/j.physletb.2012.09.017`.

[97] “Search for a W’ or techni-rho decaying into WZ in pp collisions at $\sqrt{s} = 7$ TeV”. In: *Phys.Rev.Lett* 109 (2012), p. 141801. DOI: `10.1103/PhysRevLett.109.141801`.

[98] T. Sjöstrand, S. Mrenna, and P. Z. Skands. “PYTHIA 6.4 Physics and Manual”. In: *JHEP* 05 (2006), p. 026. DOI: `10.1088/1126-6708/2006/05/026`. arXiv: `hep-ph/0603175 [hep-ph]`.

[99] Matteo Cacciari and Gavin P. Salam. “Pileup subtraction using jet areas”. In: *Phys. Lett.* B659 (2008), pp. 119–126. DOI: `10.1016/j.physletb.2007.09.077`. arXiv: `0707.1378 [hep-ph]`.

[100] Matteo Cacciari, Gavin P. Salam, and Gregory Soyez. “The Catchment Area of Jets”. In: *JHEP* 04 (2008), p. 005. DOI: `10.1088/1126-6708/2008/04/005`. arXiv: `0802.1188 [hep-ph]`.

[101] Serguei Chatrchyan et al. “Measurement of W-gamma and Z-gamma production in pp collisions at sqrt(s) = 7 TeV”. In: *Physics Letters B* 701.5 (2011), pp. 535 –555. ISSN: 0370-2693. DOI: `10.1016/j.physletb.2011.06.034`. URL: `http://www.sciencedirect.com/science/article/pii/S0370269311006551`.

[102] John M. Campbell and R. K. Ellis. “MCFM for the Tevatron and the LHC”. In: *Nucl. Phys. Proc. Suppl.* 205-206 (2010), pp. 10–15. DOI: `10.1016/j.nuclphysbps.2010.08.011`. arXiv: `1007.3492 [hep-ph]`.

[103] “Modeling of $W \to \ell\nu \not{E}_{\mathrm{T}}$ with Boson Recoil”. In: *Analysis Note* AN-2010-332 (2010).

[104] A. L. Read. “Presentation of search results: The CL(s) technique”. In: *Journal of Physics G: Nuclear and Particle Physics* 28 (10) (2002), 2693–2704. DOI: `10.1088/0954-3899/28/10/313`.

[105] L.Moneta et al. “The RooStats Project”. In: *ACAT2010 Conference Proceedings* (2011). eprint: `arXiv:1009.1003v1`.

[106] M. Bernardo and A. F. M. Smith. John Wiley & Sons, 2000. ISBN: ISBN-13:978-0471494645.

[107] Pavel M. Nadolsky et al. “Implications of CTEQ global analysis for collider observables”. In: *Phys. Rev. D* 78 (2008), p. 013004. DOI: `10.1103/PhysRevD.78.013004`. arXiv: `0802.0007 [hep-ph]`.

[108] CDF Collaboration. “Invariant Mass Distribution of Jet Pairs Produced in Association with a W boson in ppbar Collisions at sqrt(s) = 1.96 TeV”. In: *Phys.Rev.Lett* 106 (2011). DOI: `10.1103/PhysRevLett.106.171801`. URL: `http://arxiv.org/abs/1104.0699`.

[109] Estia J. Eichten, Kenneth Lane, and Adam Martin. “Technicolor Explanation for the CDF Wjj Excess”. In: *Phys. Rev. Lett.* 106 (25 June 2011), p. 251803. DOI: `10.1103/PhysRevLett.106.251803`. URL: `http://link.aps.org/doi/10.1103/PhysRevLett.106.251803`.

[110] ATLAS Collaboration. “Search for resonant WZ→ $3\ell\nu$ production in 1 $\sqrt{s} = 8$ TeV pp collisions with 13 fb^{-1} at ATLAS”. In: *ATLAS Note* ATLAS-CONF-2013-015 (2013). URL: `http://cds.cern.ch/record/1525522`.

[111] “Search for W’/technirho in WZ using leptonic final states”. In: *CMS Physics Analysis Summary* CMS-PAS-EXO-12-025 (2013).

Curriculum Vitae

PERSONAL INFORMATION

Name	Srećko Morović
Address	Lašćinska cesta 114 B Zagreb
E-mail	srecko.morovic@irb.hr, srecko.morovic@cern.ch
Phone	+385 91 508 6038 +385 1 2347 434
Citizenship	Croatian
Date and place of birth	3rd December 1980, Zagreb, Croatia
Languages	Fluent english; Basic German; Mother tongue: Croatian

EDUCATION

- 1995-1999: Classical Gymnasium in Zagreb, Croatia

- 1999-2005: Master studies at Department of Physics, Faculty of Science, University of Zagreb. Diploma thesis title: "Utjecaj grijanja i dopiranja vodikom na otpornost $Zr_{80}Ni_{20}$ metalnog stakla". Diploma advisor: doc. dr. sc. Ivan Kokanović.

- Since 2008: PhD studies at Department of Physics, Faculty of Science, University of Zagreb. Thesis title: "Measurement of W and Z pair production and search for WZ resonances at the Large Hadron Collider". Thesis advisor: dr. sc. Vuko Brigljević.

PROFESSIONAL EXPERIENCE

Since June 2007: research assistant at the Ruđer Bošković Institute, Zagreb, Croatia in the group of dr. Krešo Kadija and supervisor dr. Vuko Brigljević, working on the electroweak multiboson measurements at the CMS and LHC, and on technical aspects of the CMS detector:

- One of the main contributors to search for WZ resonances on the 2011 CMS dataset. Collaboration with the University of Wisconsin-Madison (UW) and Boston University (BU).
- One of the main contributors to WZ cross section measurement on the 2011 CMS dataset. Collaboration with Instituto de Fisica de Cantabria (IFCA), Unversidad de Oviedo (UO), BU and UW.
- Contributor to the development and commissioning of the CMS ECAL subsystem (2007). Developed ECAL web application for the CMS Run Control and Management System.
- Contributor to the development and operations of the CMS Online DQM system (2009-2011). Developed and maintained infrastructure software components of the DQM Server.
- Contributor to the development and operations of the CMS DAQ system (2012). Developed and maintained infrastructure software components of the DAQ Filter Farm.

TEACHING

- 2007/2008 and 2010/2011: Assistant teacher in a course „Računalni praktikum“ at Department of Physics, Faculty of Science, University of Zagreb
- 2011: Assistant teacher in a computing course “Numerical methods and mathematical modelling” at Department of Physics, Faculty of Science, University of Zagreb

TALKS AT CONFERENCES

Conference	"Conferences on Computing in High Energy and Nuclear Physics" (CHEP), 2010, Taipei, Taiwan.
Talk date	19th October 2010
Talk name	"CMS Online Data Quality Monitoring: Real -Time Event Processing Infrastructure"

Conference	"BSM: Beyond the Standard Model: results with the 7 TeV LHC Collision Data", 2011, ICTP, Trieste, Italy.
Talk date	20th September 2011
Talk name	"Measurement of WZ Production and search for WZ resonances with the CMS Detector" (plenary talk)

ATTENDED CONFERENCES, SCHOOLS AND COMPETITIONS

1999	30th Physics Olympiad, Padua, Italy (high school level competition)
2006	"LHC days", Split, Croatia
2008	"Trans-European School of High Energy Physics", Buymerovka, Ukraine
2008	"Physics at LHC", Split, Croatia

AWARDS AND RECOGNITIONS

2012	Annual award of the Ruder Bošković Institute (for the W'/Technicolor search paper)

COMPUTER SKILLS

- Computer languages and standards: C, C++, Python, Perl, Java, JavaScript, HTML, XML

PUBLICATIONS

1. **"Measurement of the $B_s^0 \to \mu^+\mu^-$ branching fraction and search for $B^0 \to \mu^+\mu^-$ with the CMS Experiment"**
   S. Chatrchyan *et al.* [CMS Collaboration].
   arXiv:1307.5025 [hep-ex]
   10.1103/PhysRevLett.111.101804
   Phys. Rev. Lett. **111**, 101804 (2013)

2. **"Energy calibration and resolution of the CMS electromagnetic calorimeter in pp collisions at $\sqrt{s}$ = 7 TeV"**
   S. Chatrchyan *et al.* [CMS Collaboration].
   arXiv:1306.2016
   10.1088/1748-0221/8/09/P09009
   JINST **8**, P09009 (2013)

3. **“Measurement of neutral strange particle production in the underlying event in proton-proton collisions at $\sqrt{s}$ = 7 TeV”**
S. Chatrchyan *et al.* [CMS Collaboration].
arXiv:1305.6016 [hep-ex]
10.1103/PhysRevD.88.052001
Phys. Rev. D **88**, 052001 (2013)

4. **“Study of exclusive two-photon production of W^+W^- in pp collisions at $\sqrt{s} = 7$ TeV and constraints on anomalous quartic gauge couplings”**
S. Chatrchyan *et al.* [CMS Collaboration].
arXiv:1305.5596 [hep-ex]
10.1007/JHEP07(2013)116
JHEP **1307**, 116 (2013)

5. **“Search for gluino mediated bottom- and top-squark production in multijet final states in pp collisions at 8 TeV”**
S. Chatrchyan *et al.* [CMS Collaboration].
arXiv:1305.2390 [hep-ex]
10.1016/j.physletb.2013.06.058
Phys. Lett. B **725**, 243 (2013)

6. **“Multiplicity and transverse momentum dependence of two- and four-particle correlations in pPb and PbPb collisions”**
S. Chatrchyan *et al.* [CMS Collaboration].
arXiv:1305.0609 [nucl-ex]
10.1016/j.physletb.2013.06.028
Phys. Lett. B **724**, 213 (2013)

7. **“Searches for long-lived charged particles in pp collisions at $\sqrt{s}$=7 and 8 TeV”**
S. Chatrchyan *et al.* [CMS Collaboration].
arXiv:1305.0491 [hep-ex]
10.1007/JHEP07(2013)122

8. **“Measurement of the Λ_b^0 lifetime in pp collisions at $\sqrt{s} = 7$ TeV”**
S. Chatrchyan *et al.* [CMS Collaboration].
arXiv:1304.7495 [hep-ex]
10.1007/JHEP07(2013)163
JHEP **07**, 163 (2013)

9. **“Measurement of masses in the $t\bar{t}$ system by kinematic endpoints in pp collisions at $\sqrt{s}$ = 7 TeV”**
S. Chatrchyan *et al.* [CMS Collaboration].
arXiv:1304.5783 [hep-ex]
10.1140/epjc/s10052-013-2494-7
Eur. Phys. J. C **73**, 2494 (2013)

10. **“Search for a standard-model-like Higgs boson with a mass in the range 145 to 1000 GeV at the LHC”**
S. Chatrchyan *et al.* [CMS Collaboration].
arXiv:1304.0213 [hep-ex]

10.1140/epjc/s10052-013-2469-8
Eur. Phys. J. C **73**, 2469 (2013)

11. **“Search for microscopic black holes in pp collisions at $\sqrt{s}$ = 8 TeV”**
S. Chatrchyan *et al.* [CMS Collaboration].
arXiv:1303.5338 [hep-ex]
10.1007/JHEP07(2013)178
JHEP **1307**, 178 (2013)

12. **“Studies of jet mass in dijet and W/Z + jet events”**
S. Chatrchyan *et al.* [CMS Collaboration].
arXiv:1303.4811 [hep-ex]
10.1007/JHEP05(2013)090
JHEP **1305**, 090 (2013)

13. **“Observation of a new boson with mass near 125 GeV in pp collisions at $\sqrt{s}$ = 7 and 8 TeV”**
S. Chatrchyan *et al.* [CMS Collaboration].
arXiv:1303.4571 [hep-ex]
10.1007/JHEP06(2013)081
JHEP **1306**, 081 (2013)

14. **“A New Boson with a Mass of 125 GeV Observed with the CMS Experiment at the Large Hadron Collider”**
S. Chatrchyan *et al.* [CMS Collaboration].
10.1126/science.1230816
Science **338**, 1569 (2012).

15. **“Measurement of associated production of vector bosons and top quark-antiquark pairs at sqrt(s) = 7 TeV”**
S. Chatrchyan *et al.* [CMS Collaboration].
arXiv:1303.3239 [hep-ex]
10.1103/PhysRevLett.110.172002
Phys. Rev. Lett. **110**, 172002 (2013)

16. **“Search for supersymmetry in hadronic final states with missing transverse energy using the variables α_T and b-quark multiplicity in pp collisions at $\sqrt{s}$ = 8 TeV”**
S. Chatrchyan *et al.* [CMS Collaboration].
arXiv:1303.2985 [hep-ex]
10.1140/epjc/s10052-013-2568-6
Eur. Phys. J. C **73**, 2568 (2013)

17. **“Search for the standard model Higgs boson produced in association with a top-quark pair in pp collisions at the LHC”**
S. Chatrchyan *et al.* [CMS Collaboration].
arXiv:1303.0763 [hep-ex]
10.1007/JHEP05(2013)145
JHEP **1305**, 145 (2013)

18. **“Measurement of the X(3872) production cross section via decays to J/psi pi pi in pp collisions at sqrt(s) = 7 TeV”**
S. Chatrchyan *et al.* [CMS Collaboration].
arXiv:1302.3968 [hep-ex]
10.1007/JHEP04(2013)154
JHEP **1304**, 154 (2013)

19. **“Search for a Higgs boson decaying into a b-quark pair and produced in association with b quarks in proton-proton collisions at 7 TeV”**
S. Chatrchyan *et al.* [CMS Collaboration].
arXiv:1302.2892 [hep-ex]
10.1016/j.physletb.2013.04.017
Phys. Lett. B **722**, 207 (2013)

20. **“Search for new physics in final states with a lepton and missing transverse energy in pp collisions at the LHC”**
S. Chatrchyan *et al.* [CMS Collaboration].
arXiv:1302.2812 [hep-ex]
10.1103/PhysRevD.87.072005
Phys. Rev. D **87**, 072005 (2013)

21. **“Study of the underlying event at forward rapidity in pp collisions at $\sqrt{s}$ = 0.9, 2.76, and 7 TeV”**
S. Chatrchyan *et al.* [CMS Collaboration].
arXiv:1302.2394 [hep-ex]
10.1007/JHEP04(2013)072
JHEP **1304**, 072 (2013)

22. **“Searches for Higgs bosons in pp collisions at sqrt(s) = 7 and 8 TeV in the context of four-generation and fermiophobic models”**
S. Chatrchyan *et al.* [CMS Collaboration].
arXiv:1302.1764 [hep-ex]
10.1016/j.physletb.2013.06.043
Phys. Lett. B **725**, 36 (2013)

23. **“Search for pair-produced dijet resonances in four-jet final states in pp collisions at $\sqrt{s}$ = 7 TeV”**
S. Chatrchyan *et al.* [CMS Collaboration].
arXiv:1302.0531 [hep-ex]
10.1103/PhysRevLett.110.141802
Phys. Rev. Lett. **110**, 141802 (2013)

24. **“Measurement of the $t\bar{t}$ production cross section in the all-jet final state in pp collisions at $\sqrt{s}$ = 7 TeV”**
S. Chatrchyan *et al.* [CMS Collaboration].
arXiv:1302.0508 [hep-ex]
10.1007/JHEP05(2013)065
JHEP **1305**, 065 (2013)

25. **“Measurement of the top-antitop production cross section in the tau+jets channel in pp collisions at sqrt(s) = 7 TeV”**
S. Chatrchyan *et al.* [CMS Collaboration].
arXiv:1301.5755 [hep-ex]
10.1140/epjc/s10052-013-2386-x
Eur. Phys. J. C **73**, 2386 (2013)

26. **“Search for contact interactions using the inclusive jet p_T spectrum in pp collisions at $\sqrt{s} = 7$ TeV”**
S. Chatrchyan *et al.* [CMS Collaboration].
arXiv:1301.5023 [hep-ex]
10.1103/PhysRevD.87.052017
Phys. Rev. D **87**, 052017 (2013)

27. **“Measurement of W+W- and ZZ production cross sections in pp collisions at sqrt(s) = 8 TeV”**
S. Chatrchyan *et al.* [CMS Collaboration].
arXiv:1301.4698 [hep-ex]
10.1016/j.physletb.2013.03.027
Phys. Lett. B **721**, 190 (2013)

28. **“Search for physics beyond the standard model in events with τ leptons, jets, and large transverse momentum imbalance in pp collisions at $\sqrt{s}$ = 7 TeV”**
S. Chatrchyan *et al.* [CMS Collaboration].
arXiv:1301.3792 [hep-ex]
10.1140/epjc/s10052-013-2493-8
Eur. Phys. J. C **73**, 2493 (2013)

29. **“Event shapes and azimuthal correlations in Z + jets events in pp collisions at $\sqrt{s} = 7$ TeV”**
S. Chatrchyan *et al.* [CMS Collaboration].
arXiv:1301.1646 [hep-ex]
10.1016/j.physletb.2013.04.025
Phys. Lett. B **722**, 238 (2013)

30. **“Search for supersymmetry in events with opposite-sign dileptons and missing transverse energy using an artificial neural network”**
S. Chatrchyan *et al.* [CMS Collaboration].
arXiv:1301.0916 [hep-ex]
10.1103/PhysRevD.87.072001
Phys. Rev. D **87**, 072001 (2013)

31. **“Search for supersymmetry in pp collisions at $\sqrt{s} = 7$ TeV in events with a single lepton, jets, and missing transverse momentum”**
S. Chatrchyan *et al.* [CMS Collaboration].
arXiv:1212.6428 [hep-ex]
10.1140/epjc/s10052-013-2404-z
Eur. Phys. J. C **73**, 2404 (2013)

32. **“Study of the Mass and Spin-Parity of the Higgs Boson Candidate Via Its Decays to Z Boson Pairs”**
S. Chatrchyan *et al.* [CMS Collaboration].
arXiv:1212.6639 [hep-ex]
10.1103/PhysRevLett.110.081803
Phys. Rev. Lett. **110**, 081803 (2013)

33. **“Measurements of differential jet cross sections in proton-proton collisions at $\sqrt{s} = 7$ TeV with the CMS detector”**
S. Chatrchyan *et al.* [CMS Collaboration].
arXiv:1212.6660 [hep-ex]
10.1103/PhysRevD.87.112002
Phys. Rev. D **87**, 112002 (2013)

34. **“Measurement of the $t\bar{t}$ production cross section in pp collisions at $\sqrt{s} = 7$ TeV with lepton + jets final states”**
S. Chatrchyan *et al.* [CMS Collaboration].
arXiv:1212.6682
10.1016/j.physletb.2013.02.021
Phys. Lett. B **720**, 83 (2013)

35. **“Inclusive search for supersymmetry using the razor variables in pp collisions at $\sqrt{s} = 7$ TeV”**
S. Chatrchyan *et al.* [CMS Collaboration].
arXiv:1212.6961 [hep-ex]
10.1103/PhysRevLett.111.081802
Phys. Rev. Lett. **111**, 081802 (2013)

36. **“Search for new physics in events with same-sign dileptons and b jets in pp collisions at $\sqrt{s} = 8$ TeV”**
S. Chatrchyan *et al.* [CMS Collaboration].
arXiv:1212.6194 [hep-ex]
10.1007/JHEP03(2013)037, 10.1007/JHEP07(2013)041
JHEP **1303**, 037 (2013), [Erratum-ibid. **1307**, 041 (2013)]

37. **“Search for heavy narrow dilepton resonances in pp collisions at $\sqrt{s} = 7$ TeV and $\sqrt{s} = 8$ TeV”**
S. Chatrchyan *et al.* [CMS Collaboration].
arXiv:1212.6175 [hep-ex]
10.1016/j.physletb.2013.02.003
Phys. Lett. B **720**, 63 (2013)

38. **“Search for contact interactions in $\mu^+\mu^-$ events in pp collisions at $\sqrt{s} = 7$ TeV”**
S. Chatrchyan *et al.* [CMS Collaboration].
arXiv:1212.4563 [hep-ex]
10.1103/PhysRevD.87.032001
Phys. Rev. D **87**, no. 3, 032001 (2013)

39. **“Search for heavy resonances in the W/Z-tagged dijet mass spectrum in pp collisions at 7 TeV”**

S. Chatrchyan *et al.* [CMS Collaboration].
arXiv:1212.1910 [hep-ex]
10.1016/j.physletb.2013.05.040
Phys. Lett. B **723**, 280 (2013)

40. **"Search for long-lived particles decaying to photons and missing energy in proton-proton collisions at $\sqrt{s} = 7$ TeV"**
S. Chatrchyan *et al.* [CMS Collaboration].
arXiv:1212.1838 [hep-ex]
10.1016/j.physletb.2013.04.027
Phys. Lett. B **722**, 273 (2013)

41. **"Search for exotic resonances decaying into WZ/ZZ in pp collisions at $\sqrt{s} = 7$ TeV"**
S. Chatrchyan *et al.* [CMS Collaboration].
arXiv:1211.5779 [hep-ex]
10.1007/JHEP02(2013)036
JHEP **1302**, 036 (2013)

42. **"Measurement of the ZZ production cross section and search for anomalous couplings in 2 l2l ' final states in pp collisions at $\sqrt{s} = 7$ TeV"**
S. Chatrchyan *et al.* [CMS Collaboration].
arXiv:1211.4890 [hep-ex]
10.1007/JHEP01(2013)063
JHEP **1301**, 063 (2013)

43. **"Search for new physics in events with photons, jets, and missing transverse energy in pp collisions at $\sqrt{s} = 7$ TeV"**
S. Chatrchyan *et al.* [CMS Collaboration].
arXiv:1211.4784 [hep-ex]
10.1007/JHEP03(2013)111
JHEP **1303**, 111 (2013)

44. **"Identification of b-quark jets with the CMS experiment"**
S. Chatrchyan *et al.* [CMS Collaboration].
arXiv:1211.4462 [hep-ex]
10.1088/1748-0221/8/04/P04013
JINST **8**, P04013 (2013)

45. **"Search for Z ' resonances decaying to $t\bar{t}$ in dilepton+jets final states in pp collisions at $\sqrt{s} = 7$ TeV"**
S. Chatrchyan *et al.* [CMS Collaboration].
arXiv:1211.3338 [hep-ex]
10.1103/PhysRevD.87.072002
Phys. Rev. D **87**, 072002 (2013)

46. **"Search for supersymmetry in final states with a single lepton, b-quark jets, and missing transverse energy in proton-proton collisions at $\sqrt{s} = 7$ TeV"**
S. Chatrchyan *et al.* [CMS Collaboration].
arXiv:1211.3143 [hep-ex]

10.1103/PhysRevD.87.052006
Phys. Rev. D **87**, 052006 (2013)

47. **"Search in leptonic channels for heavy resonances decaying to long-lived neutral particles"**
S. Chatrchyan *et al.* [CMS Collaboration].
arXiv:1211.2472 [hep-ex]
10.1007/JHEP02(2013)085
JHEP **1302**, 085 (2013)

48. **"Measurement of differential top-quark pair production cross sections in pp colisions at $\sqrt{s} = 7$ TeV"**
S. Chatrchyan *et al.* [CMS Collaboration].
arXiv:1211.2220 [hep-ex]
10.1140/epjc/s10052-013-2339-4
Eur. Phys. J. C **73**, 2339 (2013)

49. **"Search for supersymmetry in final states with missing transverse energy and 0, 1, 2, or at least 3 b-quark jets in 7 TeV pp collisions using the variable alphaT"**
S. Chatrchyan *et al.* [CMS Collaboration].
arXiv:1210.8115 [hep-ex]
10.1007/JHEP01(2013)077
JHEP **1301**, 077 (2013)

50. **"Measurement of the sum of WW and WZ production with W+dijet events in pp collisions at $\sqrt{s} = 7$ TeV"**
S. Chatrchyan *et al.* [CMS Collaboration].
arXiv:1210.7544 [hep-ex]
10.1140/epjc/s10052-013-2283-3
Eur. Phys. J. C **73**, 2283 (2013)

51. **"Search for heavy quarks decaying into a top quark and a W or Z boson using lepton + jets events in pp collisions at $\sqrt{s}$ = 7 TeV"**
S. Chatrchyan *et al.* [CMS Collaboration].
arXiv:1210.7471 [hep-ex]
10.1007/JHEP01(2013)154
JHEP **1301**, 154 (2013)

52. **"Measurement of the inelastic proton-proton cross section at $\sqrt{s} = 7$ TeV"**
S. Chatrchyan *et al.* [CMS Collaboration].
arXiv:1210.6718 [hep-ex]
10.1016/j.physletb.2013.03.024
Phys. Lett. B **722**, 5 (2013)

53. **"Search for pair production of third-generation leptoquarks and top squarks in pp collisions at $\sqrt{s} = 7$ TeV"**
S. Chatrchyan *et al.* [CMS Collaboration].
arXiv:1210.5629 [hep-ex]
10.1103/PhysRevLett.110.081801
Phys. Rev. Lett. **110**, 081801 (2013)

54. **“Search for third-generation leptoquarks and scalar bottom quarks in pp collisions at $\sqrt{s} = 7$ TeV”**
S. Chatrchyan *et al.* [CMS Collaboration].
arXiv:1210.5627 [hep-ex]
10.1007/JHEP12(2012)055
JHEP **1212**, 055 (2012)

55. **“Observation of long-range near-side angular correlations in proton-lead collisions at the LHC”**
S. Chatrchyan *et al.* [CMS Collaboration].
arXiv:1210.5482 [nucl-ex]
10.1016/j.physletb.2012.11.025
Phys. Lett. B **718**, 795 (2013)

56. **“Observation of Z decays to four leptons with the CMS detector at the LHC”**
S. Chatrchyan *et al.* [CMS Collaboration].
arXiv:1210.3844 [hep-ex]
10.1007/JHEP12(2012)034
JHEP **1212**, 034 (2012)

57. **“Search for excited leptons in pp collisions at $\sqrt{s} = 7$ TeV”**
S. Chatrchyan *et al.* [CMS Collaboration].
arXiv:1210.2422 [hep-ex]
10.1016/j.physletb.2013.02.031
Phys. Lett. B **720**, 309 (2013)

58. **“Search for heavy neutrinos and W[R] bosons with right-handed couplings in a left-right symmetric model in pp collisions at sqrt(s) = 7 TeV”**
S. Chatrchyan *et al.* [CMS Collaboration].
arXiv:1210.2402 [hep-ex]
10.1103/PhysRevLett.109.261802
Phys. Rev. Lett. **109**, 261802 (2012)

59. **“Search for narrow resonances and quantum black holes in inclusive and b-tagged dijet mass spectra from pp collisions at $\sqrt{s} = 7$ TeV”**
S. Chatrchyan *et al.* [CMS Collaboration].
arXiv:1210.2387 [hep-ex]
10.1007/JHEP01(2013)013
JHEP **1301**, 013 (2013)

60. **“Search for fractionally charged particles in pp collisions at $\sqrt{s} = 7$ TeV”**
S. Chatrchyan *et al.* [CMS Collaboration].
arXiv:1210.2311 [hep-ex]
10.1103/PhysRevD.87.092008
Phys. Rev. D **87**, 092008 (2013)

61. **“Search for supersymmetry in events with photons and low missing transverse energy in pp collisions at $\sqrt{s} = 7$ TeV”**
S. Chatrchyan *et al.* [CMS Collaboration].
arXiv:1210.2052 [hep-ex]

10.1016/j.physletb.2012.12.055
Phys. Lett. B **719**, 42 (2013)

62. **"Search for heavy lepton partners of neutrinos in proton-proton collisions in the context of the type III seesaw mechanism"**
S. Chatrchyan *et al.* [CMS Collaboration].
arXiv:1210.1797 [hep-ex]
10.1016/j.physletb.2012.10.070
Phys. Lett. B **718**, 348 (2012)

63. **"Measurement of the relative prompt production rate of chi(c2) and chi(c1) in pp collisions at $\sqrt{s} = 7$ TeV"**
S. Chatrchyan *et al.* [CMS Collaboration].
arXiv:1210.0875 [hep-ex]
10.1140/epjc/s10052-012-2251-3
Eur. Phys. J. C **72**, 2251 (2012)

64. **"Search for anomalous production of highly boosted Z bosons decaying to dimuons in pp collisions at $\sqrt{s} = 7$ TeV"**
S. Chatrchyan *et al.* [CMS Collaboration].
arXiv:1210.0867 [hep-ex]
10.1016/j.physletb.2013.03.037
Phys. Lett. B **722**, 28 (2013)

65. **"Search for electroweak production of charginos and neutralinos using leptonic final states in pp collisions at $\sqrt{s} = 7$ TeV"**
S. Chatrchyan *et al.* [CMS Collaboration].
arXiv:1209.6620 [hep-ex]
10.1007/JHEP11(2012)147
JHEP **1211**, 147 (2012)

66. **"Measurement of the single-top-quark t-channel cross section in pp collisions at $\sqrt{s} = 7$ TeV"**
S. Chatrchyan *et al.* [CMS Collaboration].
arXiv:1209.4533 [hep-ex]
10.1007/JHEP12(2012)035
JHEP **1212**, 035 (2012)

67. **"Search for resonant $t\bar{t}$ production in lepton+jets events in pp collisions at $\sqrt{s} = 7$ TeV"**
S. Chatrchyan *et al.* [CMS Collaboration].
arXiv:1209.4397 [hep-ex]
10.1007/JHEP12(2012)015
JHEP **1212**, 015 (2012)

68. **"Search for the standard model Higgs boson produced in association with W and Z bosons in pp collisions at $\sqrt{s} = 7$ TeV"**
S. Chatrchyan *et al.* [CMS Collaboration].
arXiv:1209.3937 [hep-ex]
10.1007/JHEP11(2012)088
JHEP **1211**, 088 (2012)

69. **“Search for a narrow spin-2 resonance decaying to a pair of Z vector bosons in the semileptonic final state”**
S. Chatrchyan *et al.* [CMS Collaboration].
arXiv:1209.3807 [hep-ex]
10.1016/j.physletb.2012.11.063
Phys. Lett. B **718**, 1208 (2013)

70. **“Evidence for associated production of a single top quark and W boson in pp collisions at $\sqrt{s}$ = 7 TeV”**
S. Chatrchyan *et al.* [CMS Collaboration].
arXiv:1209.3489 [hep-ex]
10.1103/PhysRevLett.110.022003
Phys. Rev. Lett. **110**, 022003 (2013)

71. **“Measurement of the Y1S, Y2S and Y3S polarizations in pp collisions at $\sqrt{s} = 7$ TeV”**
S. Chatrchyan *et al.* [CMS Collaboration].
arXiv:1209.2922 [hep-ex]
10.1103/PhysRevLett.110.081802
Phys. Rev. Lett. **110**, 081802 (2013)

72. **“Measurement of the top-quark mass in $t\bar{t}$ events with dilepton final states in pp collisions at $\sqrt{s} = 7$ TeV”**
S. Chatrchyan *et al.* [CMS Collaboration].
arXiv:1209.2393 [hep-ex]
10.1140/epjc/s10052-012-2202-z
Eur. Phys. J. C **72**, 2202 (2012)

73. **“Measurement of the top-quark mass in $t\bar{t}$ events with lepton+jets final states in pp collisions at $\sqrt{s} = 7$ TeV”**
S. Chatrchyan *et al.* [CMS Collaboration].
arXiv:1209.2319 [hep-ex]
10.1007/JHEP12(2012)105
JHEP **1212**, 105 (2012)

74. **“Observation of a diffractive contribution to dijet production in proton-proton collisions at $\sqrt{s} = 7$ TeV”**
S. Chatrchyan *et al.* [CMS Collaboration].
arXiv:1209.1805 [hep-ex]
10.1103/PhysRevD.87.012006
Phys. Rev. D **87**, 012006 (2013)

75. **“Search for exclusive or semi-exclusive photon pair production and observation of exclusive and semi-exclusive electron pair production in pp collisions at $\sqrt{s} = 7$ TeV”**
S. Chatrchyan *et al.* [CMS Collaboration].
arXiv:1209.1666 [hep-ex]
10.1007/JHEP11(2012)080
JHEP **1211**, 080 (2012)

76. **“Combined search for the quarks of a sequential fourth generation”**
S. Chatrchyan *et al.* [CMS Collaboration].

arXiv:1209.1062 [hep-ex]
10.1103/PhysRevD.86.112003
Phys. Rev. D **86**, 112003 (2012)

77. **“Search for pair produced fourth-generation up-type quarks in pp collisions at $\sqrt{s} = 7$ TeV with a lepton in the final state”**
S. Chatrchyan *et al.* [CMS Collaboration].
arXiv:1209.0471 [hep-ex]
10.1016/j.physletb.2012.10.038
Phys. Lett. B **718**, 307 (2012)

78. **“Search for supersymmetry in events with b-quark jets and missing transverse energy in pp collisions at 7 TeV”**
S. Chatrchyan *et al.* [CMS Collaboration].
arXiv:1208.4859 [hep-ex]
10.1103/PhysRevD.86.072010
Phys. Rev. D **86**, 072010 (2012)

79. **“Study of the dijet mass spectrum in $pp \to W+$ jets events at $\sqrt{s} = 7$ TeV”**
S. Chatrchyan *et al.* [CMS Collaboration].
arXiv:1208.3477 [hep-ex]
10.1103/PhysRevLett.109.251801
Phys. Rev. Lett. **109**, 251801 (2012)

80. **“Search for three-jet resonances in pp collisions at $\sqrt{s} = 7$ TeV”**
S. Chatrchyan *et al.* [CMS Collaboration].
arXiv:1208.2931 [hep-ex]
10.1016/j.physletb.2012.10.048
Phys. Lett. B **718**, 329 (2012)

81. **“Observation of sequential Upsilon suppression in PbPb collisions”**
S. Chatrchyan *et al.* [CMS Collaboration].
arXiv:1208.2826 [nucl-ex]
10.1103/PhysRevLett.109.222301
Phys. Rev. Lett. **109**, 222301 (2012)

82. **“Measurement of the $t\bar{t}$ production cross section in the dilepton channel in pp collisions at $\sqrt{s} = 7$ TeV”**
S. Chatrchyan *et al.* [CMS Collaboration].
arXiv:1208.2671 [hep-ex]
10.1007/JHEP11(2012)067
JHEP **1211**, 067 (2012)

83. **“Measurement of the azimuthal anisotropy of neutral pions in PbPb collisions at $\sqrt{s_{NN}} = 2.76$ TeV”**
S. Chatrchyan *et al.* [CMS Collaboration].
arXiv:1208.2470 [nucl-ex]
10.1103/PhysRevLett.110.042301
Phys. Rev. Lett. **110**, 042301 (2013)

84. **“Search for flavor changing neutral currents in top quark decays in pp collisions at 7 TeV”**
S. Chatrchyan *et al.* [CMS Collaboration].
arXiv:1208.0957 [hep-ex]
10.1016/j.physletb.2012.12.045
Phys. Lett. B **718**, 1252 (2013)

85. **“Search for a W ’ boson decaying to a bottom quark and a top quark in pp collisions at $\sqrt{s} = 7$ TeV”**
S. Chatrchyan *et al.* [CMS Collaboration].
arXiv:1208.0956 [hep-ex]
10.1016/j.physletb.2012.12.008
Phys. Lett. B **718**, 1229 (2013)

86. **“Observation of a new boson at a mass of 125 GeV with the CMS experiment at the LHC”**
S. Chatrchyan *et al.* [CMS Collaboration].
arXiv:1207.7235 [hep-ex]
10.1016/j.physletb.2012.08.021
Phys. Lett. B **716**, 30 (2012)

87. **“Search for heavy Majorana neutrinos in $\mu^+\mu^+[\mu^-\mu^-]$ and $e^+e^+[e^-e^-]$ events in pp collisions at $\sqrt{s} = 7$ TeV”**
S. Chatrchyan *et al.* [CMS Collaboration].
arXiv:1207.6079 [hep-ex]
10.1016/j.physletb.2012.09.012
Phys. Lett. B **717**, 109 (2012)

88. **“Search for pair production of first- and second-generation scalar leptoquarks in pp collisions at $\sqrt{s} = 7$ TeV”**
S. Chatrchyan *et al.* [CMS Collaboration].
arXiv:1207.5406 [hep-ex]
10.1103/PhysRevD.86.052013
Phys. Rev. D **86**, 052013 (2012)

89. **“Study of the inclusive production of charged pions, kaons, and protons in pp collisions at $\sqrt{s} = 0.9$, 2.76, and 7 TeV”**
S. Chatrchyan *et al.* [CMS Collaboration].
arXiv:1207.4724 [hep-ex]
10.1140/epjc/s10052-012-2164-1
Eur. Phys. J. C **72**, 2164 (2012)

90. **“Forward-backward asymmetry of Drell-Yan lepton pairs in pp collisions at $\sqrt{s} = 7$ TeV”**
S. Chatrchyan *et al.* [CMS Collaboration].
arXiv:1207.3973 [hep-ex]
10.1016/j.physletb.2012.10.082
Phys. Lett. B **718**, 752 (2013)

91. **“A search for a doubly-charged Higgs boson in pp collisions at $\sqrt{s} = 7$ TeV”**
S. Chatrchyan *et al.* [CMS Collaboration].
arXiv:1207.2666 [hep-ex]
10.1140/epjc/s10052-012-2189-5
Eur. Phys. J. C **72**, 2189 (2012)

92. **“Measurement of the underlying event activity in pp collisions at $\sqrt{s} = 0.9$ and 7 TeV with the novel jet-area/median approach”**
S. Chatrchyan *et al.* [CMS Collaboration].
arXiv:1207.2392 [hep-ex]
10.1007/JHEP08(2012)130
JHEP **1208**, 130 (2012)

93. **“Search for new physics in the multijet and missing transverse momentum final state in proton-proton collisions at $\sqrt{s} = 7$ TeV”**
S. Chatrchyan *et al.* [CMS Collaboration].
arXiv:1207.1898 [hep-ex]
10.1103/PhysRevLett.109.171803
Phys. Rev. Lett. **109**, 171803 (2012)

94. **“Search for supersymmetry in hadronic final states using MT2 in pp collisions at $\sqrt{s} = 7$ TeV”**
S. Chatrchyan *et al.* [CMS Collaboration].
arXiv:1207.1798 [hep-ex]
10.1007/JHEP10(2012)018
JHEP **1210**, 018 (2012)

95. **“Search for a fermiophobic Higgs boson in pp collisions at $\sqrt{s} = 7$ TeV”**
S. Chatrchyan *et al.* [CMS Collaboration].
arXiv:1207.1130 [hep-ex]
10.1007/JHEP09(2012)111
JHEP **1209**, 111 (2012)

96. **“Search for new physics with long-lived particles decaying to photons and missing energy in pp collisions at $\sqrt{s} = 7$ TeV”**
S. Chatrchyan *et al.* [CMS Collaboration].
arXiv:1207.0627 [hep-ex]
10.1007/JHEP11(2012)172
JHEP **1211**, 172 (2012)

97. **“Search for stopped long-lived particles produced in pp collisions at $\sqrt{s} = 7$ TeV”**
S. Chatrchyan *et al.* [CMS Collaboration].
arXiv:1207.0106 [hep-ex]
10.1007/JHEP08(2012)026
JHEP **1208**, 026 (2012)

98. **“Inclusive and differential measurements of the $t\bar{t}$ charge asymmetry in proton-proton collisions at 7 TeV”**
S. Chatrchyan *et al.* [CMS Collaboration].

arXiv:1207.0065 [hep-ex]
10.1016/j.physletb.2012.09.028
Phys. Lett. B **717**, 129 (2012)

99. **"Search for a light pseudoscalar Higgs boson in the dimuon decay channel in pp collisions at $\sqrt{s} = 7$ TeV"**
S. Chatrchyan *et al.* [CMS Collaboration].
arXiv:1206.6326 [hep-ex]
10.1103/PhysRevLett.109.121801
Phys. Rev. Lett. **109**, 121801 (2012)

100. **"Search for dark matter and large extra dimensions in monojet events in pp collisions at $\sqrt{s} = 7$ TeV"**
S. Chatrchyan *et al.* [CMS Collaboration].
arXiv:1206.5663 [hep-ex]
10.1007/JHEP09(2012)094
JHEP **1209**, 094 (2012)

101. **"Performance of CMS muon reconstruction in pp collision events at $\sqrt{s} = 7$ TeV"**
S. Chatrchyan *et al.* [CMS Collaboration].
arXiv:1206.4071 [physics.ins-det]
10.1088/1748-0221/7/10/P10002
JINST **7**, P10002 (2012)

102. **"Search for new physics in events with opposite-sign leptons, jets, and missing transverse energy in pp collisions at $\sqrt{s} = 7$ TeV"**
S. Chatrchyan *et al.* [CMS Collaboration].
arXiv:1206.3949 [hep-ex]
10.1016/j.physletb.2012.11.036
Phys. Lett. B **718**, 815 (2013)

103. **"Search for charge-asymmetric production of W ' bosons in top pair + jet events from pp collisions at $\sqrt{s} = 7$ TeV"**
S. Chatrchyan *et al.* [CMS Collaboration].
arXiv:1206.3921 [hep-ex]
10.1016/j.physletb.2012.09.048
Phys. Lett. B **717**, 351 (2012)

104. **"Measurement of the electron charge asymmetry in inclusive W production in pp collisions at $\sqrt{s} = 7$ TeV"**
S. Chatrchyan *et al.* [CMS Collaboration].
arXiv:1206.2598 [hep-ex]
10.1103/PhysRevLett.109.111806
Phys. Rev. Lett. **109**, 111806 (2012)

105. **"Search for narrow resonances in dilepton mass spectra in pp collisions at $\sqrt{s} = 7$ TeV"**
S. Chatrchyan *et al.* [CMS Collaboration].
arXiv:1206.1849 [hep-ex]
10.1016/j.physletb.2012.06.051
Phys. Lett. B **714**, 158 (2012)

106. **“Search for high mass resonances decaying into τ^- lepton pairs in pp collisions at $\sqrt{s} = 7$ TeV”**
S. Chatrchyan *et al.* [CMS Collaboration].
arXiv:1206.1725 [hep-ex]
10.1016/j.physletb.2012.07.062
Phys. Lett. B **716**, 82 (2012)

107. **“Search for a W' or Techni-ρ Decaying into WZ in pp Collisions at $\sqrt{s} = 7$ TeV”**
S. Chatrchyan *et al.* [CMS Collaboration].
arXiv:1206.0433 [hep-ex]
10.1103/PhysRevLett.109.141801
Phys. Rev. Lett. **109**, 141801 (2012)

108. **“Search for new physics with same-sign isolated dilepton events with jets and missing transverse energy”**
S. Chatrchyan *et al.* [CMS Collaboration].
arXiv:1205.6615 [hep-ex]
10.1103/PhysRevLett.109.071803
Phys. Rev. Lett. **109**, 071803 (2012)

109. **“Study of W boson production in PbPb and pp collisions at $\sqrt{s_{NN}} = 2.76$ TeV”**
S. Chatrchyan *et al.* [CMS Collaboration].
arXiv:1205.6334 [nucl-ex]
10.1016/j.physletb.2012.07.025
Phys. Lett. B **715**, 66 (2012)

110. **“Measurement of jet fragmentation into charged particles in pp and PbPb collisions at $\sqrt{s_{NN}} = 2.76$ TeV”**
S. Chatrchyan *et al.* [CMS Collaboration].
arXiv:1205.5872 [nucl-ex]
10.1007/JHEP10(2012)087
JHEP **1210**, 087 (2012)

111. **“Search for a light charged Higgs boson in top quark decays in pp collisions at $\sqrt{s} = 7$ TeV”**
S. Chatrchyan *et al.* [CMS Collaboration].
arXiv:1205.5736 [hep-ex]
10.1007/JHEP07(2012)143
JHEP **1207**, 143 (2012)

112. **“Search for new physics in events with same-sign dileptons and b-tagged jets in pp collisions at $\sqrt{s} = 7$ TeV”**
S. Chatrchyan *et al.* [CMS Collaboration].
arXiv:1205.3933 [hep-ex]
10.1007/JHEP08(2012)110
JHEP **1208**, 110 (2012)

113. **“Measurement of the pseudorapidity and centrality dependence of the transverse energy density in PbPb collisions at $\sqrt{s_{NN}} = 2.76$ TeV”**

S. Chatrchyan *et al.* [CMS Collaboration].
arXiv:1205.2488 [nucl-ex]
10.1103/PhysRevLett.109.152303
Phys. Rev. Lett. **109**, 152303 (2012)

114. **“Measurement of the $Lambda_b$ cross section and the $\bar{\Lambda}(b^{)}$ to $Lambda_b$ ratio with $Lambda_b$ to J/Psi Λ decays in pp collisions at $\sqrt{s} = 7$ TeV”**
S. Chatrchyan *et al.* [CMS Collaboration].
arXiv:1205.0594 [hep-ex]
10.1016/j.physletb.2012.05.063
Phys. Lett. B **714**, 136 (2012)

115. **“Search for heavy long-lived charged particles in pp collisions at $\sqrt{s} = 7$ TeV”**
S. Chatrchyan *et al.* [CMS Collaboration].
arXiv:1205.0272 [hep-ex]
10.1016/j.physletb.2012.06.023
Phys. Lett. B **713**, 408 (2012)

116. **“Studies of jet quenching using isolated-photon+jet correlations in PbPb and pp collisions at $\sqrt{s_{NN}} = 2.76$ TeV”**
S. Chatrchyan *et al.* [CMS Collaboration].
arXiv:1205.0206 [nucl-ex]
10.1016/j.physletb.2012.11.003
Phys. Lett. B **718**, 773 (2013)

117. **“Observation of a new Xi(b) baryon”**
S. Chatrchyan *et al.* [CMS Collaboration].
arXiv:1204.5955 [hep-ex]
10.1103/PhysRevLett.108.252002
Phys. Rev. Lett. **108**, 252002 (2012)

118. **“Search for anomalous production of multilepton events in pp collisions at $\sqrt{s} = 7$ TeV”**
S. Chatrchyan *et al.* [CMS Collaboration].
arXiv:1204.5341 [hep-ex]
10.1007/JHEP06(2012)169
JHEP **1206**, 169 (2012)

119. **“Search for leptonic decays of W ’ bosons in pp collisions at $\sqrt{s} = 7$ TeV”**
S. Chatrchyan *et al.* [CMS Collaboration].
arXiv:1204.4764 [hep-ex]
10.1007/JHEP08(2012)023
JHEP **1208**, 023 (2012)

120. **“Search for physics beyond the standard model in events with a Z boson, jets, and missing transverse energy in pp collisions at $\sqrt{s} = 7$ TeV”**
S. Chatrchyan *et al.* [CMS Collaboration].
arXiv:1204.3774 [hep-ex]
10.1016/j.physletb.2012.08.026
Phys. Lett. B **716**, 260 (2012)

121. **“Shape, transverse size, and charged hadron multiplicity of jets in pp collisions at 7 TeV”**
S. Chatrchyan *et al.* [CMS Collaboration].
arXiv:1204.3170 [hep-ex]
10.1007/JHEP06(2012)160
JHEP **1206**, 160 (2012)

122. **“Measurement of the mass difference between top and antitop quarks”**
S. Chatrchyan *et al.* [CMS Collaboration].
arXiv:1204.2807 [hep-ex]
10.1007/JHEP06(2012)109
JHEP **1206**, 109 (2012)

123. **“Search for anomalous t t-bar production in the highly-boosted all-hadronic final state”**
S. Chatrchyan *et al.* [CMS Collaboration].
arXiv:1204.2488 [hep-ex]
10.1007/JHEP09(2012)029
JHEP **1209**, 029 (2012)

124. **“Azimuthal anisotropy of charged particles at high transverse momenta in PbPb collisions at $\sqrt{s_{NN}} = 2.76$ TeV”**
S. Chatrchyan *et al.* [CMS Collaboration].
arXiv:1204.1850 [nucl-ex]
10.1103/PhysRevLett.109.022301
Phys. Rev. Lett. **109**, 022301 (2012)

125. **“Measurement of the Z/gamma*+b-jet cross section in pp collisions at 7 TeV”**
S. Chatrchyan *et al.* [CMS Collaboration].
arXiv:1204.1643 [hep-ex]
10.1007/JHEP06(2012)126
JHEP **1206**, 126 (2012)

126. **“Measurement of the elliptic anisotropy of charged particles produced in PbPb collisions at nucleon-nucleon center-of-mass energy = 2.76 TeV”**
S. Chatrchyan *et al.* [CMS Collaboration].
arXiv:1204.1409 [nucl-ex]
10.1103/PhysRevC.87.014902
Phys. Rev. C **87**, 014902 (2013)

127. **“Measurement of the underlying event in the Drell-Yan process in proton-proton collisions at $\sqrt{s} = 7$ TeV”**
S. Chatrchyan *et al.* [CMS Collaboration].
arXiv:1204.1411 [hep-ex]
10.1140/epjc/s10052-012-2080-4
Eur. Phys. J. C **72**, 2080 (2012)

128. **“Search for heavy bottom-like quarks in 4.9 inverse femtobarns of pp collisions at $\sqrt{s} = 7$ TeV”**
S. Chatrchyan *et al.* [CMS Collaboration].
arXiv:1204.1088 [hep-ex]

10.1007/JHEP05(2012)123
JHEP **1205**, 123 (2012)

129. **"Search for Dark Matter and Large Extra Dimensions in pp Collisions Yielding a Photon and Missing Transverse Energy"**
S. Chatrchyan *et al.* [CMS Collaboration].
arXiv:1204.0821 [hep-ex]
10.1103/PhysRevLett.108.261803
Phys. Rev. Lett. **108**, 261803 (2012)

130. **"Ratios of dijet production cross sections as a function of the absolute difference in rapidity between jets in proton-proton collisions at $\sqrt{s} = 7$ TeV"**
S. Chatrchyan *et al.* [CMS Collaboration].
arXiv:1204.0696 [hep-ex]
10.1140/epjc/s10052-012-2216-6
Eur. Phys. J. C **72**, 2216 (2012)

131. **"Measurement of the top quark pair production cross section in pp collisions at $\sqrt{s} = 7$ TeV in dilepton final states containing a τ"**
S. Chatrchyan *et al.* [CMS Collaboration].
arXiv:1203.6810 [hep-ex]
10.1103/PhysRevD.85.112007
Phys. Rev. D **85**, 112007 (2012)

132. **"Search for heavy, top-like quark pair production in the dilepton final state in pp collisions at $\sqrt{s} = 7$ TeV"**
S. Chatrchyan *et al.* [CMS Collaboration].
arXiv:1203.5410 [hep-ex]
10.1016/j.physletb.2012.07.059
Phys. Lett. B **716**, 103 (2012)

133. **"Search for $B^0_s \to \mu^+\mu^-$ and $B^0 \to \mu^+\mu^-$ decays"**
S. Chatrchyan *et al.* [CMS Collaboration].
arXiv:1203.3976 [hep-ex]
10.1007/JHEP04(2012)033
JHEP **1204**, 033 (2012)

134. **"Measurement of the cross section for production of bb^- bar X, decaying to muons in pp collisions at $\sqrt{s} = 7$ TeV"**
S. Chatrchyan *et al.* [CMS Collaboration].
arXiv:1203.3458 [hep-ex]
10.1007/JHEP06(2012)110
JHEP **1206**, 110 (2012)

135. **"Search for microscopic black holes in pp collisions at $\sqrt{s} = 7$ TeV"**
S. Chatrchyan *et al.* [CMS Collaboration].
arXiv:1202.6396 [hep-ex]
10.1007/JHEP04(2012)061
JHEP **1204**, 061 (2012)

136. **“Search for quark compositeness in dijet angular distributions from pp collisions at $\sqrt{s} = 7$ TeV”**
S. Chatrchyan *et al.* [CMS Collaboration].
arXiv:1202.5535 [hep-ex]
10.1007/JHEP05(2012)055
JHEP **1205**, 055 (2012)

137. **“Jet momentum dependence of jet quenching in PbPb collisions at $\sqrt{s_{NN}} = 2.76$ TeV”**
S. Chatrchyan *et al.* [CMS Collaboration].
arXiv:1202.5022 [nucl-ex]
10.1016/j.physletb.2012.04.058
Phys. Lett. B **712**, 176 (2012)

138. **“Inclusive b-jet production in pp collisions at $\sqrt{s} = 7$ TeV”**
S. Chatrchyan *et al.* [CMS Collaboration].
arXiv:1202.4617 [hep-ex]
10.1007/JHEP04(2012)084
JHEP **1204**, 084 (2012)

139. **“Search for the standard model Higgs boson decaying to bottom quarks in pp collisions at $\sqrt{s} = 7$ TeV”**
S. Chatrchyan *et al.* [CMS Collaboration].
arXiv:1202.4195 [hep-ex]
10.1016/j.physletb.2012.02.085
Phys. Lett. B **710**, 284 (2012)

140. **“Search for neutral Higgs bosons decaying to τ pairs in pp collisions at $\sqrt{s} = 7$ TeV”**
S. Chatrchyan *et al.* [CMS Collaboration].
arXiv:1202.4083 [hep-ex]
10.1016/j.physletb.2012.05.028
Phys. Lett. B **713**, 68 (2012)

141. **“Search for large extra dimensions in dimuon and dielectron events in pp collisions at $\sqrt{s} = 7$ TeV”**
S. Chatrchyan *et al.* [CMS Collaboration].
arXiv:1202.3827 [hep-ex]
10.1016/j.physletb.2012.03.029
Phys. Lett. B **711**, 15 (2012)

142. **“Search for the standard model Higgs boson in the H to ZZ to 2 $\ell 2\nu$ channel in pp collisions at $\sqrt{s} = 7$ TeV”**
S. Chatrchyan *et al.* [CMS Collaboration].
arXiv:1202.3478 [hep-ex]
10.1007/JHEP03(2012)040
JHEP **1203**, 040 (2012)

143. **“Search for the standard model Higgs boson in the H to ZZ to $\ell\ell\tau\tau$ decay channel in pp collisions at $\sqrt{s} = 7$ TeV”**
S. Chatrchyan *et al.* [CMS Collaboration].

arXiv:1202.3617 [hep-ex]
10.1007/JHEP03(2012)081
JHEP **1203**, 081 (2012)

144. **“Study of high-pT charged particle suppression in PbPb compared to pp collisions at $\sqrt{s_{NN}} = 2.76$ TeV”**
S. Chatrchyan *et al.* [CMS Collaboration].
arXiv:1202.2554 [nucl-ex]
10.1140/epjc/s10052-012-1945-x
Eur. Phys. J. C **72**, 1945 (2012)

145. **“Search for the standard model Higgs boson in the decay channel H to ZZ to 4 leptons in pp collisions at $\sqrt{s} = 7$ TeV”**
S. Chatrchyan *et al.* [CMS Collaboration].
arXiv:1202.1997 [hep-ex]
10.1103/PhysRevLett.108.111804
Phys. Rev. Lett. **108**, 111804 (2012)

146. **“Search for the standard model Higgs boson decaying to a W pair in the fully leptonic final state in pp collisions at $\sqrt{s} = 7$ TeV”**
S. Chatrchyan *et al.* [CMS Collaboration].
arXiv:1202.1489 [hep-ex]
10.1016/j.physletb.2012.02.076
Phys. Lett. B **710**, 91 (2012)

147. **“Combined results of searches for the standard model Higgs boson in pp collisions at $\sqrt{s} = 7$ TeV”**
S. Chatrchyan *et al.* [CMS Collaboration].
arXiv:1202.1488 [hep-ex]
10.1016/j.physletb.2012.02.064
Phys. Lett. B **710**, 26 (2012)

148. **“Search for the standard model Higgs boson decaying into two photons in pp collisions at $\sqrt{s} = 7$ TeV”**
S. Chatrchyan *et al.* [CMS Collaboration].
arXiv:1202.1487 [hep-ex]
10.1016/j.physletb.2012.03.003
Phys. Lett. B **710**, 403 (2012)

149. **“Search for a Higgs boson in the decay channel H to ZZ(*) to q qbar ℓ^- l+ in pp collisions at $\sqrt{s} = 7$ TeV”**
S. Chatrchyan *et al.* [CMS Collaboration].
arXiv:1202.1416 [hep-ex]
10.1007/JHEP04(2012)036
JHEP **1204**, 036 (2012)

150. **“Measurement of the inclusive production cross sections for forward jets and for dijet events with one forward and one central jet in pp collisions at $\sqrt{s} = 7$ TeV”**
S. Chatrchyan *et al.* [CMS Collaboration].

arXiv:1202.0704 [hep-ex]
10.1007/JHEP06(2012)036
JHEP **1206**, 036 (2012)

151. **"Suppression of non-prompt J/ψ, prompt J/ψ, and Y(1S) in PbPb collisions at $\sqrt{s_{NN}} = 2.76$ TeV"**
S. Chatrchyan *et al.* [CMS Collaboration].
arXiv:1201.5069 [nucl-ex]
10.1007/JHEP05(2012)063
JHEP **1205**, 063 (2012)

152. **"Centrality dependence of dihadron correlations and azimuthal anisotropy harmonics in PbPb collisions at $\sqrt{s_{NN}} = 2.76$ TeV"**
S. Chatrchyan *et al.* [CMS Collaboration].
arXiv:1201.3158 [nucl-ex]
10.1140/epjc/s10052-012-2012-3
Eur. Phys. J. C **72**, 2012 (2012)

153. **"Measurement of isolated photon production in pp and PbPb collisions at $\sqrt{s_{NN}} = 2.76$ TeV"**
S. Chatrchyan *et al.* [CMS Collaboration].
arXiv:1201.3093 [nucl-ex]
10.1016/j.physletb.2012.02.077
Phys. Lett. B **710**, 256 (2012)

154. **"Measurement of the charge asymmetry in top-quark pair production in proton-proton collisions at $\sqrt{s} = 7$ TeV"**
S. Chatrchyan *et al.* [CMS Collaboration].
arXiv:1112.5100 [hep-ex]
10.1016/j.physletb.2012.01.078
Phys. Lett. B **709**, 28 (2012)

155. **"Search for signatures of extra dimensions in the diphoton mass spectrum at the Large Hadron Collider"**
S. Chatrchyan *et al.* [CMS Collaboration].
arXiv:1112.0688 [hep-ex]
10.1103/PhysRevLett.108.111801
Phys. Rev. Lett. **108**, 111801 (2012)

156. **"Exclusive photon-photon production of muon pairs in proton-proton collisions at $\sqrt{s} = 7$ TeV"**
S. Chatrchyan *et al.* [CMS Collaboration].
arXiv:1111.5536 [hep-ex]
10.1007/JHEP01(2012)052
JHEP **1201**, 052 (2012)

157. **"J/ψ and ψ_{2S} production in pp collisions at $\sqrt{s} = 7$ TeV"**
S. Chatrchyan *et al.* [CMS Collaboration].
arXiv:1111.1557 [hep-ex]

10.1007/JHEP02(2012)011
JHEP **1202**, 011 (2012)

158. **“Measurement of the Production Cross Section for Pairs of Isolated Photons in pp collisions at $\sqrt{s} = 7$ TeV”**
S. Chatrchyan *et al.* [CMS Collaboration].
arXiv:1110.6461 [hep-ex]
10.1007/JHEP01(2012)133
JHEP **1201**, 133 (2012)

159. **“Measurement of the Rapidity and Transverse Momentum Distributions of Z Bosons in pp Collisions at $\sqrt{s} = 7$ TeV”**
S. Chatrchyan *et al.* [CMS Collaboration].
arXiv:1110.4973 [hep-ex]
10.1103/PhysRevD.85.032002
Phys. Rev. D **85**, 032002 (2012)

160. **“Jet Production Rates in Association with W and Z Bosons in pp Collisions at $\sqrt{s} = 7$ TeV”**
S. Chatrchyan *et al.* [CMS Collaboration].
arXiv:1110.3226 [hep-ex]
10.1007/JHEP01(2012)010
JHEP **1201**, 010 (2012)

161. **“Measurement of the weak mixing angle with the Drell-Yan process in proton-proton collisions at the LHC”**
S. Chatrchyan *et al.* [CMS Collaboration].
arXiv:1110.2682 [hep-ex]
10.1103/PhysRevD.84.112002
Phys. Rev. D **84**, 112002 (2011)

162. **“Measurement of energy flow at large pseudorapidities in pp collisions at $\sqrt{s} = 0.9$ and 7 TeV”**
S. Chatrchyan *et al.* [CMS Collaboration].
arXiv:1110.0211 [hep-ex]
10.1007/JHEP11(2011)148, 10.1007/JHEP02(2012)055
JHEP **1111**, 148 (2011), [Erratum-ibid. **1202**, 055 (2012)]

163. **“Forward Energy Flow, Central Charged-Particle Multiplicities, and Pseudorapidity Gaps in W and Z Boson Events from pp Collisions at 7 TeV”**
S. Chatrchyan *et al.* [CMS Collaboration].
arXiv:1110.0181 [hep-ex]
10.1140/epjc/s10052-011-1839-3
Eur. Phys. J. C **72**, 1839 (2012)

164. **“Performance of tau-lepton reconstruction and identification in CMS”**
S. Chatrchyan *et al.* [CMS Collaboration].
arXiv:1109.6034 [physics.ins-det]
10.1088/1748-0221/7/01/P01001
JINST **7**, P01001 (2012)

165. **“Search for a Vector-like Quark with Charge 2/3 in t + Z Events from pp Collisions at $\sqrt{s} = 7$ TeV”**
S. Chatrchyan *et al.* [CMS Collaboration].
arXiv:1109.4985 [hep-ex]
10.1103/PhysRevLett.107.271802
Phys. Rev. Lett. **107**, 271802 (2011)

166. **“Search for Supersymmetry at the LHC in Events with Jets and Missing Transverse Energy”**
S. Chatrchyan *et al.* [CMS Collaboration].
arXiv:1109.2352 [hep-ex]
10.1103/PhysRevLett.107.221804
Phys. Rev. Lett. **107**, 221804 (2011)

167. **“Measurement of the $t\bar{t}$ Production Cross Section in pp Collisions at 7 TeV in Lepton + Jets Events Using b-quark Jet Identification”**
S. Chatrchyan *et al.* [CMS Collaboration].
arXiv:1108.3773 [hep-ex]
10.1103/PhysRevD.84.092004
Phys. Rev. D **84**, 092004 (2011)

168. **“Measurement of the Differential Cross Section for Isolated Prompt Photon Production in pp Collisions at 7 TeV”**
S. Chatrchyan *et al.* [CMS Collaboration].
arXiv:1108.2044 [hep-ex]
10.1103/PhysRevD.84.052011
Phys. Rev. D **84**, 052011 (2011)

169. **“Measurement of the Drell-Yan Cross Section in pp Collisions at $\sqrt{s} = 7$ TeV”**
S. Chatrchyan *et al.* [CMS Collaboration].
arXiv:1108.0566 [hep-ex]
10.1007/JHEP10(2011)007
JHEP **1110**, 007 (2011)

170. **“Search for B(s) and B to dimuon decays in pp collisions at 7 TeV”**
S. Chatrchyan *et al.* [CMS Collaboration].
arXiv:1107.5834 [hep-ex]
10.1103/PhysRevLett.107.191802
Phys. Rev. Lett. **107**, 191802 (2011)

171. **“Search for Resonances in the Dijet Mass Spectrum from 7 TeV pp Collisions at CMS”**
S. Chatrchyan *et al.* [CMS Collaboration].
arXiv:1107.4771 [hep-ex]
10.1016/j.physletb.2011.09.015
Phys. Lett. B **704**, 123 (2011)

172. **“Measurement of the Inclusive W and Z Production Cross Sections in pp Collisions at $\sqrt{s} = 7$ TeV”**
S. Chatrchyan *et al.* [CMS Collaboration].
arXiv:1107.4789 [hep-ex]

10.1007/JHEP10(2011)132
JHEP **1110**, 132 (2011)

173. **"Dependence on pseudorapidity and centrality of charged hadron production in PbPb collisions at a nucleon-nucleon centre-of-mass energy of 2.76 TeV"**
S. Chatrchyan *et al.* [CMS Collaboration].
arXiv:1107.4800 [nucl-ex]
10.1007/JHEP08(2011)141
JHEP **1108**, 141 (2011)

174. **"Determination of Jet Energy Calibration and Transverse Momentum Resolution in CMS"**
S. Chatrchyan *et al.* [CMS Collaboration].
arXiv:1107.4277 [physics.ins-det]
10.1088/1748-0221/6/11/P11002
JINST **6**, P11002 (2011)

175. **"Search for Three-Jet Resonances in pp Collisions at $\sqrt{s} = 7$ TeV"**
S. Chatrchyan *et al.* [CMS Collaboration].
arXiv:1107.3084 [hep-ex]
10.1103/PhysRevLett.107.101801
Phys. Rev. Lett. **107**, 101801 (2011)

176. **"Search for supersymmetry in pp collisions at $\sqrt{s} = 7$ TeV in events with a single lepton, jets, and missing transverse momentum"**
S. Chatrchyan *et al.* [CMS Collaboration].
arXiv:1107.1870 [hep-ex]
10.1007/JHEP08(2011)156
JHEP **1108**, 156 (2011)

177. **"A search for excited leptons in pp Collisions at $\sqrt{s} = 7$ TeV"**
S. Chatrchyan *et al.* [CMS Collaboration].
arXiv:1107.1773 [hep-ex]
10.1016/j.physletb.2011.09.021
Phys. Lett. B **704**, 143 (2011)

178. **"Inclusive search for squarks and gluinos in pp collisions at $\sqrt{s} = 7$ TeV"**
S. Chatrchyan *et al.* [CMS Collaboration].
arXiv:1107.1279 [hep-ex]
10.1103/PhysRevD.85.012004
Phys. Rev. D **85**, 012004 (2012)

179. **"Measurement of the Underlying Event Activity at the LHC with $\sqrt{s} = 7$ TeV and Comparison with $\sqrt{s} = 0.9$ TeV"**
S. Chatrchyan *et al.* [CMS Collaboration].
arXiv:1107.0330 [hep-ex]
10.1007/JHEP09(2011)109
JHEP **1109**, 109 (2011)

180. **“Missing transverse energy performance of the CMS detector”**
S. Chatrchyan *et al.* [CMS Collaboration].
arXiv:1106.5048 [physics.ins-det]
10.1088/1748-0221/6/09/P09001
JINST **6**, P09001 (2011)

181. **“Search for New Physics with a Mono-Jet and Missing Transverse Energy in pp Collisions at $\sqrt{s} = 7$ TeV”**
S. Chatrchyan *et al.* [CMS Collaboration].
arXiv:1106.4775 [hep-ex]
10.1103/PhysRevLett.107.201804
Phys. Rev. Lett. **107**, 201804 (2011)

182. **“Search for New Physics with Jets and Missing Transverse Momentum in pp collisions at $\sqrt{s} = 7$ TeV”**
S. Chatrchyan *et al.* [CMS Collaboration].
arXiv:1106.4503 [hep-ex]
10.1007/JHEP08(2011)155
JHEP **1108**, 155 (2011)

183. **“Measurement of the Strange B Meson Production Cross Section with J/Psi ϕ Decays in pp Collisions at $\sqrt{s} = 7$ TeV”**
S. Chatrchyan *et al.* [CMS Collaboration].
arXiv:1106.4048 [hep-ex]
10.1103/PhysRevD.84.052008
Phys. Rev. D **84**, 052008 (2011)

184. **“Search for Supersymmetry in Events with b Jets and Missing Transverse Momentum at the LHC”**
S. Chatrchyan *et al.* [CMS Collaboration].
arXiv:1106.3272 [hep-ex]
10.1007/JHEP07(2011)113
JHEP **1107**, 113 (2011)

185. **“Measurement of the t-channel single top quark production cross section in pp collisions at $\sqrt{s} = 7$ TeV”**
S. Chatrchyan *et al.* [CMS Collaboration].
arXiv:1106.3052 [hep-ex]
10.1103/PhysRevLett.107.091802
Phys. Rev. Lett. **107**, 091802 (2011)

186. **“Search for Light Resonances Decaying into Pairs of Muons as a Signal of New Physics”**
S. Chatrchyan *et al.* [CMS Collaboration].
arXiv:1106.2375 [hep-ex]
10.1007/JHEP07(2011)098
JHEP **1107**, 098 (2011)

187. **“Search for Same-Sign Top-Quark Pair Production at $\sqrt{s} = 7$ TeV and Limits on Flavour Changing Neutral Currents in the Top Sector”**
S. Chatrchyan *et al.* [CMS Collaboration].

arXiv:1106.2142 [hep-ex]
10.1007/JHEP08(2011)005
JHEP **1108**, 005 (2011)

188. **“Measurement of the Top-antitop Production Cross Section in pp Collisions at $\sqrt{s} = 7$ TeV using the Kinematic Properties of Events with Leptons and Jets”**
S. Chatrchyan *et al.* [CMS Collaboration].
arXiv:1106.0902 [hep-ex]
10.1140/epjc/s10052-011-1721-3
Eur. Phys. J. C **71**, 1721 (2011)

189. **“Search for Physics Beyond the Standard Model Using Multilepton Signatures in pp Collisions at $\sqrt{s} = 7$ TeV”**
S. Chatrchyan *et al.* [CMS Collaboration].
arXiv:1106.0933 [hep-ex]
10.1016/j.physletb.2011.09.047
Phys. Lett. B **704**, 411 (2011)

190. **“Measurement of the Ratio of the 3-jet to 2-jet Cross Sections in pp Collisions at $\sqrt{s} = 7$ TeV”**
S. Chatrchyan *et al.* [CMS Collaboration].
arXiv:1106.0647 [hep-ex]
10.1016/j.physletb.2011.07.067
Phys. Lett. B **702**, 336 (2011)

191. **“Measurement of the Inclusive Jet Cross Section in pp Collisions at $\sqrt{s} = 7$ TeV”**
S. Chatrchyan *et al.* [CMS Collaboration].
arXiv:1106.0208 [hep-ex]
10.1103/PhysRevLett.107.132001
Phys. Rev. Lett. **107**, 132001 (2011)

192. **“Measurement of the $t\bar{t}$ production cross section and the top quark mass in the dilepton channel in pp collisions at $\sqrt{s} = 7$ TeV”**
S. Chatrchyan *et al.* [CMS Collaboration].
arXiv:1105.5661 [hep-ex]
10.1007/JHEP07(2011)049
JHEP **1107**, 049 (2011)

193. **“Search for First Generation Scalar Leptoquarks in the evjj channel in pp collisions at $\sqrt{s} = 7$ TeV”**
S. Chatrchyan *et al.* [CMS Collaboration].
arXiv:1105.5237 [hep-ex]
10.1016/j.physletb.2011.07.089
Phys. Lett. B **703**, 246 (2011)

194. **“Indications of suppression of excited Υ states in PbPb collisions at $\sqrt{S_{NN}}$ = 2.76 TeV”**
S. Chatrchyan *et al.* [CMS Collaboration].
arXiv:1105.4894 [nucl-ex]
10.1103/PhysRevLett.107.052302
Phys. Rev. Lett. **107**, 052302 (2011)

195. **“Search for supersymmetry in events with a lepton, a photon, and large missing transverse energy in pp collisions at $\sqrt{s} = 7$ TeV”**
S. Chatrchyan *et al.* [CMS Collaboration].
arXiv:1105.3152 [hep-ex]
10.1007/JHEP06(2011)093
JHEP **1106**, 093 (2011)

196. **“Measurement of $W\gamma$ and $Z\gamma$ production in pp collisions at $\sqrt{s} = 7$ TeV”**
S. Chatrchyan *et al.* [CMS Collaboration].
arXiv:1105.2758 [hep-ex]
10.1016/j.physletb.2011.06.034
Phys. Lett. B **701**, 535 (2011)

197. **“Long-range and short-range dihadron angular correlations in central PbPb collisions at a nucleon-nucleon center of mass energy of 2.76 TeV”**
S. Chatrchyan *et al.* [CMS Collaboration].
arXiv:1105.2438 [nucl-ex]
10.1007/JHEP07(2011)076
JHEP **1107**, 076 (2011)

198. **“Charged particle transverse momentum spectra in pp collisions at $\sqrt{s} = 0.9$ and 7 TeV”**
S. Chatrchyan *et al.* [CMS Collaboration].
arXiv:1104.3547 [hep-ex]
10.1007/JHEP08(2011)086
JHEP **1108**, 086 (2011)

199. **“Measurement of the Polarization of W Bosons with Large Transverse Momenta in W+Jets Events at the LHC”**
S. Chatrchyan *et al.* [CMS Collaboration].
arXiv:1104.3829 [hep-ex]
10.1103/PhysRevLett.107.021802
Phys. Rev. Lett. **107**, 021802 (2011)

200. **“Search for new physics with same-sign isolated dilepton events with jets and missing transverse energy at the LHC”**
S. Chatrchyan *et al.* [CMS Collaboration].
arXiv:1104.3168 [hep-ex]
10.1007/JHEP06(2011)077
JHEP **1106**, 077 (2011)

201. **“Measurement of the B^0 production cross section in pp Collisions at $\sqrt{s} = 7$ TeV”**
S. Chatrchyan *et al.* [CMS Collaboration].
arXiv:1104.2892 [hep-ex]
10.1103/PhysRevLett.106.252001
Phys. Rev. Lett. **106**, 252001 (2011)

202. **“Measurement of the differential dijet production cross section in proton-proton collisions at $\sqrt{s} = 7$ TeV”**
S. Chatrchyan *et al.* [CMS Collaboration].

arXiv:1104.1693 [hep-ex]
10.1016/j.physletb.2011.05.027
Phys. Lett. B **700**, 187 (2011)

203. **"Measurement of the Inclusive Z Cross Section via Decays to Tau Pairs in pp Collisions at $\sqrt{s} = 7$ TeV"**
S. Chatrchyan *et al.* [CMS Collaboration].
arXiv:1104.1617 [hep-ex]
10.1007/JHEP08(2011)117
JHEP **1108**, 117 (2011)

204. **"Search for Neutral MSSM Higgs Bosons Decaying to Tau Pairs in pp Collisions at $\sqrt{s} = 7$ TeV"**
S. Chatrchyan *et al.* [CMS Collaboration].
arXiv:1104.1619 [hep-ex]
10.1103/PhysRevLett.106.231801
Phys. Rev. Lett. **106**, 231801 (2011)

205. **"Search for Large Extra Dimensions in the Diphoton Final State at the Large Hadron Collider"**
S. Chatrchyan *et al.* [CMS Collaboration].
arXiv:1103.4279 [hep-ex]
10.1007/JHEP05(2011)085
JHEP **1105**, 085 (2011)

206. **"Measurement of the lepton charge asymmetry in inclusive W production in pp collisions at $\sqrt{s} = 7$ TeV"**
S. Chatrchyan *et al.* [CMS Collaboration].
arXiv:1103.3470 [hep-ex]
10.1007/JHEP04(2011)050
JHEP **1104**, 050 (2011)

207. **"Search for Physics Beyond the Standard Model in Opposite-Sign Dilepton Events at $\sqrt{s} = 7$ TeV"**
S. Chatrchyan *et al.* [CMS Collaboration].
arXiv:1103.1348 [hep-ex]
10.1007/JHEP06(2011)026
JHEP **1106**, 026 (2011)

208. **"Search for Supersymmetry in pp Collisions at $\sqrt{s} = 7$ TeV in Events with Two Photons and Missing Transverse Energy"**
S. Chatrchyan *et al.* [CMS Collaboration].
arXiv:1103.0953 [hep-ex]
10.1103/PhysRevLett.106.211802
Phys. Rev. Lett. **106**, 211802 (2011)

209. **"Search for Resonances in the Dilepton Mass Distribution in pp Collisions at $\sqrt{(s)} = 7$ TeV"**
S. Chatrchyan *et al.* [CMS Collaboration].

arXiv:1103.0981 [hep-ex]
10.1007/JHEP05(2011)093
JHEP **1105**, 093 (2011)

210. **“Search for a W' boson decaying to a muon and a neutrino in pp collisions at $\sqrt{s} = 7$ TeV”**
S. Chatrchyan *et al.* [CMS Collaboration].
arXiv:1103.0030 [hep-ex]
10.1016/j.physletb.2011.05.048
Phys. Lett. B **701**, 160 (2011)

211. **“Measurement of W^+W^- Production and Search for the Higgs Boson in pp Collisions at $\sqrt{s} = 7$ TeV”**
S. Chatrchyan *et al.* [CMS Collaboration].
arXiv:1102.5429 [hep-ex]
10.1016/j.physletb.2011.03.056
Phys. Lett. B **699**, 25 (2011)

212. **“Study of Z boson production in PbPb collisions at nucleon-nucleon centre of mass energy = 2.76 TeV”**
S. Chatrchyan *et al.* [CMS Collaboration].
arXiv:1102.5435 [nucl-ex]
10.1103/PhysRevLett.106.212301
Phys. Rev. Lett. **106**, 212301 (2011)

213. **“Search for a Heavy Bottom-like Quark in pp Collisions at $\sqrt{s} = 7$ TeV”**
S. Chatrchyan *et al.* [CMS Collaboration].
arXiv:1102.4746 [hep-ex]
10.1016/j.physletb.2011.05.074
Phys. Lett. B **701**, 204 (2011)

214. **“Strange Particle Production in pp Collisions at $\sqrt{s} = 0.9$ and 7 TeV”**
V. Khachatryan *et al.* [CMS Collaboration].
arXiv:1102.4282 [hep-ex]
10.1007/JHEP05(2011)064
JHEP **1105**, 064 (2011)

215. **“Measurement of $B\bar{B}$ Angular Correlations based on Secondary Vertex Reconstruction at $\sqrt{s} = 7$ TeV”**
V. Khachatryan *et al.* [CMS Collaboration].
arXiv:1102.3194 [hep-ex]
10.1007/JHEP03(2011)136
JHEP **1103**, 136 (2011)

216. **“Measurement of Dijet Angular Distributions and Search for Quark Compositeness in pp Collisions at $sqrts = 7$ TeV”**
V. Khachatryan *et al.* [CMS Collaboration].
arXiv:1102.2020 [hep-ex]
10.1103/PhysRevLett.106.201804
Phys. Rev. Lett. **106**, 201804 (2011)

217. **“Observation and studies of jet quenching in PbPb collisions at nucleon-nucleon center-of-mass energy = 2.76 TeV”**
S. Chatrchyan *et al.* [CMS Collaboration].
arXiv:1102.1957 [nucl-ex]
10.1103/PhysRevC.84.024906
Phys. Rev. C **84**, 024906 (2011)

218. **“First Measurement of Hadronic Event Shapes in pp Collisions at $\sqrt{(s)} = 7$ TeV”**
V. Khachatryan *et al.* [CMS Collaboration].
arXiv:1102.0068 [hep-ex]
10.1016/j.physletb.2011.03.060
Phys. Lett. B **699**, 48 (2011)

219. **“Dijet Azimuthal Decorrelations in pp Collisions at $\sqrt{s} = 7$ TeV”**
V. Khachatryan *et al.* [CMS Collaboration].
arXiv:1101.5029 [hep-ex]
10.1103/PhysRevLett.106.122003
Phys. Rev. Lett. **106**, 122003 (2011)

220. **“Inclusive b-hadron production cross section with muons in pp collisions at $\sqrt{s} = 7$ TeV”**
V. Khachatryan *et al.* [CMS Collaboration].
arXiv:1101.3512 [hep-ex]
10.1007/JHEP03(2011)090
JHEP **1103**, 090 (2011)

221. **“Measurement of Bose-Einstein Correlations in pp Collisions at $\sqrt{s} = 0.9$ and 7 TeV”**
V. Khachatryan *et al.* [CMS Collaboration].
arXiv:1101.3518 [hep-ex]
10.1007/JHEP05(2011)029
JHEP **1105**, 029 (2011)

222. **“Search for Supersymmetry in pp Collisions at 7 TeV in Events with Jets and Missing Transverse Energy”**
V. Khachatryan *et al.* [CMS Collaboration].
arXiv:1101.1628 [hep-ex]
10.1016/j.physletb.2011.03.021
Phys. Lett. B **698**, 196 (2011)

223. **“Search for Heavy Stable Charged Particles in pp collisions at $\sqrt{s} = 7$ TeV”**
V. Khachatryan *et al.* [CMS Collaboration].
arXiv:1101.1645 [hep-ex]
10.1007/JHEP03(2011)024
JHEP **1103**, 024 (2011)

224. **“Measurement of the B^+ Production Cross Section in pp Collisions at $\sqrt{s} = 7$ TeV”**
V. Khachatryan *et al.* [CMS Collaboration].
arXiv:1101.0131 [hep-ex]
10.1103/PhysRevLett.106.112001
Phys. Rev. Lett. **106**, 112001 (2011)

225. **“Search for a heavy gauge boson W ’ in the final state with an electron and large missing transverse energy in pp collisions at $\sqrt{s} = 7$ TeV”**
V. Khachatryan *et al.* [CMS Collaboration].
arXiv:1012.5945 [hep-ex]
10.1016/j.physletb.2011.02.048
Phys. Lett. B **698**, 21 (2011)

226. **“Measurement of the Inclusive Υ production cross section in pp collisions at $\sqrt{s} = 7$ TeV”**
V. Khachatryan *et al.* [CMS Collaboration].
arXiv:1012.5545 [hep-ex]
10.1103/PhysRevD.83.112004
Phys. Rev. D **83**, 112004 (2011)

227. **“Search for Pair Production of First-Generation Scalar Leptoquarks in pp Collisions at $\sqrt{s} = 7$ TeV”**
V. Khachatryan *et al.* [CMS Collaboration].
arXiv:1012.4031 [hep-ex]
10.1103/PhysRevLett.106.201802
Phys. Rev. Lett. **106**, 201802 (2011)

228. **“Search for Pair Production of Second-Generation Scalar Leptoquarks in pp Collisions at $\sqrt{s} = 7$ TeV”**
V. Khachatryan *et al.* [CMS Collaboration].
arXiv:1012.4033 [hep-ex]
10.1103/PhysRevLett.106.201803
Phys. Rev. Lett. **106**, 201803 (2011)

229. **“Search for Microscopic Black Hole Signatures at the Large Hadron Collider”**
V. Khachatryan *et al.* [CMS Collaboration].
arXiv:1012.3375 [hep-ex]
10.1016/j.physletb.2011.02.032
Phys. Lett. B **697**, 434 (2011)

230. **“Measurements of Inclusive W and Z Cross Sections in pp Collisions at $\sqrt{s} = 7$ TeV”**
V. Khachatryan *et al.* [CMS Collaboration].
arXiv:1012.2466 [hep-ex]
10.1007/JHEP01(2011)080
JHEP **1101**, 080 (2011)

231. **“Measurement of the Isolated Prompt Photon Production Cross Section in pp Collisions at $\sqrt{s} = 7$ TeV”**
V. Khachatryan *et al.* [CMS Collaboration].
arXiv:1012.0799 [hep-ex]
10.1103/PhysRevLett.106.082001
Phys. Rev. Lett. **106**, 082001 (2011)

232. **“Charged particle multiplicities in pp interactions at $\sqrt{s} = 0.9$, 2.36, and 7 TeV”**
V. Khachatryan *et al.* [CMS Collaboration].

arXiv:1011.5531 [hep-ex]
10.1007/JHEP01(2011)079
JHEP **1101**, 079 (2011)

233. **"Search for Stopped Gluinos in pp collisions at $\sqrt{s} = 7$ TeV"**
V. Khachatryan *et al.* [CMS Collaboration].
arXiv:1011.5861 [hep-ex]
10.1103/PhysRevLett.106.011801
Phys. Rev. Lett. **106**, 011801 (2011)

234. **"Prompt and non-prompt J/ψ production in pp collisions at $\sqrt{s} = 7$ TeV"**
V. Khachatryan *et al.* [CMS Collaboration].
arXiv:1011.4193 [hep-ex]
10.1140/epjc/s10052-011-1575-8
Eur. Phys. J. C **71**, 1575 (2011)

235. **"First Measurement of the Cross Section for Top-Quark Pair Production in Proton-Proton Collisions at $\sqrt{s} = 7$ TeV"**
V. Khachatryan *et al.* [CMS Collaboration].
arXiv:1010.5994 [hep-ex]
10.1016/j.physletb.2010.11.058
Phys. Lett. B **695**, 424 (2011)

236. **"Search for Quark Compositeness with the Dijet Centrality Ratio in pp Collisions at $\sqrt{s} = 7$ TeV"**
V. Khachatryan *et al.* [CMS Collaboration].
arXiv:1010.4439 [hep-ex]
10.1103/PhysRevLett.105.262001
Phys. Rev. Lett. **105**, 262001 (2010)

237. **"Search for Dijet Resonances in 7 TeV pp Collisions at CMS"**
V. Khachatryan *et al.* [CMS Collaboration].
arXiv:1010.0203 [hep-ex]
10.1103/PhysRevLett.105.211801, 10.1103/PhysRevLett.106.029902
Phys. Rev. Lett. **105**, 211801 (2010)

238. **"Observation of Long-Range Near-Side Angular Correlations in Proton-Proton Collisions at the LHC"**
V. Khachatryan *et al.* [CMS Collaboration].
arXiv:1009.4122 [hep-ex]
10.1007/JHEP09(2010)091
JHEP **1009**, 091 (2010)

239. **"CMS Tracking Performance Results from early LHC Operation"**
V. Khachatryan *et al.* [CMS Collaboration].
arXiv:1007.1988 [physics.ins-det]
10.1140/epjc/s10052-010-1491-3
Eur. Phys. J. C **70**, 1165 (2010)

240. **“First Measurement of the Underlying Event Activity at the LHC with $\sqrt{s} = 0.9$ TeV”**
V. Khachatryan *et al.* [CMS Collaboration].
arXiv:1006.2083 [hep-ex]
10.1140/epjc/s10052-010-1453-9
Eur. Phys. J. C **70**, 555 (2010)

241. **“Measurement of the charge ratio of atmospheric muons with the CMS detector”**
V. Khachatryan *et al.* [CMS Collaboration].
arXiv:1005.5332 [hep-ex]
10.1016/j.physletb.2010.07.033
Phys. Lett. B **692**, 83 (2010)

242. **“Measurement of Bose-Einstein correlations with first CMS data”**
V. Khachatryan *et al.* [CMS Collaboration].
arXiv:1005.3294 [hep-ex]
10.1103/PhysRevLett.105.032001
Phys. Rev. Lett. **105**, 032001 (2010)

243. **“Transverse-momentum and pseudorapidity distributions of charged hadrons in pp collisions at $\sqrt{s} = 7$ TeV”**
V. Khachatryan *et al.* [CMS Collaboration].
arXiv:1005.3299 [hep-ex]
10.1103/PhysRevLett.105.022002
Phys. Rev. Lett. **105**, 022002 (2010)

244. **“Transverse momentum and pseudorapidity distributions of charged hadrons in pp collisions at $\sqrt(s)$ = 0.9 and 2.36 TeV”**
V. Khachatryan *et al.* [CMS Collaboration].
arXiv:1002.0621 [hep-ex]
10.1007/JHEP02(2010)041
JHEP **1002**, 041 (2010)

245. **“Commissioning and Performance of the CMS Pixel Tracker with Cosmic Ray Muons”**
SChatrchyan *et al.* [CMS Collaboration].
arXiv:0911.5434 [physics.ins-det]
10.1088/1748-0221/5/03/T03007
JINST **5**, T03007 (2010)

246. **“Performance of the CMS Level-1 Trigger during Commissioning with Cosmic Ray Muons”**
SChatrchyan *et al.* [CMS Collaboration].
arXiv:0911.5422 [physics.ins-det]
10.1088/1748-0221/5/03/T03002
JINST **5**, T03002 (2010)

247. **“Measurement of the Muon Stopping Power in Lead Tungstate”**
SChatrchyan *et al.* [CMS Collaboration].
arXiv:0911.5397 [physics.ins-det]
10.1088/1748-0221/5/03/P03007
JINST **5**, P03007 (2010)

248. **“Commissioning and Performance of the CMS Silicon Strip Tracker with Cosmic Ray Muons”**
SChatrchyan *et al.* [CMS Collaboration].
arXiv:0911.4996 [physics.ins-det]
10.1088/1748-0221/5/03/T03008
JINST **5**, T03008 (2010)

249. **“Performance of CMS Muon Reconstruction in Cosmic-Ray Events”**
SChatrchyan *et al.* [CMS Collaboration].
arXiv:0911.4994 [physics.ins-det]
10.1088/1748-0221/5/03/T03022
JINST **5**, T03022 (2010)

250. **“Performance of the CMS Cathode Strip Chambers with Cosmic Rays”**
SChatrchyan *et al.* [CMS Collaboration].
arXiv:0911.4992 [physics.ins-det]
10.1088/1748-0221/5/03/T03018
JINST **5**, T03018 (2010)

251. **“Performance of the CMS Hadron Calorimeter with Cosmic Ray Muons and LHC Beam Data”**
SChatrchyan *et al.* [CMS Collaboration].
arXiv:0911.4991 [physics.ins-det]
10.1088/1748-0221/5/03/T03012
JINST **5**, T03012 (2010)

252. **“Fine Synchronization of the CMS Muon Drift-Tube Local Trigger using Cosmic Rays”**
SChatrchyan *et al.* [CMS Collaboration].
arXiv:0911.4904 [physics.ins-det]
10.1088/1748-0221/5/03/T03004
JINST **5**, T03004 (2010)

253. **“Calibration of the CMS Drift Tube Chambers and Measurement of the Drift Velocity with Cosmic Rays”**
SChatrchyan *et al.* [CMS Collaboration].
arXiv:0911.4895 [physics.ins-det]
10.1088/1748-0221/5/03/T03016
JINST **5**, T03016 (2010)

254. **“Performance of the CMS Drift-Tube Local Trigger with Cosmic Rays”**
SChatrchyan *et al.* [CMS Collaboration].
arXiv:0911.4893 [physics.ins-det]
10.1088/1748-0221/5/03/T03003
JINST **5**, T03003 (2010)

255. **“Commissioning of the CMS High-Level Trigger with Cosmic Rays”**
SChatrchyan *et al.* [CMS Collaboration].
arXiv:0911.4889 [physics.ins-det]
10.1088/1748-0221/5/03/T03005
JINST **5**, T03005 (2010)

256. **“Identification and Filtering of Uncharacteristic Noise in the CMS Hadron Calorimeter”**
SChatrchyan *et al.* [CMS Collaboration].
arXiv:0911.4881 [physics.ins-det]
10.1088/1748-0221/5/03/T03014
JINST **5**, T03014 (2010)

257. **“Performance of CMS Hadron Calorimeter Timing and Synchronization using Test Beam, Cosmic Ray, and LHC Beam Data”**
SChatrchyan *et al.* [CMS Collaboration].
arXiv:0911.4877 [physics.ins-det]
10.1088/1748-0221/5/03/T03013
JINST **5**, T03013 (2010)

258. **“Performance of the CMS Drift Tube Chambers with Cosmic Rays”**
SChatrchyan *et al.* [CMS Collaboration].
arXiv:0911.4855 [physics.ins-det]
10.1088/1748-0221/5/03/T03015
JINST **5**, T03015 (2010)

259. **“Commissioning of the CMS Experiment and the Cosmic Run at Four Tesla”**
SChatrchyan *et al.* [CMS Collaboration].
arXiv:0911.4845 [physics.ins-det]
10.1088/1748-0221/5/03/T03001
JINST **5**, T03001 (2010)

260. **“CMS Data Processing Workflows during an Extended Cosmic Ray Run”**
SChatrchyan *et al.* [CMS Collaboration].
arXiv:0911.4842 [physics.ins-det]
10.1088/1748-0221/5/03/T03006
JINST **5**, T03006 (2010)

261. **“Aligning the CMS Muon Chambers with the Muon Alignment System during an Extended Cosmic Ray Run”**
SChatrchyan *et al.* [CMS Collaboration].
arXiv:0911.4770 [physics.ins-det]
10.1088/1748-0221/5/03/T03019
JINST **5**, T03019 (2010)

262. **“Performance Study of the CMS Barrel Resistive Plate Chambers with Cosmic Rays”**
SChatrchyan *et al.* [CMS Collaboration].
arXiv:0911.4045 [physics.ins-det]
10.1088/1748-0221/5/03/T03017
JINST **5**, T03017 (2010)

263. **“Time Reconstruction and Performance of the CMS Electromagnetic Calorimeter”**
SChatrchyan *et al.* [CMS Collaboration].
arXiv:0911.4044 [physics.ins-det]
10.1088/1748-0221/5/03/T03011
JINST **5**, T03011 (2010)

264. **“Alignment of the CMS Muon System with Cosmic-Ray and Beam-Halo Muons”**
    SChatrchyan *et al.* [CMS Collaboration].
    arXiv:0911.4022 [physics.ins-det]
    10.1088/1748-0221/5/03/T03020
    JINST **5**, T03020 (2010)

265. **“Precise Mapping of the Magnetic Field in the CMS Barrel Yoke using Cosmic Rays”**
    SChatrchyan *et al.* [CMS Collaboration].
    arXiv:0910.5530 [physics.ins-det]
    10.1088/1748-0221/5/03/T03021
    JINST **5**, T03021 (2010)

266. **“Performance and Operation of the CMS Electromagnetic Calorimeter”**
    SChatrchyan *et al.* [CMS Collaboration].
    arXiv:0910.3423 [physics.ins-det]
    10.1088/1748-0221/5/03/T03010
    JINST **5**, T03010 (2010)

267. **“Alignment of the CMS Silicon Tracker during Commissioning with Cosmic Rays”**
    SChatrchyan *et al.* [CMS Collaboration].
    arXiv:0910.2505 [physics.ins-det]
    10.1088/1748-0221/5/03/T03009
    JINST **5**, T03009 (2010)

268. **“The CMS experiment at the CERN LHC”**
    S. Chatrchyan *et al.* [CMS Collaboration].
    10.1088/1748-0221/3/08/S08004
    JINST **3**, S08004 (2008).

269. **“Study of di-boson production with the CMS detector at LHC”**
    V. Brigljevic, D. Ferencek, S. Morovic, M. Planinic, S. Beauceron, S. Ganjour, G. Hamel de Monchenault and S. Mele *et al.*.
    10.1088/0954-3899/34/7/N01
    J. Phys. G **34**, N269 (2007).

270. **“CMS technical design report, volume II: Physics performance”**
    G. L. Bayatian *et al.* [CMS Collaboration].
    10.1088/0954-3899/34/6/S01
    J. Phys. G **34**, 995 (2007).

271. **“CMS physics technical design report: Addendum on high density QCD with heavy ions”**
    D. G. d’Enterria *et al.* [CMS Collaboration].
    10.1088/0954-3899/34/11/008
    J. Phys. G **34**, 2307 (2007).